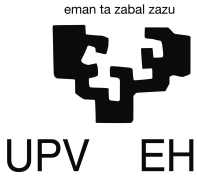


**UNIVERSIDAD DEL PAÍS VASCO**
**EUSKAL HERRIKO UNIBERTSITATEA**

**Escuela Técnica Superior de Ingeniería de Bilbao**
**Bilboko Ingeniaritza Goi Eskola Teknikoa**

**PhD Thesis**

# Compliance verification methodology for renewable generation integration. Application to island power grids

**PRESENTED BY:**

Agurtzane Etxegarai Madina

**SUPERVISED BY:**

Dr. Esther Torres Iglesias
Dr. Pablo Eguía López

2015


Servicio Editorial de la Universidad del País Vasco (UPV/EHU)
*Euskal Herriko Unibertsitateko Argitalpen Zerbitzua (UPV/EHU)*
University of the Basque Country - Editorial Service (UPV/EHU)
**ISBN: 978-84-9082-193-0**

For further requests, please send an email to the following address:
agurtzane.etxegarai@ehu.es

# Acknowledgements

This thesis is submitted in partial fulfillment of the requirements for the degree of Doctor of Philosophy (Ph. D) in Industrial Engineering by the University of the Basque Country UPV/EHU.

I am indebted to many people: colleagues, friends and family members for their interest, assistance and support, and therefore, I wish to acknowledge them hereby.

The present thesis has been carried out in the period from November 2011 to May 2015 under the supervision of Dr. Esther Torres and Dr. Pablo Eguia. I wish to thank them for supporting my research and giving me the chance to participate in the project Wind2Weak (Subprograma INNPACTO Ministerio Ciencia e Innovación), which was the starting point of this thesis. My acknowledgement also goes to the members of the Wind2Weak project belonging to Ingeteam company: Miguel Angel Rodriguez, Markel Zubiaga and Sergio Aurtenetxe.

I am also grateful to TU Clausthal, Beuth Hochschule fur Technik and Politecnico di Torino for providing a great research environment with excellent infrastructures and stimulating experiences during my research stays respectively during the summers of 2011, 2012 and 2013 under the guidance of Prof. Dr. Turschner, Prof. Dr. Borowiak and Prof. Dr. Chicco.

*Baina batez ere, urteotan ondoan izan zaituztedan guztioi eskaini nahiko nizkizueke nire eskerrik beroenak. Maldan gora nirekin sufritu duzuenoi. Bidean zehar nire umore gorabeheratsua jasan duzuenoi. Etsita nengoenean zuen laguntza luzatu didazuenoi. Eta nire lorpenekin poztu zaretenoi. Elkarrekin egin dugu, iritsi gara gailurrera. Eskerrik asko bihotzez guztioi, familia, lagun eta lankideei.*

*Anartzi, elkarrekin ametsak eraikiz jarrai dezagun.*

*Joan zirenei eta etorriko direnei. Izan zirelako gara eta garelako izango dira.*

Mungia, 2015eko Maiatza.

# Abstract

Power systems have varying characteristics, in terms of network topology, demand size and pattern, or installed power generation capacity and technology. In strong interconnected systems, voltage levels are stiff, system inertia is high and stability is rarely lost. Power supply is therefore guaranteed, and the integration of renewable energy sources is key to a diversified generation mix. In weak power grids, the penetration of non-synchronous power generation can be challenging from two perspectives: regarding the impact of variable generation assets in the power system and vice versa. For the power system, power quality issues, such as flicker, can arise due to the variability of renewable energy sources, unit commitment and dispatching can be challenging especially in weak networks with no interconnection, and stability can be compromised above certain penetration ratios. On the other hand, generation assets have to face the technical issues present in such power systems: resonance problems in extense weak power grids, great frequency excursions and propagation of low voltage dips to the whole system in island power grids, control interactions, poor power quality with the presence of flicker, unbalance, or harmonics, or voltage out of permissible ranges.

Besides, system operators often impose on to non-synchronous generators strict technical requirements, which are challenging within already technically and economically constricted system contexts such as island power grids. Firstly, generating units are not always allowed to disconnect upon the occurrence of voltage or frequency disturbances so as not to lose system stability. And secondly, power plants including those based on renewable energy sources can be requested to actively support the power system performance. Both aspects will be reviewed in the present thesis, based on most relevant regulation. In addition, grid codes should be complemented by corresponding compliance verification procedures. The current alternatives and common practices will be hereby analysed, including compliance testing by using practical tests and compliance simulation by means of simulation studies and revision against actual measurements. The alternative based on simulation has a lower cost, is easier to implement and has no side effects on the grid, even if validation is required. Thus, verification processes are streamlined for manufacturers, facility owners and system operators. However, simulation based compliance verification is yet at an early stage and basically limited to a unique requirement: Low Voltage Ride-Through (LVRT). Current procedures comprehend testing simulation models lacking data, or parameterised to represent a certain power system.

Therefore, this thesis proposes a grid code compliance verification methodology based on generic simulation models that are simple and valid for verifying grid code regulation aspects. As technical rules regarding power plant connection are deci-

dedly related to power system characteristics, island power grids have been selected as target systems. Most critical requirements in isolated power grids are Frequency Ride-Through, LVRT and voltage and current unbalance. Hence, the generic grid models will be adapted and particularised for each of the requirements, based on theoretical analysis and sensitivity studies. Finally, the parameterisation of the equivalent grid models will be developed so as to fit any power system.

The methodology will be applied to three study cases, where the installation of a renewable power plant will be studied. So, it will verified whether the generation asset is compliant with the grid codes under force, including the passive requirements Frequency Ride-Through, LVRT and voltage and current unbalance, and active requirements such as frequency response and current contribution during faults. In the first study case, a new photovoltaic plant will be installed in a medium size island grid, where only minimum information is available at the Point of Common Coupling (PCC). The second study corresponds to Terceira island, in the Açores archipelago, where a new wind farm will be installed. Static and dynamic data about the power system are available, but there is still no grid code under force to be met by renewable power plants. Finally, the methodology will be applied to the third study case consisting in the upgrade of an existing wind farm in Fuerteventura-Lanzarote subsystem in the Canaries, where both complete system data and grid code are available. The numerical application to these three study cases will back the validity of the methodology proposed in the present thesis.

**Key words:** weak power grids, island power grids, grid code, compliance verification, renewable energy sources, wind power, fault ride-through, voltage unbalance, current unbalance, frequency control, voltage control, generic model, model validation.

# Laburpena

Sistema elektrikoek zenbait ezaugarri berezi dituzte, sarearen topologiaren, energia-eskaeraren ezaugarrien eta sorkuntzako instalazioen kapazitate eta teknologiaren arabera. Elkarkonektaturiko sare elektriko sendoetan, tentsio-mailen aldaketak sumaezinak dira, sistemako inertzia altua da, eta egonkortasuna ez da normalki galtzen. Hortaz, hornidura elektrikoa bermatzen da, eta energia berriztagarrien integrazioa baliabide bat da mix energetikoa dibertsifikatzeko. Sare elektriko ahuletan, bestalde, erronka bat da energia-iturri aldakorreko sorkuntza, sorgailuek sarean edota sareak sorgailuetan duten inpaktuari dagokionez. Horrela, hornidura elektrikoaren kalitateak txarrera egin dezake, energia-iturrien aldakortasunak eragindako '*flicker*' bezalako fenomenoak direla eta; horrez gain, '*unit commitment*' eta sorkuntza-unitateen despatxua ere zaila izan daiteke kanpoko interkonexiorik gabeko sare ahuletan; eta, azkenik, sistemaren egonkortasuna kolokan jar daiteke energia berriztagarrien ratioak altuak diren egoeretan. Bestetik, sorgailuek ere jasan behar dituzte sare horietan agertzen diren arazo teknikoak: sare ahul zabaletako erresonantziak, sare isolatuetako maiztasun-desbideraketak eta tentsio-hutsen hedapenak, kontrol-elkarrekintzak, hornidura elektrikoaren kalitatea txarra -*flicker*a, desoreka eta armonikoak barne- eta maila onargarrietatik at dauden tentsioak.

Gainera, bete beharreko baldintza tekniko zorrotzak eskatzen dizkiete sistema-operatzaileek sorgailuei. Erronka handia da hori, berez teknikoki eta ekonomikoki murriztuta dauden uharte-sareetan. Alde batetik, sorgailuek sareari konektatuta jarraitu behar dute tentsio- eta maiztasun-perturbazio larriak egon arren, sistemak egonkortasuna gal ez dezan. Beste alde batetik, sorkuntzako zentralek -energia berriztagarrietan oinarritutakoak barne- aktiboki hartu behar dute parte sistemaren operazioan. Honako tesi honetan bi alderdiok berrikusiko dira, nazioarteko araudi aipagarrienetan oinarrituta. Sareko kodeak betetzen direla egiaztatzeko prozedurak ere beharrezkoak dira. Lan honetan gaurko aukera eta praktika nagusiak aztertuko dira, tokian edo laborategian burututako froga praktikoak eta neurri errealekin balioztatutako simulazio bidezko jardunbideak argituz. Simulazioan oinarritutako hautabidea merkeagoa da, errazagoa gauzatzeko orduan eta ez du zehar-efekturik sarean. Modu horretan, arrazionalizatu egiten da sareko kodeak egiaztatzea ekoizle, sortzaile eta operatzaileentzat. Hala ere, aukera hori ez dago gaur egun oso garatuta eta baldintza tekniko bakarrera mugatzen da, hots, Low Voltage Ride-Through (LVRT) delakora. Oraingo prozeduretan agertzen diren simulazio-ereduak ez dira osoak, edota parametrizatuta daude sistema elektriko jakin bat adierazteko.

Ondorioz, tesi honek simulazio-eredu generikoetan oinarritutako metodologia bat aurkeztuko du, sareko kodeen betetzea baieztatze aldera. Ereduok sinpleak baina baliozkoak dira baldintza teknikoen zeinbat alderdi egiaztatzeko. Sorkuntza elektri-

korako zentralen konexioa erregulatzen duten arau teknikoak estuki loturik daude sistema elektrikoen ezaugarriekin. Hortaz, uharte-sareak aukeratu dira azterketarako, energia berriztagarrien integrazioak berebiziko garrantzia baitu bertan. Metodologia hori uharte-sareetan erabakigarrienak diren baldintza teknikoetara mugatuko da, hau da, Frequency Ride-Through, LVRT eta tentsio- eta korronte-desoreketara. Tesian proposatutako eredu generikoak baldintza bakoitzera egokitu eta zehaztuko dira, analisi teorikoetan eta sentikortasun-azterketetan oinarrituta. Azkenik, sareko eredu baliokideen parametrizazioa argituko da, edozein saretara moldatzeko.

Metodologia hori hiru ikasketa-kasutara aplikatuko da. Hiru uharte-saretan energia berriztagarrietan oinarritutako zentral berrien edo aurretik dauden zentralen hobekuntza aztertuko dira. Horrela, sorkuntza-unitateok sare-kodeetako baldintza pasiboak (Frequency Ride-Through, LVRT eta tentsio- eta korronte-desorekak) zein aktiboak (maiztasun-erantzuna eta akatspeko korronte-injekzioa) betetzen ote dituzten egiaztatuko da. Lehen kasuan, tamaina ertaineko irla batean zentral fotovoltaiko bat instalatu nahi da; baina konexio-puntuari buruzko datu minimoak baizik ez daude eskura. Bigarren kasuan, parke eoliko berri bat eraikiko da Azore uharteetako Terceira-n; sistema elektrikoari buruzko datu estatiko eta dinamikoak ezagunak dira, baina ez dago sorgailu aldakorren konexioari buruzko araudi berezirik. Azkenik, metodologia hirugarren kasu batera aplikatuko da, Kanariar uharteetako Fuerteventura-Lanzarote azpisistemako parke eoliko baten hobekuntza aztertuz; sarearen datu estatiko eta dinamikoak ezagunak dira eta indarrean dago araudi berezi bat. Metodologia hiru ikasketa-kasuotara aplikatzeak tesian proposatutako prozedura balioztatuko du.

**Gako-hitzak**: sare ahulak, uharte-sareak, sareko kodea, energia berriztagarriak, energia eolikoa, fault ride-through, tentsio-desoreka, korronte-desoreka, maiztasun-kontrola, tentsio-kontrola, eredu generikoa, ereduen balioztapena.

# Resumen

Los sistemas eléctricos se distinguen entre sí por la topología de la red, características de la demanda, así como la capacidad y tecnología de las instalaciones generadoras. En redes eléctricas fuertemente interconectadas, las variaciones de niveles de tensión son imperceptibles, la inercia del sistema es alta y rara vez se pierde la estabilidad. El suministro eléctrico queda así garantizado y la integración de fuentes de energía renovables es clave para la diversificación del mix energético. Sin embargo, en redes consideradas débiles la penetración de generación de fuente variable supone un desafío tanto en cuanto al impacto de los generadores sobre la red, como al impacto de la red sobre los generadores. En este sentido, la calidad del suministro eléctrico puede verse perjudicada con fenómenos como el '*flicker*' ocasionado por la variabilidad de las fuentes; la programación de grupos y el despacho de unidades de generación puede resultar problemático en redes débiles sin interconexión externa; e incluso la estabilidad puede verse comprometida a partir de ciertos ratios de penetración. Por otro lado, los generadores deben afrontar los problemas técnicos presentes en dichas redes: problemas de resonancias en redes débiles extensas, grandes excursiones de frecuencia y propagación de huecos de tensión en pequeñas redes insulares, interacciones de control, baja calidad del suministro debido a la presencia de *flicker*, desequilibrios y armónicos, así como tensiones fuera de los niveles permitidos.

Además, actualmente los operadores del sistema imponen el cumplimiento de requisitos técnicos estrictos incluso a generadores no síncronos, lo cual es especialmente exigente en sistemas de por sí limitados técnica y económicamente como las redes insulares. Por un lado, los generadores deben permanecer conectados a la red bajo graves perturbaciones de tensión y frecuencia, de modo que el sistema no pierda la estabilidad. Por otro lado, las centrales de generación, incluyendo aquellas basadas en fuentes de energía renovables, deben en ocasiones contribuir activamente a la operación del sistema. Ambos aspectos serán revisados en la presente tesis, basándose en las normativas internacionales más relevantes. Además, los códigos de red deben completarse con los correspondientes procedimientos de verificación. En la presente tesis se analizarán las alternativas y prácticas habituales, incluyendo pruebas prácticas, in situ o en laboratorio, o herramientas de simulación con validación mediante medidas reales. La alternativa basada en simulación tiene un coste más bajo, es más fácil de implementar y no tiene efectos colaterales en la red, aunque los modelos de simulación deben ser validados. De este modo, los procesos de verificación se racionalizan para fabricantes, generadores y operadores. Sin embargo, la verificación del cumplimiento del código de red basada en herramientas de simulación se encuentra poco desarrollado y limitada básicamente a un único requisito: Low Voltage Ride-Through (LVRT). Además, los procedimientos existentes incluyen modelos de simulación incompletos o parametrizados de modo que representan un

sistema eléctrico concreto.

Por lo tanto, la presente tesis propone una metodología de verificación del cumplimiento de código de red basada en modelos de simulación genéricos, simples y válidos. Dado que las normas técnicas de conexión de centrales de generación eléctricas están unívocamente unidas a las características de los sistemas eléctricos, se han seleccionado las redes insulares donde la integración de fuentes de energía renovables es de vital importancia. Así mismo, la metodología se limita a los requisitos técnicos más críticos en pequeñas redes insulares: Frequency Ride-Through, LVRT y desequilibrios de tensión y corriente. Los modelos genéricos se adaptarán y particularizarán para cada uno de estos requisitos, en base a estudios analíticos y de sensibilidad de los parámetros más influyentes. Finalmente, se llevará a cabo la parametrización de los modelos equivalentes de red, de modo que se puedan ajustar a cualquier tipo de red.

La metodología se aplicará a tres casos de estudio, donde se estudiarÃą la instalación o mejora de centrales de generación renovable en tres redes insulares. De este modo, se verificará si las unidades de generación cumplen con los códigos de red en vigor incluyendo requisitos pasivos como Frequency Ride-Through, LVRT y desequilibrios de tensión y corriente, así como los requisitos activos de respuesta de frecuencia y contribución de corriente durante faltas. En el primer caso de estudio, se contempla la instalación de una planta fotovoltaica en una pequeña isla, donde únicamente se dispone de información mínima en el punto de conexión. El segundo caso de estudio incluye la isla de Terceira en las Azores, donde se instalará un nuevo parque eólico. Se dispone de datos estáticos y dinámicos del sistema eléctrico, pero no existe ninguna regulación técnica específica sobre la conexión de generadores variables. Por último, la metodología se aplicará a un tercer caso que consiste en la ampliación de un parque eólico existente en el subsistema de Fuerteventura-Lanzarote en las Islas Canarias. En este caso, se dispone de datos estáticos y dinámicos sobre la red y hay una regulación en vigor. La aplicación de la metodología a estos tres casos de estudio apoyará la validez del procedimiento propuesto en esta tesis.

**Palabras clave:** redes débiles, redes insulares, código de red, energías renovables, energía eólica, fault ride-through, desequilibrios de tensión, desequilibrios de corriente, control de frecuencia, control de tensión, modelo genérico, validación de modelos.

# Contents

**Abstract** v

**Laburpena** vii

**Resumen** ix

**List of Figures** xvii

**List of Tables** xxi

**Acronyms** xxv

## I Introduction 1

**1 Introduction** 3
- 1.1 Background . . . 3
  - 1.1.1 Technical issues in isolated power grids . . . 4
  - 1.1.2 Economic issues in isolated power grids . . . 6
  - 1.1.3 Integration of renewable power generation in isolated power grids . . . 7
- 1.2 Statement of objectives . . . 9
- 1.3 Outline of the thesis . . . 9

## II State of the art 11

**2 Review of grid codes** 13
- 2.1 Introduction . . . 13
- 2.2 Review and comparison of technical requirements . . . 14
  - 2.2.1 Operating ranges . . . 15
  - 2.2.2 Active power . . . 15
  - 2.2.3 Frequency control . . . 16
  - 2.2.4 Reactive power . . . 17
  - 2.2.5 Voltage control . . . 19
  - 2.2.6 Fault ride-through . . . 20
  - 2.2.7 Synthesis of requirements . . . 23
- 2.3 Analysis of current and future grid code requirements . . . 24
  - 2.3.1 Influence of power grid strength and characteristics on grid codes 24

2.3.2 Future regulatory aspects . . . . . 28

**3 Grid code compliance verification 31**
3.1 Introduction . . . . . 31
3.2 Renewable power generation modelling and simulation . . . . . 32
3.2.1 Challenges regarding renewable power generation modelling . 32
3.2.2 Root Mean Square (RMS) against ElectroMagnetic Transient (EMT) models . . . . . 34
3.2.3 Generic models against proprietary models . . . . . 36
3.3 Renewable power generation model validation . . . . . 37
3.3.1 Test data collection . . . . . 38
3.3.2 Model simulation . . . . . 41
3.3.3 Model validity acceptance rules . . . . . 42
3.4 Verification of the compliance of technical requirements . . . . . 43
3.4.1 Review of compliance verification practices . . . . . 43
3.4.2 Certification procedures . . . . . 47

**III Compliance verification methodology for renewable generation integration into island power grids 53**

**4 A compliance verification methodology 55**
4.1 Introduction . . . . . 55
4.2 Theoretical framework of the proposed methodology . . . . . 57
4.2.1 Generic grid model . . . . . 57
4.2.2 Particular grid model . . . . . 58
4.2.3 Parameterised grid model . . . . . 58
4.3 Practical implementation of the proposed methodology . . . . . 59
4.3.1 Definition of the grid code compliance tests . . . . . 59
4.3.2 Application of the methodology . . . . . 64
4.4 Validation of the proposed methodology . . . . . 64

**5 Frequency Ride-Through 67**
5.1 Introduction . . . . . 67
5.2 Frequency dip definition . . . . . 67
5.3 Theoretical analysis . . . . . 68
5.3.1 System frequency response model for a single generating unit 68
5.3.2 System frequency response model for the whole power system 74
5.4 Grid model and event representation . . . . . 79
5.4.1 Particular grid model . . . . . 79
5.4.2 Sensitivity of the particular grid model parameters . . . . . 80
5.4.3 Parameterisation of grid model for grid code compliance verification . . . . . 81

**6 Low Voltage Ride-Through 83**
6.1 Introduction . . . . . 83
6.2 Voltage dip definition . . . . . 83

6.3 Theoretical analysis . . . 85
6.3.1 Voltage divider model . . . 85
6.3.2 Dynamic unregulated model . . . 87
6.3.3 Dynamic regulated model . . . 95
6.4 Grid model and event representation . . . 97
6.4.1 Particular grid model . . . 97
6.4.2 Sensitivity of particular grid model parameters . . . 97
6.4.3 Parameterisation of grid model for grid code compliance verification . . . 102

**7 Voltage and current unbalance 105**
7.1 Introduction . . . 105
7.2 Voltage unbalance definition . . . 106
7.3 Theoretical analysis . . . 107
7.3.1 Analysis of asymmetrical short-circuit faults . . . 107
7.3.2 Analysis of series faults . . . 108
7.3.3 Analysis of unbalanced loads . . . 111
7.3.4 Summary of unbalancing cases . . . 113
7.4 Grid model and event representation . . . 114
7.4.1 Particular grid model . . . 114
7.4.2 Sensitivity of particular grid model parameters . . . 115
7.4.3 Parameterisation of grid model for grid code compliance verification . . . 119

**IV Numerical application of the compliance verification methodology 123**

**8 Practical application: a medium size island 125**
8.1 Introduction . . . 125
8.2 Parameterisation of particular grid models . . . 126
8.2.1 Adjustment results . . . 126
8.2.2 Verification of the parameterisation . . . 127
8.3 Practical application of the methodology . . . 128

**9 Practical application: Terceira island 137**
9.1 Introduction . . . 137
9.2 Performance analysis . . . 137
9.2.1 Description of operation scenarios . . . 138
9.2.2 Operation in steady-state . . . 139
9.2.3 Transient operation . . . 140
9.2.4 Synthesis . . . 146
9.3 Parameterisation of grid models . . . 147
9.3.1 Adjustment results . . . 148
9.3.2 Verification of the parameterisation . . . 150
9.4 Practical application of the methodology . . . 151

**10 Practical application: Fuerteventura-Lanzarote islands 159**
10.1 Introduction . . . 159
10.2 Performance analysis . . . 159
10.2.1 Description of operation scenarios . . . 160
10.2.2 Operation in steady-state . . . 161
10.2.3 Transient operation . . . 162
10.2.4 Synthesis . . . 169
10.3 Parameterisation of grid models . . . 170
10.3.1 Adjustment results . . . 171
10.3.2 Verification of the parameterisation . . . 173
10.4 Practical application of the methodology . . . 174

**V Conclusions and future work 181**

**11 Conclusions and future research 183**
11.1 Conclusions . . . 183
11.2 Main contributions . . . 186
11.3 Scientific production . . . 187
11.4 Future research lines . . . 188

**VI Appendices 191**

**A Influence of System Frequency Response (SFR) study model on frequency response 193**
A.1 Single generating unit models . . . 193
A.2 Whole power system models . . . 195

**B Application of symmetrical components for unbalancing phenomena 199**
B.1 Introduction . . . 199
B.2 Shunt faults . . . 199
B.2.1 Connection of sequence circuits . . . 199
B.2.2 Current calculation . . . 200
B.2.3 Voltage calculation . . . 201
B.3 Series faults . . . 202
B.3.1 Connection of sequence circuits . . . 202
B.3.2 Sequence voltage drop calculation . . . 204
B.3.3 Sequence current calculation . . . 206
B.4 Unbalanced loads . . . 207
B.4.1 Connection of sequence circuits . . . 207
B.4.2 Sequence voltage calculation . . . 210
B.4.3 Sequence current calculation . . . 212

**C Numerical application 215**
C.1 Introduction . . . 215

C.2 Power plant model description . . . . . 215
C.3 Model parameterisation: Case 1 . . . . . 216
C.3.1 Photovoltaic power plant: description and parameterisation . 216
C.3.2 Parameterised grid model . . . . . 220
C.4 Model parameterisation: Case 2 . . . . . 222
C.4.1 Wind farm: description and parameterisation . . . . . 222
C.4.2 Parameterised grid model . . . . . 223
C.5 Model parameterisation: Case 3 . . . . . 225
C.5.1 Wind farm: description and parameterisation . . . . . 225
C.5.2 Parameterised grid model . . . . . 226

**D Terceira island** **229**
D.1 Introduction . . . . . 229
D.2 Characteristics of the power system in Terceira . . . . . 229
D.2.1 Characteristics of transmission lines . . . . . 229
D.2.2 Description of generator characteristics . . . . . 229
D.2.3 Power transformers . . . . . 232
D.3 Case study . . . . . 232
D.3.1 Load scenarios . . . . . 232
D.3.2 Generation dispatch . . . . . 233

**E Fuerteventura-Lanzarote system** **237**
E.1 Introduction . . . . . 237
E.2 Characteristics of the power system Fuerteventura-Lanzarote . . . . 237
E.2.1 Characteristics of transmission lines . . . . . 237
E.2.2 Description of generator characteristics . . . . . 238
E.2.3 Power transformers . . . . . 240
E.3 Case study . . . . . 240
E.3.1 Load scenarios . . . . . 240
E.3.2 Generation dispatch . . . . . 240

**Bibliography** **244**

# List of Figures


1.1 Simplified power system model . . . . . 5

2.1 Comparison of PQ diagrams . . . . . 18
2.2 Comparison of UQ diagrams for wind farms . . . . . 19
2.3 Comparison of LVRT requirements in the grid codes under review . 21
2.4 HVRT requirement in Australia and Spain . . . . . 23
2.5 Comparison of the Tasmanian frequency standard with the Australian mainland . . . . . 25
2.6 Comparison of LVRT requirements in insular and extrapeninsular territories with peninsula, in Spain . . . . . 26
2.7 Comparison of LVRT requirements in insular and metropolitan territories, in France . . . . . 26

3.1 General validation process . . . . . 38
3.2 Low voltage ride-through test equipment principle based on voltage divider . . . . . 40
3.3 Test circuit for model acceptance testing . . . . . 41
3.4 General Verification Process . . . . . 50
3.5 Procedimiento de Verificación, Validación y Certificación (PVVC): model of the equivalent electrical grid . . . . . 51

4.1 General grid power modelling procedure . . . . . 57
4.2 Generic grid test model . . . . . 58
4.3 Frequency ride-through limits . . . . . 59
4.4 Frequency droop response . . . . . 60
4.5 LVRT profiles . . . . . 61
4.6 Active current injection requirement . . . . . 62
4.7 Reactive current injection requirement . . . . . 63
4.8 Single-line scheme for the application of the methodology . . . . . 64
4.9 General renewable generation plant verification procedure . . . . . 66

5.1 Frequency deviation after an active power mismatch . . . . . 68
5.2 Reduced block diagram of a generic power plant based on a first-order function . . . . . 72
5.3 Reduced block diagram of a generic power plant based on a first-order function . . . . . 73
5.4 Particular grid model for frequency analysis . . . . . 79
5.5 Effect of parameters on frequency response . . . . . 81

6.1 Typical voltage dip . . . . . 84
6.2 Characteristic parameters on a fault induced voltage dip . . . . . 85
6.3 Simplified circuit for voltage dip calculation . . . . . 85
6.4 SMIB model . . . . . 88
6.5 Equivalent circuit during a fault . . . . . 89
6.6 Power angle curve during unbalanced faults . . . . . 90
6.7 A two machine power system . . . . . 94
6.8 Effect of AVR on transient stability . . . . . 96
6.9 Particular grid model for voltage dip analysis . . . . . 98
6.10 Effect of parameters on voltage dip magnitude . . . . . 99
6.11 Effect of parameters on voltage dip recovery . . . . . 99
6.12 Effect of parameters on voltage response . . . . . 100
6.13 Effect of generic model on voltage dip . . . . . 102

7.1 Types of short-circuits . . . . . 108
7.2 Series fault types . . . . . 109
7.3 Unequal series impedance . . . . . 109
7.4 Single-phase load between phases B and C . . . . . 111
7.5 Three-phase load in ungrounded star connection . . . . . 112
7.6 Three-phase load in delta connection . . . . . 112
7.7 Particular grid model for voltage unbalance . . . . . 114
7.8 Effect of fault type on negative voltage and current unbalance magnitude 115
7.9 Effect of short-circuit type and grid strength on the propagation of VUF . . . . . 116
7.10 Effect of $R/X$ on the propagation of VUF (1PhG) . . . . . 116
7.11 Effect of fault type on negative voltage and current unbalance magnitude 117
7.12 Effect of feeder length on VUF for unequal series impedance . . . . . 117
7.13 Effect of SCR ratio on VUF for single-phase load . . . . . 118
7.14 Effect of power system strength and phase shift on VUF (Case 1, only amplitude unbalance) . . . . . 119
7.15 Effect of power system strength on VUF (Case 1, only amplitude unbalance) . . . . . 119
7.16 Effect of power system strength on VUF (Case 3, mixed unbalance) 119

8.1 Case 1: verification of the adjustment of frequency ride-through . . . 129
8.2 Case 1: verification of the rest of parameters . . . . . 130
8.3 Case 1: validation of the procedure for frequency ride-through . . . . 132
8.4 Case 1: validation of the procedure for frequency response . . . . . 132
8.5 Case 1: validation of the procedure for LVRT . . . . . 133
8.6 Case 1: validation of the procedure for VUF . . . . . 134

9.1 Voltage levels in steady-state at 15 kV in Terceira island . . . . . 139
9.2 Frequency deviation after loss of generation in Terceira island . . . . 141
9.3 Frequency deviation after load loss in Terceira island . . . . . 142
9.4 Voltage dip magnitude after a three-phase fault at Serra do Cume . 143
9.5 Voltage dips in Terceira island . . . . . 143
9.6 Frequency deviation for a short-circuit at PESC bus . . . . . 144

9.7 Frequency deviation for a short-circuit at different locations . . . . . 144
9.8 Voltage dip magnitude after a fault at SEBJ30 . . . . . 144
9.9 Voltage dip magnitude at SEQR30 . . . . . 145
9.10 Voltage unbalance in Terceira island . . . . . 146
9.11 Voltage after Vinha Brava-Vitoria line loss . . . . . 146
9.12 Case 2: verification of adjustment of frequency ride-through . . . . . 151
9.13 Case 2: verification of the rest of parameters . . . . . 152
9.14 Case 2: validation of the procedure for frequency ride-through . . . . 154
9.15 Case 2: validation of the procedure for frequency response . . . . . 154
9.16 Case 2: validation of the procedure for LVRT . . . . . 155
9.17 Case 2: validation of the procedure for VUF . . . . . 156

10.1 Frequency deviation after loss of generation in Fuerteventura-Lanzarote 162
10.2 Frequency deviation under valley demand in Fuerteventura-Lanzarote 163
10.3 Frequency deviation after load loss in Fuerteventura-Lanzarote . . . 164
10.4 Voltage dip magnitude after a fault at Punta Grande . . . . . 164
10.5 Voltage dip magnitude after a fault at Matas Blancas . . . . . 165
10.6 Frequency deviation during short-circuit at Punta Grande . . . . . 165
10.7 Voltage dip during unbalanced faults at Punta Grande in Fuerteventura-Lanzarote . . . . . 166
10.8 Voltage dip magnitude at Montaña Mina 66 kV (I) . . . . . 167
10.9 Voltage dip magnitude at Montaña Mina 66 kV (II) . . . . . 168
10.10 Two-phase short-circuit at Montaña Mina 66 kV . . . . . 168
10.11 Case 3: verification of adjustment of frequency ride-through . . . . . 174
10.12 Case 3: verification of the rest of parameters . . . . . 175
10.13 Case 3: validation of the procedure for frequency ride-through . . . . 177
10.14 Case 3: validation of the procedure for frequency response . . . . . 177
10.15 Case 3: validation of the procedure for LVRT . . . . . 178
10.16 Case 3: validation of the procedure for VUF . . . . . 179

A.1 Study of Egido model . . . . . 195
A.2 Comparison of single reheat steam turbine-generator models . . . . . 196
A.3 Comparison of SFR models for a multi-generator system . . . . . 196

B.1 Sequence circuit connection for a single-phase short-circuit . . . . . 199
B.2 Sequence circuit connection for a double-phase short-circuit . . . . . 200
B.3 Sequence circuit connection for a double-phase to ground short-circuit 200
B.4 Sequence circuit connection for unequal series impedances . . . . . 204
B.5 Sequence circuit connection for one phase open . . . . . 205
B.6 Sequence circuit connection for two open phases . . . . . 205
B.7 Sequence circuit connection for single-phase load . . . . . 210
B.8 Sequence circuit connection for three-phase load in ungrounded star 210
B.9 Sequence circuit connection for three-phase load in grounded star . . 211
B.10 Sequence circuit connection for a three-phase load in delta connection 211

C.1 Converter RMS model in block diagrams . . . . . 216
C.2 PV plant connection layout . . . . . 217

C.3 First-order turbine-governor model . . . . . 221
C.4 Wind farm connection layout in Terceira . . . . . 222
C.5 Wind farm connection layout in Lanzarote . . . . . 226

D.1 Single line diagram of Terceira island . . . . . 230

E.1 Single line diagram of Fuerteventura-Lanzarote system . . . . . 238

# List of Tables


2.1 Grid codes under study . . . . . 14
2.2 Remain connected frequency ranges . . . . . 15
2.3 Primary frequency control requirements for conventional generation 17
2.4 Primary frequency control requirements for non-synchronous generating units . . . . . 18
2.5 Voltage control requirements . . . . . 20
2.6 Active power recovery upon fault clearance . . . . . 22
2.7 Synthesis of remain connected requirements . . . . . 24
2.8 Synthesis of active requirements . . . . . 24
2.9 Remain connected frequency ranges . . . . . 27
2.10 Parameters for UQ inner envelope . . . . . 27

3.1 Renewable generation modelling and validation requirements in the countries under study . . . . . 33
3.2 Grid code compliance verification in the countries under study . . . 44

4.1 Synthesis of remain connected requirements . . . . . 56
4.2 Synthesis of grid code compliance tests . . . . . 63
4.3 Summary of study cases for the validation of the methodology . . . . 65

5.1 Synthesis of simplified models for prime movers . . . . . 70
5.2 Parameters of TGOV1 model reheat steam turbine . . . . . 80

6.1 Shunt reactances representing different types of faults (I) . . . . . 89
6.2 Shunt reactances representing different types of faults (II) . . . . . 89
6.3 Voltage dip magnitude for unbalanced faults . . . . . 92
6.4 Shunt reactances representing different types of faults (III) . . . . . 92
6.5 Parameters of the voltage divider model . . . . . 97
6.6 Voltage dip magnitude adjustment . . . . . 104

7.1 Summary of unbalancing cases . . . . . 114
7.2 Theoretical load characteristics adjustment for a given CUF . . . . . 120
7.3 Theoretical load characteristics adjustment for a given VUF . . . . . 121

8.1 Initial data for Case 1 . . . . . 125
8.2 Case 1: parameterisation of particular grid model for frequency ride-through . . . . . 126
8.3 Case 1: parameterisation of particular grid model for LVRT (SEIE) . 127
8.4 Case 1: parameterisation of particular grid model for LVRT (SEPE) 127

8.5 Case 1: parameterisation of particular grid model for unbalance . . . 127
8.6 Case 1: parameterised grid model validation results . . . . . 128
8.7 Case 1: frequency ride-through test cases . . . . . 131
8.8 Case 1: LVRT test cases . . . . . 131
8.9 Case 1: unbalance test cases . . . . . 134
8.10 Case 1: summary of grid code compliance verification . . . . . 135

9.1 Characteristics of PCC in Terceira island . . . . . 138
9.2 Summary of study cases in Terceira island . . . . . 138
9.3 Frequency after loss of generation in Terceira island . . . . . 141
9.4 Synthesis of performance results in Terceira island . . . . . 147
9.5 Case 2: parameterisation of particular grid model for frequency ride-through . . . . . 148
9.6 Case 2: parameterisation of particular grid model for LVRT . . . . . 149
9.7 Case 2: parameterisation of particular grid model for unbalance . . . 149
9.8 Case 2: parameterised grid model validation results . . . . . 150
9.9 Case 2: frequency ride-through test cases . . . . . 153
9.10 Case 2: unbalance test cases . . . . . 155
9.11 Case 2: summary of grid code compliance verification . . . . . 157

10.1 Characteristics of PCC in Lanzarote island . . . . . 160
10.2 Summary of study cases in Fuerteventura-Lanzarote . . . . . 160
10.3 Frequency after loss of generation in Fuerteventura-Lanzarote . . . . 163
10.4 Frequency after loss of load in Fuerteventura-Lanzarote . . . . . 164
10.5 Voltage unbalance due to single-phase faults under *Study Case 6* . . 167
10.6 Synthesis of performance results in Fuerteventura-Lanzarote . . . . . 169
10.7 Synthesis of test cases with possible adjustment values . . . . . 171
10.8 Case 3: parameterisation of particular grid model for frequency ride-through . . . . . 172
10.9 Case 3: parameterisation of particular grid model for LVRT . . . . . 172
10.10 Case 3: parameterisation of particular grid model for unbalance . . . 172
10.11 Case 3: theoretical model verification results . . . . . 173
10.12 Case 3: frequency ride-through test cases . . . . . 176
10.13 Case 3: unbalance test cases . . . . . 178
10.14 Case 3: summary of grid code compliance verification . . . . . 180

A.1 Typical frequency minimum time range in different power systems . 193
A.2 Parameter estimation for a single generating unit . . . . . 194
A.3 Comparison of SFR models . . . . . 194
A.4 Parameter estimation for 2 generating units . . . . . 196
A.5 Frequency response for the multi-generator system . . . . . 197

C.1 Case 1: system impedance data (20 kV 100 MVA base) . . . . . 217
C.2 Case 1: inverter and static generator ratings . . . . . 217
C.3 Case 1: parameters of Control Module . . . . . 218
C.4 Case 1: parameters of Converter Module (LVRT) . . . . . 218
C.5 Case 1: parameters of Converter Module (Reactive current injection) 219

C.6 Case 1: parameters of Converter Module (Active current injection) . 219
C.7 Case 1: relay parameters . . . . . 219
C.8 Case 1: parameterisation of particular grid model for frequency ride-through . . . . . 220
C.9 Parameters of first-order turbine-governor model . . . . . 220
C.10 Parameters of Automatic Voltage Regulator (AVR) model SEXS . . 221
C.11 Case 1: parameterisation of particular grid model for voltage unbalance 221
C.12 Case 2: system impedance data (30 kV 100 MVA base) . . . . . 222
C.13 Case 2: inverter and static generator ratings . . . . . 223
C.14 Case 2: parameters of Converter Module (LVRT) . . . . . 223
C.15 Case 2: parameters of Converter Module (Active current injection) . 223
C.16 Case 2: relay parameters . . . . . 224
C.17 Case 2: parameterisation of particular grid model for frequency ride-through . . . . . 224
C.18 Parameters of First-order turbine-governor model . . . . . 224
C.19 Case 2: parameterisation of particular grid model for voltage unbalance 225
C.20 CASE 3: system impedance data (66 kV 100 MVA base) . . . . . 226
C.21 Case 3: inverter and static generator ratings . . . . . 226
C.22 Case 3: parameterisation of particular grid model for frequency ride-through . . . . . 227
C.23 Parameters of First-order turbine-governor model . . . . . 227
C.24 Case 3: parameterisation of particular grid model for voltage unbalance 228

D.1 Parameters of 30 kV transmission lines in Terceira island . . . . . 231
D.2 List of power stations in Terceira island . . . . . 231
D.3 Technical data from Belo Jardim power plant (G1BJ-G10BJ) . . . . 231
D.4 Voltage regulator model SEXS technical data from the thermal power plants in Terceira island . . . . . 232
D.5 Speed regulator model DEGOV1 technical data from Belo Jardim power plant (G1BJ-G10BJ) . . . . . 232
D.6 Fully rated converter parameters in Terceira island . . . . . 232
D.7 Power transformer characteristics in Terceira island . . . . . 233
D.8 Power transformer characteristics at Belo Jardim . . . . . 233
D.9 Power transformer characteristics at Serra do Cume . . . . . 233
D.10 Load scenarios in Terceira island, 2012 . . . . . 234
D.11 Thermal generation scenarios in Terceira island . . . . . 234
D.12 On-line generators for each study case in Terceira island . . . . . 235

E.1 Parameters of 66 kV transmission lines in Fuerteventura-Lanzarote system . . . . . 239
E.2 List of models . . . . . 239
E.3 List of power stations in Fuerteventura-Lanzarote system . . . . . 239
E.4 Technical data from the thermal power plant Punta Grande, Lanzarote 240
E.5 Technical data from the thermal power plant Las Salinas, Fuerteventura 241
E.6 Speed regulator model DEGOV1 technical data from the thermal power plant at Punta Grande . . . . . 241

E.7 Speed regulator model DEGOV1 technical data from the thermal power plant at Las Salinas . . . . . 242
E.8 Speed regulator model GAST technical data from the thermal power plants in Fuerteventura-Lanzarote . . . . . 242
E.9 Voltage regulator model IEEET1 technical data from the thermal power plants in Fuerteventura-Lanzarote system . . . . . 242
E.10 Power transformer characteristics at Punta Grande . . . . . 243
E.11 Power transformer characteristics at Las Salinas . . . . . 243
E.12 Power transformer characteristics at wind park substations . . . . . 243
E.13 Power transformer characteristics at wind park substations . . . . . 243
E.14 Load scenarios in Fuerteventura-Lanzarote, 2013 . . . . . 244
E.15 Thermal generation scenarios in Fuerteventura-Lanzarote system . . 244
E.16 Cost functions in Lanzarote and Fuerteventura . . . . . 245
E.17 On-line generators in Punta Grande for each study case . . . . . 245
E.18 On-line generators in Las Salinas for each study case . . . . . 246

# Acronyms

**AUFLS** Automatic Under Frequency Load Shedding

**AVR** Automatic Voltage Regulator

**CCUF** Complex Current Unbalance Factor

**CLUF** Complex Load Unbalance Factor

**CRC** Composite Regulating Characteristic

**CSC** Combined Short-Circuit

**CUF** Current Unbalance Factor

**CVUF** Complex Voltage Unbalance Factor

**DFIG** Doubly Fed Induction Generator

**EDF** Electricité de France

**EHV** Extra High Voltage

**EMT** ElectroMagnetic Transient

**FACTS** Flexible AC Transmission System

**FRC** Frequency Response Characteristic

**FRT** Fault Ride-Through

**FSM** Frequency Sensitive Mode

**HV** High Voltage

**HVRT** High Voltage Ride-Through

**HVDC** High Voltage Direct Current

**LFSM** Limited Frequency Sensitive Mode

**LUF** Load Unbalance Factor

**LVRT** Low Voltage Ride-Through

**LVUR** Line Voltage Unbalance Rate

**MV** Medium Voltage

**NI** Northern Ireland

**OP** Operating Procedure

**PCC** Point of Common Coupling

**PECAN** Plan Energético de Canarias

**PLL** Phase-Locked Loop

**PMSG** Permanent Magnet Synchronous Generator

**PO** Procedimientos de Operación

**PSS** Power System Stabilizer

**PVVC** Procedimiento de Verificación, Validación y Certificación

**PVUR** Phase Voltage Unbalance Rate

**REE** Red Eléctrica de España

**RES** Renewable Energy Sources

**RMS** Root Mean Square

**ROCOF** Rate-of-Change-of-Frequency

**SCIG** Squirrel Cage Induction Generator

**SCR** Short-Circuit Ratio

**SEI** Systèmes Energétiques Insulaires

**SEIE** Sistemas Eléctricos Insulares y Extrapeninsulares

**SEPA** Sistema Eléctrico de Serviço Público dos Açores

**SEPE** Sistema Eléctrico Peninsular Español

**SFR** System Frequency Response

**SMIB** Single Machine Infinite Bus

**TPP** Thermal Power Plant

**TSO** Transmission System Operator

**UFLS** Under Frequency Load Shedding

**UVLS** Under Voltage Load Shedding

**VSC** Voltage Source Converter

**VSG** Voltage Sag Generator

**VUF** Voltage Unbalance Factor

**WF** Wind Farm

**WPP** Wind Power Plant

**WTG** Wind Turbine Generator

**ZVRT** Zero Volt Ride-Through

# Part I

# Introduction

# Chapter 1

# Introduction

## 1.1 Background

Although a large proportion of power systems worldwide are large strongly interconnected systems, there is an increasing interest in isolated or poorly interconnected systems, called weak power grids. Weak power grids can be classified as subsystems connected to the main grid via weak interconnections, such as loads at remote locations and offshore wind farms, and autonomous power grids without connection to the main grid, e.g. islands, microgrids temporarily disconnected from the mains, or remote rural areas. This thesis focuses on the second category: isolated power grids which are weak by nature.

Standard IEEE 1204 [1] defines a weak Alternating Current (AC) power grid according to its static and dynamic performance:

1. AC system impedance may be high relative to AC power at the point of connection, i.e. short-circuit power at the point of connection may be low.

2. AC system mechanical inertia may be inadequate relative to the AC power infeed.

The first condition is met in wide area weak power grids, usually operated at medium voltage levels with long radial feeders and low $X/R$ ratios. In small island power grids, both static and dynamic aspects do often apply. In addition, power is supplied by few generating groups, mostly fed by diesel or heavy oil, with small unit power and low inertia. Overall, generators are large with respect of the system load for economic reasons [2] and so, higher reserve margins than in interconnected systems are necessary. Demand patterns depend on the climate and the activity. Thus, minimum to maximum demand ratios are low in tropical isolated power grids, while islands with seasonal tourism activity have low load in winter and high load in summer.

The static power strength is characterised by the short-circuit power level, which is low in weak power grids. However, the measure only applies to the Point of Common Coupling (PCC) from the grid point of view. It is therefore convenient to take into account the generation connected to the PCC, using a grid stiffness index such as

the *Short-Circuit Ratio (SCR)*:

$$SCR = \frac{S_{sc}}{S_n} \tag{1.1}$$

where, $S_n$ is the installed capacity of the generation power plant and $S_{sc}$ the short-circuit level at the PCC.

A power grid is considered strong for SCR values above 20 [3] to 25 [4] and weak for SCR values below 6 to 10 [5], although other reference values might be found in literature.

On the other hand, dynamic weakness of a power network can be characterised by the overall inertia constant H (seconds) and the composite frequency response characteristic $\beta$ (MW/Hz), which relates the active power response of a system to a change in frequency. The composite power/frequency characteristic of a power system depends on the combined effect of the droops of all generators and on the frequency response of all the loads in the system. Island power grids have a low inertia and regulation capability.

Aforementioned characteristics of weak power grids result into technical and economic issues which can constrain the secure operation of power systems, especially regarding renewable energy sources.

### 1.1.1 Technical issues in isolated power grids

The frequency and duration of unsafe situations in weak grids is much greater than in high performance strong grids. Electricity supply interruption duration is also significantly higher. Based on collected operational data, [6] points out that incidents of loss of generating units are quite common and cause serious problems in non-interconnected grids. On the other hand, weak grids are mainly composed of rural overhead networks, where faults occur more frequently than in strong interconnected power grids and fault clearing times are usually longer.

Aforementioned disturbance patterns, in addition to inherent characteristics of weak power systems, lead to technical issues related to voltage and frequency regulation, and stability.

**Voltage regulation** Weak power systems experience significant fluctuations in bus voltages, both in steady-state and under dynamic events. In addition, under weak grid condition, voltage sensitivity with respect of reactive power is high, which means that the same amount of reactive support (injection or absorption) results in larger voltage deviations. Based on the simplified power system in Figure 1.1, the relation between reactive power and voltage control can be clarified.

The voltage drop between the sending end (Bus 1) and the receiving end (Bus 2) is:

$$\Delta V = \frac{R_s \cdot P + X_s \cdot Q}{E} + j \cdot \frac{X_s \cdot P - R_s \cdot Q}{E} = \Delta V_p + j \cdot \Delta V_q \tag{1.2}$$

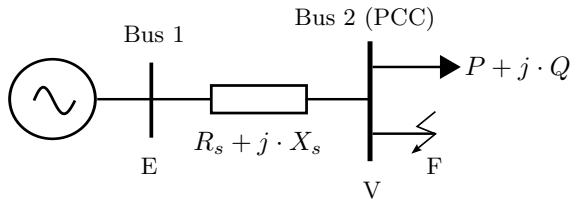


**Figure 1.1. Simplified power system model**

Transmission networks are mostly inductive, although $X/R$ ratio tends to be lower in weak power grids. Therefore, reactive power is proportional to voltage drop and so, voltage magnitude is mainly controlled by reactive power exchange in transmission networks. However, in more resistive networks both active and reactive power do affect voltage. In weak power grids, source impedance is higher, and hence, even low reactive power injection produces a high impact on voltage.

**Frequency regulation** The swing equation in (1.3) relates active power and frequency, showing that any active power mismatch results in a frequency deviation in a power system ruled by synchronous generation.

$$2 \cdot H \cdot \frac{d^2\delta}{dt^2} = P_m - P_e - K_D \cdot \frac{d\delta}{dt} \tag{1.3}$$

where $H$ is the inertia constant, $\delta$ load angle, $P_e$ electromagnetic power, $P_m$ mechanical power, and $K_D$ damping factor.

Based on (1.3), it can be concluded that after an active power mismatch the initial frequency gradient (Rate of Change of Frequency ROCOF) and deviation of frequency in steady-state ($\Delta f_{ss}$) depend on the mismatch magnitude $\Delta P$, inertia $H$, system frequency response and regulating capacity $R$, and damping $K_D$ (Equations (1.4) and (1.5)).

$$ROCOF = \frac{\Delta P}{2 \cdot H} \tag{1.4}$$

$$\Delta f_{ss} = \frac{\Delta P}{K_D + \frac{1}{R}} \tag{1.5}$$

Frequency regulation is primarily troublesome in isolated power grids. In fact, both ROCOF and steady-state frequency deviation following an active power mismatch result into high values, because of their low inertia constant, low regulating capability and big size of generators with respect of the total load. Therefore, frequency stability issues could happen [7], especially in isolated systems with high renewable energy penetration, contributing with dismissable inertia, as generators are usually not required to actively support frequency.

**Stability** Both voltage and frequency issues could lead to instability.

Frequency instability is more common in island power grids, whereas voltage stability is a major concern in vast area weak power grids.

Transient stability can also be compromised in weak power grids during short-circuits. On one hand, the magnitude of a voltage dip following a fault results into higher values at a point with low short-circuit power, i.e. low strength, as indicated by (1.6) for a three-phase fault based on Figure 1.1. On the other hand, transient stability might be lost sooner in weak power grids because of low system inertia (mainly in island grids), and longer fault duration. Besides, in small isolated power grids severe voltage dips can easily propagate to the whole power system.

$$V_{dip}(p.u.) = V_{pf,Bus1}(p.u.) \cdot \frac{Z_f}{Z_{s,1} + Z_f} = V_{pf,Bus1}(p.u.) \cdot \frac{Z_f}{\frac{V_{pf,PCC}^2}{S_{sc,PCC}} + Z_f} \tag{1.6}$$

where $Z_f$ is the fault impedance at fault point F, $Z_{s,1}$ the positive sequence source impedance, and $V_{pf}$ the pre-fault voltage at Bus 2. Short-circuit power at the PCC is represented by $S_{sc,PCC}$.

### 1.1.2 Economic issues in isolated power grids

Special mention should be made of economic aspects in insular power systems. These power systems are usually burdened with additional costs stemming from their insularity, as electricity must be generated on-site. This aspect affects negatively the cost of electricity by burdening the tariff with increased fuel (due to import and transportation) and operating costs. Most insular systems operate with generation margins around 30-40 % in order to increase reliability, which implies higher costs compared to 15-20 % in mainland [8]. In the case of the French SEI operated by EDF overcost can double prices in mainland France [9], even if some solidarity policies are often applied. The same applies in other island grids such as the Spanish isolated power grids.

In addition, market and investment situation in islands is very closely related to population density: the smaller the population, the smaller the market. Therefore, the challenge of establishing a sustainable energy system is greater, and as a result, most islands do not enjoy many options for diversifying their energy supply and usually rely on oil-fired diesel engine generation for their power generation [8]. This situation does not smooth the way to a competitive market, and adapted economic models have to be adopted in some islands.

Aforementioned economic drawbacks do also have an impact on grid code aspects. On one hand, a sustainable integration of renewable energies in weak power grids requires new assets to participate on voltage and frequency ancillary services, which have an economic cost for the system. On the other hand, technically demanding performance of generators involves an investment by manufacturers. Both aspects could be compromised in economically constrained power systems, such as islands.

### 1.1.3 Integration of renewable power generation in isolated power grids

Several studies have been carried out to determine limiting factors for renewable power generation integration. Most research has been focused on wind power integration. Ideally, the only limit to the wind power generation in an isolated system would be its instantaneous power demand [10]. However, some limitations apply to wind penetration. Technical, resource and economic limitations are mentioned in literature [11]. Resource is not a limitation in most island grids. However, the economics of wind generation will tend to get worse as penetration increases. Partly, because of additional costs of dealing with technical issues, and partly, because wind generation does not match electrical demand, leading to lower average electricity prices for electricity and eventually substantial curtailment [12].

Regarding technical limitations, voltage and frequency regulation, and stability issues, troublesome 'per se' in weak power grids, become more important with an increasing penetration of Renewable Energy Sources (RES), which are highly variable and intermittent. In addition, insular power grids cannot import energy from neighbouring power systems and cannot export renewable energy in excess. And, due to their small-size, they cannot take advantage of the '*portfolio*' effect [13]. Those factors result into dispatching, reliability, security and power quality issues [14].

1. RES are considered non-dispatchable and can be subject to output power limitations, related with technical constraints of the conventional generating units, namely the minimum loading levels of the thermal units (technical minima) [15].

2. Islands with RES show often rapid changes in both demand and generation [16], as RES are highly variable and intermittent. Diesel generators, base to many isolated power grid generation, cannot always follow these variations, as their step load capability is approximately 50-75 % of the remaining capacity due to the dynamics of the turbo-lag [17].

3. In small-size power grids with medium voltage distribution networks, the power quality issues may become a serious concern because of the proximity of RES to loads. Renewable source discontinuity and variability can generate voltage fluctuations above the flicker limit, harmonics, voltage variations, voltage dips and voltage unbalances [18].

4. Renewable power generation technologies are commonly based on non-synchronous machines with no inherent inertia. Hence, larger frequency deviations happen upon any large power mismatch event. As renewable energy sources replace synchronous generation, they have to take on frequency and voltage control functions previously in charge of conventional generating units.

In order to avoid technical issues due to a massive integration of renewable energies, the penetration of this type of generation has been limited in some power systems. These limits vary across the power systems, depending on the specific circumstances prevailing in each autonomous system, both in terms of conventional units (e.g.

production technology, control capabilities, etc.) and RES generating units (e.g. in the case of wind farms, size and technology of the wind turbines, dispersion of wind turbines on the island, etc.). A share of RES of 15 % is widely established as the upper-limit on power systems [19]. On the other hand, in some networks the maximum penetration of RES is set by law. Electricité de France (EDF) policy is to limit in real time at 30 % the part of non-predictable renewable to avoid the risk of black-out [20]. In autonomous island grids of Greece, such as Crete, wind farm generation is limited at 30 % of the instantaneous demand [21]. Similarly, Ireland's Electricity Supply Board (ESB) suggested that wind power levels should be limited to 30 % of instantaneous load during daytime, with possibly a higher contribution at nights [22]. In Sardinia penetration is limited to 400 MW for 1200 MW of minimum load [23]. In the Australian small isolated systems, such as Tasmania, a maximum of 40 % of instantaneous consumption is permitted, although primary reserve is bigger than in aforementioned cases [24]. Therefore, those limits to the output of RES generation assets results into power curtailments during their operation. In other cases, the penetration of renewable energies is based on a minimum Short-Circuit Ratio (SCR) level required for the connection of generation assets. In interconnected power grids, some grid codes require a minimum source strength for the connection of non-synchronous generation. In German VDN grid code, an initial value of 6 is required, whereas in Denmark and in Portugal the limit is set on 10 and on 5 in Spain [25, 26].

However, curtailment is not a solution, because the maximisation of the integration of RES into island grids is called to be a solution in order to assure their self-reliance and energy supply security [27]. Therefore, new initiatives and innovative projects have been promoted regarding following matters: efficient energy management systems including forecasting techniques and demand side management [28], optimal exploitation and efficient short-term operation of RES [13, 29], upgrade of power networks and assets, more flexible and high-performance thermal plants [8], new control algorithms in RES converters [30–32], or external assets providing active power storage (e.g. batteries, hydro-pumping, flywheel...) [14]. In addition, several system operators include in their grid codes strict frequency and active power, and/or voltage and reactive power requirements. Even more, RES are being requested to actively contribute in the power system control and security, as conventional synchronous generation technologies do. Therefore, reliable grid equivalent models are necessary so as to emulate most critical disturbances and operation situations in island grids. Adequate grid models would provide a useful tool during grid code compliance procedures, as well as to test protection and control algorithms.

## 1.2 Statement of objectives

This thesis proposes a new methodology to validate the integration of new renewable generation to install in isolated power grids. Compliance simulation models will be developed, with a double objective: to enable a valid emulation of static and dynamic behaviour of insular power grids under most frequent and critical disturbances and operation scenarios, and to provide power generating facility owners and manufacturers with a validation benchmark in order to verify grid code fulfilment.

Partial objectives of the thesis are also listed below.

- Review of technical characteristics in isolated power grids.
- Review of grid code requirements in relevant power grids.
- Review of procedures for verification, validation and certification of grid code requirements in relevant power grids.
- Development of generic grid code compliance simulation models.
- Methodology to adapt generic grid models to isolated weak power grids characteristics.
- Theoretical analysis of dynamic frequency, voltage dip and voltage unbalance.
- Characterisation of steady-state and dynamic performance of real medium size island grids.
- Practical application and verification of the proposed methodology.

## 1.3 Outline of the thesis

The thesis is divided into three major parts. First, grid code requirements for renewable energy integration under force in well-known power grids are reviewed, as well as procedures for verification, validation and certification cited in literature. Then, a methodology for the verification of the integration of renewable power generation is proposed to be applied in island grids is proposed. Finally, the methodology is applied to three cases.

**Part I. Introduction**

Part I consists of Chapter 1 and presents the introduction to the thesis. The background and motivation are explained, as starting point and cornerstone for the description of the objectives to be fulfilled within the present work. The contents of the thesis are also outlined, briefly summarising each chapter.

**Part II. State of the art**

Part II reviews the state of the art regarding the two main topics of the thesis. On the one hand, relevant grid codes are synthesised in Chapter 2. On the other, grid code compliance verification procedures regarding non-synchronous generation assets are reviewed in Chapter 3.

**Part III. Methodology for the verification of the integration of renewable power generation into island power grids**

Part III encompasses the methodology proposed in this thesis for the verification of the integration of renewable power generation in isolated weak power grids. First, the simulation based compliance verification is introduced in Chapter 4. Then, three grid code requirements and corresponding disturbances are theoretically analysed: Frequency Ride-Through in Chapter 5, Low Voltage Ride-Through in Chapter 6, and voltage and current unbalance in Chapter 7. Based on these studies, a generic simulation model is particularised and parameterised for each event, in accordance with the characteristics of the grid at the connecting point and the corresponding grid code limits.

**Part IV. Practical application of the compliance verification methodology**

The compliance verification methodology is applied to three study cases: a general case in order to validate the theoretical analysis of the three events under study in Chapter 8, the island of Terceira where the integration of renewable generation assets is not ruled by any technical regulation as presented in Chapter 9, and finally, the Fuerteventura-Lanzarote system based on the Sistemas Eléctricos Insulares y Extrapeninsulares (SEIE) grid code, which is in Chapter 10.

**Part V. Conclusions and future research**

Chapter 11 indicates the conclusions and contributions of the work developed in the thesis. Possible future research lines are as well outlined.

**Appendices**

Appendices are gathered at the end of the document and develop some theoretical and practical aspects that complement the document. Appendix A studies the influence of the SFR study model on frequency response. Appendix B presents the connection of sequence circuits for short-circuits, series faults and unbalanced loading. Sequence currents and voltages are calculated for all three cases. Appendix C details power plant modelisation for the three practical applications: the general case, Terceira island, and Fuerteventura-Lanzarote system. The power systems in Terceira island and Fuerteventura-Lanzarote system are described respectively in Appendix D and Appendix E, including the network topology, and the characteristics of the power plants and substations in the systems. Besides, demand and generation scenarios are listed, together with the unit commitment and generation dispatch.

# Part II

# State of the art

# Chapter 2

# Review of grid codes in weak power grids

## 2.1 Introduction

Environmental constraints leading to a carbon-free society are driving the change to a larger penetration of renewable energy sources as power generation agents. However, best resources are often located at remote or even isolated regions. The integration of variable energy sources in such weak power grids poses many technical and economic issues. Both aspects have an impact on the development of grid codes, that is worth analysing.

Grid code evolution has been extensively studied in the literature, mainly focused on technical requirements for large wind power plants. Thorough analysis and comparison of grid codes were conducted most recently in [33–40]. However, grid codes are under constant revision and information update is necessary. Even if harmonisation efforts are being launched by international organisms, e.g. the European Wind Energy Association (EWEA) and the European Network of Transmission System Operators for Electricity (ENTSO-E), differences between system operator requirements continue to be considerable. Reasons for the differences are often a result of environmental conditions, government policies, local utility practices, network strength and characteristics, and grid asset types present in the system [33, 34]. Although existing literature is wide for strong power systems, information is sparse regarding small and weak power grids [41].

Therefore, this chapter studies differences between technical requirements imposed on to generation assets influenced by the strength and characteristics of the power system. Thus, countries with very distinct characteristics have been selected for the study: a large power system with weak subsystems such as Australia (as counterpart to Tasmania island); leading countries in renewable energy penetration and policies, e.g. United Kingdom and Denmark; interconnected regions including isolated territories with a specific regulation such as France, including some isolated systems outside the metropolitan France operated by Electricité de France (EDF), called Systèmes Energétiques Insulaires (SEI) and Spanish extra-peninsular and insular territories known as Sistemas Eléctricos Insulares y Extrapeninsulares (SEIE); or island territories such as Ireland and New Zealand. The grid codes under study are

listed in Table 2.1. Technical requirements applying to both synchronous and non-synchronous generating units at transmission networks have been studied, in order to focus the analysis on the constraints imposed by power system characteristics, mainly oriented to weak and isolated power systems.

**Table 2.1. Grid codes under study**

| Region | Title |
|---|---|
| Australia | *National Electricity Rules Version* [42] |
| Denmark | *Technical regulation 3.2.5* [43]<br>*Technical regulation 3.2.3* [44] |
| France SEI | *Referentiel Technique HTB* [45] |
| United Kingdom | *The Grid Code* [46] |
| Northern Ireland | *SONI Grid Code* [47] |
| Republic of Ireland | *EirGrid Grid Code* [48] |
| New Zealand | *Electricity Industry Participation Code* [49] |
| Spain SEIE | *OP SEIE 1* [50]<br>*OP SEIE 12.2 (Draft)* [51] |
| Tasmania | *Tasmanian Frequency Operating Standard Review* [52] |

This chapter is organised as follows. Section 2.2 compares the most outstanding technical regulations in the power systems under study, followed by a comparative discussion of the influence of power grid strength and characteristics on current and future regulatory aspects in Section 2.3.

## 2.2 Review and comparison of technical requirements

Technical requirements applying to both synchronous and non-synchronous generating units at transmission networks have been studied, in order to focus the analysis on the constraints imposed by power system characteristics, mainly oriented to weak and isolated power systems. Among the grid codes reviewed, three different approaches regarding generation assets have been identified. Technical regulation in Australia and New Zealand is technologically neutral, whereas Ireland, Denmark and UK have a separate grid code specifically for wind power. Finally, grid codes in France SEI and Spanish SEIE not only apply to wind power but also to other intermittent energy technologies.

As grid code review and comparison can become cumbersome due to significant differences between system operator requirements even regarding structure and terminology, the generic grid code format proposed by the EWEA in [53] has been used as a basis for the analysis hereafter. The requirements have been classified into six

groups: operating ranges, active power, frequency control, reactive power, voltage control and fault ride-through.

### 2.2.1 Operating ranges

Continuous operation of generating units is required around the rated frequency, usually between 49 and 51 Hz (Table 2.2). Transiently, generators shall remain connected being allowed to operate during some limited time periods for frequency values outside this band. Minimum and maximum frequencies correspond to 47 and 52 Hz as a general rule, respectively. However, in France SEI the band enlarges up to 44-54 Hz. New Zealand South Island has also a wider band than the average: 45-55 Hz. These frequency excursions could correspond either to slow phenomena or to disturbances leading to frequency excursions such as e.g. generation loss and short-circuit faults.

Outside continuous operating bands, generators must withstand with disconnecting short time periods, as indicated in Table 2.2. In the case of Denmark, it only applies to Wind Turbine Generators (WTGs) with a rating higher than 25 kW. The continuous operating range in that case is 49.5-50.2 Hz.

**Table 2.2. Remain connected frequency ranges**

| Frequency (Hz) | Denmark | SEI | UK | Ireland | SEIE |
|---|---|---|---|---|---|
| 52-54 | | 5 s | | | |
| 51.5-52 | 15 min | Cont. | 15 min | 60 min | 1 h |
| 51-51.5 | | | 90 min | | Cont. |
| 50.5-51 | | | Cont. | | |
| 49.5-50.5 | Cont. | | | Cont. | |
| 49-49.5 | 5 h | | | 60 min | |
| 48-49 | 30 min | | 90 min | | |
| 47.5-48 | 3 min | 3 min | | | 1 h |
| 47-47.5 | 20 s | | 20 s | 20 s | 3 s |
| 46-47 | | | | | |
| 44-46 | | 30 s | | | |

Table 2.2 applies for normal operation voltage levels, normally situated in a ±10 % band. Some grid codes require generators to continue operating out of this band for limited time periods. Requirements in French islands, Spanish SEIE and Denmark include a voltage-frequency graph for frequency and voltage rating capability of generating power plants in steady-state, as recommended in EWEA's generic grid code format.

### 2.2.2 Active power

Active power control is the ability of power plants to regulate their active power output to a defined level and at a defined ramp rate. Currently, most grid codes require to implement this feature not only to synchronous generation, but also to renewable power generation installations.

Except for the French islands, the rest of the grid codes under study limit active power ramp rates, corresponding to the gradient control mode. Most grid codes exempt from ramp-down rates on purpose for low wind conditions and underfrequency response mode. Regulation from EirGrid is the most complete regarding the ramp rate requirement, to be met not only by generation assets, but also by demand side units and interconnectors. Generators should have a ramp-up and ramp-down capability of at least 1.5 % of installed capacity. For wind farms, ramp rate average values measured over 1 and 10 min are specified for any situation, being applicable to every operation including start up, normal operation and shut down. It shall be possible to vary each of these two maximum ramp rate settings independently over a range between 1 and 30 MW per minute. The ramp rate settings shall be specified by the system operator previously to the operation date.

In the Australian grid code, there is such a requirement for scheduled and semi-scheduled generators, limiting ramp-up and ramp-down rates to the lower of 3 MW/min or 3 % of the maximum capacity (with a minimum requirement of 1 MW/min). The same limit of 3 % of maximum capacity is required in Northern Ireland for centrally dispatched generating units, set up as a minimum. Specific ramp requirement is issued for wind farms, which in turn shall have a positive ramp rate controller capable of being set within a range from 1 MW per minute to 10 MW per minute under normal operating conditions, and including a zero ramp rate setting, in order to block that feature.

In SEIE power systems in Spain, generators are requested to be able of limiting ramp-up and ramp-down rates (not related to decrease in primary energy source production) according to orders from the system operator. In contrast, in New Zealand the grid code leaves ramp-rate requirement for intermittent generators to be agreed between generators and system operators.

Regarding active power production constraint, in Northern Ireland, the active power restriction can be between 50 % and 100 % of the maximum instantaneous production. In the Republic of Ireland, wind farms can be also requested to operate at a restricted output value indicated as set-point by the system operator.

The Danish grid code requires the absolute production constraint, delta production constraint and power gradient constraint modes. After receiving a setpoint change order, execution must start within 2 s and be completed not later than 30 s. The accuracy of the control performed must not deviate by more than $\pm 2$ % of the setpoint value or by $\pm 0.5$ % of the rated power.

Finally, any grid code which indicates a frequency response mode requires to apply the delta constraint function, although it is only specifically mentioned in the Danish grid code. This feature is further explained in next subsection.

### 2.2.3 Frequency control

Regarding frequency control, conventional generating units are requested to participate in primary frequency control, implemented through a speed governor system, so as not to decrease active power generation during frequency drops and not to

increase active power generation during frequency rises. Speed governors shall have a droop between 2 % and 8 % with a maximum permitted dead-band, as indicated in Table 2.3.

**Table 2.3. Primary frequency control requirements for conventional generation**

| Region | Droop | Dead-band | Response time |
|---|---|---|---|
| France SEI | 3-8 % | ±15 mHz | 15 s |
| UK | 3-5 % | ±15 mHz | – |
| Northern Ireland | 4 % | – | – |
| Republic of Ireland | – | ±15 mHz | 30 s |
| New Zealand | 0-7 % | – | – |
| Spain SEIE | 2-5 % | ±30 mHz | 30 s |

Besides, in regions with large penetration of variable source power generation or frequency regulation issues (such as isolated power grids), renewable generating units are also called to participate in frequency control, with an automatic variation of the generated power output in relation to the frequency in the system. Two types of frequency regulation are cited in the literature.

- Frequency Sensitive Mode (FSM) or frequency regulation with droop characteristic: generators are compelled to provide frequency response for low and high frequencies, respectively increasing or decreasing their output.
- Limited Frequency Sensitive Mode (LFSM): generators are only compelled to provide partial frequency response, normally for high frequencies, reducing their output at a given rate.

In the grid code issued by National Grid, both LFSM and FSM can be instructed. For LFSM, in response to an increase in system frequency above 50.4 Hz a minimum rate of 2 % of output per 0.1 Hz deviation shall be decreased. Maximum execution time depends on the device used for accomplishing this feature, with a maximum time of 5 min.

In most grid codes, primary frequency control is compulsory, although in the Spanish SEIE some installations can be exempted from this service depending on the characteristics of the isolated power system. If frequency response is based on a speed governor or analogous device, corresponding action parameter values are shown in Table 2.4 for non-synchronous generating units. In some grid codes, during low voltage events (e.g. under 0.85 p.u. in the case of the SEIE), this regulation feature may be disabled.

### 2.2.4 Reactive power

All grid codes under study include specific reactive power capability limits. However, they differ on the point at which the requirement is specified, voltage range at the

**Table 2.4: Primary frequency control requirements for non-synchronous generating units**

| Region | Droop | Dead-band | Response time |
|---|---|---|---|
| France SEI | 3-8 % | ±15 mHz | 15 s |
| Northern Ireland | 4 % | – | – |
| Republic of Ireland | – | ±15 mHz | 30 s |
| New Zealand | 0-7 % | – | – |
| Spain SEIE | 2-6.66 % | ±30 mHz to ±200 mHz | 30 s |

Note: in the UK, the same requirements are applied to synchronous and non-synchronous generating units.

connection point, as well as the method for measuring the reactive power capability, either expressed in terms of power factor or reactive power. In the case of synchronous generating units, generator performance charts specify their reactive power capability limits. Minimum short-circuit ratio is also usually stated, as in the case of UK (0.4 for units under 1600 MVA and 0.5 for larger units) or Northern Ireland (0.5). For non-synchronous generators, such as WTGs, grid codes specify reactive power capability in terms of PQ and UQ diagrams. In Figure 2.1 reactive power limits for non-conventional power plants are compared in terms of reactive to active power (PQ diagram), except for Australia and New Zealand which are technologically neutral. In Figure 2.1 only the operating limits are considered without taking into account voltage conditions.

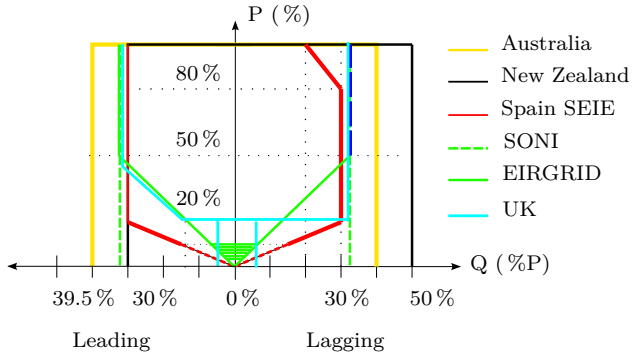


**Figure 2.1. Comparison of PQ diagrams**

In the Spanish grid code, the reactive power generation requirement is reduced above 80 % of the power output, as the need for voltage control is lower at high levels of active power and the simultaneous generation of maximum active and reactive power increases cost. Reactive power requirement is also reduced for low power output: below 50 % in the EirGrid code, and below 20 % in the Spanish case. In both cases, 10 % is indicated as limit value, where compliant operation is still desirable with a certain flexibility. The Danish grid code for wind farms sets different requirements

as a function of the rated power of the wind farm. So, largest installations have to comply with more stringent requirements and be able to manage wider reactive power ranges.

Terminal voltage limitations also affect reactive power capability of variable generators. Hence, grid codes indicate voltage limits for the obligatory compliance of the reactive power requirement. For inductive compliance, Spanish regulation sets a maximum voltage limit of 1.05 p.u. and for capacitive condition, a minimum limit of 0.95 p.u. In New Zealand, voltage thresholds depend on the voltage level, with 1.1 and 0.95 p.u. for 220 and 110 kV transmission networks in case of inductive capability and 1.1 and 0.9 p.u. for capacitive capability. Some grid codes specify reactive power versus voltage characteristic separately from the reactive range, by means of a UQ chart (Figure 2.2). The most and less restrictive requirements correspond respectively to Spanish islands and Northern Ireland. For non-synchronous generators, lagging capability may diminish as terminal voltage increases because of converter current constraints. Leading capability normally grows with the increase of terminal voltage [54].

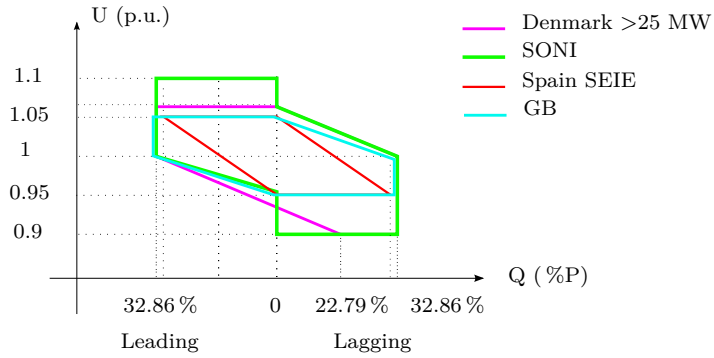


**Figure 2.2. Comparison of UQ diagrams for wind farms**

### 2.2.5 Voltage control

Regarding voltage control for non-synchronous generators, all three control modes (reactive power, power factor and voltage control) are selectable in Ireland (both Republic of Ireland and Northern Ireland), Denmark, Spain and Australia. The latter includes this condition both for WTGs based on synchronous and asynchronous machines. On the contrary, the UK grid code only indicates voltage control mode, regardless of the generation technology. The voltage control mode and set-points can be changed on-line in some regions, as for the SEIE case.

Fast response of voltage control is of highest importance, and therefore, most important parameters in the grid codes under study for intermittent power generating units are summarised in Table 2.5. Comparison is not straightforward, as parameter definition often is not consistent. The National Grid regulation is the most stringent, due to the conditions of fast settling time and high resolution.

**Table 2.5. Voltage control requirements**

| Region | Slope | Rise time | Settling time | Resolution |
|---|---|---|---|---|
| Australia | – | 2 s for a 5 % step | – | 0.5 % |
| Denmark | – | – | 10 s | 0.1 kV |
| UK | 2-7 % | 1 s for a 90 % | 2 s | 0.25 % |
| Ireland | 1-10 % | 1 s for a 90 % | 20 s | – |
| Spain SEIE | 0-25 | 1 s for a 90 % | 1 min | 0.01 p.u. |

### 2.2.6 Fault ride-through

During short-circuits, voltage drops in all (three-phase fault) or at least some of the phases (unbalanced faults). During unbalanced short-circuits, voltage can as well swell in some of the phases. So, two requirements can be defined in relation to Fault Ride-Through (FRT): LVRT for voltage drops and High Voltage Ride-Through (HVRT) for voltage swells. HVRT is less common, but present in some interconnection rules.

All reviewed grid codes include LVRT requirements. Same rules for any type of generation apply in Australia, French SEI and UK power systems, whereas in Denmark, any generation power plant with a rated power higher than 1.5 MW must ride-through low voltage dips. Different profiles are applied to synchronous and wind power generation. In the case of synchronous generation, shorter duration faults must be withstood in Western Denmark, which is a weaker power system compared to Eastern Denmark.

Figure 2.3 shows comparative graphs with the LVRT requirements in the grid codes under study. New Zealand profile has not been included in the figure, as it is not still accepted as a rule (but expected to be included in future versions of the grid code [55, 56]). Separate requirements are proposed to be met by generators connected to the North Island and the South Island. Besides, regarding grid voltage before the FRT event, a prefault voltage value of 0.9 p.u. is considered in contrast to other grid codes. Regarding UK for faults shorter than 140 ms no specific profile is mentioned. It is stated that any generator connected to the transmission grid should be able to withstand zero volt voltage dips for a total clearance time of 140 ms. For faults longer than 140 ms a FRT profile is indicated. In the case of Australia, hypothesis mentioned in [57] have been taken into account for the 250 kV network, as only maximum fault clearance times as a function of the voltage level are stated.

In most of the technical regulations under study, the Zero Volt Ride-Through (ZVRT) requirement is stated, which could pose some difficulty to non-synchronous generating units such as WTGs to comply with. However, the compliance is required at the high voltage terminals of the interconnection transformer, i.e. PCC. Therefore, taking into account booster transformers and interconnection cables, a higher voltage would have to be ridden through at the generator terminals. On the other hand, the Irish grid code requires the most stringent profile regarding voltage recovery, with a lower slope, which depends on the electrical machines present in the power grid and

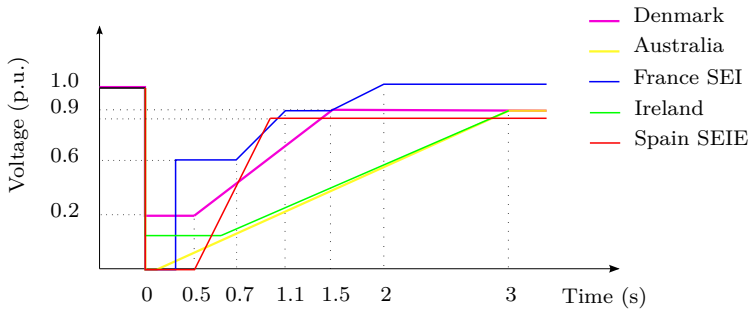


**Figure 2.3. Comparison of LVRT requirements in the grid codes under review**

power grid characteristics. The presence of induction type machines, slow voltage control systems or weak power grids can result into slow voltage recoveries.

Although only envelopes corresponding to three-phase faults have been represented in Figure 2.3, some grid codes require separate characteristics depending on the short-circuit type. It is the case for the Spanish SEI, where a less stringent profile is required to be withstood by generating units during two-phase short-circuits, with a lowest value of voltage of 0.5 p.u. In Australia (and therefore in Tasmania), three-phase short-circuits have to be ridden-through during shorter times if compared to the rest of the short-circuit types, i.e. 120 ms versus 250 ms in 250 kV networks. Both EirGrid and SONI Transmission System Operators (TSOs) indicate a LVRT profile to be withstood in all phases or any of the phases. Hence, a single envelope specifies the requirements upon any short-circuit, balanced or unbalanced. In Denmark, recurrent short-circuits have to be withstood in the case of unbalanced faults. In addition, wind power plants have to comply with the requirements if at least two independent faults occur within 2 min. In UK, a zero LVRT requirement has to be met upon the occurrence of a solid three-phase or unbalanced earth fault.

In addition, a feature which is being required in many codes is active and reactive power contribution during faults and after fault clearance. French islands do have a LVRT profile, but no requirement regarding active support of wind farms during the disturbed regime until recovery. Grid codes issued by EirGrid and REE for Spanish islands set conditions for active power during faults. In the Republic of Ireland, wind farms shall provide active power in proportion to retained voltage, and in the SEIE during disturbances and for voltages under 0.95 p.u. active current injection shall be within a certain area. The requirement shall be complied with until voltage recovery. In Denmark, active power must be maintained during voltage dips, even if a reduction in active power is acceptable. Upon the clearance of the fault, a fast recovery of active power generation is required in many regions as indicated in Table 2.6. Australian grid code sets the most stringent condition.

Regarding the time delay of the active power recovery, it should be delayed until the post-fault voltage is stabilised. An immediate increase of active power could cause voltage fluctuations and instability, especially in weak power grids [58]. From this perspective, the time delay should be as long as possible. The least stringent grid code, i.e. France SEI, requires a time delay of maximum 10 s, but values below

**Table 2.6. Active power recovery upon fault clearance**

| Region | Time (s) | P ( % of pre-fault P) |
|---|---|---|
| Australia | 0.1 s after clearance | 95 % |
| Denmark | 0.5 s after voltage recovery | 90 % |
| France SEI | 10 s after clearance | 95 % |
| UK | 0.5 s after clearance | 90 % |
| Ireland | 1 s after voltage recovery | 90 % |

1 second are mostly found. This requirement is due to the load demand in the transmission grid. Hence, there is a conflict of interest between the voltage stability support and the demand for a quick active power recovery. The limit value should therefore be set dependent on the voltage stability situation in the grid, leading to higher values in weak power grids. Regarding the gradient of the active power recovery, it is independent of the voltage stability situation and depends on the machine ratings. High gradients may impose stress on the components of a WTG. Finally, the minimum level of active power is of highest importance for transient stability and should be kept below the maximum transferable limit.

Regarding reactive power support during LVRT, its maximum level and gradient are normally specified. The maximum level of reactive power influences the voltage control capability and transient stability. On the other hand, a high post-fault reactive power generation can impose overvoltages. Hence, it is necessary to down-ramp the reactive power when the voltage recovers. According to the Australian grid code, generation assets shall provide capacitive reactive current of at least the greater of its pre-disturbance reactive current and 4 % of the maximum continuous current for each 1 % reduction with respect to its pre-fault level during faults. Both EirGrid and SONI require to maximise reactive current within reactive power capability of the WTGs. Spanish regulation for islands indicates a more detailed reactive current behaviour, both during voltage dip and subsequent recovery, where reactive current is expressed as a linear function with several sections for different voltage ranges. For voltage values below 0.1 p.u. and above 1.15 converters are allowed to be blocked, and not to inject current into the grid. However, as soon as the system recovers, the blocking must be suppressed. Danish grid code states that reactive power must be controlled to support voltage with a linear graph requiring a maximum of 100 % $I_Q/I_N$ injection from 60 % to 20 % of voltage during faults. Below 20 % of voltage disconnection is allowed, and hence no reactive power is required.

LVRT requirements are usually expressed using positive sequence. However, in the Spanish grid code it is specified that reactive current can be injected/absorbed in the three phases (i.e. positive sequence current only), or in the faulty phases as synchronous generators do (i.e. using positive and negative sequence currents). The latter option is preferred. In addition, the system operator shall be able to indicate the reactive current to be injected by the wind farm.

In recent years, similar voltage-time profiles have also been defined for overvoltage

or voltage swell conditions, caused by large load switching, capacitor energising or faults in the network. This feature is in turn referred to as HVRT, and among the grid codes under study, it applies in the SEIE and Australia for both synchronous and non-synchronous generation, following the graph in Figure 2.4. A highest value of respectively 1.25 and 1.3 p.u. has to be withstood during 50 ms. Lowest overvoltages have corresponding longer remain connected times following a linear and exponential evolution, respectively, with a maximum time of 1 s.

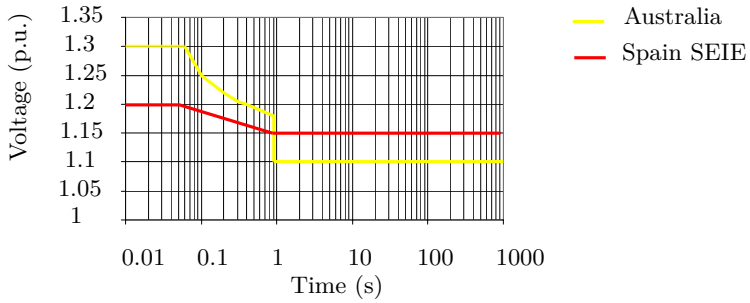


**Figure 2.4. HVRT requirement in Australia and Spain**

### 2.2.7 Synthesis of requirements

The technical requirements under review can be broadly divided into two categories:

- Operating ranges for both steady-state and transient performance, during which generation assets are not allowed to disconnect from the grid. These requirements are often named as *remain connected requirements* or *passive requirements*.
- Active requirements under which generation assets shall contribute to frequency and voltage control in the system.

Remain connected requirements are summarised in Table 2.7, classified in three categories: voltage, frequency and power quality. Except for power quality, which often is regulated by international standards or only pointed out in distribution grid codes, the rest of the requirements are indicated in almost any grid code under study, except for the HVRT and phase angle jump. In contrast, active requirements are not widely harmonised and applied to RES. Main current active requirements are summarised in Table 2.8.

**Table 2.7. Synthesis of remain connected requirements**

| Requirement | AUST | DEN | SEI | UK | ROI | NI | NZ | SEIE |
|---|---|---|---|---|---|---|---|---|
| Freq. range | ✓ | ✓ | ✓ | ✓ | ✓ | ✓ | ✓ | ✓ |
| Freq. ride-through | | ✓ | ✓ | ✓ | ✓ | ✓ | ✓ | ✓ |
| Freq. gradient | ✓ | | | | ✓ | ✓ | | ✓ |
| Voltage range | ✓ | ✓ | ✓ | ✓ | ✓ | ✓ | ✓ | ✓ |
| LVRT | ✓ | ✓ | ✓ | ✓ | ✓ | ✓ | ✓ | ✓ |
| HVRT | ✓ | | | | | | | ✓ |
| Phase jump | | ✓ | | | | | | ✓ |
| Unbalance | | | | ✓ | ✓ | ✓ | | ✓ |
| Flicker | ✓ | ✓ | ✓ | ✓ | ✓ | ✓ | ✓ | ✓ |
| Harmonics | ✓ | ✓ | ✓ | ✓ | ✓ | ✓ | ✓ | ✓ |

Note. AUST: Australia, DEN: Denmark, SEI:France SEI, UK:United Kingdom, ROI: Republic of Ireland, NI: North Ireland, NZ: New Zealand, and SEIE: Spanish SEIE.

**Table 2.8. Synthesis of active requirements**

| Requirement | AUST | DEN | SEI | UK | ROI | NI | NZ | SEIE |
|---|---|---|---|---|---|---|---|---|
| P regulation for low frequencies[a] | AAS[c] | | | ✓ | ✓ | | | ✓ |
| P regulation for high frequencies[a] | AAS[c] | | | ✓ | ✓ | | | ✓ |
| Inertial response[b] | | | | | | | | ✓ |
| P support during FRT | ✓ | | | ✓ | ✓ | ✓ | | ✓ |
| Q support during FRT | ✓ | | | ✓ | ✓ | ✓ | | ✓ |

[a]: Primary frequency regulation

[b]: Mentioned as future requirement in the Spanish SEIE grid code

[c]: AAS corresponds to Automatic Access Standard

## 2.3 Analysis of current and future grid code requirements in relation to grid power characteristics

### 2.3.1 Influence of power grid strength and characteristics on grid codes

Grid codes shall be adapted to technical constraints in the corresponding power grid, such as the network strength and the characteristics of generation technologies. In [59] the impact of regulatory scenarios on the development of renewable energy on islands is studied. In this section, the influence of weakness and isolation of the power

grid on the interconnection conditions imposed by system operators to grid users is analysed. With that purpose in mind, selected grid codes under study have been compared to those applying in the corresponding stronger continental networks.

**Tasmania versus mainland Australia** The mainland Australian regulatory framework rules in the Tasmanian transmission network, except for the frequency operating standard. Limits for continuous operation in normal operation are equal: 49.85 and 50.15 Hz. On the other hand, limits for maximum and minimum frequency are wider in both power systems for island operation, as frequency excursions in the system result into higher values without interconnection. But underfrequency and overfrequency thresholds (49 and 51 Hz) and remain connected frequency bands are even greater in Tasmania. Figure 2.5 compares operational frequency ranges in the Australian mainland system and in the Tasmanian power grid, based on [52]. Tasmanian frequency standard requires a more restrictive frequency ride-through profile compliance.

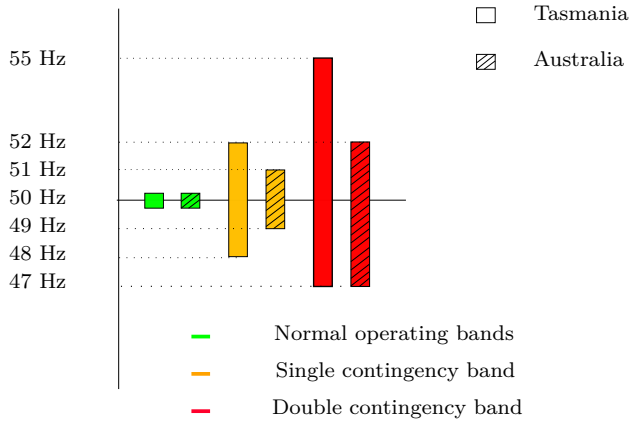


**Figure 2.5: Comparison of the Tasmanian frequency standard with the Australian mainland**

**SEIE versus peninsular Spain** Figure 2.6 compares LVRT profiles required respectively in peninsular and insular Spain. The latter regulation is more restrictive. Deeper voltages must be ridden through in the insular territories, where a zero volt condition must be withstood for grounded short-circuits. In the case of two-phase faults, a lowest value of 0.5 p.u. must be withstood in the islands, and 0.6 p.u. in the peninsula.

There are also notable differences regarding active and reactive current support. The grid code in the SEIE sets the same requirements for reactive and active current for any type of short-circuit, whereas in peninsular Spain different conditions are indicated, with more stringent requirements for balanced faults. In peninsular Spain, during and after any type of fault no reactive nor active power shall be consumed. Exceptionally, consumption of reactive and active power is permitted (on the contrary to SEIE regulation), with lower maximum reactive current and higher maximum active current consumption permitted for unbalanced faults. In addition, du-

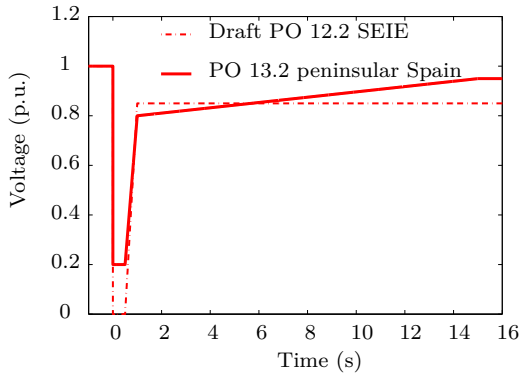


**Figure 2.6: Comparison of LVRT requirements in insular and extrapeninsular territories with peninsula, in Spain**

ring short-circuits, lower reactive current generation is required in peninsular Spain for voltages under 0.95 p.u. Therefore, regulation in the peninsula is less stringent regarding dynamic support during LVRT.

**SEI versus continental France** For generation connected to high voltage networks, the LVRT requirement in the French islands is the same as in metropolitan France. However, at lower transmission levels, a shorter zero voltage has to be withstood, with a slower recovery (Figure 2.7). No active or reactive power support is required during a voltage dip in any French territory.

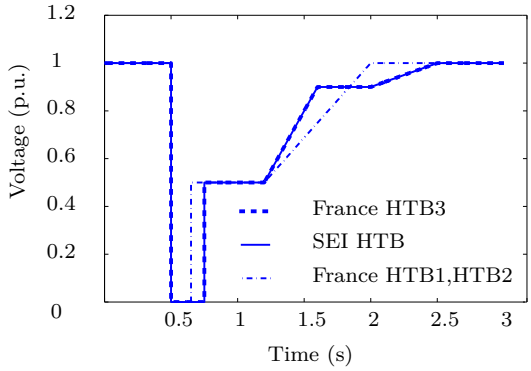


**Figure 2.7: Comparison of LVRT requirements in insular and metropolitan territories, in France**

**ENTSO-E** The ENTSO-E has proposed a common set of requirements for grid connection [60], where specific values to be assigned to various parameters depend on the type and region of the power generating module. Power generating modules are categorised depending on the connecting point voltage and maximum capacity of the generator. Four categories are defined: type A, B, C and D. For the first three types connecting point is below 110 kV, and for type D, at 110 kV or above.

While requirements applicable to type A are basic level requirements, increasing requirements are imposed on to the other types. On the other hand, five synchronous areas are designated in the ENTSO -E grid code: Continental Europe, Nordic system, United Kingdom, Ireland and Baltic system.

With regard to frequency ranges, slight differences appear depending on the synchronous area. Any synchronous area should be capable of continuous operation for frequencies between 49 and 51 Hz. However, outside this band, generators should be able to withstand exceptional frequency ranges during determined time periods. In the case of United Kingdom, frequency bands are not only timely longer, but also wider, i.e. lower minimum and higher maximum frequencies have to be withstood by generators in this synchronous area (Table 2.9). On the contrary, with regard to voltage bands, United Kingdom and Ireland have to withstand narrower operation ranges during shorter times. As instance in Ireland, a type D generator has to remain connected under a voltage range between 0.9 and 1.05 p.u., while in continental Europe the band enlarges to 0.85-1.1 p.u.

**Table 2.9. Remain connected frequency ranges**

| Frequency (Hz) | Continental Europe | Ireland | UK |
|---|---|---|---|
| 47-47.5 | | | 20 s |
| 47.5-48.5 | $\geq$ 30 min | 90 min | 90 min |
| 48.5-49 | $\geq$ 47.5-48.5 band | $\geq$ 90 min | $\geq$ 90 min |
| 49-51 | Cont. | Cont. | Cont. |
| 51-51.5 | 30 min | 90 min | 90 min |
| 51.5-52 | | | 15 min |

Reactive power capability of the generating units is also defined depending on the synchronous area of application. UQ graphs can be customer defined, provided that the graph is inside the maximum fixed outer envelope and meets maximum ranges as indicated in Table 2.10. Reactive power range for power module units is lower than for synchronous generators, but no general pattern in function of the weakness of the synchronous area can be extracted.

**Table 2.10. Parameters for UQ inner envelope**

| Area | Max. $Q/P_{max}$ (SG) | Max. $Q/P_{max}$ (WF) | Voltage range |
|---|---|---|---|
| Continental EU | 0.95 p.u. | 0.75 p.u. | 0.225 p.u. |
| Nordic | 0.95 p.u. | 0.95 p.u. | 0.15 p.u. |
| United Kingdom | 0.95 p.u. | 0.66 p.u. | 0.1 p.u. |
| Ireland | 1.08 p.u. | 0.66 p.u. | 0.218 p.u. |
| Baltic | 1.0 p.u. | 0.8 p.u. | 0.22 p.u. |

Note: SG stands for synchronous generation and WF for wind farms

Finally, it can be concluded that the ENTSO-E grid code is more demanding for weaker synchronous areas, as smaller generating units installed outside continental

Europe are requested to comply with the same level of requirements than much bigger generators in continental Europe.

**Conclusions** Regarding the influence of a power system strength and characteristics on the grid code, it can be concluded that the main differences between the technical regulation in interconnected power systems and weak power systems are the following:

- Wider operating ranges. Weak power systems have usually more onerous technical requirements for generators than those found in larger, interconnected grids.
- More stringent primary frequency response requirements, especially in isolated power grids. In order to provide support under low frequencies, generation assets based on RES can be requested to curtail their power output.
- A wider range of power factor is usually required for weak areas, especially during low power output, as voltage fluctuations can be large.
- Fault ride-through requirements are more onerous. Concerning voltage dip magnitude to be ridden through, ZVRT is common practice. Voltage recovery after a fault can be slow in weak power grids, and hence some restrictions on power restoration can be imposed both regarding active and reactive power. Active power recovery cannot be too fast, as important overvoltages can happen. Regarding reactive power, active contribution is often requested.

However, grid codes are in constant evolution, because of advances in generation and new trends in regulation. Special attention shall be paid to the regulatory frame regarding the integration of generation assets in weak power grids, adapting requirements in order to achieve a stable, secure and sustainable power supply, and so, overcome voltage and frequency regulation and stability issues.

### 2.3.2 Future regulatory aspects

The study of the latest drafts of international grid codes shows that more stringent requirements are to be imposed, especially concerning large renewable power generation installations and weak power systems. In order to take advantage of the existing resources and assure the security of the supply, system operators may require more demanding features. Specifically, following aspects are expected to be included in future grid codes for non-conventional power generation: (1) reactive power support during the fault period, (2) inertia emulation, (3) power oscillations damping, (4) other features such as black-start and island operation capability. In other words, non-conventional power plants will be designated to fully comply with requirements formerly meant only for synchronous generators. Hence, new devices and techniques such as power plant controllers will be necessary to achieve compliance [61].

On the other hand, FRT requirements were initially imposed only on to wind farms, but later some grid codes (e.g. Ireland) have stated the obligation of also synchronous generating units to ride-through extremely low voltages during faults. Therefore, the tendency is to conceive technologically neutral grid codes, as proposed by the

ENTSO-E grid code. Harmonisation processes have been launched, both for structure (EWEA) and for requirements (ENTSO-E). This type of processes are necessary at least to fix some terminology and common requirement types, but power system characteristics must be also taken into account.

# Chapter 3

# Current procedures and practices on grid code compliance verification

## 3.1 Introduction

Grid codes include the electrical performance to be complied by generating units. Demonstrating grid code compliance and achieving a grid connection agreement are, therefore, essential milestones in the development of a power plant project. The increase in renewable generation plants formed by a large number of individual generating units poses a challenge to system operators, in terms of connection process and plant modelling management. In order to cope with these issues, both compliance procedures based on testing and simulation, and modelling and validation requirements for renewable generation plants have already been established in many countries.

According to ENTSO-E [60], compliance testing is defined as the process of verification that power generating facilities comply with the specifications and requirements provided by the grid code. It can be carried out, for example, before starting operation of new installations. The verification should include the revision of documentation (including technical data and models), the verification of the requested capabilities of the facility by practical tests and simulation studies and the validation of the model performance based on actual measurements. This compliance shall be maintained throughout the lifetime of the facility. Hence, power plants shall undergo periodical compliance monitoring processes, in order to verify that their technical capabilities are maintained and simulation models are still valid.

A grid code verification plan is as important as the regulation itself and it should not need to leave room for interpretation regarding how each requirement shall be assessed. Unfortunately, not every grid code is complemented by a clear and detailed compliance verification plan.

Grid code evolution has been extensively studied in the literature, mainly focused on technical requirements for large Wind Power Plants (WPPs). Thorough analysis and comparison of grid codes were conducted most recently in [33–40, 62]. However, grid code verification and generation unit and system certification procedures are still at an early stage, and information is sparse, scattered [35] or focused on specific countries [63]. Often it can also be found within grid code review documents [64]. A

review of modelling and simulation requirements for variable generation in the grid codes would also be useful [65] and previous works can be found in [57, 66].

Therefore, this chapter aims to carry out an updated review of the international regulations and current practices regarding the verification and certification of the electrical performance in renewable generation systems, mainly focused on wind power generation. The countries analysed are Australia, Denmark, Ireland, New Zealand, Spain and UK. The selection covers a broad spectrum of countries with different power system structures and different levels of renewable energy penetration, whose grid codes were also reviewed in Chapter 2. Besides, German technical guidelines have also been included in this study, as their verification, validation and certification procedures for generating systems are pioneering in Europe.

This chapter is organised as follows. Section 3.2 describes renewable power generation asset modelling and simulation requirements, reviewing generic model development initiatives. Simulation models must be accompanied by validation tests to show the validity of the models. Model validation practices and practical set-ups are indicated in Section 3.3. Finally, compliance verification procedures regarding technical requirements in grid codes are gathered in Section 3.4, with special emphasis on certification procedures in Spain and Germany.

## 3.2 Renewable power generation modelling and simulation

Grid code requirements regarding data, modelling and simulation have been previously reviewed in [57, 66]. [66] gathers practices by several system operators regarding modelling requirements, ranging from Argentina -where non-confidential and non-black box models are required for all WPPs above 10 MW- and Croatia -where no generator model is required before connecting a generator-. However, the enquiry was carried out in 2005, and since then, modelling requirements have evolved. Therefore, requirements regarding modelling and simulation in the countries under study are hereby described and compared, including the application scope, model characteristics, and simulation requirements. Table 3.1 indicates the documents containing modelling and validation prescriptions required by system operators for renewable generation. Regulations are often complemented by guidelines with a more specific explanation. This is the case for most of the countries under study.

### 3.2.1 Challenges regarding renewable power generation modelling

In the traditional power systems, it was not necessary to include renewable power generation models in dynamic simulations, because penetration was still low and, regarding wind generation, disconnection during disturbances was a usual practice. Nowadays, situation has reversed and variable generation assets can even affect system stability. Therefore, many grid codes require manufacturers and generators to supply valid dynamic models.

**Table 3.1: Renewable generation modelling and validation requirements in the countries under study**

| Country | Title |
|---|---|
| Australia | *National Electricity Rules* [67]<br>*Generating System Model Guidelines* [68]<br>*Data and Model Requirements for generating systems of less than 30 MW* [69]<br>*Dynamic Model Acceptance Guideline* [70] |
| Denmark | *Technical regulation 3.2.5. for wind power plants with a power output greater than 11 kW* [71] |
| Germany | *FGW Technical Guidelines for Power Generating Units Part 3, Determination of electrical characteristics of power generating units and systems connected to MV, HV and EHV grids* [72]<br>*FGW Technical Guidelines for Power Generating Units Part 4, Demands on Modelling and Validating Simulation Models of the Electrical Characteristics of Power Generating Units and Systems* [73] |
| Republic of Ireland | *EirGrid grid code* [48] |
| New Zealand | *Connecting and Dispatching New Generation in New Zealand. Overview* [74]<br>*Asset Capability Information Overview. Guideline* [75] |
| Spain | *OP 9.0 Información intercambiada con el operador del sistema* [76]<br>*Guía descriptiva del procedimiento de puesta en servicio* [77]<br>*Requisitos de los modelos de instalaciones eólicas, fotovoltaicas y todas aquellas que no utilicen generadores síncronos directamente conectados a la red* [78]<br>*Condiciones de validación y aceptación de los modelos* [79] |
| UK | *The Grid Code* [46]<br>*Guidance Notes-Power Park Modules* [80] |

Main challenges reported in the literature regarding renewable power generation modelling are [81, 82]:

- Generators are usually based on power electronic devices. Thus, modelling can pose some issues, especially regarding control systems and algorithms which are often proprietary.
- Available models typically represent only large signal performance, but the impact of renewable generators on small signal performance needs also to be assessed.
- Performance under unbalanced network conditions, caused by unbalanced faults or asymmetric line impedances and loads, can impact significantly power electronic control systems and is difficult to model using only positive-sequence models. Hence, some grid codes require models that can represent both balan-

ced and unbalanced situations.

- In some areas, such as Australia, it is becoming more common to connect renewable generation in weak points of the network. Concerns about simulation model accuracy under these circumstances is highlighted in some references [63, 83].
- The aggregation approach might not be adequate to represent a large wind farm by a single equivalent for all cases. This can be the case for large wind farms with multiple feeders, where the response of individual or groups of turbines might be different, or power plants where generators are operating at different speed. The equivalencing of collector, transformer and compensation devices might show the same issues.

Among the countries under study, in Australia all new generating plants must provide validated models, regardless of the technology. Requirements regarding modelling are technology-neutral, as technical requirements imposed on to generation assets in the grid code [81]. In the Danish grid code, synchronous generators, as well as wind farms with a power output greater than 1.5 MW, must supply a valid dynamic model. The minimum capacity for wind power plants with the obligation to supply modelling information is set to 5 MW in the Republic of Ireland, as well as in the UK, where it applies to any power park module type, i.e. generating units powered by an intermittent power source. In Germany all generators are subject to dynamic model provision, unlike New Zealand where little information can be found with regard to asset modelling.

In most of the countries under review, aggregated models are accepted. In any case, in Australia the model aggregation methodology must be clearly specified and in Denmark, it must be proved that aggregation does not significantly impact simulation results. The aggregate models of wind farms must include in some cases the central park level controller (Australia), as well as the collector network (Ireland).

The scope of application normally includes both the generating unit and the complete generation system. In Australia, the complete wind or solar power plant model includes any dynamic reactive power support and the power plant controller. The German regulation indicates the modelling requirements at generating unit level, whereas modelling fundamentals for power generation system are only described as a framework for future application. Installation models shall include generating units, transformers, cables, reactive power compensation systems and the external grid. In Ireland, the wind farm model shall include the WTG models, converter controls, reactive compensation and protection relays.

### 3.2.2 Root Mean Square (RMS) against ElectroMagnetic Transient (EMT) models

Static and dynamic simulations are needed for operational, planning, interconnection and plant design purposes. System models are required at three general levels [73, 84]:

- Load flow and short-circuit models are used for basic design studies.

- Positive sequence or RMS models have traditionally been used for system integration studies and stability studies. Perfect balanced conditions are assumed and stability issues under study tend to be bounded within a small frequency band around the fundamental frequency of the system.

- Detailed three-phase EMT level models are necessary to study the effect of fast transients and electromagnetic interference, which require higher frequency components.

Generally, positive sequence RMS models must be handed in by manufacturers. This is the case for large power plants in Australia, Germany, and UK. In Denmark, it must be possible to use the simulation models for RMS balance and unbalance studies. Besides, the grid code indicates that models must be valid for a frequency range of 47-53 Hz and 0-1.4 p.u. of voltage.

The bandwidth of dynamic models is directly related to the required simulation time-step and, thus, to the resulting simulation speed. EMT models result into smaller time-steps and longer simulation times. However, they are necessary, because phenomena such as Subsynchronous Resonance (SSR), Subsynchronous Torsional Interaction (SSTI) or the study of behaviour of variable generators in weak nodes of a power system require detailed models. For instance, in Australia, detailed EMT-type models must be provided when seeking assessment of the model for a SCR lower than three. In addition, transient stability models should have a bandwidth of at least 0.05Hz to 10Hz. On the other hand, EirGrid regulation indicates that dynamic models must represent features likely to be relevant to angular and voltage stability. However, using EMT-type models for the whole system can be impracticable if the connecting network is large [63]. So, some simplifications need to be assumed. For instance, positive-sequence EMT models are used for routine stability studies in Australia [63].

When the power system topology and simulated disturbances are balanced, positive sequence models are adequate. However, unbalanced conditions can affect power electronics and, therefore, are required to be studied. It can be performed by using three-phase RMS or EMT simulations. In addition, positive sequence models might not be adequate for representing sufficient details of the converter control system [63].

Related to the model type, model minimum constants and simulation time steps are often specified. In Australia, transient stability models must allow numerically stable and accurate performance for time step-sizes down to 1 ms. Time constants of less than 5 ms should only be included if their inclusion is critical. Regarding model time constants, dynamics under 5 ms and 10 ms must be discarded in Spain and in the UK respectively. In Ireland, simulation time steps must be higher than 5 ms, whereas in Germany the limit is set on 10 ms, even if it must be demonstrated that simulations with different increment sizes obtain equivalent results. Last, simulation models in Denmark must be capable of using numerical equation solvers with variable time steps.

Besides, system operators often specify the software simulation package. On the whole, the preferred option is *PSS/E* from *Siemens*. In UK, the model structure and complexity must be suitable to be integrated in *Powerfactory* from *DigSILENT*. However, model could be implemented in the software package chosen by the manufacturer. In Denmark and New Zealand, there is no indication about the software simulation package to be used. However, according to [82], the system operator in New Zealand performs steady-state, dynamic and transient networks analysis using *DigSILENT Powerfactory*.

### 3.2.3 Generic models against proprietary models

Regarding dynamic modelling requirements, system operators and manufacturers have conflicting perspectives [57]. System operators prefer to use standard models that represent with sufficient accuracy the plant performance and are simple enough to be included in large network simulation runs. On the contrary, equipment manufacturers are concerned with achieving a high degree of accuracy and protecting their intellectual property. They are reluctant to disclose details of their products and, hence, models are often not standardised. Proprietary models include user-written positive-sequence models and three-phase detailed equipment models. However, in recent times manufacturer-specific models have become available in software tools such as *DigSILENT* [82].

In Australia, black box type representations are not accepted by the system operator and functional block diagrams, as well as model source code, is compulsory for generating systems over 30 MW, preferably in source code formats FORTRAN and FLECS. In Denmark, simulation models must be supplied in the form of block diagrams using primarily transfer functions and accompanied by model descriptions. Models consisting of compiled code are acceptable provided the source code is also sent. In any case, encrypted parts are not acceptable. Black box modelling is allowed for individual WTGs making up a wind farm with a power output greater than 25 MW. In Germany, a grey box approach is adopted. Even if during generating unit certification black box models are accepted, they must be accompanied by simplified open models. In Spain, user models shall be provided as open code objects in FLECS or FORTRAN programming languages.

During recent years, the need of harmonised generic model standards for the different parts and applications of power systems has been enhanced [85]. The development of generic models regarding variable generators has been mainly focused on wind power. During recent years, generic models representing different types of wind turbines and their controls have been published and provided for power system studies [65, 84]. They allow simulating the typical behaviour of wind generator types and control concepts and are well suited for general power system planning studies or feasibility studies. Wind speed variations have been commonly neglected in proposed generic WTG models, as it can be considered constant during the simulation period -up to 20 seconds in typical transient stability simulations [86]-. Generic models not only have been proposed for wind farms, but also for solar photovoltaic generation [87], reactive power compensation equipment (SVC, STATCOM) [88] or High Voltage Direct Current (HVDC) [89, 90]. In the United States, many of the initiatives come

from the Western Electricity Coordinating Council (WECC), whereas the National Renewable Energy Laboratory (NREL) has been engaged in an extensive model validation project aimed at testing the models against field measurements and refining the WECC generic models if needed. Models proposed by the WECC are included in *PSS/E*, *PSLF* and *PowerWorld* software packages. Internationally, IEC 61400-27-1 is an ongoing effort to standardise generic simulation models of individual wind turbines for transient stability simulation in large power systems. The main differences with regard to WECC models is that a common modular structure applies to all wind turbine types and the turbine and plant model are separated [91]. A future release of IEC 61400-27-2 will include the plant controller.

For generating systems of less than 30 MW, the Australian Energy Market Operator (AEMO) accepts the use of generic models for connection studies (e.g. standard IEEE models for synchronous generators or IEC/WECC generic wind farm models) provided that the model can reasonably represent the plant components of the generating system and the SCR is reasonably high [69]. In Ireland, user-written models must be supplied if there is no suitable library model. Similarly, in Spain a list with preferred models regarding conventional generation assets, as well as wind and photovoltaic power, reactive compensation systems such as Flexible AC Transmission System (FACTS) and protection relays, has been released. For synchronous generators, IEEE standard, CIM and PSS/E preferred models are indicated, whereas for renewable generation, generic models in PSS/E are stated. If none of these models allows to represent adequately the dynamic performance, user-written models are also accepted. In the UK, the use of standard models is encouraged.

However, generic models might be inadequate for studies aiming to improve or assess equipment details [82]. Besides, the validity of generic models for system frequency disturbances is still pending [84, 86]. Generic models have been tested against vendor models, but should be compared to actual recorded disturbance monitoring.

## 3.3 Renewable power generation model validation

The purpose of model validation is to ensure the correct performance of control systems and validate the computer models used for stability analysis [92]. Consequently, model parameters must represent adequately the dynamic performance of the device being modelled for power system studies [84]. Thus, along with the requirement for simulation models, there is an increasing demand in the grid codes to assure the proximity of models and physical behaviour [93]. Table 3.1 indicates the documents containing validation prescriptions required by system operators, which are strongly related to modelling requirements. Model validation is compulsory in all the countries.

There is considerable international experience regarding the validation of synchronous generator models [92, 94–97]. Validation methods are mainly based on staged tests, involving off-line tests such as enhanced short-circuit tests and partial load rejection tests [92], and frequency response testing covering Standstill Frequency Response (SSFR), Open Circuit Frequency Response (OCFR) and On Line Frequency

Response (OLFR) described in [92, 98]. These processes take significant time and are expensive, and might be harmful for the generating units [97]. An on-line disturbance monitoring based methodology is presented in [97], where validation is carried out by comparison with generator measurements recorded during system events. Then, parameters can be optimised through an automated iterative simulation approach. In addition, reactive capability, excitation system and governor testing is also extensively described in literature [92].

There is less experience regarding validation with generation based on renewable energy sources, and it is mainly focused on wind power. Validation must ensure that wind turbine models represent the turbine characteristics with sufficient accuracy, especially during severe transient disturbances.

Figure 3.1 illustrates the main steps that are necessary to evaluate the correspondence of a model with reality, based on a model definition [84, 93]:

1. Collect actual data from the modelled devices, which can be recorded or measured during tests.
2. Simulate the same set of tests or events during the data collection process on the model.
3. Compare measured or recorded data to simulation results and decide if the validation is acceptable or the model parameters should be adjusted.

Each of the steps is further explained in next subsections.

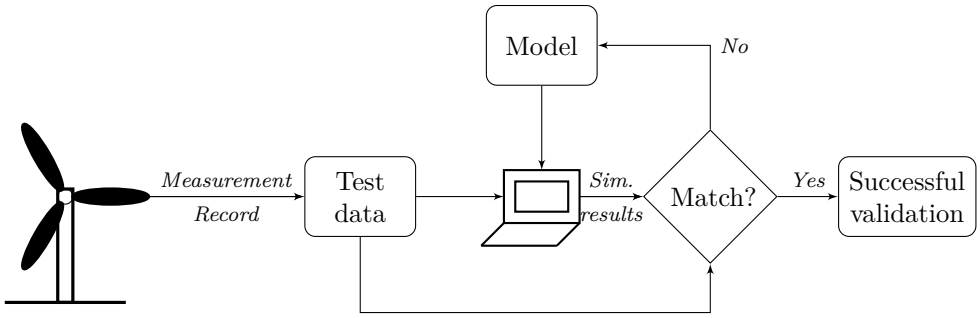


**Figure 3.1. General validation process**

### 3.3.1 Test data collection

In the early stages of the development of standard models, generic RMS models were validated against manufacturer detailed EMT models using a similar simulation tool [82]. It is an easy method, but it has some shortcomings regarding the model assumptions and the area of application. However, parallel validation of positive-sequence RMS against EMT models could be necessary for generation assets connected to weak power grids [63].

Currently, validation is mostly carried out by testing. Tests can be carried out on-site or off-site, via factory, laboratory or test beds [99]. On-site or field tests are more realistic and, as a consequence, are generally preferred by system operators. In Australia model validation must be carried out with on-site tests whenever possible. In Spain, the validation report shall include results obtained under real tests, even if test benches are accepted. In Ireland, both test types are accepted, because validation is based on the comparison of simulation results with actual observed behaviour of a prototype under laboratory conditions and/or actual observed behaviour of the real WTG as installed and connected to a transmission or distribution network. In Germany, the use of bench tests is permitted only if the behaviour of the generating unit is equal to the free-field measurement or when free-field testing equipment is used, as mentioned in standard IEC61400-21.

However, real tests might have some impact on the nearby grid users, so significant cost and test-time reductions can be obtained via proper factory testing [100]. Repeatability of the tests is also possible and, thus, it is much easier to identify any equipment problem, if necessary.

Model validation is required for different transient conditions, depending on the country. Generally, dynamic models are validated by testing the generating unit performance under faults. Thus, LVRT capability of the generation asset under test is evaluated. In these cases, staged testing is a preferable option, with two factory implementation options [82, 101]:

- Staged generator testing: it can be carried out using the turbine generator and controls alone, without the blades, during manufacturing process or at a dedicated test facility.
- Staged full-scale testing: a full-scale turbine is subjected to electrical disturbances at dedicated test facilities.

Factory test set-ups for short-circuit emulation are called *voltage dip generators*, which are able to emulate the actual network impedance during a fault. Four types of emulators have been proposed in the literature [100, 102–104]: generator based, shunt impedance based, transformer based, and full converter based emulators. Full converters have the advantage to be able to emulate any voltage waveform [100], not only voltage dips but also active and reactive power steps, or voltage and frequency changes, as presented in [105]. Some commercial testing solutions have been patented such as the Megha for LVRT tests or QuEST Lab, also able to carry out HVRT or phase angle jump tests [106], which are aimed for on-site tests.

The most common approach among the countries under review is based on the shunt impedance based voltage dip generator as a voltage divider, proposed in standard IEC61400-21 [107] (Figure 3.2). German and Danish validation tests are based on this standard. In the case of Germany, it can be used to validate both WTGs and photovoltaic generation units, for which the power at the DC side could be supplied by a suitable source. It has the advantage that it can be easily constructed and the setup is quite similar to a real fault situation, and thus, a realistic voltage dip is obtained [100]. The impedance $Z_2$ emulates the fault impedance. The voltage dip

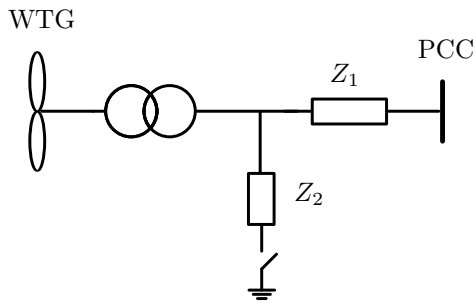


**Figure 3.2: Low voltage ride-through test equipment principle based on voltage divider**

starts when the circuit breaker is closed, and ends when the breaker opens and clears the fault current. The impedance $Z_1$ is needed in order to limit the influence of the voltage dip in the supplying grid. In order to be able to set the remaining voltage level during the dip, according to the grid code requirements, the impedance values have to be adjusted accordingly, or a shunt impedance bank can also be used [104]. In the German regulation, the impedances employed in the testing equipment must have an $X/R$ ratio of at least 3. The SCR at the connection point must be at least 3. The Fault Ride-Through (FRT) tests must be performed for three-phase and two-phase faults at partial and full load. The test is aimed both for model validation and compliance verification for LVRT requirement. Nonetheless, other test benches other than a short-circuit simulator based on the voltage divider principle, are permitted, such as grid simulators or transformer-based testing equipment.

For weak connection points, on-site staged fault testing is usually more appropriate [63]. Several methods exist for the implementation of on-site staged fault testing, including the fuse-wire method, the dropped conductor method and the direct earthing method. A practical set-up and results of the latter method are presented in [63].

However, other non-fault disturbance tests are also required in Australia, Denmark, Republic of Ireland or UK. In Australia, general model acceptance tests are fault disturbance tests (three-phase-to-ground) and non-fault disturbance tests, such as step response test on machine active and reactive power, or grid voltage magnitude, rate of change of frequency and step response test on grid voltage angle. The same case studies are required for wind farms and synchronous generators, although additional case studies are stated for each one: regarding LVRT for variable generation technologies, and regarding excitation sytems, and governors for synchronous generators. Model acceptance tests are also indicated for dynamic reactive support plants and HVDC links. Model acceptance set-up for wind farms is shown in Figure 3.3. A similar set-up is proposed for synchronous generation, although the connection arrangement of the generating unit is slightly different. Models are expected to work for a range of the simulation parameters rather than for specific settings. Fault disturbance tests must consider factors such as fault duration, grid SCR, grid $X/R$ ratio, pre-fault load levels, or fault $X/R$ ratio. For each test, a combination of study cases are presented based on varying aforementioned factors.

In Denmark, aside from voltage drop tests, model behaviour under voltage increase

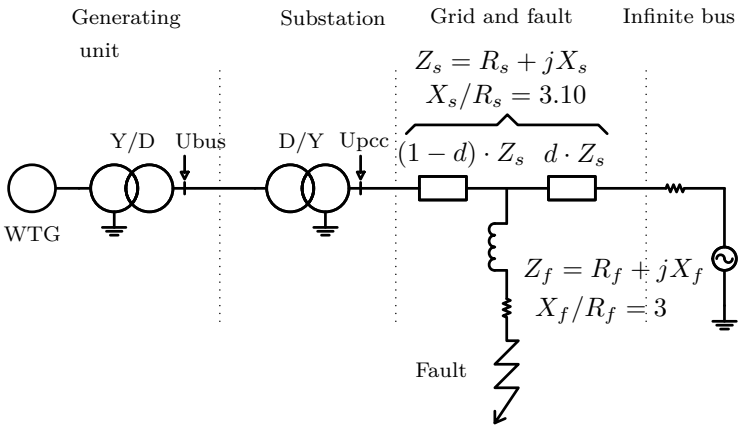


**Figure 3.3. Test circuit for model acceptance testing**

and frequency variations must be tested and results shall be obtained from test stations or measurement at commercial systems. In Germany, dynamic generating unit models are validated for LVRT requirement and at power station level, focuses on active and reactive power. Finally, the conditions validated in Ireland must be similar to those of interest, such as short-circuit levels, severe faults, voltage excursions, or large wind variations.

Test data can also be collected by opportunistic testing, also called on-line monitoring [82]. Thus, measurement equipment installed on-site records naturally power system disturbances used to validate the simulation models. However, transient model validation requires three-phase fault events, which rarely occur, and in any case, they seldom present the sufficient magnitude. Therefore, validation against single-phase short-circuits has been carried out in some cases [82, 108], as measurements were considered valid and it was reported to be a successful approach also for synchronous generators [97]. Otherwise, long-term monitoring approach can be used, and progressive model validation can be performed [63].

### 3.3.2 Model simulation

Model acceptance processes are often based on play-back techniques [84]. The simulation model is fed with recorded measurements from the low voltage terminals of the actual device. Accordingly, the same set of tests or events can be reproduced. In that case, the grid impedance and the dynamic behaviour of the grid is not included in the model. This choice is called open-loop model validation. Play-back techniques are more commonly used with positive-sequence models [63]. However, open-loop validation could lead to error, if the correlation between wind speed and voltage is not taken into account [109] and if the non-linear characteristics of the step-up transformer are omitted [63].

An analogous technique is reported in [108], in use by WECC for some time. It is achieved with the aid of a modified classical generator model (GENCLS) capable

of holding terminal voltage and frequency as specified in an input file with actual records. However, for some simulation software packages, it is not possible to use an external file to establish a fictitious voltage. So, two alternatives are possible:

- Simulation of a similar event by adjusting disturbance conditions.
- Application of a specific voltage profile using a user-written model.

The latter option is adopted for wind farm simulation in Spain, in the case of grid code compliance verification. On the other hand, closed-loop model validation entails a farm level model being connected to the rest of the network [63]. The validation of an entire WPP is reported in [84], using recorded voltage and current at PCC level. However, according to the experience of system operators in Australia, a number of high-speed data recorders at several locations are necessary, including the low and medium voltage terminals of critical nodes [63].

### 3.3.3 Model validity acceptance rules

Model simulation should provide an adequate match that captures the relevant dynamics and properly represents the dynamic response of the plant [84]. Few grid codes indicate the minimum accuracy level. For instance, in Denmark, the accuracy of simulations models must be kept within ±10 % for voltage, active power, active current, reactive power and reactive current. The actual accuracy shall be documented in the validation report. In Germany, the accuracy tolerances depend on the parameter under study ranging from 2 % to 7 %. In Australia, accuracy requirements are detailed for both load flow and short-circuit models, and transient and oscillatory stability models. Regarding load flow models, the deviation of the plant model from the actual plant response for active power and reactive power must not exceed 10 % of the total change in that quantity, and the model must not show characteristics that are not present in the actual plant response. These accuracy requirements apply also for transient stability models and further specifications are indicated for control system models, time domain responses including non-linear responses or performance and responses to switching or controlled sequence events.

If simulation and test results show a different behaviour from the generation asset, model parameter values can be adjusted or derived upon the observance of test response or through internal measurements [81]. However, unlike the case of synchronous machines, for power electronic interfaced technologies it is not generally possible to derive most model parameters directly from time-domain analysis of on-site test results nor from frequency domain transfer function testing [63]. Indeed, parameter tuning based on curve fitting against on-site testing measurements has to take into account a wide range of operating conditions.

Type validation is admitted in most regulations. In Australia validation on a single generating unit would be sufficient, as the same performance is observed in other units of the same type. However, factory and/or type tests alone are not sufficient for model validation, so a long-monitoring program must also be established [81].

## 3.4 Verification of the compliance of technical requirements

Manufacturers and generators must prove compliance with the technical connection requirements included in the grid codes under force. There are two alternatives to carry out this compliance verification [60]: practical tests or simulation, provided that the generating unit model has been validated. Each approach has its own advantages and disadvantages, and the risk and costs of both methods have to be assessed. Testing represents the real behaviour of the power system, but it has a high cost and can have side effects on the system if it is performed on-site. On the contrary, simulation does not involve any additional charge and it is harmless. However, validation of the model against field measurements is necessary. In general, on-site testing is the primary approach expected to be applied [63]. However, compliance verification can be also performed through a combination of both techniques, including on-site testing, comparative simulation studies, long-term monitoring and provision of overseas test experiences [63].

In addition, the relative size of the generating system has to be taken into consideration, as well as the type of generation technology and the location at which requirements are expected to be met. Regarding generation systems based on renewable energy sources, power plants are made up of several small size generating units, but grid code requirements are expected to be met at the PCC. Therefore, depending on the technical rule under study, verification shall be carried out on two levels [110]: a single generating unit, and the entire plant level.

### 3.4.1 Review of compliance verification practices

Comparison of compliance verification practices in the countries under study is a demanding task, since procedures are related to heterogenous grid code structures and requirements. Besides, the degree of detail, structure and even terminology employed in the relevant documents is heterogenous. Nonetheless, following are gathered the most remarkable international compliance testing practices and rules. This section introduces general requirements and practices regarding generating system performance verification in order to comply with grid codes under force. Reference documents for the countries under study are summarised in Table 3.2.

**Australia** As stated in [111], during commissioning applicants must demonstrate that their generating system meets the performance standards. Wherever practicable, the performance must be demonstrated by testing. However, these tests cannot demonstrate that the performance standards are met under all system conditions. Indeed, some requirements cannot be demonstrated by testing. The actual plant performance must meet the expected behaviour within predefined and agreed tolerances. Commissioning tests are undertaken considering power system conditions at the time of commissioning. However, the comparison of actual results with simulation results provides reasonable evidence that the generator can remain in service for the full range of power system conditions.

**Table 3.2. Grid code compliance verification in the countries under study**

| Country | Title |
|---|---|
| Australia | *Commissioning requirements for generating systems* [111]<br>*Template for Generator Compliance Programs* [112] |
| Denmark | *Technical regulation 3.2.5. for wind power plants with a power output greater than 11 kW* [71]<br>*Appendix 5.1. Wind power plants with a power output range of 1.5 MW to 25 MW* [113]<br>*Appendix 5.1. Wind power plants with a power output greater than 25 MW* [114] |
| Germany | *FGW Technical Guidelines for Power Generating Units Part 3, Determination of electrical characteristics of power generating units and systems connected to MV, HV and EHV grids* [72] |
| Republic of Ireland | *Grid Code Compliance Test Procedure* [115]<br>*EirGrid grid code* [48] |
| New Zealand | *Companion Guide for Testing of Assets* [116] |
| Spain | *Procedure for verification, validation and certification of the requirements of the Procedimientos de Operación (PO) 12.3 on the response of wind farms and photovoltaic plants in the event of voltage dips* [117] |
| UK | *The Grid Code* [46]<br>*Guidance Notes-Power Park Modules* [80] |

The rules do not detail any specific commissioning test. Instead, as technologies, types and the specific installation may vary from site to site, tests are expected to be tailored to the requirements of the equipment. In order to assist the applicant, typical tests for synchronous and non-synchronous machines are outlined based on former practices. For some of the rules more than a testing and monitoring method is proposed, along the required testing frequency and the basis for compliance assessment.

Some of the performance standards can be fully demonstrated based on on-site tests, such as power quality, protection system, active power control, monitoring and control requirements or power station auxiliary supplies. However, reactive power cannot be fully demonstrated on-site for the full voltage range. Voltage disturbances or contingencies are also unlikely to be demonstrated on field. Only the limits of the protection system related to these requirements may be proved. Regarding frequency control, the actual performance of the system under frequency variations cannot be demonstrated on-site. With respect to voltage and reactive power control, the actual performance of the generating system during all oscillations considering all system conditions is unlikely to be demonstrated on-site, but the performance of the system may be partially demonstrated through model validation. Some of the rules can as well be tested by modelling and simulation of the plant, such as fault level, partial

load rejection, or responsiveness of governor system. The response to voltage disturbance, frequency control, impact on network capability and voltage and reactive power control can also be demonstrated through model validation.

**Denmark** In Denmark, verification requirements depend on the generating unit technology and size, analogously to grid code requirements. Regarding wind power plants, plant owners are responsible for ensuring that generating assets comply with technical regulation and to provide some documentation in accordance with the total rated power of the power plant at the point of connection [43]. Even small wind power plants above 11 kW require type-approval and power quality verification according to standard IEC 61400-21 [107], apart from other documents. In addition, wind power plants with a power output above 1.5 MW need to verify the capability of the power plant to remain connected during voltage drops, and dynamic simulation is an acceptable verification method [43]. [113] and [114] contain guidelines for implementing commissioning tests for wind power plants respectively with a rated output over 1.5 MW and up to 25 MW, and over 25 MW. Regarding electrical conditions, tolerance to frequency and voltage deviations, and power quality are listed for verification, and many items can be verified by using simulation models. For instance, under normal operation, wind farms must withstand phase-angle jumps without disconnecting and the compliance can be verified by using a simulation model. LVRT requirements regarding balanced and unbalanced short-circuits can also be assessed with simulation models. In any case, set-ups for testing or simulation are not indicated.

**Germany** The grid connection regulations to be verified are listed below.

- Active and reactive power generation depending on the primary power supply
- Active power control for defined setpoints and frequency deviations
- Power quality
- Performance during faults (LVRT)
- Cut-in conditions
- Performance of protective devices

The aim of the LVRT test is to determine whether the generating unit is capable of detecting voltage dips and riding through them, as well as providing current during the voltage dip. The voltage dip detection methodology must be described. Testing, measurement and verification of the unit performance can be carried out in accordance with standard IEC61400-21 for any of the requirements. Test benches can be used for:

- Active and reactive power provision based on predefined set-points
- Transition behaviour of active and reactive power provision based on predefined set-points
- Reduction of output power with overfrequency
- PQ capability

- Performance during faults

In some cases, if the safety of the unit is not guaranteed, tests cannot be carried out with the unit running. In order to verify the voltage regulation requirement, the test can be carried out on a test bench by means of a suitable grid or via adjustment of the rated voltage in the control system. Flicker determination can be carried out on-site, by using a test bench on the actual grid or an AC network simulator.

Regarding the compliance at system level, only measurement of harmonic current is described in the reference document.

**New Zealand** Generation assets must pass through testing at the commissioning stage. There is no compliance requirement in the connection rules, but an explanatory guide for asset testing has been released by the System Operator (Transpower) covering routine tests and commissioning tests. Routine tests are designed to ensure that the generators are able to meet the technical requirements, as well as to verify operational ranges and limits of the generating plant, and steady-state performance, including over-under frequency performance. Initial tests apply to all generators above 1 MW, but test types differ depending on generation technologies. Detailed test programs for synchronous generators and wind generators are indicated. Regarding FRT, the test entails applying a fault to the grid and monitoring the wind farm response. The test must confirm that the coordinated control systems operate correctly and also allow the validation of the model. In addition, this test must confirm that the wind farm stays connected during under frequency excursions.

**Republic of Ireland** The reference document encompasses major technical requirements for wind farms, including active power management, transmission system voltage requirements and signals, communication and control. In each section, a series of tests are defined, in order to be performed at wind farm level. For each test, the following items are described: purpose, instrumentation, procedure and pass-criteria. All tests can be carried out on-site without additional equipment, with exception of the frequency response compliance test of wind farms. Since the grid frequency cannot be changed at will, this test requires to be emulated by means of injection of a frequency signal into the wind farm controller to simulate appropriate changes of frequency.

**Spain** Only verification regarding LVRT requirement included in the Operating Procedure (OP) 12.3 is documented. The verification procedure is explained in Subsection 3.4.2, within the certification procedure.

**United Kingdom** Compliance processes for both synchronous generators and power park modules are included in the grid code document. Tests for the final operational notification must include:

- Reactive capability tests, that shall be performed by modifying the voltage set-point of the voltage control scheme
- Voltage control system tests, that can also be used to validate the excitation system or voltage system model. The voltage control system shall be perturbed

with a series of step injections to the voltage reference, and where possible, multiple up-stream transformer taps.

- Governor or frequency control system tests, that can also be used to validate the governor or frequency control system model. Frequency modulation is possible by using a frequency injection signal.
- FRT tests for power plants above 100 MW

For each compliance test, the description, purpose, required results and assessment criteria are given. However, measurement and acceptance requirements are not indicated. If a power park contains two or more identical generating units, compliance testing may be reduced if the first unit completes the full testing.

Regarding FRT, manufacturers can demonstrate compliance using tests carried out with the facilities available. However, manufacturers are expected to replicate each fault type (three-phase, phase-phase, two-phase to earth and single-phase to earth) with varying magnitudes. The tests should illustrate any changes in characteristics or internal operating modes that depend upon fault severity, such as active and reactive power fault contribution and power recovery characteristic. The tests should be performed on a single power park unit using a test circuit based on the voltage divider.

Data and performance characteristics with respect to certain grid code requirements are registered by manufacturer for specific non-synchronous generating units. Then, simulation studies must be submitted to the system operator to demonstrate compliance with the connection conditions. The reactive capability of the generator must be demonstrated by a load flow simulation study. On the other hand, voltage control, reactive power stability and FRT capability of power park modules shall be proved by means of dynamic simulation series.

### 3.4.2 Certification procedures

Showing compliance with grid codes is especially challenging regarding renewable power generation systems, and is best done by compliance certification [118]. According to the international standard ISO/IEC 17000:2004, certification is a third-party attestation related to products, processes, systems or persons, whereas attestation includes the issue of a statement, based on a decision following the review, that fulfilment of specified requirements (e.g. guidelines, codes and standards) has been demonstrated. The review itself covers the verification of the suitability, adequacy and effectiveness [119].

Certification is generally achieved in two steps. Firstly, a type of generating unit must obtain a **Type Certificate** based on one or more country specific grid codes according to the relevant certification procedure. A recognised certification system for WTGs is IEC 61400-22 [120], that includes the evaluation of design, type-testing and manufacturing, as well as an optional type characteristic measurements module (power quality and noise). Procedures for assessing compliance regarding power quality requirements are gathered in IEC 61400-21 [107], including voltage quality

(emissions of flicker and harmonics), voltage drop response, power control (control of active and reactive power), grid protection and reconnection time. The type certification process ends with the issuance of a certificate, maintained and verified over time.

In a second step, a site specific **Project Certificate** must be issued for each power plant, e.g. wind farm, based on site specific data and the type certificate. In Europe, the most complete and documented certification procedures regarding grid code verification are the *Procedure for Verification, Validation and Certification of the Requirements of the OP 12.3 on the Response of Wind Farms in the Event of Voltage Dips (PVVC)* in Spain [117], and the German *Technical Guidelines for Power Generating Units. Part 8. Certification of the electrical characteristics of power generating units and systems in the medium, high- and highest voltage grids* [121], which describe the procedures to certify wind power installations according to their corresponding grid codes. A theoretical and practical comparison between both certification systems can be found in [35].

#### 3.4.2.1 Germany: FGW-TG8 procedure

The FGW-TG8 document [121] describes the procedure for the preparation and issue of a unit and system certification in accordance with the German grid connection regulations. The scope of the guideline is limited to the electrical characteristics impacting load flow, grid stability and voltage quality in an electrical grid. The document is complemented by documents [72] and [73].

To certify new generating units the applicant must provide:

- Verification of type testing according to FGW-TG3 [72], proved by the test report that includes measurement data.
- A comprehensive computer based model of the power generating unit, which may be encapsulated as a black box model, and executable in commercial grid analysis applications. This model needs to be suitable for the representation of the measuring situation of the type tests in accordance with FGW-TG3 [72], in order to facilitate verification of the model simulation based on measuring results.
- An open, where necessary simplified, model of the power generating unit. This open model must allow the certifier to follow the logical links between control loops in the relevant system controls. The degree of detail of the open model must be clarified in advance between the certification authority and the manufacturer. In some cases it may be sufficient to present block diagrams. It is necessary to comprehensively describe fault detection for verification of performance in a fault situation.

Model validation is performed based on the comprehensive computed-based unit model, by comparing simulation results to the measured data given in the test report, as well as on the basis of simulation results for test specifications for a variety of defined setpoints and/or grid conditions. Model validation is completed by inspecting the aforementioned open model.

The document also includes the procedure for generating system certification. To certify power generating systems the applicant must provide:

- Details on all the units connected in the system, including unit certificates, product certificates and/or test reports.
- Details on the electrical components of the system, where applicable component certificates must be provided. This includes all operational resources in the system internal grid up to the grid connection point. Single line diagrams must be provided.
- Details on the grid connection point, grid operator and connection regulation. The characteristic data of the public grid (short-circuit power and impedance phase angle) are provided by the grid operator.

To certify old systems, the applicant must provide verification of type testing according to FGW-TG3. Furthermore, the document must contain the specification of the original power generating unit and the specifications on the retrofitted power generating unit. Model validation is not included in this procedure [35].

#### 3.4.2.2 Spain: PVVC procedure

The PVVC defines two possible processes to verify the conformity of wind farms with the response requirements established in OP 12.3 for FRT: the *General Verification Process* and the *Particular Verification Process*. The General Verification Process consists of verifying that the wind farm does not disconnect and that the requirements stated on the OP 12.3 are met. Three actions must be completed: testing, model validation and, finally, wind farm simulation. Regarding test procedure, field tests are preferred. WTG simulation model validity must be accredited by a model validation report confirmed by measurements in the field tests. Next, the simulation models of all dynamic elements of the wind farm must be integrated inside a wind farm simulation model. Using this model, a wind farm simulation has to be carried out evaluating its response. A WTG with an accredited test report constitutes a unit type. A generator of the same manufacturer and with the same characteristics can avoid to have to repeat field tests. Wind farms with a verified wind farms report are considered a wind farm type (i.e. project type). Figure 3.4 shows the three steps of the general verification process.

As an alternative to the general procedure, the particular verification process obtains the direct wind farm verification by testing the dynamic elements of the wind farm and without having to carry out computer simulations. Hence, model validation and wind farm simulation are not needed.

The particular verification process is faster and cheaper than the general verification process [35]. Hence, wind turbine manufacturers and wind farm operators may prefer this process if the WTG can be tested and can ride through the voltage dip test defined in the particular verification process. However, the general verification process is necessary in those wind farms whose wind turbines can not ride through the voltage dip defined in the particular process and a compensating system is installed at the wind farm substation to fulfill the OP 12.3 requirement [35].

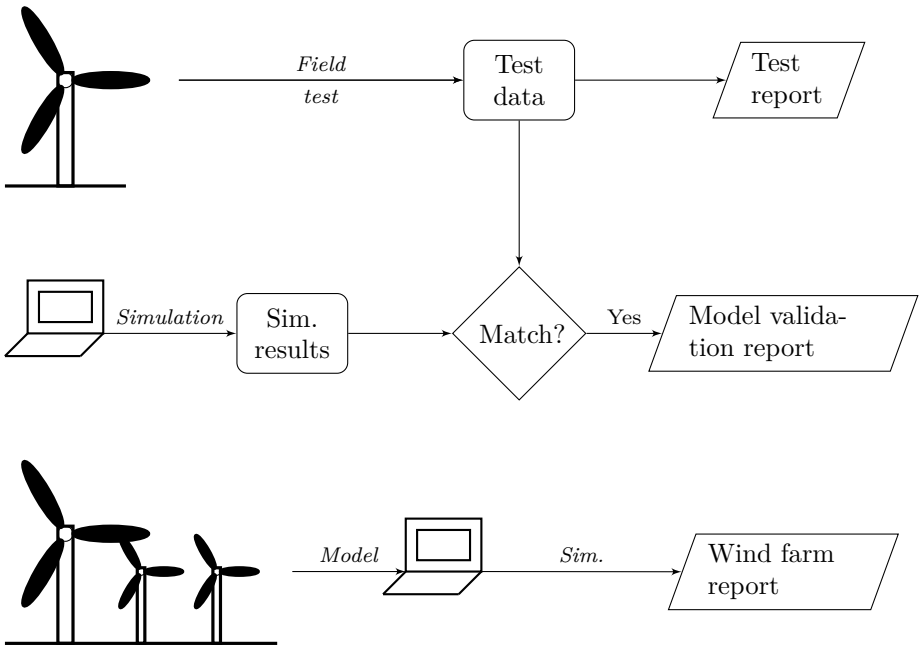


**Figure 3.4. General Verification Process**

**Test procedure** As testing equipment, the use of a voltage dip generator using an inductive divider is recommended. Other types of dip generators are accepted, but resulting residual voltages must be similar to those defined in the document. Four test categories are defined from the combination of partial and full load operating point, and three phase and two phase voltage dips: three-phase short-circuits at partial and full load, and two-phase isolated short-circuits at partial and full load. The definition and conditions under which the test is carried out depend on the objective of the test: for model validation -general verification process- or observance of FRT -particular verification process-.

**Model validation procedure** The generating unit model validation consists of three steps:

- Instantaneous voltage and current values are recorded for all the test categories. The duration of comparison window is 1 second, with 100 ms before the voltage dip.
- The manufacturers models must reproduce each of the tests carried out in the field. For that purpose, the test bench must be modelled as a voltage source set to the time series of the measured values, in the case of a WTG.
- The model is considered validated when the difference between simulation and test for active and reactive power does not exceed 10 % in the 85 % of the cases.

**Wind farm simulation procedure** In order to carry out a wind farm simulation, the model of the wind farm shall be based on validated WTG models. Existing reac-

tive compensation devices, cables, step-up transformer and internal lines must be also modelled. WTG aggregation is accepted. In addition, the interconnection substations has also to be represented by a MV/HV transformer and the evacuation line until the PCC. The rest of the power system (the external grid) must be modelled so that the fault clearance at the PCC reproduces the usual voltage profile in Spain: a sudden increase upon the clearing of the fault and a slower recovery afterwards. This profile has to be fixed and independent of the location of the wind farm. The single line scheme is shown in Figure 3.5, based on the reference document. The Union for the Coordination of the Transmission of Electricity (UCTE) equivalent includes a synchronous generator that reflects the UCTE system. To take into account the dynamics of the closest grid, a synchronous generator is included, as well as a load, modelled as a constant current and constant impedance asset. Data of the synchronous generators and their excitation systems are indicated. The fault reactance is adjusted so as to have a voltage magnitude of 0.2 p.u. and 0.6 p.u. during respectively a three-phase and a two-phase short-circuit. Parameter values can be found in the reference document.

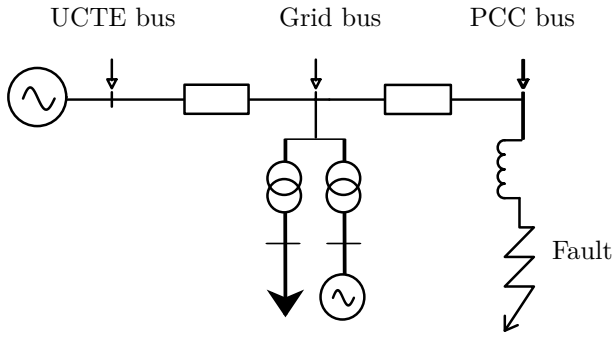


**Figure 3.5. PVVC: model of the equivalent electrical grid**

For each of the four test categories, it must be shown that:

- The wind farm remains connected during the voltage dip. Therefore, the simulation model must include the protection relays. If the wind farm model is not based on unit aggregation, the loss of generated active power must not exceed 5 % of the pre-fault value.
- Voltage and current levels at WTG terminals must be compared to test values and admitted error tolerances are defined (2 % for residual voltage level).
- Exchanges of active and reactive power must be as described in the technical requirement. Measurement techniques and power calculating methodologies for testing and simulation are indicated in the reference document.

For existing wind farms, simplified WTG models can be used, as usually no data to model the installations exists. If the wind turbines have an accredited test report, general library models can be included in the wind farm simulation. The models must consist of a current/voltage source and protections, so as to meet the limits

of the report. If the requirements to use library models are not fulfilled, validated models of WTGs must be provided by the manufacturers and the validation must be carried out according to the PVVC.

**Verification of requirements for photovoltaic plants** Annex II of the reference document indicates the verification of the requirements in OP 12.3 for photovoltaic plants. The testing process is based on feeding the AC side of the photovoltaic conversion system by a system that simulates voltage dips. The conversion system shall be tested by a continuous source at its DC part, either consisting of a set of photovoltaic modules or a DC power supply. Regarding the voltage dip generator, it can be:

- An inductive generator similar to the set-up proposed for WTGs.
- A power electronics device or other device able to simulate a variable AC voltage with the profile as defined in the technical requirement.

Regarding test validation criteria, active power must be within indicated ranges, the system disconnection must be less than one in three consecutive tests, injected current during the dip must meet specified requirements and the residual stress level and time during the load test must be as indicated.

# Part III

# Compliance verification methodology for renewable generation integration into island power grids

# Chapter 4

# A compliance verification methodology based on generic simulation models

## 4.1 Introduction

When connecting new generation assets, integration studies must be performed in order to guarantee power system safety and stability. Therefore, two aspects have to be considered: the impact of the new generation assets on the power grid, and vice versa. Whenever grid code regulations (if existing) are met, both objectives are covered. Hence, new generation assets must prove grid code compliance. For older generating units, periodic tests are usually performed. As a consequence, grid codes must be complemented by corresponding compliance verification procedures.

As overviewed in Chapter 3, there are two alternatives to carry out a verification plan: compliance testing by using practical tests and compliance simulation by means of simulation studies and revision against actual measurements. The alternative based on simulation has a lower cost, is easier to implement and has no side effects on the grid, even if validation is required. However, system operators mostly approve of type validations, including generating units and power plants with the same characteristics. Thus, verification processes are streamlined for manufacturers, facility owners and system operators. However, simulation based compliance verification is yet at an early stage and basically limited to a unique requirement: Low Voltage Ride-Through (LVRT). Moreover, procedures comprehend testing simulation models lacking data, or parameterised to represent a certain power system. It is the case of Spanish PVVC [117]. Therefore, generic power system models valid for verifying grid code regulation aspects are necessary. As technical rules regarding power plant connection are decidedly related to power system characteristics, those generic models should be accompanied by a methodology for parameterisation so as to fit any power system.

Hence, this thesis proposes a methodology to verify the integration of renewable power generation into isolated power grids using a simulation procedure beyond LVRT requirement. Two main objectives are pursued:

1. Enable a valid emulation of static and dynamic behaviour of insular power grids under most frequent or critical disturbances and operation scenarios by using simplified grid equivalent models.

2. Provide power generating facility owners and manufacturers with generic simulation models in order to verify grid code compliance.

Grid codes are strongly dependent on power grid characteristics. The scope of this thesis is limited to island grids because (1) RES integration is key for a sustainable and self-reliant energetic future, and (2) testing and evaluating emerging technologies before installed in field is especially important in remotely located power systems [14]. As a consequence, simulation procedures for most critical rules in this kind of power grids are hereby presented, based on technical issues described in Chapter 2. Three aspects are hereby covered, for being critical in isolated grids.

1. **Frequency Ride-Through:** frequency excursions are high in island power grids. As a consequence, generation interconnection rules often require to ride-through these deviations, remaining connected and even in some cases, modifying the power output of the generating units so as to contribute to system stability, i.e. frequency response.

2. **Low Voltage Ride-Through:** voltage dip magnitude following short-circuits can be higher in weak power grids. In addition, their duration is longer and undervoltages can quickly propagate to the whole network in island grids. So, transient stability can be compromised. As a consequence, grid codes often require non-synchronous generators to contribute to system performance by remaining connected and even in some cases, by controlling their active and reactive power output.

3. **Voltage and current unbalance:** unbalance is a quite common power quality issue in weak power grids. International standards indicate several methods to define and measure this phenomenon, and some interconnection rules require generation assets to remain connected under unbalanced voltage and current situations.

Table 4.1 summarises the requirements further studied and analysed in this thesis. Each of the requirements is theoretically analysed in following chapters. Corresponding grid events are analytically characterised, in order to obtain a grid model able to emulate each of the phenomena and adjust them so as to reproduce grid code requirements. Some of the cited requirements are associated to active support requirements, that are studied as a whole.

**Table 4.1. Synthesis of remain connected requirements**

| Requirement | Grid event | Chapter |
|---|---|---|
| Frequency ride-through | Frequency dip/swell | Chapter 5 |
| Low Voltage Ride-Through | Voltage dip | Chapter 6 |
| Voltage and current unbalance | Unbalance | Chapter 7 |

The present chapter is organised as follows. Firstly, Section 4.2 presents and describes the methodology encompassing the theoretical framework. This thesis follows the current standardisation trend, and hence, a generic and simple simulation model is proposed. This model can be valid for any of the grid code requirements under analysis, after particularising and parameterising it to fit the target power system. Section 4.3 describes the grid code compliance tests and the application of the methodology. Finally, the validation of the procedure is explained in Section 4.4.

## 4.2 Theoretical framework of the proposed methodology

The methodology presented in this thesis proposes a generic and reduced grid model as equivalent system suitable for both simulating the static and dynamic performance of a selected power system for interconnection and design purposes, and for verifying the compliance of grid code requirements. Depending on the disturbance to be represented and sensitivity studies of the model parameters, the **generic grid model** must be particularised, and so obtain a **particular grid model**. Finally, the grid model has to be parameterised based on grid characteristics and grid code limits, resulting into a **parameterised grid model**. Thus, the model is ready to be simulated connected to the power plant model under study. The procedure is illustrated in Figure 4.1.

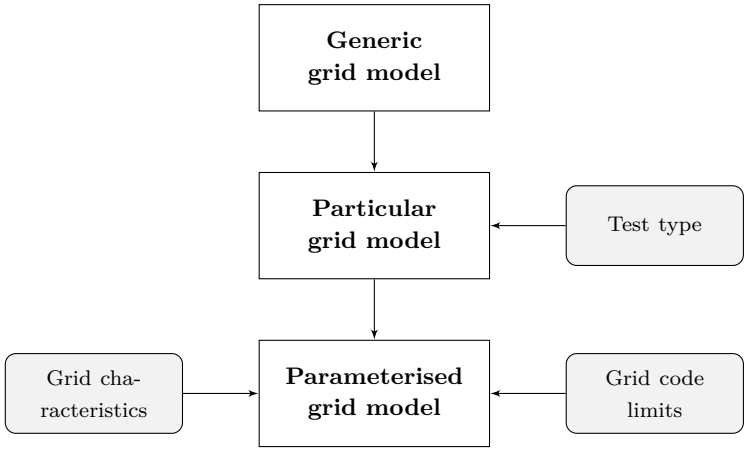


**Figure 4.1. General grid power modelling procedure**

### 4.2.1 Generic grid model

Power system models must represent all the elements in the system in order to replicate the performance of the power grid: power plants to generate electricity, transmission and distribution lines to transfer electricity and loads as final consumers. The premises of the grid model are to be generic, simple and valid for a wide range

of operation scenarios and system topologies and characteristics. The T-shaped simple grid model in Figure 4.2 meets all the requirements. It is partially based on the model included in the Spanish PVVC procedures [117]. *Generator 1* represents the bulk power system, while *Generator 2* serves to introduce neighbouring generator influence to the PCC. Electrical distances are limited by series impedances $Z_{l1}$ and $Z_{l2}$. Finally, a load is included in order to model demand and establish power flow.

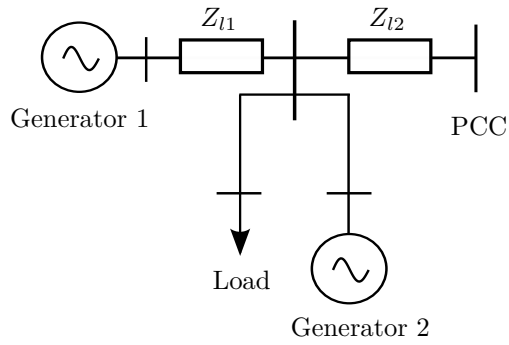


**Figure 4.2. Generic grid test model**

### 4.2.2 Particular grid model

Depending on the test event under study, the generic test model can be simplified regarding its topology. In some cases, only a generator is necessary; in other cases, line impedances can be avoided. Particular grid models of each of the phenomena under study are proposed in this thesis, based on theoretical analysis and sensitivity studies.

### 4.2.3 Parameterised grid model

Based on the equations ruling the operation of the particular grid model for the disturbance under study, the parameters of the model must be adjusted so as to obtain limit values imposed by interconnection regulation. However, the objectives of the methodology hereby presented are twofold. The methodology serves to verify grid code fulfilment, but also as simple test circuit to reproduce the operation of the power system under analysis. Therefore, under the latter assumption, the parameterisation of the particular grid model can be based on system data. If information about the complete detailed model is available, reduction or equivalencing techniques can be applied, in order to obtain a parameterised equivalent grid model. If not, the parameterisation can be based on the static data at the PCC, i.e. voltage level and short-circuit power, which are usually publicly provided by system operators. Dynamic parameters of generating systems can be based on typical values.

## 4.3 Practical implementation of the proposed methodology

The methodology described in Section 4.2 constitutes the theoretical framework, which must be adapted to the power system topology and characteristics, as well as operation scenarios and limit values. This thesis focuses on weak power grids regarding isolated systems. Hence, the test circuit has to cover most common operation situations and practices, as well as critical technical requirements to be met by generation assets there. So, selected compliance tests are hereby listed and described. Finally, the practical application of the methodology is explained.

### 4.3.1 Definition of the grid code compliance tests

Compliance testing is performed by certified test laboratories, in order to prove compliance of the equipment with national, international, or industry standards. In this thesis, equipment under test are generation assets based on renewable energy sources. Compliance verification requires a limited number of well-defined and carefully executed reproducible tests. Therefore, tests must be divided into simple items including a straight-forward description, a valid verification procedure and pass/fail objectives. In other words, what to assess, how to assess and passing criteria shall be indicated.

#### 4.3.1.1 Frequency Ride-Through

Frequency ride-through is related to the ability of generating units to remain connected during frequency excursions. Frequency deviations during dynamic operation are mainly due to power mismatch events or short-circuit faults. Six tests have been defined related to dynamic frequency requirements, based on most frequent requirements in the reviewed grid codes. Figure 4.3 illustrates the frequency ride-through requirement.

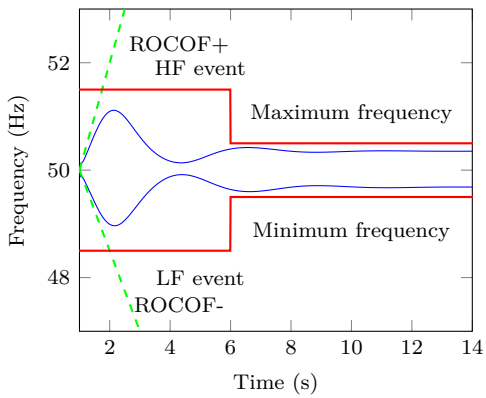


**Figure 4.3. Frequency ride-through limits**

1. **Maximum frequency**: ability of a power generating unit to remain connected under frequencies above rated value. Parameter: $f_{max}$.
2. **Minimum frequency**: ability of a power generating unit to remain connected under frequencies below rated value. Parameter: $f_{min}$.
3. **High frequency event**: ability of a power generating unit to remain connected with an overfrequency event during a determined time period. Some grid codes may include more than one high frequency event. Parameters: $f_{ss,h}$ *and time*.
4. **Low frequency event**: ability of a power generating unit to remain connected with an underfrequency event during a determined time period. Some grid codes may include more than one low frequency event. Parameters: $f_{ss,l}$ *and time*.
5. **Positive Rate-of-Change-of-Frequency (ROCOF)**: ability of a power generating unit to remain connected with a positive ROCOF with increasing frequency. Parameter: $+ROCOF$.
6. **Negative ROCOF**: ability of a power generating unit to remain connected with a negative ROCOF with decreasing frequency. Parameter: $-ROCOF$ .

These tests must be carried out with the frequency response control disabled.

#### 4.3.1.2 Frequency Response

Some grid codes include the requirement of providing primary frequency control based on droop with a certain dead-band for high frequencies. In some cases, the frequency response feature even encompasses low frequency situation, so that generating units must increase their output. For renewable generation, this is not always possible as it depends on the primary energy availability, and in any case, it requires previous operation at a curtailed power output. Figure 4.4 illustrates frequency response based on droop characteristic.

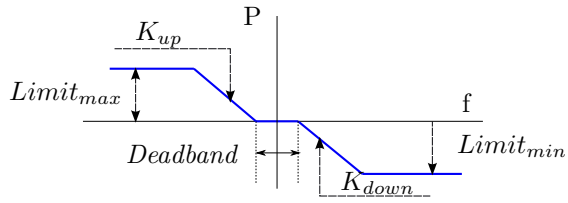


**Figure 4.4. Frequency droop response**

Inertia-based frequency response is out of the scope of this thesis, as it is seldom a requirement, but a future trend in grid codes under study.

Two tests have been defined related to frequency response requirement.

1. **Primary frequency control for high frequencies**: ability of a power generating unit to decrease the power output for frequencies above rated value. Parameters: $K_{down}$, $Limit_{min}$, *deadband*.
2. **Primary frequency control for low frequencies**: ability of a power generating unit to increase the power output for frequencies under rated value. Parameters: $K_{up}$, $Limit_{max}$, *deadband*.

#### 4.3.1.3 Low Voltage Ride-Through

Fault ride-through requirement is based on the capability of generating units to remain connected under faults. LVRT is related to voltage dips, mainly caused by short-circuit faults. During balanced faults, all faulted phases undergo undervoltage. On the other hand, unbalanced faults result in undervoltage in the faulted phases, but also in overvoltage in the healthy phases. Figure 4.5 illustrates the LVRT requirement, including main characteristic profiles found in literature. Three main characteristics can be found: square dips determined by a lowest voltage value, step profiles emulating protection settings with definite trip times, and envelopes with a ramp recovery (polygonal profile), which best match voltage dips with a smooth recovery.

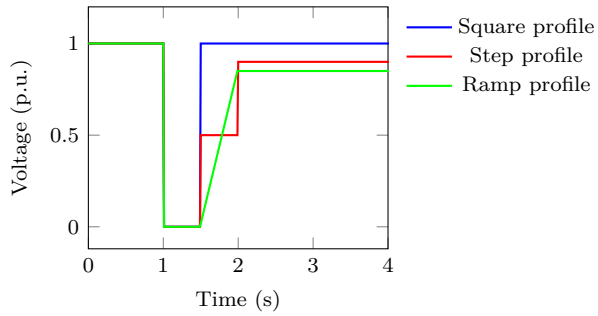


**Figure 4.5. LVRT profiles**

Two tests have been defined regarding LVRT requirements, based on the most relevant grid codes.

1. **Balanced Low Voltage Ride-Through**: ability of a power generating unit to remain connected during a symmetrical voltage dip. Parameters: either *voltage dip magnitude and time* or *a voltage against time profile*.
2. **Unbalanced Low Voltage Ride-Through**: ability of a power generating unit to remain connected during an asymmetrical voltage dip. Parameters: either *voltage dip magnitude and time* or *a voltage against time profile*.

#### 4.3.1.4 Output current during faults

It is related to the LVRT requirement. Some regulations require active support during faults from renewable generation, besides remaining connected. Four tests have been defined, based on the most relevant grid codes.

1. **Active current injection during balanced faults**: ability of a power generating unit to generate active power during a balanced fault, in order to support system stability. Parameter: *active current injection profile (current against voltage)*. Figure 4.6 illustrates an active current injection characteristic during undervoltage, based on three reference points: $(V_{a1}, I_{a1})$, $(V_{a2}, I_{a2})$, $(V_{a3}, I_{a3})$. Dashed lines indicate maximum and minimum limits that are included in some grid codes such as in the SEIE.
2. **Active current injection during unbalanced faults**: ability of a power generating unit to generate active power during an unbalanced fault, in order to support system stability. Parameter: *active current injection profile (current against voltage)*.
3. **Reactive current injection during faults**: ability of a power generating unit to generate/absorb reactive power during a fault, in order to support system stability. Parameter: *reactive current injection profile (current against voltage)*. Figure 4.7, based on the Spanish grid code, illustrates reactive current injection characteristic during undervoltage and overvoltage, based on several reference points: $(V_{q1}, I_{q1})$, $(V_{q2}, I_{q2})$, $(V_{q3}, I_{q3})$,..., $(V_{q7}, I_{q7})$.
4. **Reactive current injection during unbalanced faults**: ability of a power generating unit to generate active power during an unbalanced fault, in order to support system stability. Parameter: *reactive current injection profile (current against voltage)*.

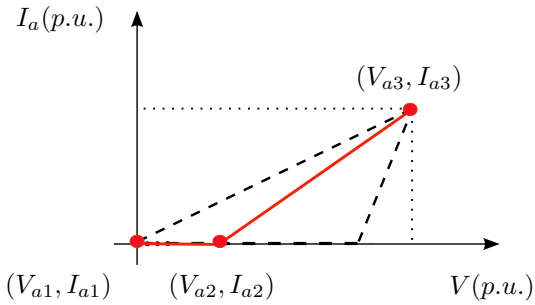


**Figure 4.6. Active current injection requirement**

#### 4.3.1.5 Unbalance requirement

Voltage and current unbalance are mainly caused by unbalanced power generation sources, short-circuit faults, series faults, and unbalanced loading. Two tests have been defined related to unbalance requirement.

1. **Voltage unbalance**: ability of a power generating unit to remain connected during a voltage unbalance. Parameter: Voltage Unbalance Factor (VUF).
2. **Current unbalance**: ability of a power generating unit to remain connected during a voltage unbalance. Parameter: Current Unbalance Factor (CUF).

Frequency protection functions and frequency response be must disabled.

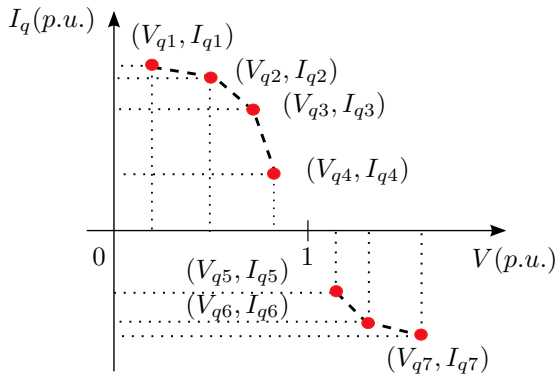


**Figure 4.7. Reactive current injection requirement**

#### 4.3.1.6 Synthesis of the grid code compliance tests

Table 4.2 summarises the grid code compliance tests, indicating a test identification code that is used later in the practical application cases in Chapter 8, Chapter 9 and 10.

**Table 4.2. Synthesis of grid code compliance tests**

| Id | Compliance test |
|---|---|
| A1 | Maximum frequency |
| A2 | Minimum frequency |
| A3 | High frequency event |
| A4 | Low frequency event |
| A5 | Positive ROCOF |
| A6 | Negative ROCOF |
| A7 | Primary frequency control for high frequencies |
| A8 | Primary frequency control for low frequencies |
| B1 | Balanced LVRT |
| B2 | Unbalanced LVRT |
| B3 | Active current injection during balanced fault |
| B4 | Reactive current injection during balanced faults |
| B5 | Active current injection during unbalanced faults |
| B6 | Reactive current injection during unbalanced faults |
| C1 | Voltage unbalance |
| C2 | Current unbalance |

For remain connected requirements, two events must be simulated by adjusting the simplified equivalent grid for each of the compliance tests: an event outside the permitted range in the grid code (indicated suffix -1 in test identificator, e.g. A1-1), and an event within the permitted range (indicated suffix -2 in test identificator, e.g. A1-2). For active support requirements, generator contribution must be showed by simulating an event within limits (suffix -2).

### 4.3.2 Application of the methodology

After the generic grid model has been particularised and parameterised, the generation system model under verification or study has to be included in the complete set-up so as to carry out the simulation. The electrical configuration of the whole system is described in Figure 4.8, where the wind farm is connected to the grid at the PCC by means of a step-up transformer and an interconnection line. The connecting network is represented by a grid equivalent, which corresponds to the parameterised grid model. Regarding other generation technologies, the wind farm shall be replaced, but the layout in Figure 4.8 is valid.

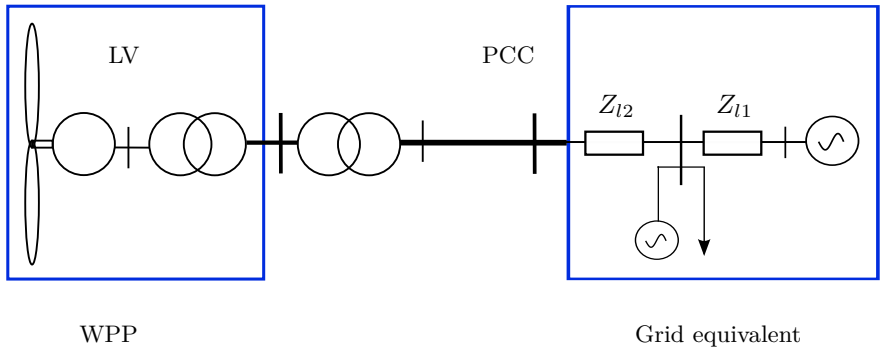


**Figure 4.8. Single-line scheme for the application of the methodology**

The generation asset model must include the complete model of the renewable generation power plant, including the generating units (generator and control models), as well as the cables connecting the units and the interconnection interface with the external network (until the PCC), as some operation performance indexes must be verified at the connecting point. If the validation methodology is to be applied during a grid code compliance certification, the simulation model is expected to meet the system operator requirements concerning model detail as seen in Chapter 3. In some cases, aggregated models are accepted for representing the whole generation system.

## 4.4 Validation of the proposed methodology

The power system target type in this thesis are island power grids, defined as weak networks without significant external interconnection. Therefore, the proposed methodology must be validated by real study cases.

Three possible cases can be made out regarding the objectives of the methodology, size of the island, available data and grid code under force, summarised in Table 4.3. The rule for the island size is based on [14].

- **Case 1**. It is a general case regarding a medium size isolated power grid with unknown dynamic system data nor grid code under force.

- **Case 2**. Medium size isolated power grid with known dynamic system data but no grid code under force.
- **Case 3**. Bigger size isolated power grid with known dynamic system data and grid code under force.

**Table 4.3. Summary of study cases for the validation of the methodology**

| Case | Size | Static data | Dynamic data | Grid code |
|---|---|---|---|---|
| **Case 1** | Medium | ✓ | $\chi$ | $\chi$ |
| **Case 2** | Medium | ✓ | ✓ | $\chi$ |
| **Case 3** | Big | ✓ | ✓ | ✓ |

The connection point of study, where the renewable energy source installation is to be located, must be known. Hence, the voltage level and short-circuit power at the PCC are provided by the system operator. If dynamic data about the target power grid is missing, typical values on other similar size islands can be used. Besides, some islands, because of their small size or low penetration of RES, have no interconnection rules for generation assets. However, some limits can be set after a deep study of the power grid, with both steady-state and dynamic analyses, requirements from other similar systems can be adopted, or typical operation can be emulated following the same adjustment methodology.

The general certification procedure is outlined in Figure 4.9, where depending on the requirement the pass or fail condition means remaining connected (remain connected requirements), or contributing actively to support the system (active support requirements).

The validity of the parameterised model shall be verified by checking if the generated disturbance meets the grid code limits. If the model is used for integration studies and a detailed model of the power system is available, simulation results of the complete and simplified grid models have to be compared, so as to verify whether the error is within acceptable ranges. The limit accuracy error between theoretical and simulation model has been set to 10 % in this thesis, based on Australian [122] and Danish [71] regulation.

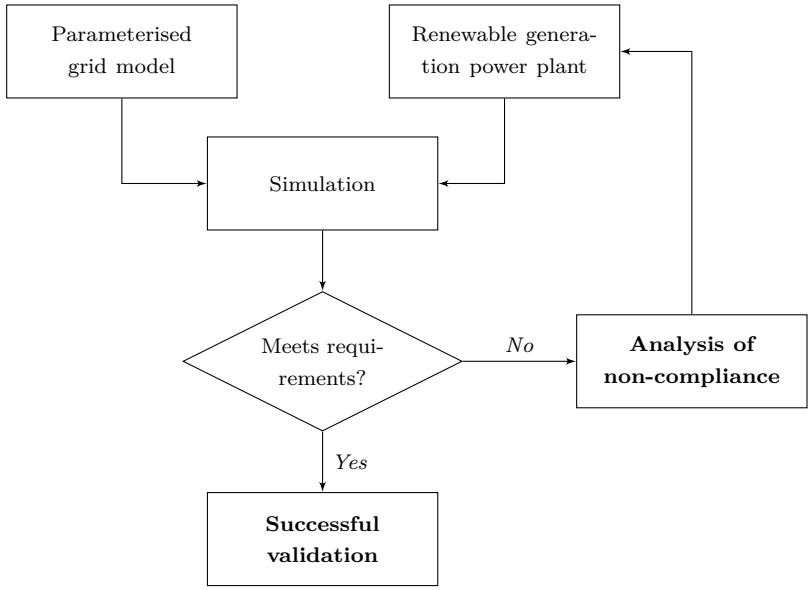


**Figure 4.9. General renewable generation plant verification procedure**

# Chapter 5

# Frequency Ride-Through

## 5.1 Introduction

Frequency in power systems is related to the balance between generation and demand. So, any imbalance in active power results in a frequency deviation. If a large load is suddenly connected to (or disconnected from) the power system, or if a generating unit is suddenly disconnected by the protection equipment, the frequency in the system changes: when load exceeds the generating capacity, frequency drops; otherwise, frequency rises.

A model to estimate frequency deviation after a power mismatch event is essential for adjusting frequency relays in load shedding schemes, estimating the amount of necessary spinning reserve, or calculating the amount of load reconnection or wind power generation [123]. In this thesis, it is used to reproduce usual frequency deviations in island power grids and to verify the grid code compliance of renewable power plants.

The present chapter reviews analytical models to characterise frequency deviation and is organised as follows. In Section 5.2, characteristic parameters regarding frequency deviations are defined. In Section 5.3, frequency dips are studied considering a unique generating unit and the whole power system. As a result, a particular grid model able to emulate frequency excursions is introduced in Section 5.4, simplifying the initially proposed model following a sensitivity study. Finally, in Subsection 5.4.3 the formulae leading to the parameterised grid model are presented.

## 5.2 Frequency dip definition

The response of a power system to a power imbalance can be described in four stages, depending on the duration of the dynamics involved [124]: rotor swings in generators, frequency drop, primary control by turbine-governor systems, and secondary control by central regulators.

After the first stage of rotor swings, the power imbalance results in an increase or a decrease in frequency depending on the generation-load unbalance. The frequency rises or decays with a constant slope, since still no primary frequency control action takes place. The participation of each generator during this stage depends on its

inertia. The lower the inertia, the faster is the frequency variation. Later, primary controls of turbine-governor systems act and try to recover the balance. The contribution of each generator is basically a function of its governor droop, the speed of the turbine-governor system response and the amount of available spinning reserve. Finally, within a time frame of one or several minutes, secondary control action and energy supply system dynamics prevail in frequency dynamics.

In the present study, focus is put on primary frequency regulation, because low values of frequency can be attained in isolated power grids before secondary regulation reacts due to the high presence of Diesel engines. Figure 5.1 shows the evolution of frequency after a power unbalance and the effect of the primary regulation action. As it is shown, a frequency drop event shows three main characteristic parameters: **Rate-Of-Change Of Frequency** (ROCOF) between points A and B, **minimum frequency** ($f_{min}$) also called **frequency nadir** at point B, and the **steady-state frequency deviation** ($\Delta f_{ss}$) at point C.

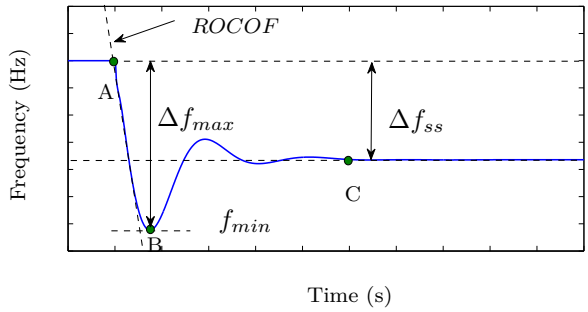


**Figure 5.1. Frequency deviation after an active power mismatch**

In case of a frequency rise, a frequency maximum appears at point B and a positive steady-state frequency deviation is obtained as a result of primary frequency response.

## 5.3 Theoretical analysis

The aggregate load-frequency behaviour following load-generation imbalance in isolated power systems can be represented by System Frequency Response models. Following are introduced SFR models for single generating units, and for systems made up of several generating units, as cornerstones to the simplified model which is proposed in this thesis for frequency ride-through requirement.

### 5.3.1 System frequency response model for a single generating unit

SFR models for estimating frequency response are based on power generating unit's and load's response to a change in electric power. A detailed model of a generating

unit results into a high-order transfer function, which complicates the computation of frequency response. As a first simplifying hypothesis, the generator excitation is not represented in the SFR model and the level of excitation is assumed constant [125], since mainly turbine-governor systems affect short-term frequency dynamics [126].

Mechanical and electrical characteristics of synchronous machines considered in stability and frequency response studies are based on the equation of motion or swing equation indicated in (5.1).

$$\frac{2 \cdot H}{\omega_s} \cdot \frac{d^2\delta}{dt^2} = T_m - T_e - \frac{K_D}{\omega_s} \cdot \frac{d\delta}{dt} \tag{5.1}$$

where $H$ is the inertia constant, defined as the kinetic energy in watt-seconds at rated speed divided by the VA base, $\omega_s$ is the rated angular speed, $T_e$ electromagnetic torque in $N \cdot m$, $T_m$ mechanical torque in $N \cdot m$, $K_D$ damping factor in p.u. torque / p.u. speed deviation and $\delta$ generator angle in $rad$.

Rewriting (5.1) in terms of power:

$$2 \cdot H \cdot \frac{d^2\delta}{dt^2} = P_m - P_e - K_D \cdot \frac{d\delta}{dt} \tag{5.2}$$

In general, power system loads are a composite of a variety of electrical devices. Electrical power for resistive loads is independent of frequency. But in the case of motor loads, electrical power changes with frequency to changes in motor speed. The overall frequency-dependent characteristic of composite load may be expressed as:

$$P_e = P_l + D \cdot \omega \tag{5.3}$$

where $P_l$ is non-frequency sensitive load, $D \cdot \omega$ frequency-sensitive load and $D$ the load-damping constant. The damping constant is expressed as a percent change in load for one percent change in frequency. Typical values of D are 1 to 2 percent. A value of $D$ =2 means that a 1 % change in frequency would cause a 2 % change in load [127].

Prime mover models are high-order. However, by simplifying the model of the turbine-governor system, the computational cost can be remarkably reduced. Hence, some simplifying hypothesis are assumed in the literature. These assumptions consist on ignoring slow system dynamics, non-linearities in the system and reducing transfer function order of the models, e.g. by considering contribution to frequency response of poles close to origin is negligible, and close zero-pole pair cancellation if within unity circle. Hence, most systems can be approximated by a first or second order equivalent function. Typically, steam-driven turbines can be modelled by first-order transfer functions, whereas gas-driven or diesel-driven combustion turbines might require second-order models [125].

In the literature, mostly reheat-type steam boiler plants have been considered. A second-order equivalent transfer function is proposed in [127], whereas [125] is based on a first-order function. Both authors apply some of the abovementioned simplifying hypothesis. However, both models have the drawback that they only apply to reheat steam turbine type generation. On the other hand, [123] and [126] propose valid models for a variety of generation technologies with different governors, fitting the response of any detailed generating unit model into an equivalent low-order model (first-order and second-order correspondingly) by means of parameter estimation. [126] includes also generator power-output limitations, yielding into a non-linear model.

Let us consider the generic second-order transfer function of a prime mover in (5.4), as proposed in [126].

$$K_i \cdot \frac{1 + b_{1,i} \cdot s + b_{2,i} \cdot s^2}{1 + a_{1,i} \cdot s + a_{2,i} \cdot s^2} \tag{5.4}$$

The parameter $K_i$ represents the gain of the turbine-governor system, which is usually the inverse of the governor droop. The parameters $a_{1,i}$, $a_{2,i}$, $b_{1,i}$ and $b_{2,i}$ correspond to the dominant poles and possible zeros of the turbine-governor system. In [123] and [126] some (or all) of the coefficients are adjusted such that the response of the model resembles as much as possible the response of the complete model of a turbine-governor system. Optionally, these parameters can also be obtained from field tests. Table 5.1 summarises some simplified models proposed in literature based on the generic second-order transfer function.

**Table 5.1. Synthesis of simplified models for prime movers**

| **Reference** | $K_i$ | $b_{1,i}$ | $b_{2,i}$ | $a_{1,i}$ | $a_{2,i}$ |
|---|---|---|---|---|---|
| Kundur [127] | $1/R_i$ | $\mathrm{F}_{HP} \cdot \mathrm{T}_{RH}$ | 0 | $\mathrm{T}_{RH}+\mathrm{T}_{CH}$ | $\mathrm{T}_{RH} \cdot \mathrm{T}_{CH}$ |
| Anderson [125] | $1/R_i$ | $\mathrm{F}_{HP} \cdot \mathrm{T}_{RH}$ | 0 | $\mathrm{T}_{RH}$ | 0 |
| Egido [123] | $1/R_i$, tunable | 0 | 0 | Tunable | 0 |
| Sigrist [126] | $1/R_i$ | Tunable | Tunable | Tunable | Tunable |

Based on Anderson model for a reheat-type steam boiler plant, the main parameters for frequency characterisation can be calculated as indicated in (5.5) for ROCOF, in (5.6) for frequency deviation in steady-state ($\Delta f_{ss}$) and in (5.9) for frequency minimum.

**Initial ROCOF or frequency gradient**

$$\lim_{t \to 0} ROCOF = \frac{P_0}{2 \cdot H} = \frac{P_0}{M} \tag{5.5}$$

**Frequency deviation in steady-state**

$$\Delta f_{ss} = \lim_{t \to +\infty} \Delta\omega(t) = \frac{R \cdot P_0}{D \cdot R + K_m} = \frac{P_0}{D + \dfrac{K_m}{R}} \tag{5.6}$$

In some references $K_m = 1$ is assumed [127]. Hence, (5.6) can be further simplified:

$$\Delta f_{ss} = \frac{P_0}{D + \dfrac{1}{R}} \tag{5.7}$$

**Frequency minimum** Minimum frequency is attained when the derivative of frequency deviation (ROCOF) equals zero. That happens at instant $t_{min}$:

$$t_{min} = \frac{\arctan(\dfrac{\omega_r}{\varsigma \cdot \omega_n}) - \phi}{\omega_r} \tag{5.8}$$

Hence, frequency nadir or minimum frequency shall be calculated as:

$$f_{min} = \Delta\omega(t_{min}) = \left(\frac{R \cdot P_0}{D \cdot R + K_m}\right) \cdot \left[1 + \alpha \cdot e^{-\varsigma \cdot \omega_n \cdot t_{min}} \cdot \sin(\omega_r \cdot t_{min} + \phi)\right] \tag{5.9}$$

where:

$$\omega_n^2 = \frac{R \cdot D + K_m}{2 \cdot H \cdot T_{RH} \cdot R} \tag{5.10}$$

$$\varsigma = \frac{2 \cdot H \cdot R + T_{RH} \cdot (D \cdot R + K_m \cdot F_{HP})}{2 \cdot (D \cdot R + K_m)} \cdot \omega_n \tag{5.11}$$

$$\alpha = \sqrt{\frac{1 - 2 \cdot T_{RH} \cdot \varsigma \cdot \omega_n + T_{RH}^2 \cdot \omega_n^2}{1 - \varsigma^2}} \tag{5.12}$$

$$\omega_r = \omega_n \cdot \sqrt{1 - \varsigma^2} \tag{5.13}$$

$$\phi = \phi_1 - \phi_2 = tan^{-1}\left(\frac{\omega_r \cdot T_{RH}}{1 - \varsigma \cdot \omega_n \cdot T_{RH}}\right) - tan^{-1}\left(\frac{\sqrt{1 - \varsigma^2}}{-\varsigma}\right) \tag{5.14}$$

Initial rate of change of frequency and steady-state frequency do not strongly depend on prime mover parameters. However, minimum frequency strongly depends on the transfer function of the turbine-governing system. [123] proposes a methodology to calculate minimum frequency after generation loss in a power system valid for

any type generation technology, in which speed governor and prime mover detailed models are replaced by a first-order model as represented in Figure 5.2:

$$P_m = \frac{k}{T \cdot s + 1} \cdot \Delta\omega \tag{5.15}$$

where $T$ is the time constant and $k$ the gain of the transfer function.

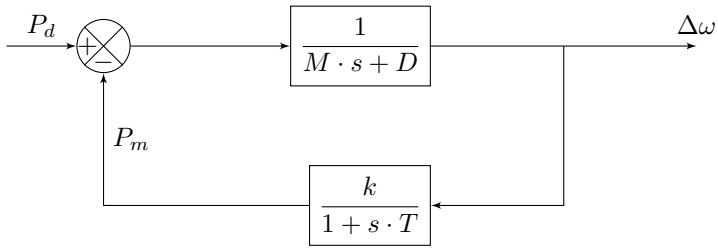


**Figure 5.2: Reduced block diagram of a generic power plant based on a first-order function**

The values of parameters $k$ and $T$ of the first order transfer function are obtained by fitting the response of the model to the response of the detailed model whose behaviour is intended to be reproduced. Two ways of obtaining these parameters are proposed in [123]. On one hand, $k$ can be calculated from the detailed model to obtain the same droop, as indicated by (5.16).

$$k = \frac{1}{R} = \frac{P_0}{\Delta f_{ss}} \tag{5.16}$$

Then, $T$ can be estimated by fitting the response of the first-order model to the detailed model. Non-linear regression technique can be used for that purpose. Frequency minimum happens in the first seconds after the generation loss. So, short-term behaviour is of interest. To improve the fitting in those first seconds after the disturbance, parameters are computed taking into account only the first seconds of data. Alternatively, both $k$ and $T$ can be estimated using a non-linear regression technique, resulting in a better minimum frequency estimation.

Frequency response for the approximated first-order model can be obtained solving the equation in (5.17) using the inverse Laplace transform. Frequency response in both Laplace and time domain is indicated by (5.17) and (5.18).

$$\Delta\omega(s) = \frac{P_0 \cdot (1 + T \cdot s)}{2 \cdot H \cdot T \cdot s^2 + (2 \cdot H + D \cdot T) \cdot s + (D + K)} \tag{5.17}$$

$$\Delta\omega(t) = \frac{P_0}{D + k} \cdot \left[1 + \frac{e^{-\varsigma \cdot \omega_n \cdot t}}{\sqrt{1 - \varsigma^2}} \cdot (T \cdot \omega_n \cdot sin(\omega_r \cdot t) - sin(\omega_r \cdot t + \theta_1))\right] \tag{5.18}$$

where:

$$\theta_1 = acos(\varsigma) \tag{5.19}$$

$$\omega_n = \sqrt{\frac{D+k}{2 \cdot H \cdot T}} \tag{5.20}$$

$$2 \cdot \varsigma\omega_n = \frac{2 \cdot H + T \cdot D}{2 \cdot H \cdot T} \tag{5.21}$$

$$\omega_r = \omega_n \cdot \sqrt{1-\varsigma^2} \tag{5.22}$$

It results in an initial frequency gradient equal to that calculated in (5.5), i.e. $ROCOF = P_0/M$. The steady-state frequency deviation results from solving (5.23).

$$\Delta f_{ss} = \frac{P_0}{D+k} \tag{5.23}$$

On the other hand, the frequency minimum is attained at instant $t_{min}$.

$$t_{min} = \frac{1}{\omega_r} \cdot atan\frac{\omega_n \cdot T \cdot \sqrt{1-\varsigma^2}}{\omega_n \cdot T \cdot \varsigma - 1} \tag{5.24}$$

However, [123] proposes a simple method to obtain the frequency minimum. Indeed, to compute the maximum frequency deviation the important effect is the output of the turbine-governor in the first seconds after the loss of generation, when the prime mover is excited by a quasi-linear decay of frequency which corresponds to a ramp-like input. Then, the input to the prime mover system can be modelled by 5.5 and the closed-loop can be broken yielding to the model in Figure 5.3.

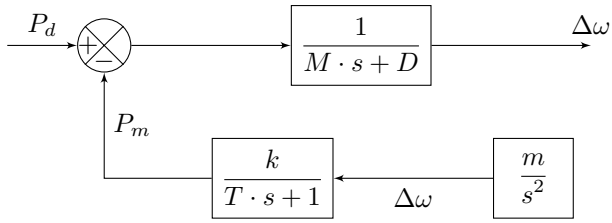


**Figure 5.3: Reduced block diagram of a generic power plant based on a first-order function**

Defining a ramp gain $C$, maximum frequency deviation can be expressed as:

$$\Delta\omega_{max} = \frac{P_0}{2 \cdot C} \tag{5.25}$$

where $C$ is a value between 0 and $k$. The maximum value for $C$, $C_{max}$, is the value at the instant in which frequency is minimum ($t_{min}$), which is pointed out by Egido as the most suited value.

The following non-linear equation system has to be solved:

$$\begin{cases} C = k \cdot \left[1 - \dfrac{T}{t_{min}} \cdot \left(1 - e^{-t_{min}/T}\right)\right] & (5.26) \\ t_{min} = \dfrac{2 \cdot H}{C} & (5.27) \end{cases}$$

Any iterative numerical method, such as Newton-Raphson, can be employed to solve the equation system formed by (5.26) and (5.27). [123] proposes a further simplification consisting in assuming a typical value for $t_{min}$ and obtain a sensible value for the ramp gain $C$.

### 5.3.2 System frequency response model for the whole power system

The response of the power system is driven by the response of all connected generating units and depends furthermore on the extension of the network, connected loads, etc. However, in small isolated power systems, the influence of the network on short-term frequency dynamics and especially on inter-machine oscillations is usually negligible [126], [128]. Neglecting inter-machine oscillations in short-term frequency dynamics by neglecting synchronising power and transmission performance results in an average or uniform frequency. Therefore, the network can be omitted, and load demand and power generation can be considered as concentrated on a single bus.

Initial frequency gradient and steady-state frequency deviation can be calculated for a given generator using (5.5) and (5.6), regardless of the prime mover technology. As power systems are composed of multiple parallel generating units, both parameters can be computed using a composite regulating model with an equivalent regulation $R_{eq}$, system inertia $H_{eq}$ and system load damping $D$.

**Initial ROCOF or frequency gradient** In a power system with multiple generators, when some generation is lost, system frequency starts to drop. Assuming that all generators remain in synchronism, they slow down at approximately the same rate.

$$ROCOF = \frac{P_{0,T}}{2 \cdot \sum_{i=1}^{n} \dfrac{H_i \cdot S_i}{S_T}} = \frac{\Delta P_0}{2 \cdot H_{eq}} \tag{5.28}$$

where $H_{eq}$ is the equivalent inertia constant of a power system made up of multiple generating units.

**Frequency deviation in steady-state** When two or more generators with droop governor characteristics are connected to a power system, there is a unique frequency at which they share a load change.

By representing the system with a single equivalent generator, equivalent droop can be calculated as:

$$R_{eq} = \frac{P_{Neq}}{\sum_{i=1}^{n} \frac{P_{Ni}}{R_i}} \tag{5.29}$$

As $P_{Neq} = \sum_{i=1}^{n} P_{Ni}$:

$$R_{eq} = \frac{1}{\sum_{i=1}^{n} \frac{1}{R_i}} \tag{5.30}$$

Thus, the composite power/frequency characteristic of a power system depends on the combined effect of the droops of all generator speed governors. It also depends on the frequency characteristics of all the loads in the system. For a system with n generators and a composite load-damping constant of $D$, the steady-state frequency deviation following a total active power change in the system $\Delta P_{0,T}$ is given by:

$$\Delta f_{ss} = \frac{P_{0,T}}{(1/R_1 + 1/R_2 + \cdots + 1/R_n) + D} = \frac{\Delta P_0}{1/R_{eq} + D} \tag{5.31}$$

It has been assumed that the speed-droop characteristic of an individual generator unit is linear over the full range of power and frequency variations. In practice, the output power of each turbine is limited by its technical parameters. If a turbine is operating at its upper power limit, then a decrease in the system frequency does not produce a corresponding increase in its power output. Consequently, the generation characteristic of the system is dependent on the number of units operating away from their limit at part load, i.e. on the *spinning reserve* [124].

**Frequency minimum** Power systems are composed of multiple parallel generating units, and frequently there are several characteristic types of generation each possessing a distinct dynamic response. Therefore, each generating unit should be modelled separately to exactly calculate its frequency behaviour in the system. So, the SFR model would be of high order, and its performance a very complex function of many system variables. Therefore, following levels of simplification have been proposed in the literature to compute frequency response in a power system. Chan proposes in [129] a delay model to represent the valve motion (fast time constants) and a canonical model for each turbine slow time constants. Anderson considers all generators in the power system to be identical [125]: identical technology and identical parameter values. Therefore, they can be replaced by an equivalent generating unit. Aik considers all generators in the power system to be of identical technology or dynamic

response structure, but with different values of parameters [130]. Egido considers all generator with governor and prime mover systems represented by linear first-order systems, resulting in a non-linear *N+1* equation system [123]. The aim of the method is the calculation of the minimum frequency in the system. Sigrist proposes a non-linear multi-generator SFR model, with equivalent inertia and the whole generation and load demand connected to the same bus [126]. Turbine-governor systems are represented by first or second order systems.

Following, frequency minimum calculation has been developed using methods proposed by Anderson, Aik and Egido, which are the most straightforward method to estimate the value of frequency minimum. The selected SFR models are all linear and do not take into account the generator output limitations. Therefore, they are only valid for small disturbances [126].

For a power system with $n$ simplified reheat steam generators, frequency deviation is:

$$\sum_{i=1}^{n} 2 \cdot H_i \cdot s \cdot \Delta\omega = \left[ \sum_{i=1}^{n} P_{SP,i} - \sum_{i=1}^{n} \left( \frac{K_{m,i}}{R_i} \cdot \frac{1 + F_{HP,i} \cdot T_{RH,i} \cdot s}{1 + T_{RH,i}} \right) \cdot \Delta\omega \right] - \sum_{i=1}^{n} P_{e,i} \tag{5.32}$$

where $H_i$ is the inertia constant of generating unit $i$, $\Delta\omega$ represents frequency deviation in the system, $P_{SP,i}$ the individual active power set-point, $K_{m,i}$ the individual effective gain constant, $R_i$ the individual droop constant, $F_{HP,i}$ the fraction of power generated by the high pressure section in each turbine, $T_{RH,i}$ the time constant of the reheater of each unit, and $P_{e,i}$ the individual electrical power. All parameters must be expressed on a common base.

In this case, only a change in $P_e$ ($\Delta P_{SP} = 0$) is of interest. Hence, a new system input variable $P_d$ can be defined, which is positive for a generation power increase (or load decrease) and negative for a load increase (or generation decrease). In addition, the inertial-load dynamic response of the whole system is represented by an equivalent inertia $H_{eq}$ and equivalent damping constant $D$ and (5.32) can be simplified as follows:

$$(2 \cdot H_{eq} \cdot s + D) \cdot \Delta\omega = \sum_{i=1}^{n} \left( \frac{K_{m,i}}{R_i} \cdot \frac{1 + F_{HP,i} \cdot T_{RH,i} \cdot s}{1 + T_{RH,i} \cdot s} \right) \cdot \Delta\omega - P_d \tag{5.33}$$

If total power mismatch in the system is $P_{0,T}$, frequency deviation can be computed as:

$$\Delta\omega = \frac{-P_{0,T}(s)}{(2 \cdot H_{eq} \cdot s + D)} \cdot \frac{1}{1 + \sum_{i=1}^{n} \frac{K_{m,i}}{R_i} \cdot \frac{1 + F_{HP,i} \cdot T_{RH,i} \cdot s}{1 + T_{RH,i} \cdot s}} \tag{5.34}$$

Anderson assumes that every generator has an identical dynamic response (all turbine-governor parameters are identical), but different governor droops [125]. Hence:

$$\Delta\omega = \frac{-P_{0,T}(s)}{(2 \cdot H_{eq} \cdot s + D)} \cdot \frac{1}{1 + \frac{K_m \cdot (1 + F_{HP} \cdot T_{RH} \cdot s)}{1 + T_{RH} \cdot s} \cdot \sum_{i=1}^{n} \frac{1}{R_i}} \tag{5.35}$$

Based on (5.30), the calculation of frequency deviation can be further simplified:

$$\Delta\omega = \frac{-P_{0,T}(s)}{(2 \cdot H_{eq} \cdot s + D)} \cdot \frac{1}{1 + \frac{K_m \cdot (1 + F_{HP} \cdot T_{RH} \cdot s)}{1 + T_{RH} \cdot s} \cdot \frac{1}{R_{eq}}} \tag{5.36}$$

Aik in [130] also considers that reheat steam-boiler plants are dominant in the power system, but with different values for parameters $R_i$, $F_{HP,i}$, $(1 - F_{HP,i})$, $T_{RH,i}$ and $K_{m,i}$. After a sudden load-generation imbalance represented by a step function of magnitude $P_{0,T}$, expressing the equation as a sum of partial fractions:

$$\Delta\omega(s) = P_{0,T} \cdot \sum_{i=1}^{n+1} \frac{A_i}{p_i} \cdot \left( \frac{1}{s} - \frac{1}{s - p_i} \right) \tag{5.37}$$

where $A_i$ is real or complex, $p_i$ is a root and may be real or a complex conjugate-pair. In time domain, the response of the $n + 1$ order SFR model is given by:

$$\Delta\omega(t) = P_{0,T} \cdot \sum_{i=1}^{n+1} \frac{A_i}{p_i} \cdot \left(1 - e^{p_i \cdot t}\right) \cdot U(t) \tag{5.38}$$

The nature of the load-frequency model response depends on the roots in (5.38). For all real roots, it is monotonically decreasing function of time, whereas if the roots have at least one complex-conjugate pair $\sigma \pm ujw_n$, the response is a damped sinusoidal function of time.

On the other hand, based on Egido in [123], frequency deviation evolution in time domain can be calculated as:

$$\Delta\omega(t) = \frac{P_0}{2 \cdot H_{eq}} \cdot t + \frac{1}{4 \cdot H_{eq}} \cdot \sum_{i=1}^{n} C_i \cdot m \cdot t^2 \tag{5.39}$$

Time for minimum frequency $t_{min}$ is calculated as:

$$t_{min} = \frac{P_0}{\sum_{i=1}^{n} C_i \cdot m} = \frac{2 \cdot H_{eq}}{\sum_{i=1}^{n} C_i} \tag{5.40}$$

And therefore, maximum frequency deviation is:

$$\Delta\omega_{max} = f_{min} = \frac{P_0}{2 \cdot \sum_{i=1}^{n} C_i} \tag{5.41}$$

If $C_{max,i}$ at the instant of $t_{min}$ is chosen as the value for $C_i$, it results into a non-linear $n+1$ equation system:

$$\begin{aligned} C_1 &= K_1 \cdot \left(1 - \frac{T_1}{t_{min}} \cdot \left(1 - e^{\frac{-t_{min}}{T_1}}\right)\right) \\ &\vdots \\ C_n &= K_n \cdot \left(1 - \frac{T_n}{t_{min}} \cdot \left(1 - e^{\frac{-t_{min}}{T_n}}\right)\right) \end{aligned} \tag{5.42}$$

Had all the $N$ units the same averaged ramp gain, $C_1 = C_2 = \cdots = C_N = C$, minimum frequency would be:

$$f_{min} = \frac{P_0}{2 \cdot N \cdot C} \tag{5.43}$$

Based on (5.41) or (5.43), an equivalent ramp gain constant can be defined, hereinafter called $C_{eq}$.

$$C_{eq} = \sum_{i=1}^{n} C_i = K_{eq} \cdot \left(1 - \frac{T_{eq}}{t_{min}} \cdot \left(1 - e^{\frac{-t_{min}}{T_{eq}}}\right)\right) \tag{5.44}$$

where $K_{eq} = \sum_{i=1}^{n} K_i$ and $T_{eq} = \sum_{i=1}^{n} T_i$.

Hence, (5.40) and (5.41) can be rewritten and so, a multi-generator system can be substituted by an equivalent generator with $K_{eq}$ and $T_{eq}$.

$$t_{min} = \frac{2 \cdot H_{eq}}{C_{eq}} \tag{5.45}$$

$$f_{min} = \frac{P_0}{2 \cdot C_{eq}} \tag{5.46}$$

Alternatively, frequency response can be analytically calculated based on this equivalent generating unit using inverse Laplace transform.

After the analysis of system frequency response model for a whole power system, it can be concluded that the calculation of initial frequency gradient and frequency deviation in steady-state is straightforward, while different methods have been proposed in the literature for the more complex frequency nadir calculation. Appendix A compares their performance based on some numerical examples.

## 5.4 Grid model and event representation

In this section, the generic grid model introduced in Chapter 4 has been particularised in order to characterise frequency response in isolated power systems, based on the theoretical analysis in Section 5.3 and taking into account the sensitivity of the grid model parameters. Finally, equations leading to the parameterisation of the particular grid model are presented.

### 5.4.1 Particular grid model

Based on the theoretical analysis, it can be concluded that only generator and load modelling are necessary to reproduce a frequency excursion after a power mismatch in a power system, as a unique frequency is considered in the whole power system. The particular grid model for frequency deviation is shown in Figure 5.4.

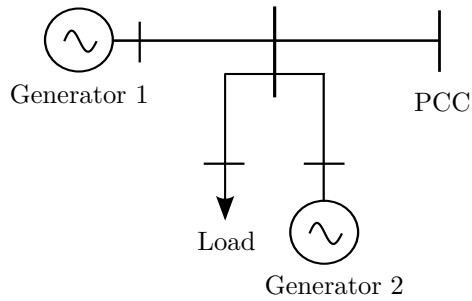


**Figure 5.4. Particular grid model for frequency analysis**

*Generator 2* represents the biggest generator on-line in the system and *Generator 1* is the equivalent of the rest of the generating units. Load influence in the system is represented by the aggregated load in Figure 5.4. Load aggregation can include frequency independent and frequency dependent load assets, characterised by the load damping factor. On the other hand, the power mismatch in the system can be reproduced with the disconnection of *Generator 2* for underfrequency events. If a frequency rise must be emulated, it can be done by partly disconnecting the load, composed by assets *Load 1* and *Load 2*. *Load 2* must be disconnected for overfrequency events. Alternatively, a load step can be simulated based on a single load asset.

If non-synchronous generation is installed in the power system (e.g. wind power), its impact can be included in the load modelling, represented as a negative load

omitting any dynamics [126]. Hence, decoupled power generation can be modelled as a generating unit, but with zero inertia $H_i$ and zero gain $K_i$. Or, as a negative load.

### 5.4.2 Sensitivity of the particular grid model parameters

A reheat turbine modelled by the standard IEEE model TGOV1 [131] has been considered for illustrative purpose. Parameter values are pointed out in Table 5.2, based on [127]. $T_1$ corresponds to $T_{CH}$, $T_2$ to $T_{RH}$, $T_3 = F_{HP} \cdot T_{RH}$, $D_t$ represents load damping and $R$ the droop constant in a tandem-compound single reheat turbine of fossil-fuelled unit.

**Table 5.2. Parameters of TGOV1 model reheat steam turbine**

| Parameter | Value |
|---|---|
| $T_1$ | 0.3 s |
| $T_2$ | 7 s |
| $T_3$ | 2.1 s |
| $A_t$ | 1 |
| $D_t$ | 0 |
| $V_{min}$ | 0 p.u. |
| $V_{max}$ | 1.2 p.u. |
| $R$ | 0.05 |
| $H$ | 4 s |

Figure 5.5 shows the frequency response sensitivity of model parameters on droop, turbine time constants, inertia and load damping. Although all parameters under study impact on the system frequency response, it can be observed that power mismatch and droop are those more strongly related as they alter all characteristic parameters of frequency response. The influence of spinning reserve has not been included, but studies in the literature state that the smaller the spinning reserve, the bigger the drop in frequency due to the loss of power [128].

In addition, the influence of the SFR study model has also been studied, because the selection of the computing method for frequency response shows different degrees of accuracy depending on the scenario under study. The study is annexed in Appendix A. As a conclusion, it can be stated Kundur and Anderson methods are only valid for thermal power stations, whereas Egido model can fit any type of generation. However, the simplification of the resolution of the equation system is only valid for power systems with small power mismatches below $P_0 < 0.1 p.u.$ For higher power losses, the equation system has to be solved directly.

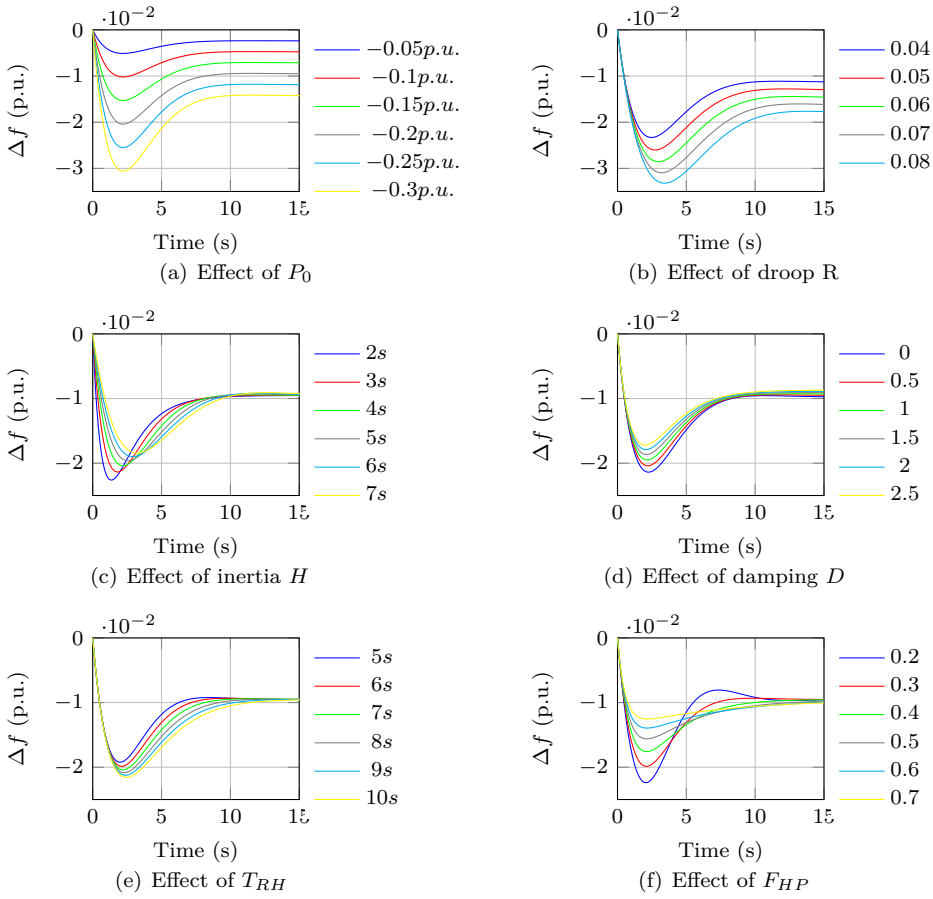


(a) Effect of $P_0$ (b) Effect of droop R

(c) Effect of inertia $H$ (d) Effect of damping $D$

(e) Effect of $T_{RH}$ (f) Effect of $F_{HP}$

**Figure 5.5. Effect of parameters on frequency response**

### 5.4.3 Parameterisation of grid model for grid code compliance verification

$P_0$ power mismatch is the only common parameter present in the calculation of the three characteristic parameters of dynamic frequency performance: initial ROCOF, steady-state frequency deviation and frequency minimum. In addition, the impact on the system frequency response is very high (Figure 5.5). Therefore, the dynamic frequency event can be represented based on the particular grid model in Figure 5.4 by the trip (frequency dip) of *Generator 2* or partial disconnection of load (frequency swell), with a power of $P_0$. The rest of parameters affecting frequency performance belong to *Generator 1* and to the aggregated load, for systems where load damping is important. If not, the load will be modelled as a constant power load.

Regarding generator parameterisation, two options are possible. On one hand, if parameters of generators in the system are already known, equivalent values $H_{eq}$, $R_{eq}$, $C_{eq}$ or $T_{eq}$ can be calculated from parameters of the individual generators. On

the other hand, if no dynamic data about the generators is available, generators can be adjusted according to typical values in isolated systems or to the specific values of the power grid under study. The worst scenario for frequency deviation must be considered, i.e. low demand and low system inertia, which often corresponds to highest renewable energy instantaneous penetration with dismissable contribution.

Below are summarised expressions for the independent adjustment of parameter $P_0$ to obtain a certain ROCOF, $f_{ss}$ and $f_{min}$.

**Initial ROCOF**

$$P_0 = ROCOF \cdot 2 \cdot H_{eq} \tag{5.47}$$

where $H_{eq}$ is calculated using (5.28).

**Steady-state frequency deviation**

$$P_0 = f_{ss} \cdot \left( \frac{1}{R_{eq}} + D \right) \tag{5.48}$$

where $R_{eq}$ is calculated using (5.30).

**Frequency minimum** For small disturbances, $P_0 < 0.1 p.u.$, frequency minimum can be most conveniently estimated following Egido method, as it considers power systems made up of generators with different technologies.

$$P_0 = f_{min} \cdot 2 \cdot C_{eq} \tag{5.49}$$

where $C_{eq}$ is calculated using (5.44) and (5.45).

For larger mismatches, the first-order step response shall be calculated by directly solving the firs-order function.

$$P_0 = \Delta\omega \cdot \frac{D + K_{eq}}{\left[ 1 + \frac{e^{-\varsigma \cdot \omega_n \cdot t}}{\sqrt{1-\varsigma^2}} \cdot (T_{eq} \cdot \omega_n \cdot sin(\omega_r \cdot t) - sin(\omega_r \cdot t + \theta_1) \right]} \tag{5.50}$$

where:

$$t_{min} = \frac{1}{\omega_r} \cdot atan \frac{\omega_n \cdot T_{eq} \cdot \sqrt{1-\varsigma^2}}{\omega_n \cdot T_{eq} \cdot \varsigma - 1} \tag{5.51}$$

where $T_{eq}$ and $K_{eq}$ are calculated using (5.44). Parameter $T_i$ of the individual first-order turbine-governor models must be tuned on open-loop against the complete model.

# Chapter 6

# Low Voltage Ride-Through

## 6.1 Introduction

Voltage dips are short duration reductions in RMS voltage mainly caused by short circuits, overloads, starting of large motors, and transformer saturation [132]. Most issues are associated with fault caused voltage dips. Therefore, this chapter focuses on this sort of disturbance analysis.

The interest in voltage dips has traditionally been focused on their impact on end-user equipment [133]. However, apart from being a power quality problem, voltage dips constitute today a major potential threat in networks with high distributed generation penetration [134]. On the event of a voltage dip, it has been noted that the simultaneous shut-down of large numbers of wind generators connected to the electrical system could happen. As a result, many power system operators have established new operating procedures which define the characteristics of the voltage-time response that wind farms and other RES must be able to ride-through, in terms of depth, duration and profile, as well as the exchange of active and reactive power to be met during the disturbance.

This chapter reviews analytical models to characterise voltage dips in power systems and it is organised as follows. In Section 6.2, characteristic parameters regarding voltage dips are defined. In Section 6.3 voltage dips are studied considering three models: a voltage divider model, a dynamic unregulated model, and a dynamic regulated model. As a result, a particular grid model able to emulate voltage dips is introduced in Section 6.4, simplifying the initially proposed model following a sensitivity study and presenting the formulae leading to the parameterised grid model.

## 6.2 Voltage dip definition

Different definitions have been proposed in the literature to describe voltage dips. The most extended one defines a voltage dip as a decrease in RMS voltage to values between 0.1 to 0.9 p.u. at the power frequency for durations from 0.5 cycles to 1 minute, reported as the remaining voltage [135].

Figure 6.1 shows a voltage dip due to a three-phase fault. As a voltage dip concerns a drop in voltage magnitude, it is often represented by plotting the RMS voltage

as a function of time, which is calculated or derived from the instantaneous voltage data. This is referred to as *voltage versus time characteristic*, also called *single-event characteristics*, and it allows identifying the main parameters of voltage dips: RMS magnitude during the event and dip duration [133]. Dip magnitude is defined as the minimum RMS voltage, divided in two concepts: voltage drop magnitude or depth of the voltage dip and residual voltage, as shown in Figure 6.1. They are usually expressed as percentage values ( %).

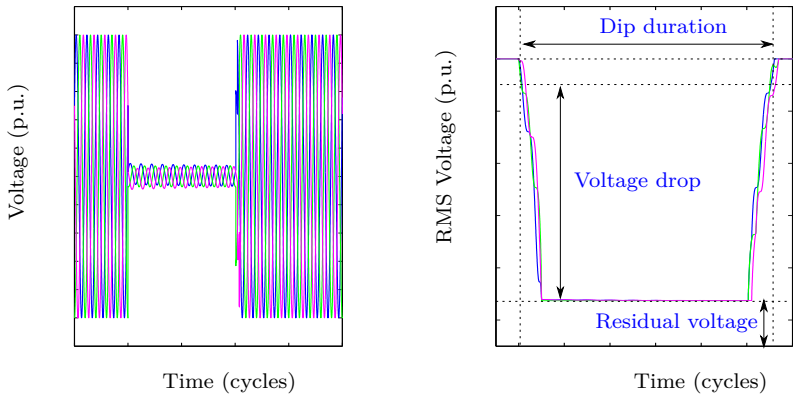


**Figure 6.1. Typical voltage dip**

This characterisation is correct for single-phase systems, three-phase balanced faults and for rectangular-shaped dips, where the voltage profile has a sharp drop at the beginning and a sharp rising at the end. But in some cases, this assumption is no more valid due to the special voltage dips with a long post fault recovery. The shape of the voltage dip depends strongly on the underlying cause. A voltage dip due to a fault is characterised by a sudden drop in voltage and a quite fast voltage recovery (depending on the reactive support), while a voltage dip due to motor starting is characterised by a sudden drop but a smooth recovery.

The present study is focused on fault induced voltage dips. A voltage dip event shows following RMS characteristic parameters (Figure 6.2): (1) **pre-fault voltage**, (2) **voltage dip magnitude**, (3) **minimum voltage**, (4) **dip duration**, (5) **fast recovery voltage**, (6) **maximum overvoltage** and (7) **instant of maximum overvoltage**, and (8) **post-fault voltage**.

In addition, for three-phase unbalanced dips the three individual phases are affected differently. In that case, the most affected phase is taken as dip magnitude and the duration is the longest of the three durations [136]. Voltage dips also involve other features such as phase-angle jump, point-on-wave of dip initiation and point-on-wave of dip recovery, waveform distortion and phase unbalance [137], but those aspects are out of the scope of this thesis.

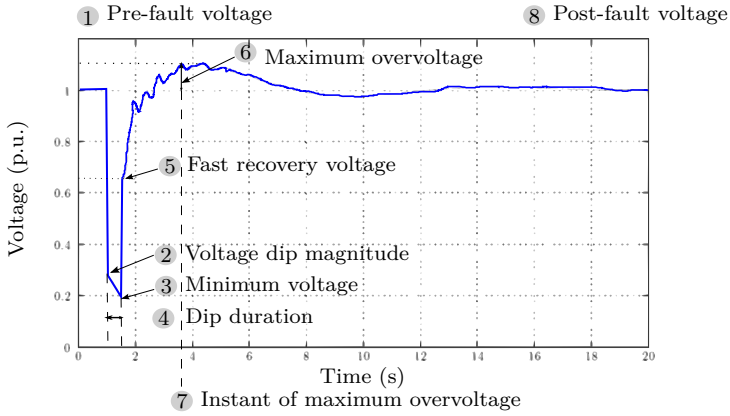


**Figure 6.2. Characteristic parameters on a fault induced voltage dip**

## 6.3 Theoretical analysis

The theoretical analysis of voltage dip calculation has been carried out using three models. First, a simple voltage divider model has been considered to introduce basic concepts. In real networks, voltage dip characterisation is more complicated and depends strongly on the dynamics of the electrical machines included in the power system. It is specially remarkable that voltage recovery is not instantaneous and it can be analysed through dynamic unregulated and regulated models, introducing transient stability concepts as well. The action of protection relays is not taken into account in this study.

### 6.3.1 Voltage divider model

To introduce basic ideas, consider a radial distribution feeder supplied from a bus bar that also supplies a sensitive load or installation, where a fault happens at point F. It is a simple voltage divider (Figure 6.3), where $\underline{Z}_s$ is the source impedance and $\underline{Z}_f$ is the feeder impedance between the PCC and the fault point, including the fault impedance if it is considered. Using an equivalent grid model, the application of the fault results into a square shaped voltage dip.

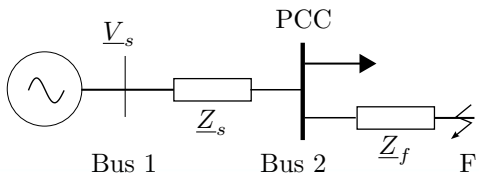


**Figure 6.3. Simplified circuit for voltage dip calculation**

This radial network, widely present in weak or isolated power systems, represents a voltage divider. In meshed networks, such as transmission systems, the concept of

voltage divider model is still useful [138], even if the feeders and the source impedance are not easy to identify. Therefore, the calculation of voltages in meshed transmission systems can be carried out with the network impedance matrix [139].

Expressions for the calculation of sequence voltages $\underline{V}_{a0}$, $\underline{V}_{a1}$ and $\underline{V}_{a2}$ at the PCC are listed in Appendix B for different fault conditions, where source impedance $\underline{Z}_s$ corresponds to the equivalent impedance $\underline{Z}$. Therefore, $\underline{Z}_1 = \underline{Z}_{s,1}$, $\underline{Z}_2 = \underline{Z}_{s,2}$, and $\underline{Z}_0 = \underline{Z}_{s,0}$.

The voltage divider model is useful to calculate the value of the parameter *voltage dip magnitude*. Pre-fault voltages are normally assumed equal to 1 p.u. For more accurate calculations, a load flow study should be made and so, the pre-fault voltages accurately obtained. However, it is hereby considered for the analytical expressions. Based on symmetrical components (Appendix B), voltage dip magnitude can be calculated as follows:

**Three-phase short-circuit** For the simplest case of a symmetrical short-circuit, the voltage dip magnitude at the PCC is indicated in (6.1).

$$|\underline{V}_A(pu)| = \left|\underline{V}_{pf}\right| \cdot \frac{\left|\underline{Z}_f\right|}{\left|\underline{Z}_f + \underline{Z}_s\right|} \tag{6.1}$$

**Single-phase short-circuit** Considering the sequence impedances, the voltage dip magnitude (per unit) in phase A at the PCC can be calculated as:

$$|\underline{V}_A(pu)| = \left|\underline{V}_{pf}\right| \cdot \frac{\left|3 \cdot \underline{Z}_f\right|}{\left|\underline{Z}_{s,1} + \underline{Z}_{s,2} + \underline{Z}_{s,0} + 3 \cdot \underline{Z}_f\right|} \tag{6.2}$$

Reference [136] indicates the expression for voltage dip magnitude in solidly-grounded and impedance-grounded systems. In solidly-grounded systems, source impedances in the three components are often about equal, resulting in the same magnitude as for three-phase short-circuits:

$$|\underline{V}_A(pu)| = \left|\underline{V}_{pf}\right| \cdot \frac{\left|\underline{Z}_f\right|}{\left|\underline{Z}_f + \underline{Z}_{s,1}\right|} \tag{6.3}$$

On the other hand, in resistance or high-impedance grounded systems, the zero-sequence source impedance differs significantly from the positive and negative sequence source impedances. As a consequence, (6.3) cannot be applied.

**Double-phase short-circuit** Considering the sequence impedances, the voltage dip magnitude (per unit) in phase A at the PCC can be calculated as:

$$|\underline{V}_A(pu)| = \left|\underline{V}_{pf}\right| \cdot \frac{\left|2 \cdot \underline{Z}_{s,2} + \underline{Z}_f\right|}{\left|\underline{Z}_{s,1} + \underline{Z}_{s,2} + \underline{Z}_f\right|} \tag{6.4}$$

And in faulty phases B and C:

$$|\underline{V}_B(pu)| = \left|\underline{V}_{pf}\right| \cdot \left| \frac{\left(\underline{Z}_{s,2} + \underline{Z}_f\right) \cdot \underline{a}^2 + \underline{Z}_{s,2} \cdot \underline{a}}{\underline{Z}_{s,1} + \underline{Z}_{s,2} + \underline{Z}_f} \right| \tag{6.5}$$

If all sequence components are assumed to be equal ($\underline{Z}_{s,1} = \underline{Z}_{s,2} = \underline{Z}_{s,0}$), and $\left|\underline{V}_{pf}\right| = 1$ p.u., $|\underline{V}_A(pu)| = 1$ p.u. Further simplifying with $\underline{Z}_f = 0$, voltage in phases B and C is $|\underline{V}_B(pu)| = |\underline{V}_C(pu)| = 0.5$ p.u.

**Double-phase-to-ground short-circuit** Considering the sequence impedances and $Z_f = 0$, the voltage dip magnitude (per unit) in phase A at the PCC can be calculated as:

$$|\underline{V}_A(pu)| = \left|\underline{V}_{pf}\right| \cdot \left| \frac{3 \cdot \underline{Z}_{s,2} \cdot \underline{Z}_{s,0} + 6 \cdot \underline{Z}_{s,2} \cdot \underline{Z}_t}{\underline{Z}_{s,1} \cdot \left(\underline{Z}_{s,0} + \underline{Z}_{s,2} + 3 \cdot \underline{Z}_t\right) + \underline{Z}_{s,2} \cdot \left(\underline{Z}_{s,0} + 3 \cdot \underline{Z}_t\right)} \right| \tag{6.6}$$

And in faulty phase B:

$$|\underline{V}_B(pu)| = \left|\underline{V}_{pf}\right| \cdot \left| \frac{\underline{Z}_{s,0} \cdot \underline{Z}_{s,2} + \underline{Z}_{s,2} \cdot \left(\underline{Z}_{s,0} + 3 \cdot \underline{Z}_t\right) \cdot \left(\underline{a}^2 + \underline{a}\right)}{\underline{Z}_{s,1} \cdot \left(\underline{Z}_{s,0} + \underline{Z}_{s,2} + 3 \cdot \underline{Z}_t\right) + \underline{Z}_{s,2} \cdot \left(\underline{Z}_{s,0} + 3 \cdot \underline{Z}_t\right)} \right| \tag{6.7}$$

If all sequence components are assumed to be equal ($\underline{Z}_{s,1} = \underline{Z}_{s,2} = \underline{Z}_{s,0}$), and $\left|\underline{V}_{pf}\right| = 1$ p.u., $|\underline{V}_A(pu)| = 1$ p.u. Further simplifying with $\underline{Z}_f = 0$ and $\underline{Z}_t = 0$, voltage in faulty phases B and C, $|\underline{V}_B(pu)| = |\underline{V}_C(pu)| = 0$ p.u.

### 6.3.2 Dynamic unregulated model

Using the voltage divider model, only voltage dip magnitude can be characterised. If the evolution of voltage during a fault is to be studied, dynamic models are better suited. In these models, system dynamics, mainly represented by generator dynamics, are taken into account. In this subsection, generator dynamics without voltage regulation are analysed. First, the transient performance of a single generating unit connected to an infinite bus is presented, which helps to understand the calculation of voltage dip for a multi-machine system.

#### 6.3.2.1 Single Machine Infinite Bus (SMIB) model

Consider the system shown in Figure 6.4 consisting of a generator delivering power to a large system represented by an infinite bus through a line of reactance $X_l$.

For a simpler analysis, the synchronous generator can be modelled using a classical model, composed of a voltage source $E'$ behind a transient reactance $X'_d$. Classical model assumes that transient saliency is ignored, and mechanical power and generator e.m.f. are constant. $E'$ and $X'_d$ correspond to the transient period, which mostly affects the first oscillations of the generator and therefore, transient stability. The

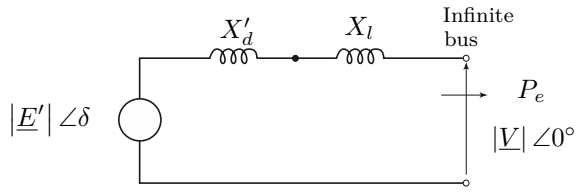


**Figure 6.4. SMIB model**

voltage magnitude $E'$ remains constant and the angle $\delta$ varies following the mechanical oscillations of the rotor. It can be deduced that the electric power given by the synchronous generator is:

$$P_e = \frac{|\underline{E}'| \cdot |\underline{V}|}{X_{eq}} \sin \delta = P_{max} \cdot sin\delta \tag{6.8}$$

where $X_{eq}$ is the equivalent reactance between the machine and the infinite bus in (6.9).

$$X_{eq} = X_l + X'_d \tag{6.9}$$

During short-circuits, electrical power generated by synchronous machines decreases, while mechanical power remains constant. So, based on swing equation, a short-circuit initially accelerates generators and brakes motors. The rate-of-change-of-speed of the synchronous machines is determined by the power mismatch level and the inertia constant. Swing equation is transformed taking into account the expression of the electrical power generated by the machine in (6.8).

$$\frac{2 \cdot H}{\omega_s} \cdot \frac{d^2\delta}{dt^2} = P_m - \frac{|\underline{V}| \cdot |\underline{E}'|}{X_{eq}} - D \cdot \frac{d\delta}{dt} \tag{6.10}$$

Three different states accompanying a disturbance can be identified with three, generally different, values of $X_{eq}$: (i) the pre-fault state when the reactance $X_{eq} = X_{eq,pref}$; (ii) the fault state when $X_{eq} = X_{eq,f}$, and (iii) the post-fault state when $X_{eq} = X_{eq,postf}$.

During a short-circuit fault, the electric power delivered by a synchronous generator depends on the short-circuit type, fault point and fault impedance, which result in different $X_{eq,f}$ values. Based on power system in Figure 6.4 and considering a short-circuit at the terminals of the generator, the equivalent circuit during the fault is shown in Figure 6.5.

According to Figure 6.5, voltages $E'$ and $V$ are directly connected by an equivalent fault reactance $X_{eq,f}$ obtained using the star-delta transformation.

$$X_{eq,f} = X'_d + X_l + \frac{X'_d \cdot X_l}{\Delta X_f} \tag{6.11}$$

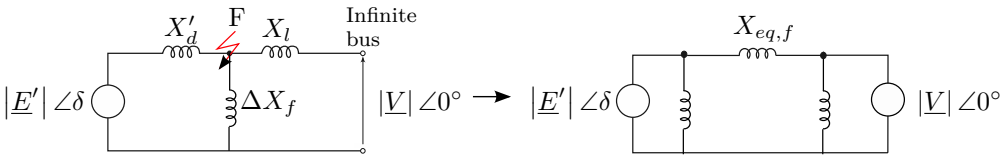


**Figure 6.5. Equivalent circuit during a fault**

where $\Delta X_f$ is the fault shunt reactance at the faulted point. The use of symmetrical components allows any type of fault to be represented in the positive-sequence network by a fault reactance $\Delta X_f$ connected between the point of the fault and the neutral as shown in Figure 6.5. The value of the shunt fault impedance $\Delta X_f$ depends on the type of fault and is given in Table 6.1 where $X_1$, $X_2$ and $X_0$ are respectively the positive, negative, and zero sequence Thevenin equivalent reactances as seen from the fault terminals [124].

**Table 6.1. Shunt reactances representing different types of faults (I)**

| **Type** | 3Ph | 2PhG | 2Ph | 1Ph |
|---|---|---|---|---|
| $\Delta X_f$ | $X_f$ | $X_f + \dfrac{(X_2 + X_f) \cdot (X_0 + X_f + 3 \cdot X_t)}{X_2 + X_0 + 2 \cdot X_f + 3 \cdot X_t}$ | $X_f + X_2$ | $X_2 + X_0 + 3 \cdot X_f$ |

The circuit diagram in Figure 6.5 corresponds to the positive-sequence network so that when $X_{eq,f}$ in (6.11) is used in the power-angle characteristic, only the torque and power due to the flow of positive-sequence currents is accounted for. The expressions can be further simplified by considering a null fault reactance and equal values of sequence reactances ($X_1 = X_2 = X_0$). Hence, shunt reactances representing different types of fault have the values indicated in Table 6.2. The corresponding power-angle characteristics during the fault are illustrated in Figure 6.6.

**Table 6.2. Shunt reactances representing different types of faults (II)**

| **Type** | 3Ph | 2PhG | 2Ph | 1Ph |
|---|---|---|---|---|
| $\Delta X_f$ | 0 | $\dfrac{X_1}{2}$ | $X_1$ | $2 \cdot X_1$ |

In addition, the accelerating torque for unbalanced faults is smaller than that for three-phase faults, and so, the rotor accelerates less rapidly and the rotor angle at the clearing instant is smaller. As a result, stability margins are larger.

In order to characterise a voltage dip caused by a short-circuit at the faulted bus (or an other bus in the power system), the transient behaviour of the synchronous generator shall be studied, determining the load angle $\delta$ at every instant. Therefore, Equation (6.10) shall be solved using numerical integration techniques. If the study case is simplified considering a power system without damping ($D = 0$) and with no electrical power during the fault (e.g. a bolted three-phase short-circuit), (6.10) can

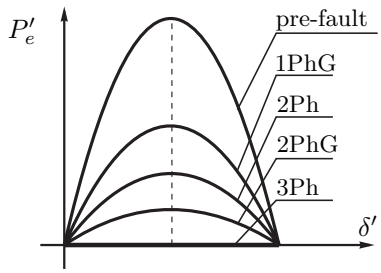


**Figure 6.6. Power angle curve during unbalanced faults**

be solved by direct integration. The solution for $\delta$ calculation in the case of a bolted three-phase short-circuit is:

$$\delta = \frac{P_m \cdot \omega_s}{4 \cdot H} \cdot t^2 + \delta_0 \tag{6.12}$$

At the fault clearing instant, $t = t_{dip}$. As a result, $\delta_1$ can be calculated according to (6.13).

$$\delta_1 = \frac{P_m \cdot \omega_s}{4 \cdot H} \cdot t_{dip}^2 + \delta_0 \tag{6.13}$$

For the rest of the cases (i.e. non-bolted three-phase short-circuits or unbalanced short-circuits) load angle $\delta$ at the fault clearing instant shall be computed using **numerical methods**. Indeed, during short-circuits other than bolted three-phase short-circuits, the synchronous generator can only supply electrical power $P_e$ as indicated below.

$$P_e(\delta) = P_{max,fault} \cdot \sin\delta \tag{6.14}$$

where maximum active power $P_{max,fault}$ is:

$$P_{max,fault} = \frac{|\underline{V}| \cdot |\underline{E}'|}{X_{eq,f}} \tag{6.15}$$

As a consequence, for short-circuits other than bolted three-phase short-circuits or with damping, (6.16) shall be solved:

$$\frac{d^2\delta}{dt^2} = \frac{\left(P_m - P_e(\delta) - D \cdot \frac{d\delta}{dt}\right) \cdot \omega_s}{2 \cdot H} \tag{6.16}$$

Besides, the calculation of the evolution of the load angle $\delta$, helps determine if transient stability is guaranteed. For this purpose, though, a simpler method can be used, without needing to solve the swing equation: the **equal area criterion**.

Stability is maintained in the system whenever the acceleration area is smaller than deceleration area. However, this method can only be applied to a SMIB system or to a power system composed by two generators.

Using the SMIB model, a voltage dip can be characterised with the calculation of the characteristic parameters indicated on Figure 6.2.

**Voltage dip magnitude** The voltage dip magnitude at fault point F in Figure 6.5 can be computed as:

$$\underline{V}_F = 1j \cdot \Delta X_f \cdot \underline{I}_f \tag{6.17}$$

Being $I_f$ the fault current:

$$\underline{I}_f = \frac{\underline{V}_{eq}}{1j \cdot (X_{eq} + \Delta X_f)} \tag{6.18}$$

$\underline{V}_{eq}$ is the equivalent voltage of the synchronous generator and the infinite bus. Applying Millman's theorem:

$$\underline{V}_{eq} = \left( \frac{\underline{V}}{1j \cdot X_l} + \frac{E' \angle \delta_0}{1j \cdot X'_d} \right) \cdot 1j \cdot X_{eq} \tag{6.19}$$

For this case, $X_{eq}$ is:

$$X_{eq} = \frac{X_l \cdot X'_d}{X_l + X'_d} \tag{6.20}$$

And the initial rotor angle of the generator can be calculated as:

$$\delta_0 = \arcsin \frac{P_m \cdot X_{eq,pref}}{|\underline{V}| \cdot |\underline{E}'|} \tag{6.21}$$

Therefore, the voltage dip magnitude can be calculated as:

$$|\underline{V}_F| = \Delta X_f \cdot \frac{|\underline{V}_{eq}|}{X_{eq} + \Delta X_f} \tag{6.22}$$

However, as indicated before, Figure 6.5 only represents the positive sequence circuit, and hence, $\underline{V}_F$ is the positive sequence voltage. Therefore, in order to compute voltage at faulted point, all three sequence voltages shall be added up. Equation (6.22) is verified only for three-phase short-circuits. For unbalanced faults, expressions in Table 6.3 shall be taken into account. Double-phase-to-ground faults have not been considered, because they are not generally mentioned in most of the grid codes under review in Chapter 2.

**Table 6.3. Voltage dip magnitude for unbalanced faults**

| Fault type | Voltage dip magnitude |
|---|---|
| Single-phase-to-ground | $\left\|\underline{V}_F\right\| = 3 \cdot X_f \cdot \frac{\left\|\underline{V}_{eq}\right\|}{Xeq + \Delta X_f}$ (6.23) |
| Two-phase | $\left\|\underline{V}_F\right\| = \left(2 \cdot X_2 + X_f\right) \cdot \frac{\left\|\underline{V}_{eq}\right\|}{Xeq + \Delta X_f}$ (6.24) |

Therefore, a generalised form for voltage dip magnitude calculation can be adopted for any shunt fault type:

$$\left|\underline{V}_F\right| = \Delta' X_f \cdot \frac{\left|\underline{V}_{eq}\right|}{X_{eq} + \Delta X_f} \tag{6.25}$$

Where $\Delta' X_f$ also depends on the fault type as indicated in Table 6.4.

**Table 6.4. Shunt reactances representing different types of faults (III)**

| **Fault type** | 3Ph | 2Ph | 1Ph |
|---|---|---|---|
| $\Delta' X_f$ | $X_f$ | $2 \cdot X_2 + X_f$ | $3 \cdot X_f$ |

**Minimum voltage** This parameter represents the voltage value at the clearing instant and can be obtained by (6.26) with $V_{eq}$ evaluated at $\delta = \delta_1$. As a result:

$$\left|\underline{V}_{min}\right| = \Delta' X_f \cdot \frac{\left|\underline{V}_{eq}\left(\delta_1\right)\right|}{X_{eq} + \Delta X_f} \tag{6.26}$$

$$\underline{V}_{eq}\left(\delta_1\right) = \left(\frac{\underline{V}}{1j \cdot X_l} + \frac{E' \angle \delta_1}{1j \cdot X'_d}\right) \cdot 1j \cdot X_{eq} \tag{6.27}$$

Comparing (6.19) and (6.27), it can be observed that the only difference is the angle $\delta_1$ between the machine and the infinite bus. This angle depends on many parameters, such as the initial state (angle $\delta_0$), the generator inertia, the fault duration, the fault type and fault impedance, as it results from solving (6.16).

**Fast recovery voltage** The fast recovery voltage corresponds to the voltage value immediately after the fault clearing. In first instance, the value of the load angle $\delta$ shall be computed at the fault clearing instant, i.e. $\delta_1$, as done for the calculation

of *minimum voltage*. However, during the first post-fault instants, the synchronous generator supplies the following electrical power:

$$P_e(\delta) = P_{max,postf} \cdot \sin\delta = \frac{|\underline{V}| \cdot |\underline{E}'|}{X_{eq,postf}} \tag{6.28}$$

where $P_{max}$ is the maximum active power after the fault. It equals the pre-fault power if the power system recovers totally from the short-circuit. If not (e.g. a double circuit line only recovers one of the feeders), the equivalent impedance for the power delivery results into higher values, and therefore, the maximum active power being supplied by the generator is lower.

Hence, the fast recovery voltage can be calculated in complex form as indicated by (6.29).

$$\underline{V}_{rec} = E'\angle\delta_1 - \frac{(E'\angle\delta_1 - V)\cdot 1j\cdot X'_d}{1j\cdot(X_l + X'_d)} = \frac{E'\angle\delta_1\cdot 1j\cdot X_l + V\cdot 1j\cdot X'_d}{1j\cdot(X_l + X'_d)} \tag{6.29}$$

$$|\underline{V}_{rec}| = \frac{1}{X_l + X'd}\cdot\sqrt{(X_l\cdot E'\cdot cos(\delta_1) + V\cdot X'_d)^2 + (X_l\cdot E'\cdot sin(\delta_1))^2} \tag{6.30}$$

**Maximum overvoltage** In order to compute the maximum overvoltage and the instant of maximum overvoltage (corresponding to the first swing oscillation of the generator), maximum value of (6.31) shall be calculated. Therefore, in order to compute the maximum overvoltage magnitude, Equation (6.32) shall be derived and equaled to 0.

$$\underline{V}(\delta) = E'\angle\delta - \frac{(E'\angle\delta - V)\cdot 1j\cdot X'_d}{1j\cdot(X_l + X'_d)} = \frac{E'\angle\delta\cdot 1j\cdot X_l + V\cdot 1j\cdot X'_d}{1j\cdot(X_l + X'_d)} \tag{6.31}$$

$$|\underline{V}(\delta)| = \frac{1}{X_l + X'd}\cdot\sqrt{(X_l\cdot E'\cdot cos(\delta) + V\cdot X'_d)^2 + (X_l\cdot E'\cdot sin(\delta))^2} \tag{6.32}$$

The maximum overvoltage does not correspond to the LVRT requirement, but to the HVRT requirement which is out of the scope of this thesis.

#### 6.3.2.2 Two machine system

In a system with two machines (Figure 6.7), one of the machines must be generating and the other must be motoring.

Therefore, considering a lossless interconnection line:

$$P_{m,1} = -P_{m,2} = P_m \tag{6.33}$$

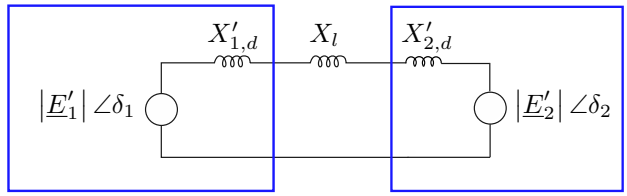


**Figure 6.7. A two machine power system**

$$P_{e,1} = -P_{e,2} = P_e \tag{6.34}$$

Dismissing damping constants, swing equations can be rewritten like:

$$\frac{2 \cdot H_1}{\omega_s} \cdot \frac{d\omega_1}{dt} = P_{m,1} - P_{e,1} = P_m - P_e \tag{6.35}$$

$$\frac{2 \cdot H_2}{\omega_s} \cdot \frac{d\omega_2}{dt} = P_{m,2} - P_{e,2} = P_e - P_m \tag{6.36}$$

Subtracting (6.35) and (6.36):

$$\frac{d\left(\omega_1 - \omega_2\right)}{dt} = \omega_s \cdot \frac{H_1 + H_2}{H_1 \cdot H_2} \cdot \left(P_m - P_e\right) \tag{6.37}$$

Considering $\delta = \delta_1 - \delta_2$ and $\omega = \omega_1 - \omega_2$ and defining an equivalent inertia $H_{eq}$, Equation (6.39) is obtained:

$$H_{eq} = \frac{H_1 \cdot H_2}{H_1 + H_2} \tag{6.38}$$

If Generator 1 is of quite large capacity in comparison with Generator 2, the case corresponds to a SMIB [140].

$$\frac{2 \cdot H_{eq}}{\omega_s} \cdot \frac{d\omega}{dt} = P_m - P_e \tag{6.39}$$

where:

$$P_e = \frac{\left|\underline{E}'_1\right| \cdot \left|\underline{E}'_2\right|}{X'_{d,1} + X'_{d,2} + X_l} \cdot sin\delta \tag{6.40}$$

#### 6.3.2.3 Multi-machine power systems

For the calculation of voltage dip characteristic parameters in multi-machine power systems, a power flow shall be solved in a first instance. Then, individual power swing equations of each machine must be computed based on the admittance matrix of the system. As an instance, for a two machine system (6.35) and (6.36) must be solved.

However, multi-machine systems can be simplified taking into account the following hypotheses:

1. Find out coherent machines that oscillate simultaneously for being electrically close (i.e. two generators at the same power plant) [141].
2. Reduce a two-machine system to an equivalent system made up of a single generator with equivalent inertia connected to a infinite bus [142].

A fault inducing a voltage dip can lead to transient instability. To study transient stability in multi-machine systems, equal area criterion can be widely used, but following simplifications are considered to reduce the original system to a single machine infinite bus system:

- Divide the machines in the system into two groups: the critical machines that are responsible for the loss of synchronism, and the remaining non-critical ones.
- Replace the two groups by two equivalent machines.
- Replace these machines by an equivalent single machine, infinite bus system (Section 6.3.2.2).
- Evaluate the system stability using the equal area criterion.

### 6.3.3 Dynamic regulated model

The transient power-angle characteristic for an unregulated generator has been derived assuming that the excitation is constant. In practice, synchronous generators are equipped with an AVR which tries to maintain voltage at the generator terminals constant by adjusting the value of the excitation voltage, and, consequently, $E_f$.

When a fault occurs, the generator terminal voltage drops and the large regulation error $\Delta V = V_{ref} - V_g$ forces the AVR to increase the generator field current. However, the field current does not change immediately due to a delay depending on the gain and time constants of the AVR, and on the time constant of the generator field winding. Therefore, $E_g$ does not remain constant as indicated as hypothesis for the unregulated model.

The effect of AVR action on transient stability is shown in Figure 6.8, assuming a non-solid three-phase fault at $\delta = \delta_2$ [124]. When no AVR is present (Figure 6.8(a)), this system may lose stability. The effect of the AVR, shown in Figure 6.8(b), is to increase the field current leading to an increase in the transient emf $E'$. This increase in $E'$ can be accounted for by drawing a family of power-angle characteristics $P_{E'}(\delta)$ for different values of $E'$.

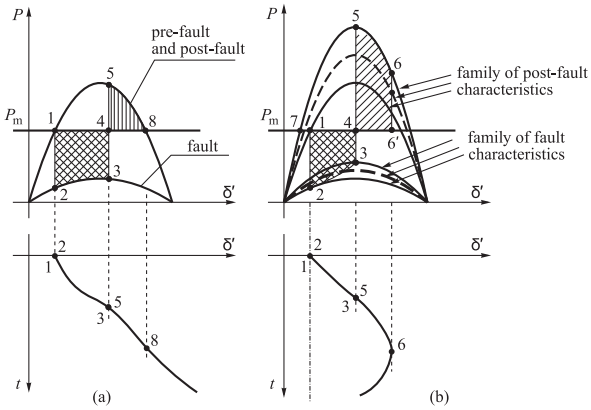


**Figure 6.8. Effect of AVR on transient stability**

Under typical assumptions, the synchronous generator can be modelled by the following set of non-linear differential equations:

$$\frac{2 \cdot H}{\omega_s} \cdot \frac{d^2\delta}{dt^2} = P_m - E'_q \cdot I_q - D \cdot \frac{d\delta}{dt} \tag{6.41}$$

$$\frac{dE'_q}{dt} = \frac{1}{T'_{d0}} \cdot \left(E_{fd} - E'_q - (X_d - X'_d) \cdot I_d\right) \tag{6.42}$$

where $E_{fd}$ is the equivalent emf in the exciter coil, $E'_q$ is the transient emf due to field flux linkage, $T'_{d0}$ is the direct-axis open-circuit transient time constant of the generator, $X_d$ the synchronous reactance, $X'_d$ the transient reactance, $I_d$ and $I_q$ are direct and quadrature axis components of stator current.

If the excitation system is a high gain static system and the terminal voltage is measured using a transducer with first-order dynamics, $E_{fd}$ can be expressed as:

$$E_{fd} = K_a \cdot (V_c + V_{pss}) \tag{6.43}$$

$$\frac{V_{tr}}{dt} = \frac{1}{T_r} \cdot (-V_{tr} + V_t) \tag{6.44}$$

where $V_{tr}$ and $T_r$ are the output and time constant of the voltage transducer, $K_a$ is the gain of the exciter amplifier, $V_t = \sqrt{\left(E'_q - X'd \cdot I_d\right)^2 + \left(X'_d \cdot I_q\right)^2}$ is the generator terminal voltage and $V_c$ is the input to the exciter (output of the designed controller).

## 6.4 Grid model and event representation

In this section, the generic grid model introduced in Chapter 4 has been particularised in order to characterise voltage dips in isolated power systems, based on the theoretical analysis in Section 6.3 and taking into account the sensitivity of the grid model parameters. Finally, equations leading to the parameterisation of the particular grid model are presented.

### 6.4.1 Particular grid model

Two different grid models are hereby proposed to obtain the characteristic behaviour of island power grids during voltage dips. The **divider model** in Figure 6.9(a) and the more complex **T-shaped model** in Figure 6.9(b), based on [117]. In both particular models, the load asset establishes the power flow in the system. A short-circuit must be applied at point F to simulate the appearance of a voltage dip. $Z_{l2}$ limits voltage dip magnitude at PCC and $Z_{l1}$ represents the source impedance. Regarding the generating units:

- **Voltage divider model** (Figure 6.9(a)): *Generator 1* stands as the equivalent generating unit of the whole power system. For emulating a square shaped dip, *Generator 1* must be modelled as an ideal voltage source, disregarding its dynamics. For a polygonal voltage dip, *Generator 1* must be modelled as a synchronous generator, including controls.
- **T-shaped model** (Figure 6.9(b)): *Generator 2* represents the generator which is closer to the fault point and *Generator 1* is the equivalent of the rest of the generating units. Both generators must include controls.

### 6.4.2 Sensitivity of particular grid model parameters

#### 6.4.2.1 Voltage divider model

The analysis of the sensitivity of the voltage divider model parameters related to voltage dip is based on Figure 6.9 (a) with values indicated in Table 6.5. Parameter values has been selected based on typical medium-size islands.

**Table 6.5. Parameters of the voltage divider model**

| Parameter | Value |
|---|---|
| $U_N$ | 30 kV |
| $S_{sc}$ | 100 MVA |
| $P_{load}$ | 20 MW |

Note: Source is totally inductive.

Voltage dip magnitude depends on pre-fault voltage, short-circuit type, short-circuit power, impedance fault, and $R/X$ ratio. The pre-fault voltage has been excluded from the sensitivity study, as it is normally assumed to be 1 p.u. $Z_{l2}$ includes the

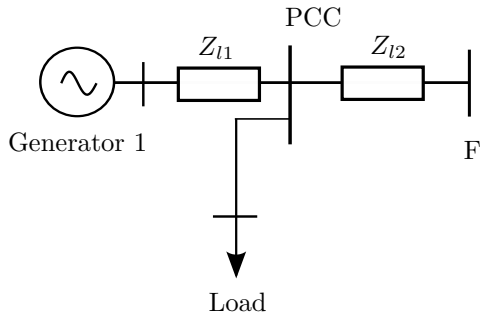


(a) Voltage divider model

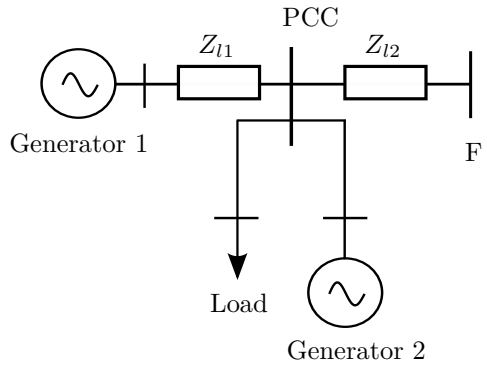


(b) T-shaped model

**Figure 6.9. Particular grid model for voltage dip analysis**

impedance of the feeder from the PCC until the fault point F, with a bolted fault. Figure 6.10 shows the voltage dip magnitude sensitivity with respect of short-circuit type and power system strength.

**Short-circuit type** $\underline{Z}_{l1,1} = \underline{Z}_{l1,2}$ are considered equal as hypothesis, representing the source impedance. In addition, for the study, two types of power systems are considered: solidly grounded transmission systems (where $\underline{Z}_{l1,1} = \underline{Z}_{l1,2} = \underline{Z}_{l1,0}$) and solidly grounded distribution systems (where $\underline{Z}_{l1,0} = 2.5 \cdot \underline{Z}_{l1,1}$).

Figure 6.10(a) illustrates the effect of the short-circuit type on the voltage dip magnitude at the PCC. Voltage dips caused by two-phase short-circuits only reach 0.5 p.u. For the rest of short-circuit types, dip magnitude is 0 p.u. at the fault point (as the fault impedance $Z_{l2}$ is assumed null). Nonetheless, as distance to fault point increases, three-phase, single-phase and two-phase-to-ground shortcircuits in solidly grounded distribution systems have a higher magnitude than the rest of faults.

**Short-circuit power** The dependence of voltage dip magnitude on short-circuit power was analytically derived for three-phase short-circuits in Chapter 1. Weak power grid show low short-circuit power values. Therefore, voltage dip magnitude is

deeper. Figure 6.10(b) shows the effect of short-circuit on voltage dip magnitude at the PCC, based for the voltage divider model. A totally inductive 30 kV network and a bolted three-phase short-circuit have been considered for illustration purpose.

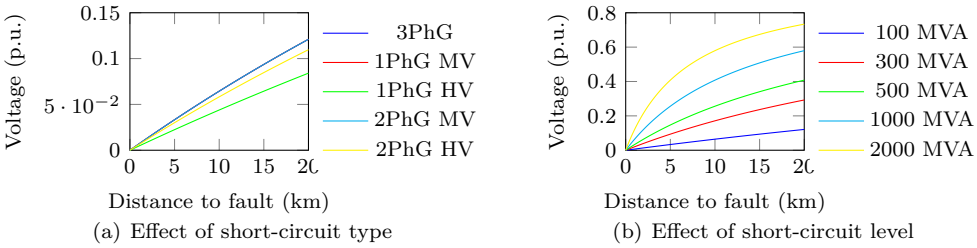


(a) Effect of short-circuit type (b) Effect of short-circuit level

**Figure 6.10. Effect of parameters on voltage dip magnitude**

**Voltage recovery** If instead of considering *Generator 1* as a voltage source with dismissable internal impedance, it is modelled as a controlled synchronous generator, the voltage dip envelope shows a polygonal shape: voltage dip magnitude is not constant, voltage recovery is not instantaneous, and some overvoltage can appear on recovery.

Based on the voltage divider model in Figure 6.9(a) with parameters in Table 6.5, voltage recovery has been analysed for three-phase short-circuits. The generator size and the line impedance have been modified in order to analyse their impact on voltage recovery, illustrated in Figure 6.11. It can be concluded that as voltage source is stronger, recovery is faster and with lower post-fault overvoltage. On the other hand, the closer the voltage source to the PCC, the higher is overvoltage. In any case, post-fault overvoltage seems to be linked to the fast recovery voltage. For lower fast recovery voltages, resulting postfault voltage is higher. These two aspects are more important than voltage regulator parameters for this case study.

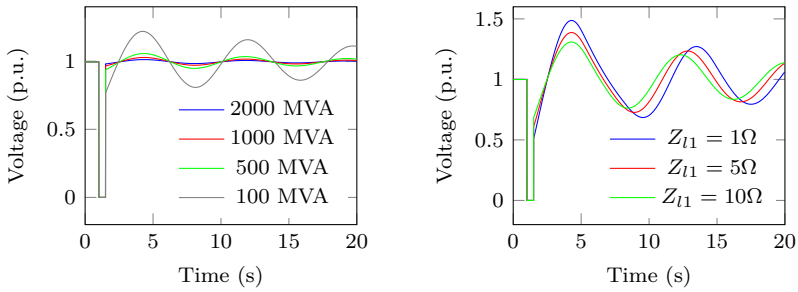


(a) Effect of $G_1$ strength (b) Effect of feeder length

**Figure 6.11. Effect of parameters on voltage dip recovery**

#### 6.4.2.2 T-shaped model

The sensitivity study is based on the particular grid model in Figure 6.9(b) parameterised as indicated in [117], considered as base case. Fault impedance is represented by $Z_f$, and not by $Z_{l2}$. Some of the parameters under study only affect voltage during the disturbance, but others influence the pre-fault, during fault and post-fault situations, e.g. short-circuit power, $X/R$ relation or pre-fault voltage. Results are plotted in Figure 6.12.

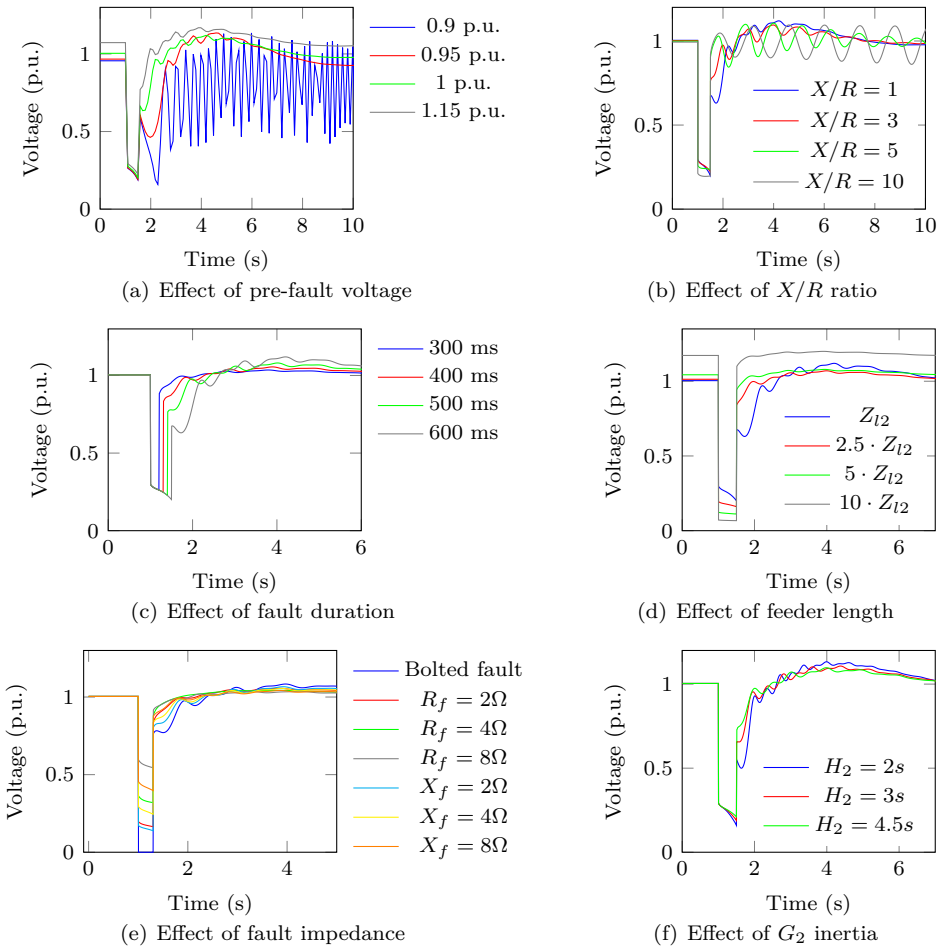


(a) Effect of pre-fault voltage

(b) Effect of $X/R$ ratio

(c) Effect of fault duration

(d) Effect of feeder length

(e) Effect of fault impedance

(f) Effect of $G_2$ inertia

**Figure 6.12. Effect of parameters on voltage response**

**Short-circuit type** On the base case study, different types of short-circuits have been applied with the same fault impedance $\underline{Z}_f = 1i \cdot 4.067\Omega$. For any type of fault except for double-phase short-circuits, the voltage magnitude and minimum voltage are very similar. For two-phase faults magnitude is above $0.5 \cdot V_{pf}$ p.u. The fastest

recovery corresponds to single-phase-to-ground faults, resulting in an almost square-shaped dip. Two-phase and two-phase-to-ground faults have a very similar recovery behaviour, in any case faster than for three-phase faults.

**Pre-fault voltage** The influence of the pre-fault voltage is illustrated in Figure 6.12(a). The test is performed by changing the voltage reference at the slack bus *Bus 1*. Therefore, voltage level at PCC bus is modified from the base case. Although it hardly affects during the disturbance, it does the voltage recovery. For lower pre-fault voltages,the fast recovery voltage decreases. Therefore, recovery is slower. For low reference voltages, the fast recovery voltage is too small and unable to recover stability.

$X/R$ **relation of feeder impedances** Figure 6.12(b) shows the sensitivity of $X/R$ relation. For more resistive feeders, voltage dip is deeper, but fast recovery voltage is higher on the other hand.

**Fault duration** Figure 6.12(c) shows the sensitivity of fault duration. Minimum voltage is lower for longer faults, as well as fast recovery voltage. Therefore, voltage recovery is slower for longer faults, and above the critical clearing time, the system loses stability.

**Short-circuit power** The short-circuit power at the PCC in the base case is 4827.4 MVA, as it represents a continental strong power system. As the short-circuit impedance strongly depends on the line impedance $Z_{l2}$, the latter has been modified in order to study the influence of the grid strength on voltage dips. However, it does not only affect voltage during the fault, but also in the pre-fault situation, as seen in Figure 6.12(d). In weaker grids, pre-fault and post-fault voltages are higher, voltage dip magnitude and minimum voltage are lower, but the voltage recovery also seems faster.

**Fault impedance** Figure 6.12(e) shows the sensitivity of fault impedance. For bolted three-phase faults, dip magnitude is zero, and as fault impedance increases, so does voltage dip magnitude. Voltage during fault is lower if fault impedance is considered inductive, as the power system is mostly inductive. Voltage recovery is slightly slower for lower dip magnitude values.

**Generator inertia** As observed in Figure 6.12(f), lower inertia constants lead to a slightly lower voltage dip and recovery is slower. The inertia of the generating unit that is closer to the fault point has more relevance.

**Voltage regulation system** As seen theoretically for the dynamic regulated model, the transient behaviour of a synchronous machine depends on the AVR system if present, but also on generator parameters. Regarding the excitation system, it can be concluded that the most influencing generator is the most electrically close to the PCC. For longer duration faults (e.g. 500 ms), transient stability is lost sooner if the closest generation has no excitation system. Regarding the generator parameters, it can also be seen that the most influencing generator is the most electrically close to the PCC (*Generator 2*).

**Comparison with voltage divider model** In order to compare the voltage divider model and the T-shaped model, two alternatives have been analysed. Firstly, the T-shaped model based on [117] has been simplified. Results are shown in Figure 6.13(a), compared to the base case based on [117]. If *Generator 2* is left out of service (G2 OOS), voltage drops in the transmission lines are high, and lower impedance values must be configured so as to solve the power flow: $Z_{l1} = Z_{l2} = 0.5$ p.u. have been selected in this case. The three-phase short-circuit at the PCC with $Z_f = 4.067\Omega$ results now into a square-shaped dip. Alternatively, if *Generator 1* is disconnected (G1 OOS), it also results into a divider model. Voltage dip is not square under that case, but recovery is still faster than the base case. Secondly, the voltage divider model with parameters in Table 6.5 has been converted into a T-shaped model by installing a second generator *Generator 2* (G2 in service) in the load bus, generating 10 MW. Figure 6.13(b) shows that recovery is slower than in the base case voltage divider model and that post-fault overvoltage is lower.

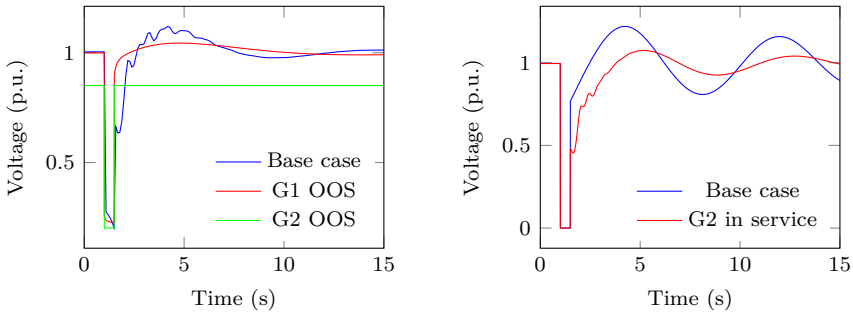


(a) T-shaped (b) Voltage divider

**Figure 6.13. Effect of generic model on voltage dip**

### 6.4.3 Parameterisation of grid model for grid code compliance verification

The voltage divider model is adequate as a first approach, and can be suitable for most small and medium size isolated systems. However, the T-shaped model is necessary to characterise voltage dips in wider networks, as well as to study transient stability.

LVRT profiles in the grid codes can be *square*, *step* or *ramp* profiles (Figure 4.5). For square dips, it is only necessary to adjust dip magnitude. Step profiles respond to the action of protection relays, which is out of the scope of the thesis. Ramp profiles represent a slower recovery, depending on generator dynamics, grid topology and voltage regulation. As overviewed in Section 6.3, analysis is complex under those factors and and analytical adjustment results into high-order equations. Therefore, only voltage dip magnitude is parameterised hereby. For both voltage dip models, voltage dip magnitude depends, among other factors, on the short-circuit power at the fault point and fault impedance. Therefore, particular grid models can be

tuned based on both those parameters: $Z_{l2}$ representing the fault impedance and $Z_{l1}$ limiting the short-circuit power at the fault point. $Z_{l1} = \frac{V_F^2}{S_{sc,F}}$. Short-circuit power must correspond to maximum values, attained under peak demand scenario. In small and medium size island grids, voltage source internal impedance is not dismissable. Generator parameters and voltage regulators must be set to typical values.

Considering an inductive power system source for simplicity, Table 6.6 indicates fault impedance values for resistive and inductive fault impedances for a given voltage dip magnitude and different short-circuit types. Resistive faults are commonly considered in real cases. However, [117] considers fault reactances as calculation is streamlined and reactive power requirements are higher under that assumption for WTGs. In the case of two-phase short-circuits, voltage dip magnitude corresponds to phase B for a fault between phases B and C. In the voltage divider model, $V_{eq}$ corresponds to the pre-fault voltage in p.u. and $X_{eq}$ to the positive sequence source reactance. For the T-shaped model, $V_{eq}$ is the equivalent voltage of both generator buses and $X_{eq}$ the equivalent positive sequence reactance. The voltage minimum and the fast recovery voltage can be calculated using (6.27) and (6.30) based on the parameterisation for dip magnitude. Two-phase-to-ground faults are out of the scope of the parameterisation because parameterisation results into high order equations and this type of fault is not generally mentioned in most of the grid codes under review in Chapter 2.

**Table 6.6. Voltage dip magnitude adjustment**

| Type | Resistive fault | Inductive fault |
|---|---|---|
| **3Ph** | $R_f = \dfrac{\lvert\underline{V}_{dip}\rvert \cdot X_{eq}}{\sqrt{\lvert\underline{V}_{eq}\rvert^2 - \lvert\underline{V}_{dip}\rvert^2}}$ (6.45) | $X_f = \dfrac{\lvert\underline{V}_{dip}\rvert \cdot X_{eq}}{\lvert\underline{V}_{eq}\rvert - \lvert\underline{V}_{dip}\rvert}$ (6.46) |
| **1Ph** | $R_f = \dfrac{\lvert\underline{V}_{dip}\rvert \cdot X_{eq}}{\sqrt{\lvert\underline{V}_{eq}\rvert^2 - \lvert\underline{V}_{dip}\rvert^2}}$ (6.47) | $X_f = \dfrac{\lvert\underline{V}_{dip}\rvert \cdot X_{eq}}{\lvert\underline{V}_{eq}\rvert - \lvert\underline{V}_{dip}\rvert}$ (6.48) |
| **2Ph** | $R_f = \dfrac{-b_1 \pm \sqrt{b_1^2 - 4 \cdot a_1 \cdot c_1}}{2 \cdot a_1}$ (6.49) | $X_f = \dfrac{-b_2 \pm \sqrt{b_2^2 - 4 \cdot a_2 \cdot c_2}}{2 \cdot a_2}$ (6.50) |
| Note: | $a_1 = \lvert\underline{V}_{dip}\rvert^2 - \lvert\underline{V}_{eq}\rvert^2$<br>$b_1 = -\lvert\underline{V}_{eq}\rvert^2 \cdot X_{eq}$<br>$c_1 = X_{eq}^2 \cdot \left(4 \cdot \lvert\underline{V}_{dip}\rvert^2 - \lvert\underline{V}_{eq}\rvert^2\right)$ | $a_2 = \lvert\underline{V}_{eq}\rvert^2 - \lvert\underline{V}_{dip}\rvert^2$<br>$b_2 = X_{eq} \cdot \left(\lvert\underline{V}_{eq}\rvert^2 - 4 \cdot \lvert\underline{V}_{dip}\rvert^2\right)$<br>$c_2 = X_{eq}^2 \cdot \left(\lvert\underline{V}_{eq}\rvert^2 - 4 \cdot \lvert\underline{V}_{dip}\rvert^2\right)$ |

# Chapter 7

# Voltage and current unbalance

## 7.1 Introduction

Voltage unbalance as a power quality issue is quite a common phenomenon, particularly in weak AC systems [143], because sources of unbalance can arise from multiple unsymmetrical conditions. It has been identified that unbalanced voltages can occur in weak power grids even during normal operation [144]. On one hand, insular weak power grids are mainly composed by distribution networks, which are prone to unbalanced voltage because of prevailing single phase loads, unbalanced phase impedance or combination of both [145], [146]. Generation sources might also contribute to unbalance. As an instance, photovoltaic systems connected to the grid produce structural unbalance and unbalance due to partial shading [147]. Single phase distributed generation also contribute to unbalance as they generate power on only one phase. Asymmetrical short-circuit faults do as well cause temporarily unbalanced regime and their study is of interest as they are more common than symmetrical shunt faults. Therefore, voltage unbalance is characterised in this chapter depending on the three main unbalancing factors: **asymmetrical short-circuit faults**, **series faults**, and **unbalanced loads**. Current unbalance is not generally considered a power quality parameter according to current standards [148], with a few exceptions. However, it is worth studying it, because it is a root cause of the aforementioned voltage unbalance phenomena.

This chapter reviews analytical models to characterise voltage and current unbalance in power systems and it is organised as follows. In Section 7.2, characteristic parameters regarding voltage and current unbalance are defined. In Section 7.3 voltage and current unbalance is analitically studied referred to three phenomena: asymmetrical short-circuits, series faults, and unbalanced loads. Unbalanced sources are out of the scope of this thesis. A particular grid model able to emulate voltage unbalance is introduced in Section 7.4, simplifying the initially proposed model following a sensitivity study. Subsection 7.4.3 introduces formulae leading to the parameterised grid model.

## 7.2 Voltage unbalance definition

A three-phase power system is called balanced if the three-phase voltages and currents have the same amplitude and are phase shifted by 120° with respect to each other. If these conditions are not met, the system is unbalanced.

Several parameters have been proposed to quantify the level of voltage and current unbalance. The most used concepts are described below.

**VUF** It is defined as the ratio of the negative sequence voltage component to the positive sequence voltage component, and therefore, subindex − is added accordingly. The percentage negative voltage unbalance factor is given by:

$$VUF_{-}(\%) = \frac{|\underline{V}_2|}{|\underline{V}_1|} \cdot 100 = K_{u-} \cdot 100 \tag{7.1}$$

Strictly speaking, VUF should also take into consideration zero sequence voltage component. Therefore, a similar ratio is sometimes defined for the homopolar versus direct magnitude ratio as well, called the **homopolar unbalance factor** $VUF_0$. However, most power systems are compensated and zero sequence currents cannot flow in those systems.

**CUF** Correspondent unbalance factors can be defined for current unbalance: CUF.

$$CUF_{-}(\%) = \frac{|\underline{I}_2|}{|\underline{I}_1|} \cdot 100 = K_{i-} \cdot 100 \tag{7.2}$$

Reference [149] introduces the concept of **total current unbalance factor** as the sum of negative and homopolar current unbalance factor. Correspondingly, a **total voltage unbalance factor** $TVUF$ could also be defined as:

$$TVUF(\%) = VUF_{-}(\%) + VUF_0(\%) \tag{7.3}$$

An easier approximate way to calculate the voltage asymmetry is:

$$VUF(\%) = \frac{S_L}{S_{sc}} \cdot 100 \tag{7.4}$$

This ratio only uses the apparent power of the load $S_L$ and the short-circuit power $S_{sc}$ of the supply circuit.

**Complex Voltage Unbalance Factor (CVUF)** It is an extension of VUF. It is defined as the ratio of the negative sequence voltage phasor to the positive sequence voltage phasor [150], and therefore, subindex − is added accordingly. Their ratio

results in a complex number, whose angle represents the lag between the negative and positive sequences. The percentage voltage unbalance factor is given by:

$$CVUF\_(\,\%) = \frac{\underline{V}_2}{\underline{V}_1} \cdot 100 = K_u \cdot 100\angle\Theta_u \tag{7.5}$$

The corresponding definition for current can also be introduced: Complex Current Unbalance Factor (CCUF).

**Load Unbalance Factor (LUF)** It is defined as the ratio between the maximum current and the balanced current absorbed by a three-phase load. It can also be expressed as a function of load phase impedances. Unbalance in phase A with respect to phases B and C can be expressed as:

$$LUF(\,\%) = \frac{|\underline{I}_a|}{|\underline{I}_b|} \cdot 100 = \frac{|\underline{Z}_a|}{|\underline{Z}_b|} \cdot 100 \tag{7.6}$$

In the previous definitions, sequence voltages are necessary for some unbalance measurements. Therefore, the theoretical analysis is further based on the symmetrical components theory, also called the Stokvis-Fortescue theorem.

## 7.3 Theoretical analysis

Voltage and current unbalance can arise because of transient disturbances such as short-circuit and series fault, as well as because of unbalanced loading in the power system. Therefore, the following theoretical characterisation of unbalance focuses on all three situations.

### 7.3.1 Analysis of asymmetrical short-circuit faults

In three-phase systems, shunt faults can result into balanced or unbalanced faults as indicated in Figure 7.1. The connection of the sequence circuits for short-circuits and expressions for voltage and current calculation at PCC are annexed in Appendix B. Based on above-mentioned expressions, Complex Voltage Unbalance Factor (CVUF) and Complex Current Unbalance Factor (CCUF) have been computed at the PCC for the different types of faults.

**Single-phase short-circuit**

$$CVUF = -\frac{\underline{Z}_2}{\underline{Z}_2 + \underline{Z}_0 + 3 \cdot \underline{Z}_f} \tag{7.7}$$

$$CCUF = 1 \tag{7.8}$$

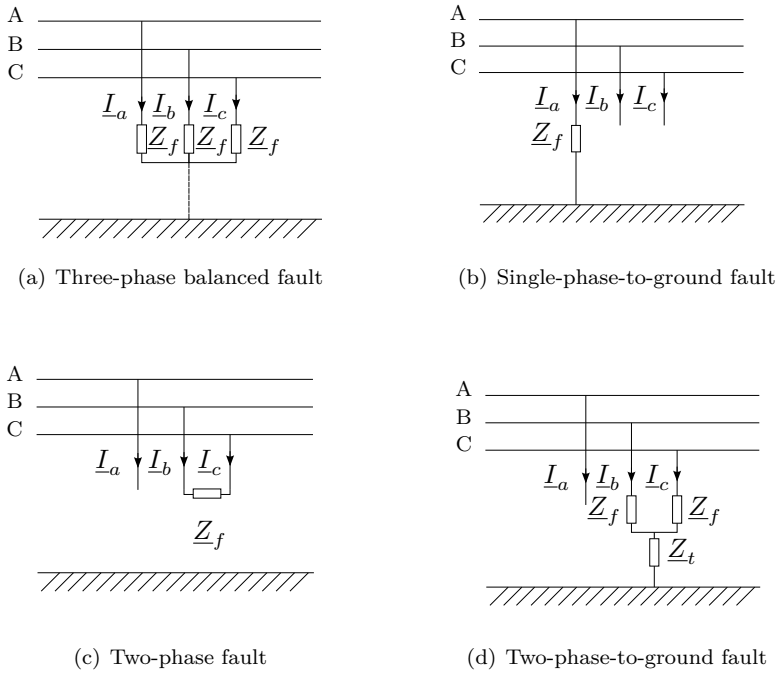


(a) Three-phase balanced fault

(b) Single-phase-to-ground fault

(c) Two-phase fault

(d) Two-phase-to-ground fault

**Figure 7.1. Types of short-circuits**

**Double-phase short-circuit**

$$CVUF = \frac{\underline{Z}_2}{\underline{Z}_2 + \underline{Z}_f} \tag{7.9}$$

$$CCUF = -1 \tag{7.10}$$

**Double-phase-to-ground short-circuit**

$$CVUF = \frac{\underline{Z}_2 \cdot \left(\underline{Z}_0 + \underline{Z}_f + 3 \cdot \underline{Z}_t\right)}{\left(\underline{Z}_2 + \underline{Z}_0 + 2 \cdot \underline{Z}_f + 3 \cdot \underline{Z}_t\right) \cdot \left(\underline{Z}_f + \underline{Z}\right)} \tag{7.11}$$

where: $\underline{Z} = \dfrac{\left(\underline{Z}_2 + \underline{Z}_f\right) \cdot \left(\underline{Z}_0 + \underline{Z}_f + 3 \cdot \underline{Z}_t\right)}{\underline{Z}_2 + \underline{Z}_0 + 2 \cdot \underline{Z}_f + 3 \cdot \underline{Z}_t}$

$$CCUF = -\frac{\underline{Z}_0}{\underline{Z}_2 + \underline{Z}_0} \tag{7.12}$$

### 7.3.2 Analysis of series faults

Another source of unbalance in power systems is the appearance of series faults. Common unbalances are a blown fuse or broken conductor, hereinafter called **one**

**open phase** (Figure 7.2(a)) and two blown fuses or open conductors, hereinafter called **two open phases** (Figure 7.2(b)). The loss of any phase may result in a notable reduction of voltage on one or more phases and a corresponding increase in voltage unbalance.

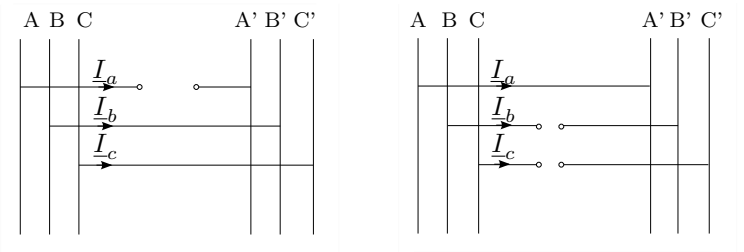


(a) One phase open (b) Two open phases

**Figure 7.2. Series fault types**

**Unequal phase impedances** are also included in this analysis (Figure 7.3). Unequal mutual impedances can arise as a result of asymmetrical electromagnetic coupling between the conductors of untransposed/partially transposed single circuit or multi-circuit transmission and distribution overhead lines, including a wide range of possible combinations between magnitudes and angles of the respective series impedances of phases A, B and C [151]. It also includes any other asymmetrical structure of network elements, such as transformers.

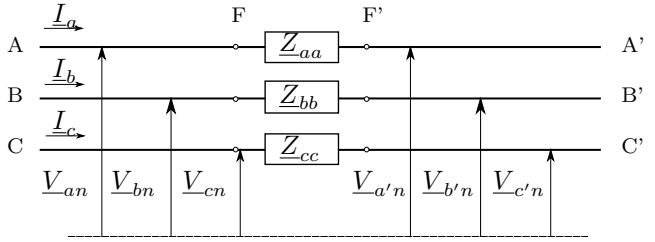


**Figure 7.3. Unequal series impedance**

In Figure 7.3 only self impedances of each phase $\underline{Z}_{aa}$, $\underline{Z}_{bb}$ and $\underline{Z}_{cc}$ are considered, as mutual impedances between phases have been neglected as they are often small compared to self impedances [152]. Among the wide range of possible combinations between magnitudes and angles of the self impedances, $\underline{Z}_{aa} \neq \underline{Z}_{bb} = \underline{Z}_{cc}$ is considered.

In series faults, there is no fault point in the sense described for shunt faults. Rather, there are two fault points, indicated with $F$ and $F'$, at both sides of the unbalance. Thus, the sequence network is still that of a completely symmetrical system, and the unbalanced portion is isolated outside the sequence network [152]. The connection of the sequence circuits for series faults, as well as the mathematical derivation can

be found in Appendix B. Current direction is assumed to be from $F$ to $F'$, and a voltage drop is shown in the assumed direction of current.

It must be remarked that load current must be included for these series unbalances, as the current is dependent on the load or difference between the system voltages on either side of the open. Load would be connected at terminals $A'$, $B'$ and $C'$. If load is omitted as it is common for the shunt faults, no current would be able flow in the networks. Balanced loading is considered for analysis purpose, as simultaneous unbalancing conditions are not considered.

Voltage and current during the series fault have been calculated between the faulted points $F$ and $F'$ and its positive, negative and zero components are indicated in Appendix B. Complex Voltage Unbalance Factor at terminals $A'$, $B'$ and $C'$ has been computed. A balanced three-phase voltage system is considered at phases $A$, $B$ and $C$. Therefore, negative voltage unbalance at load PCC can be calculated as indicated by (7.13). Complex Current Unbalance Factor has also been computed.

$$CVUF = \frac{-\underline{\Delta V}_{a2}}{\underline{V}_{pf} - \underline{\Delta V}_{a1}} \tag{7.13}$$

**Unequal impedances**

$$CVUF = -\frac{\underline{Z}_2 \cdot \underline{Z}}{\left(\underline{Z}_2 + \underline{Z}_0 + 2 \cdot \underline{Z}_{bb} + \dfrac{\underline{Z}_{aa} - \underline{Z}_{bb}}{3}\right)} \tag{7.14}$$

where: $\underline{Z} = \dfrac{(\underline{Z}_0 + \underline{Z}_{bb}) \cdot \left(\dfrac{\underline{Z}_{aa} - \underline{Z}_{bb}}{3}\right)}{\underline{Z}_0 + \underline{Z}_{bb} + \dfrac{\underline{Z}_{aa} - \underline{Z}_{bb}}{3}}$

$$CCUF = -\frac{\underline{Z}_0 + \underline{Z}_{bb}}{3 \cdot (\underline{Z}_2 + \underline{Z}_0) + 5 \cdot \underline{Z}_{bb} + \underline{Z}_2} \tag{7.15}$$

**One open phase**

$$CVUF = \frac{\underline{Z}_2 \cdot (\underline{Z}_0 + \underline{Z}_{bb})}{\underline{Z}_1 \cdot (\underline{Z}_2 + \underline{Z}_0 + 2 \cdot \underline{Z}_{bb})} \tag{7.16}$$

$$CCUF = -\frac{\underline{Z}_0 + \underline{Z}_{bb}}{2 \cdot \underline{Z}_{bb} + \underline{Z}_2 + \underline{Z}_0} \tag{7.17}$$

**Two open phases**

$$CVUF = \frac{\underline{Z}_2}{\underline{Z}_1} \tag{7.18}$$

$$CCUF = 1 \tag{7.19}$$

### 7.3.3 Analysis of unbalanced loads

Large loads in power systems are mostly three-phase symmetrical. A great number of existing small single-phase loads does not exceedingly distort the symmetry, as these loads are distributed almost evenly to all three phases and statistical variation in powers drawn by each phase is usually insignificant. Unbalance is mainly caused by large single-phase loads, such as single-phase electric railways or big single-phase electric furnaces. Unlike a short circuit condition, these unbalanced situations often exist for a long time before being detected.

This study focuses on both **one single-phase loads connected to line and phase voltages** (Figure 7.4), and **unbalanced three-phase loads connected in ungrounded and grounded star** (Figure 7.5), as well as in **delta** (Figure 7.6). Ungrounded star and delta three-phase loads are equivalent respectively to three single phase loads connected to phase and line voltages, respectively. The connection of the sequence circuits for unbalanced load, as well as the mathematical derivation can be found in Appendix B. Among the possible combinations between magnitudes and angles of the load impedances, for three-phase loads in star connection $\underline{Z}_a \neq \underline{Z}_b = \underline{Z}_c$ is assumed. For line connected three-phase loads, $\underline{Z}_{bc} \neq \underline{Z}_{ab} = \underline{Z}_{ca}$ is assumed.

Regarding three-phase loads, three kind of unbalance types can arise [148]: only amplitude unbalance (phase shifts between the phasors are equal), only phase unbalance (amplitudes of phasors are equal) and mixed unbalance (amplitude unbalance along with phase unbalance).

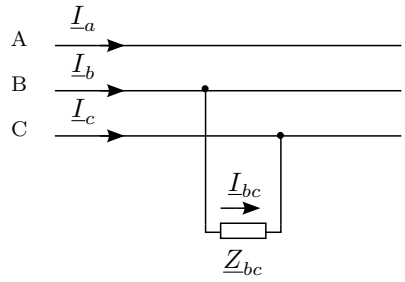


**Figure 7.4. Single-phase load between phases B and C**

Voltage due to unbalanced load has been calculated at the PCC of the load and its positive, negative and zero sequence components are indicated in Appendix B. Based on those expressions, Complex Voltage Unbalance Factor and Complex Current Unbalance Factor have been computed for unbalancing load situations under study. Load unbalance can be further characterised by Complex Load Unbalance Factor (CLUF).

**Single-phase load**

$$CVUF = \frac{\underline{Z}_2}{\underline{Z}_2 + \underline{Z}_{bc}} \tag{7.20}$$

$$CCUF = -1 \tag{7.21}$$

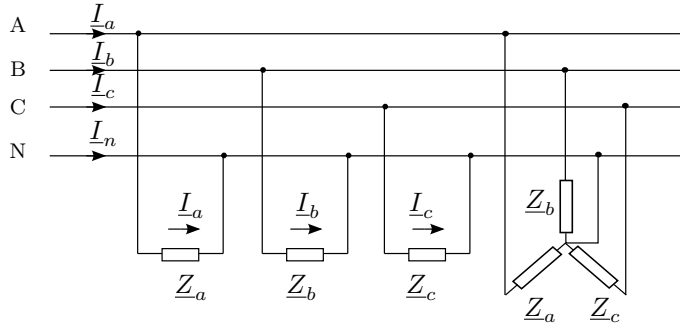


**Figure 7.5. Three-phase load in ungrounded star connection**

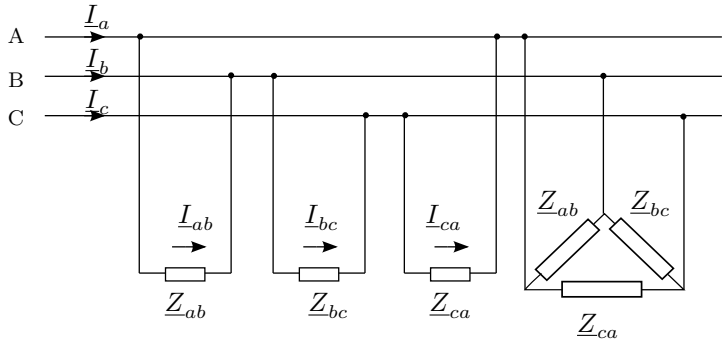


**Figure 7.6. Three-phase load in delta connection**

### Three-phase load in ungrounded star connection

$$CVUF = \frac{\underline{Z}_2 \cdot (\underline{Z}_a - \underline{Z}_b)}{\underline{Z}_b \cdot (2 \cdot \underline{Z}_2 + \underline{Z}_b + 2 \cdot \underline{Z}_a) + \underline{Z}_a \cdot \underline{Z}_2} \tag{7.22}$$

Voltage unbalance for a three-phase load in ungrounded star connection could therefore be calculated using (7.23). Negative voltage unbalance depends on the source strength in relation to the power drawn by the load and on the phase difference between source and load. In addition, it is also influenced by load unbalance type and degree, characterised by CLUF.

$$CVUF = \frac{\underline{CLUF} - 1}{2 + \underline{CLUF} + \dfrac{\underline{Z}_b}{\underline{Z}_2} \cdot (1 + 2 \cdot \underline{CLUF})} \tag{7.23}$$

$$CCUF = -\frac{\underline{Z}_a - \underline{Z}_b}{2 \cdot \underline{Z}_b + \underline{Z}_a + 3 \cdot \underline{Z}_2} \tag{7.24}$$

$$CCUF = \frac{\underline{CLUF} - 1}{2 + \underline{CLUF} + 3 \cdot \dfrac{\underline{Z}_2}{\underline{Z}_b}} \tag{7.25}$$

**Three-phase load in grounded star connection**

$$CVUF = \frac{\underline{Z}_2 \cdot \underline{Z}^{'}}{\left(\underline{Z}_2 + \underline{Z}_0 + 2 \cdot \underline{Z}_b + \dfrac{\underline{Z}_a - \underline{Z}_b}{3}\right) \cdot \left(\underline{Z}_b + \underline{Z}^{''}\right)} \tag{7.26}$$

where: $\underline{Z}^{'} = \dfrac{(\underline{Z}_0 + \underline{Z}_b) \cdot \left(\dfrac{\underline{Z}_a - \underline{Z}_b}{3}\right)}{\underline{Z}_0 + \underline{Z}_b + \dfrac{\underline{Z}_a - \underline{Z}_b}{3}}$ and $\underline{Z}^{''} = \dfrac{(\underline{Z}_2 + \underline{Z}_b) \cdot (\underline{Z}_0 + \underline{Z}_b) \cdot \left(\dfrac{\underline{Z}_a - \underline{Z}_b}{3}\right)}{\underline{Z}_2 + 2 \cdot \underline{Z}_b + \underline{Z}_0 + \dfrac{\underline{Z}_a - \underline{Z}_b}{3}}$

$$CCUF = -\frac{(\underline{Z}_0 + 3 \cdot \underline{Z}_N + \underline{Z}_b) \cdot \left(\dfrac{\underline{Z}_a - \underline{Z}_b}{3}\right)}{2 \cdot \underline{Z}_b + \underline{Z}_2 + \underline{Z}_0 + 3 \cdot \underline{Z}_N + \dfrac{\underline{Z}_a - \underline{Z}_b}{3}} \tag{7.27}$$

**Three-phase load in delta connection** Formulae for ungrounded star load can be applied.

### 7.3.4 Summary of unbalance cases

By inspection of sequence circuit connection for the unbalancing phenomena under study (Appendix B), it can be concluded that:

- Single-phase short-circuit and two open phases are equivalent considering $\underline{Z}_f = \underline{Z}_{aa}$.
- Two-phase short-circuit and single-phase load are equivalent considering $\underline{Z}_f = \underline{Z}_{bc}$.
- Two-phase-to-ground short-circuit and one open phase are equivalent considering $\underline{Z}_t = \underline{Z}_f = 0$.
- Unequal impedances and grounded star load are equivalent considering $\underline{Z}_{aa} = \underline{Z}_a$ and $\underline{Z}_{bb} = \underline{Z}_b$.
- Any load in ungrounded star connection can be converted into a delta load and vice versa.

Therefore, the unbalancing cases can be gathered into five general cases as indicated in Table 7.1. Thus, particular grid model parameterisation can be simplified as study cases are reduced.

**Table 7.1. Summary of unbalancing cases**

| Case | Subcase | Phenomenon |
|---|---|---|
| 1 | a | Single-phase short-circuit |
| | b | Two open phases |
| 2 | a | Two-phase short-circuit |
| | b | Single-phase load |
| 3 | a | Two-phase-to-ground short-circuit |
| | b | One open phase |
| 4 | a | Unequal series impedance |
| | b | Three-phase load in grounded star connection |
| 5 | a | Three-phase load in ungrounded star connection |
| | b | Three-phase load in delta connection |

## 7.4 Grid model and event representation

### 7.4.1 Particular grid model

The particular grid model proposed for voltage unbalance characterisation is introduced in Figure 7.7, where *Generator 2* has been excluded. $Z_{l1}$ limits the short-circuit power at the PCC and $Z_{l2} = 0$ for series faults and unbalanced loading. Regarding asymmetrical short-circuits, $Z_{l2}$ represents the fault impedance or distance to the fault from the PCC. Load must be balanced for asymmetrical short-circuit and series faults, whereas it represents the unbalanced loading for the third case.

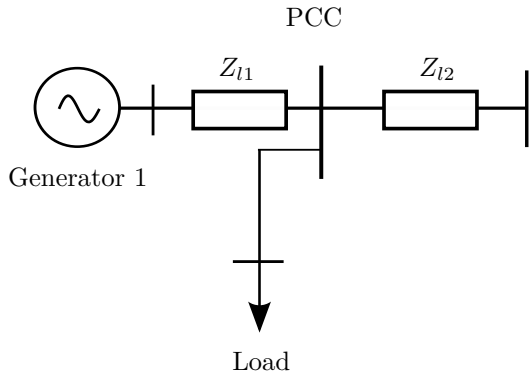


**Figure 7.7. Particular grid model for voltage unbalance**

### 7.4.2 Sensitivity of particular grid model parameters

It is important to study the sensitivity of the magnitude of the negative unbalance factor with respect to system parameters and fault characteristics, in order to derive a simplified power system model valid to characterise unbalance in island grids. Therefore, sensitivity analysis have been performed for unbalanced short-circuits, series faults and unbalanced loads based on the particular grid model in Figure 7.7. Rated voltage in the system is 66 kV.

#### 7.4.2.1 Sensitivity analysis of asymmetrical short-circuits

Following factors have been studied: type of short-circuit, strength of the power system, $R/X$ factor of the power system, and distance to the faulted point.

As first step, following simplifying hypothesis have been assumed: all three sequence source impedances are equal, $\underline{Z}_f = 0$, $\underline{V}_{pf} = 1 p.u.$, and $\underline{Z}_t = 0$.

**Type of short-circuit** It can be easily derived that under those assumptions VUF only depends on the short-circuit type. The highest negative voltage unbalance occurs for double-phase and double-phase-to-ground short-circuit with a %100 of unbalance, as plotted in Figure 7.8. Therefore, voltage unbalance at the faulted pointed does not depend on the power system strength nor on the $R/X$ ratio, which characterise weak power grids.

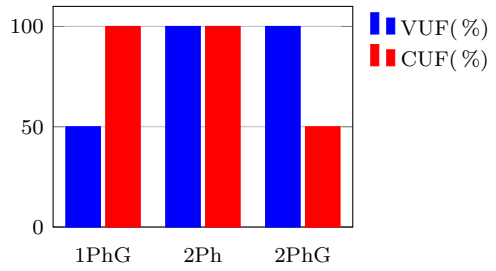


**Figure 7.8: Effect of fault type on negative voltage and current unbalance magnitude**

Regarding current unbalance, assuming as only simplifying hypothesis that all three sequence source impedances are equal, magnitude of CUF is 100 % for single-phase and double-phase short-circuits, and 50 % for double-phase-to-ground short-circuits.

**Distance to the fault** On the other hand, dependence between voltage unbalance and distance to the fault has also been studied in Figure 7.9. Results show that the propagation of the voltage unbalance depends on power system characteristics, such as short-circuit power and $R/X$ ratio. As distance to the faulted point increases, VUF decreases, especially in stronger power grids (1000 MVA). In weaker power grids (100 MVA), is only slightly attenuated. The unbalance reduction in relation with short-circuit power appears to a greater extent for double-phase-to-ground faults.

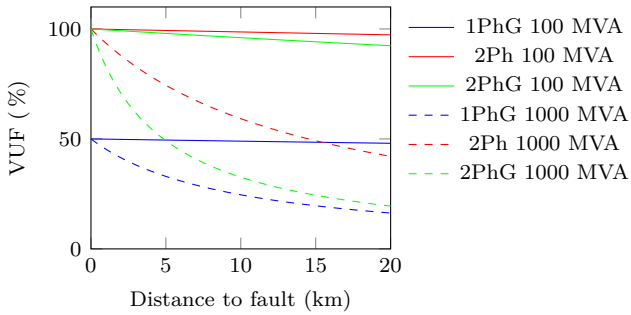


**Figure 7.9: Effect of short-circuit type and grid strength on the propagation of VUF**

**$R/X$ ratio of the power system** Figure 7.10 plots the voltage unbalance at the PCC under single-phase short-circuits for weak and strong power grids (with respectively 100 MVA and 1000 MVA short-circuit power in a 66 kV network) in function of the $X/R$ ratio of the source. Considering a totally inductive feeder, voltage unbalance propagation is lower in more inductive power sources. The effect can be clearly seen in strong power grids, where voltage unbalance is dramatically attenuated.

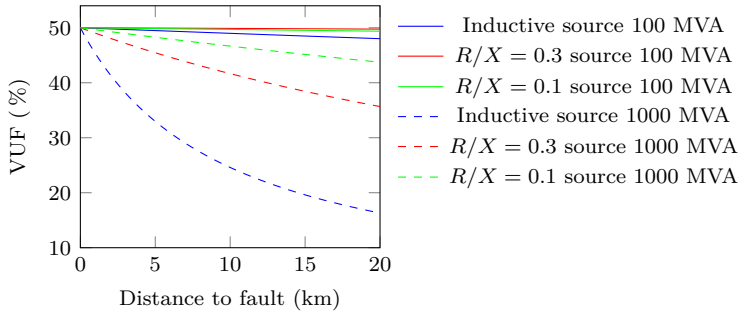


**Figure 7.10. Effect of $R/X$ on the propagation of VUF (1PhG)**

It can be concluded that in weak power grids voltage unbalance mainly depends on the short-circuit type. Regarding current unbalance, factors are always constant considering all sequence impedances equal. For both unbalance factors, values between 50 % and 100 % are reached.

#### 7.4.2.2 Sensitivity analysis of series faults

Following factors have been studied: type of series fault, loading of the power system, strength of the power system, $R/X$ factor of the power system, and length of the faulted feeder. As first step, all three sequence source impedances are assumed equal, and load connected at $A'B'C'$ end is considered to be connected in grounded star.

**Type of series fault** It can be easily derived that under those assumptions, negative voltage unbalance factor is constant for one phase open and two phases open conditions as shown in Figure 7.11, with respectively 50 % and 100 % of negative voltage unbalance at load terminals. For unbalanced series impedance situation,

negative voltage unbalance factor reaches values close to 0 %. Regarding current unbalance, a constant 100 % value results under two open phase situation. Under the above assumed hypothesis, current unbalance is also held constant at 50 % for an open phase. For unbalanced series impedance situation, negative current unbalance factor reaches values around 14 %.

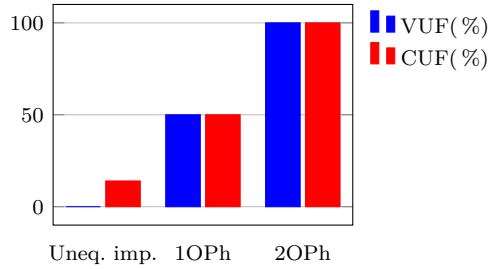


**Figure 7.11: Effect of fault type on negative voltage and current unbalance magnitude**

**Other factors** The effect of loading, strength and $R/X$ ratio of the power system has been studied. Though, the influence of these factors is negligible. However, the length of the faulted feeder is relevant, although in all cases unbalance factors are under 1 %. Figure 7.12 shows that unbalance increases almost linearly with feeder length, but always remaining at very low levels. So as to highlight the small magnitude of the impact, unrealistically long feeder lengths in island grids have been considered.

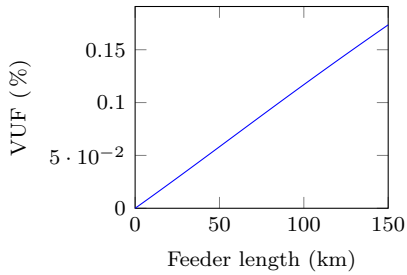


**Figure 7.12. Effect of feeder length on VUF for unequal series impedance**

It can be concluded that unbalance factors under 50 % are reached only under unequal impedance phenomenon. However, unbalance factors are hardly adjustable, because aspects such as loading, strength and $R/X$ ratio of the source have very low effect.

#### 7.4.2.3 Sensitivity analysis of unbalanced loading

Following factors have been studied: type of unbalanced load connection, unbalance type (amplitude and/or phase unbalance), $X/R$ ratio of source and load, and strength of the power system.

**Single-phase load connected to line voltage** Voltage unbalance caused by a single-phase load connected to line voltage depends on both the short-circuit power at the PCC and power drawn by the load. Therefore, it depends on the SCR and on the power factor difference between source and load, as stated in (7.28), if positive and negative sequence impedances are assumed to be equal.

$$CVUF = \frac{1}{1 + \frac{\underline{S}_{sc}}{\underline{S}_l}} = \frac{|\underline{S}_{sc}| \cdot e^{j \cdot \varphi_{source}}}{|\underline{S}_l| \cdot e^{j \cdot \varphi_{load}}} = \frac{e^{j \cdot (\varphi_{source} - \varphi_{load})}}{SCR} \tag{7.28}$$

Figure 7.13 shows the results based on a single load connected to line voltage with different power factor values. Voltage unbalance decreases with the strength of the power grid, whereas it increases as the load is more resistive.

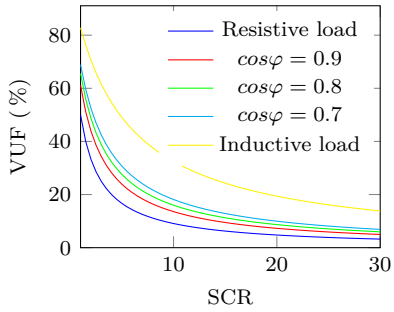


**Figure 7.13. Effect of SCR ratio on VUF for single-phase load**

On the other hand, CUF is constant under any circumstance, with a value of 100 %.

**Three-phase loads** Three-phase unbalanced loads can have amplitude and/or phase unbalance. For only amplitude unbalance, voltage unbalance is scarcely related to phase difference between source and load (Figure 7.14), but depends strongly on the load unbalance degree and strength of the power system. As observed in Figure 7.15, voltage unbalance curves tend to very low values close to zero as power system strength increases. In addition, voltage unbalance increases if unbalanced phase draws less current, i.e. as CLUF magnitude is higher.

Only phase unbalance has also been analysed. With higher phase shift difference voltage unbalance increases. However, in stronger power grids, all the cases show similar low values. Finally, mixed load unbalance has been studied in Figure 7.16.

It can be concluded that negative voltage unbalance depends on source strength and $R/X$ ratio, power drawn by the load and its power factor, as well as on load unbalance type and degree. Single-phase load creates a higher voltage unbalance than three-phase unbalanced loads.

On the other hand, current unbalance increases with power system strength, whereas phase shift only affects current unbalance in weak power grids. In stronger grids the influence is barely noticeable.

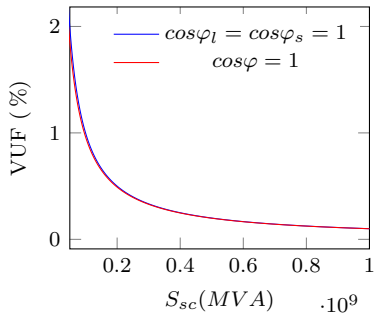


**Figure 7.14: Effect of power system strength and phase shift on VUF (Case 1, only amplitude unbalance)**

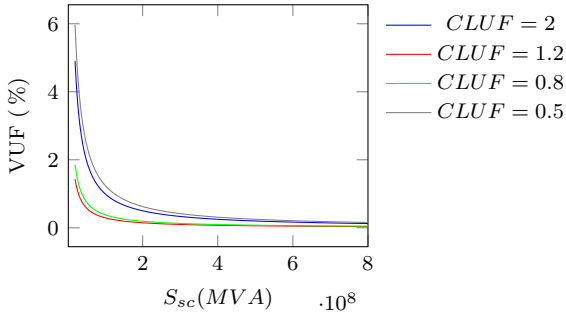


**Figure 7.15: Effect of power system strength on VUF (Case 1, only amplitude unbalance)**

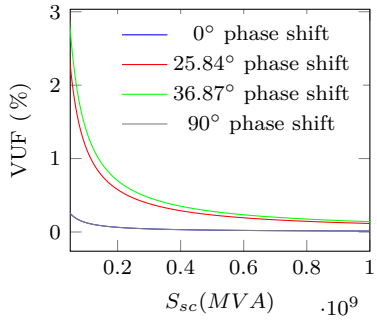


**Figure 7.16. Effect of power system strength on VUF (Case 3, mixed unbalance)**

### 7.4.3 Parameterisation of grid model for grid code compliance verification

The cases summarised in Table 7.1 can be divided into two categories: long-term and temporary unbalancing phenomena. Shunt faults, and one and two open phase series faults belong to the last category; unequal series impedance and load unbalance are inherent in power systems, especially at distribution voltage level. However, unequal series impedance barely causes any voltage unbalance, as shown in Section 7.3.2 and

temporary unbalancing phenomena cause high voltage and current unbalances.

Therefore, the theoretical adjustment for grid code compliance verification focuses on unbalanced loading. Current grid code limits for current unbalance values stay between 0.1 % and 5 % and for voltage unbalance, between 0.7 and 2 %. In all reviewed grid codes, only the limit for unbalance magnitude is considered. Therefore, VUF and CUF parameters have been chosen to measure voltage and current unbalance.

Based on the sensitivity study and in order to simplify the analytical calculation, an inductive voltage source and resistive loads have been assumed in the particular grid model (Figure 7.7). In addition, in small and medium size island grids, voltage source internal impedance is not dismissable. For three-phase loads, only magnitude unbalance is considered. Formulae for adjustment under those assumptions are indicated in Tables 7.2 and 7.3, where $X_2$ is the negative sequence source impedance at the PCC, $K_u$ the magnitude of voltage unbalance, $LUF$ load unbalance factor as the ratio between phase A and B impedance, and $K_i$ the magnitude of current unbalance. For current unbalance adjustment, only three-phase loads are considered, because single-phase loads always result in a 100 % of current unbalance magnitude. $Z_{l1}$ must be adjusted to the lowest short-circuit power scenario, which generally results in a higher unbalance, as highlighted in the sensitivity study. For three-phase loads, $R_a = LUF \cdot R_b$.

**Table 7.2. Theoretical load characteristics adjustment for a given CUF**

| **Unbalancing case** | **Theoretical adjustment** |
|---|---|
| Ungrounded star 3Ph load | $R_b = \dfrac{3 \cdot X_2 \cdot K_i}{\sqrt{(LUF-1)^2 - K_i^2 \cdot (2+LUF)^2}}$ (7.29) |

**Table 7.3. Theoretical load characteristics adjustment for a given VUF**

| Unbalancing case | Theoretical adjustment |
|---|---|
| Single-phase load | $R_{bc} = \sqrt{\left(\frac{X_2}{K_u}\right)^2 - X_2^2}$ (7.30) |
| Ungrounded star 3Ph load | $R_b = \frac{X_2 \cdot \sqrt{(LUF-1)^2 - K_u^2 \cdot (2+LUF)^2}}{K_u \cdot (1+2 \cdot LUF)}$ (7.31) |

# Part IV

# Numerical application of the compliance verification methodology

# Chapter 8

# Practical application: a medium size island

## 8.1 Introduction

The methodology proposed in this thesis will be validated by the application to three island study cases. This chapter verifies the methodology with **Case 1**: a medium size island, with no dynamic data available and no grid code under force. It is considered as the general case.

The initial data about the medium size island under study is summarised in Table 8.1, based on data in [153]. It has been assumed that a new photovoltaic plant is planned to be installed.

This chapter is organised as follows. First, particular grid models worked out after the theoretical analysis in previous chapters have been been parameterised based on typical values in similar islands and limits in relevant grid codes. Then, the validity of the particular grid models has been verified in Section 8.2. Finally, the performance of the new renewable power plant model connected to the parameterised grid model has been tested by means of simulation in Section 8.3.

**Table 8.1. Initial data for Case 1**

| Parameter | Value |
|---|---|
| Peak load | 12.9 MW |
| Valley load | 5.9 MW |
| Voltage at PCC | 20 kV |
| $S_{sc,max}$ at PCC | 100 MVA |
| $S_{sc,min}$ at PCC | 60 MVA |

## 8.2 Parameterisation of particular grid models

For each of the three requirements under study, the particular grid has been parameterised based on corresponding formulae in Chapter 5, 6 and 7 of Part III. As only static data in Table 8.1 is available, the adjustment has been carried out based on typical values in similar size islands and limits imposed by selected grid codes. Particular grid models have been adjusted to obtain certain values at the PCC, as technical requirements are indicated at that point. The parameterised grid model has been simulated with *PowerFactory* simulation software package and results compared to adjustment values, so as to verify the validity of the theoretical formulae proposed in Part III.

### 8.2.1 Adjustment results

**Frequency ride-through** The results of the adjustment methodology for the parameterisation of frequency ride-through are stated in Table 8.2. Limits are based on the grid code requirements in the SEIE. Regarding the equivalent generator *Generator 1*, its rated power is $S_N = 10$ MVA, with $H_{eq} = 2.16s$, $R_{eq} = 0.061$ and $T_{eq} = 6.1s$ for the generation scenario under study, corresponding to valley load. The rated capacity of *Generator 2* is $S_N = 5$ MVA and the rest of the characteristics is as for *Generator 1*. The target system is a medium size island, and hence, the loss of a single generator can result into a high proportion of the total installed capacity. So, the values for maximum and minimum frequency have been calculated with (5.50).

**Table 8.2: Case 1: parameterisation of particular grid model for frequency ride-through**

| Test | Parameter | Limit | $G_2$ | Load 1 | Load 2 |
|---|---|---|---|---|---|
| A1 | $fmax$ | 52 Hz | - | 3.95 MW | 1.95 MW |
| A2 | $f_{min}$ | 47 Hz | 1.95 MW | 2.95 MW | 2.95 MW |
| A3 | $f_{ss,h}$ | 50.25 Hz | - | 4.67 MW | 1.23 MW |
| A4 | $f_{ss,l}$ | 49.75 Hz | 0.82 MW | 2.95 MW | 2.95 MW |
| A5 | $ROCOF+$ | 2 Hz/s | - | 3.31 MW | 2.59 MW |
| A6 | $ROCOF-$ | -2 Hz/s | 1.73 MW | 2.95 MW | 2.95 MW |

**LVRT** For LVRT, the divider model has been selected as particular grid model because distances between assets in the island are short. The adjustment for LVRT has been carried out based on SEIE requirements. Only dip magnitude has been adjusted. The results of the adjustment methodology are stated in Table 8.3. Resistive faults and inductive sources have been assumed, based on the sensitivity study in Chapter 6. $Z_{l1}$ has been calculated so as to obtain the maximum short-circuit power at the PCC taking into account the generator internal impedance. $Z_{l2}$ has been adjusted in function of the dip magnitude.

Weak power grids generally set very low minimum dip magnitudes to ride-through. As seen in Chapter 2, in most of the cases a ZVRT is required. However, it order to

**Table 8.3. Case 1: parameterisation of particular grid model for LVRT (SEIE)**

| Test | Parameter | Limit | $Z_{l1}$ | $Z_{l2}$ | $G_1$ | Load |
|---|---|---|---|---|---|---|
| B1-SEIE | $V_{dip,3Ph}$ | 0 p.u. (0.5 s) | $0.64j \cdot \Omega$ | 0 | 25 MVA | 12.9 MW |
| B2-SEIE | $V_{dip,1Ph}$ | 0 p.u. (0.5 s) | $0.64j \cdot \Omega$ | 0 | 25 MVA | 12.9 MW |
| B2-SEIE | $V_{dip,2Ph}$ | 0.5 p.u. (0.5 s) | $0.64j \cdot \Omega$ | 0 | 25 MVA | 12.9 MW |

prove the validity of the parameterisation for LVRT, grid code requirements for peninsular Spain (Sistema Eléctrico Peninsular Español (SEPE)) have been used also. In the SEPE, voltage dip magnitude to ride-through must be 0.2 p.u. for all short-circuit types unless two-phase faults, where a lowest value of 0.6 p.u. is indicated. Table 8.4 indicates the parameterisation of the particular grid model for the SEPE.

**Table 8.4. Case 1: parameterisation of particular grid model for LVRT (SEPE)**

| Test | Parameter | Limit | $Z_{l1}$ | $Z_{l2}$ | $G_1$ | Load |
|---|---|---|---|---|---|---|
| B1-SEPE | $V_{dip,3Ph}$ | 0.2 p.u. (0.5 s) | $0.64j \cdot \Omega$ | 0.8165Ω | 25 MVA | 12.9 MW |
| B2-SEPE | $V_{dip,1Ph}$ | 0.2 p.u. (0.5 s) | $0.64j \cdot \Omega$ | 0.8165Ω | 25 MVA | 12.9 MW |
| B2-SEPE | $V_{dip,2Ph}$ | 0.6 p.u. (0.5 s) | $0.64j \cdot \Omega$ | 1.432Ω | 25 MVA | 12.9 MW |

**Unbalance** Unbalance limits are based on SEIE grid code for CUF (5 %) and VUF (2 %). The results of the adjustment methodology are stated in Table 8.5. All sequence impedances have been considered equal and a value of $LUF = 2$ for three-phase loads. The selected scenario is valley demand with minimum short-circuit value ($S_{sc,min}$), as voltage unbalance results into higher values.

The single load corresponds to $P_{bc} = 1.2$ MW and the three-phase load $P_a = 1MW$ and $P_b = P_c = 2MW$. For the CUF adjustment, resulting active power absorbed by the unbalanced load is $P_a = 64.1MW$ and $P_b = P_c = 128.2MW$, values that are over the capacity and stability limits of the power grid.

**Table 8.5. Case 1: parameterisation of particular grid model for unbalance**

| Test | Parameter | Limit | $Z_{l1}$ | $G_1$ | Load |
|---|---|---|---|---|---|
| C1 | VUF | 2 % | $1.07 \cdot j\Omega$ | 15 MVA | $R_{bc} = 333.43\Omega$<br>$R_a = 133\Omega$, $R_b = 66.5\Omega$ |
| C2 | CUF | 5 % | $1.07 \cdot j\Omega$ | 15 MVA | $R_a = 2.08\Omega$, $R_b = 1.04\Omega$ |

## 8.2.2 Verification of the parameterisation

The validity of the parameterised grid model has been verified by means of simulation. The parameterised models have been implemented with *PowerFactory* Digsilent software package as indicated in Appendix C. Then, the simulation results have

been benchmarked against the grid code limits in use in each requirement. Figure 8.1 shows the results of the adjustment for *Frequency Ride-Through* requirement. The adjustment for the rest of requirements can be verified in Figure 8.2. Grid code limits are plotted with discontinuous line, in green for two-phase short-circuits and in red for the rest of the fault types.

The relative errors between the theoretical model and the simulation results have been computed for each technical requirement and can be looked up in Table 8.6. The error for LVRT has been computed, but the dip envelope has been also compared against the SEIE profile. Errors are within ±10 %. Hence, theoretical expressions for the particular grid model adjustment can be hereby validated, as well as the parameterised grid models.

**Table 8.6. Case 1: parameterised grid model validation results**

| Test | Parameter | Limit | Result | Error ( %) | Verification |
|---|---|---|---|---|---|
| A1 | $fmax$ | 52 Hz | 51.97 Hz | 0.058 % | ✓ |
| A2 | $f_{min}$ | 47 Hz | 46.94 Hz | 0.13 % | ✓ |
| A3 | $f_{ss,h}$ | 50.25 Hz | 50.248 Hz | -0.004 % | ✓ |
| A4 | $f_{ss,l}$ | 49.75 Hz | 49.751 Hz | 0.002 % | ✓ |
| A5 | ROCOF+ | 2 Hz/s | 1.94 Hz/s | -3 % | ✓ |
| A6 | ROCOF- | -2 Hz/s | -1.95 Hz/s | -2.5 % | ✓ |
| B1-SEIE | $V_{dip,3Ph}$ | 0 p.u. | 0 p.u. | 0 % | ✓ |
| B2-SEIE | $V_{dip,1PhG}$ | 0 p.u. | 0 p.u. | 0 % | ✓ |
| B2-SEIE | $V_{dip,2Ph}$ | 0.5 p.u. | 0.49 p.u. | 2 % | ✓ |
| B1-SEPE | $V_{dip,3Ph}$ | 0.2 p.u. | 0.193 p.u. | -3.5 % | ✓ |
| B2-SEPE | $V_{dip,1PhG}$ | 0.2 p.u. | 0.193 p.u. | -3.5 % | ✓ |
| B2-SEPE | $V_{dip,2Ph}$ | 0.6 p.u. | 0.62 p.u. | 3.33 % | ✓ |
| C1 (1Ph load) | VUF | 2 % | 2 % | 0 % | ✓ |
| C1 (3Ph load) | VUF | 2 % | 1.99 % | -0.5 % | ✓ |

## 8.3 Practical application of the methodology

A new photovoltaic plant with a rated capacity of 1.78 MA is planned to be installed in the island. The PCC of the PV plant has the characteristics indicated in Table 8.1. Even for the worst case, SCR results into high values. The power plant is connected to the substation PCC with an overhead line of 5 km. The photovoltaic plant has been modelled with *PowerFactory* software package, based on a grey-box user model and parameterised according to values indicated in Appendix C, where the user model and the equivalent grid model are also described. The methodology has been applied

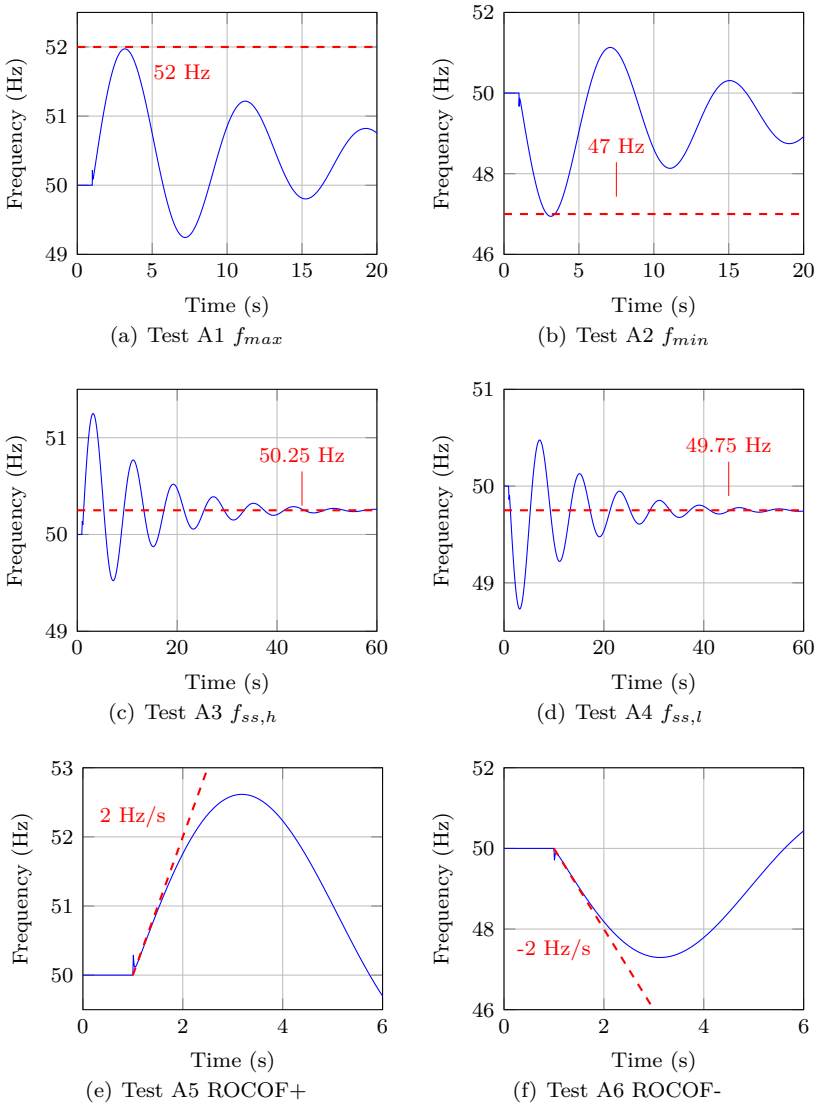


(a) Test A1 $f_{max}$ (b) Test A2 $f_{min}$

(c) Test A3 $f_{ss,h}$ (d) Test A4 $f_{ss,l}$

(e) Test A5 ROCOF+ (f) Test A6 ROCOF-

**Figure 8.1. Case 1: verification of the adjustment of frequency ride-through**

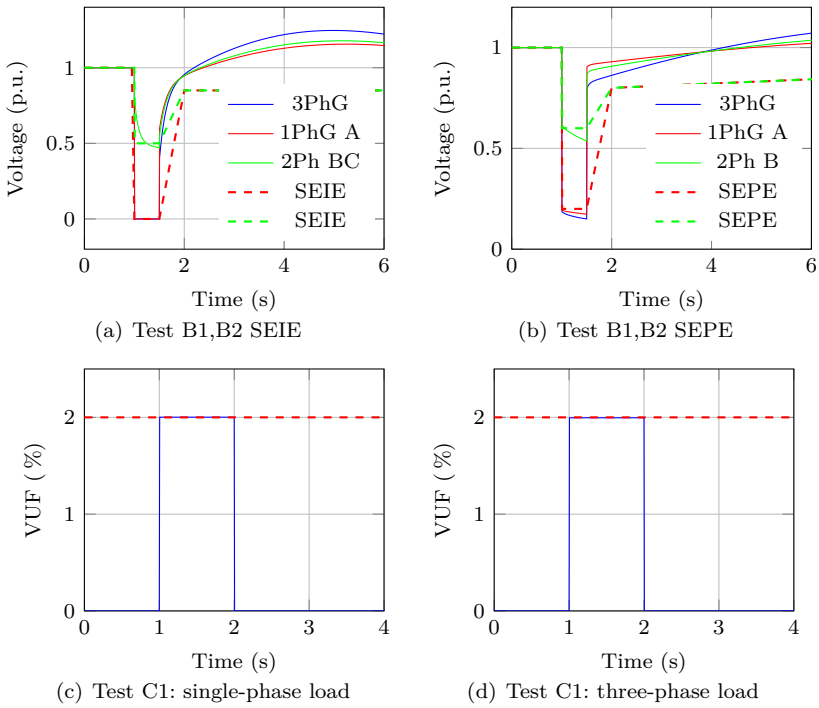


**Figure 8.2. Case 1: verification of the rest of parameters**

so as to verify if the new power plant complies with the technical provisions in the SEIE grid code regarding the requirements under study.

For remain connected requirements, two events have been simulated by adjusting the simplified equivalent grid for each of the compliance tests defined in Chapter 4: an event outside the permitted range in the grid code in the SEIE (indicated suffix -1 in test identificator), and an event within the permitted range (indicated suffix -2 in test identificator). Limit values are based on grid code provisions as indicated in Section 8.2. For active support requirements, generator contribution is showed by simulating an event within limits (suffix -2).

**Frequency ride-through** Frequency ride-through test cases are listed in Table 8.7. For *Frequency ride-through* verification, the frequency response block of the plant has been disabled, so as to be able to observe the trip of the plant when frequency is beyond permitted values. This feature can be achieved by conveniently adjusting the protection relay settings of the generation asset. In addition, for a better observance of ROCOF events, under/overfrequency protection relays have been disabled for test cases A5 and A6. Test cases A3 and A4 have not been considered, because only primary protection relays have been configured in the model.

Figure 8.3 plots the system frequency and power output of the power plant for each case. The power output is expressed in p.u. with respect of initial power reference.

**Table 8.7. Case 1: frequency ride-through test cases**

| Test case | Parameter | Limit | Test value |
|---|---|---|---|
| A1-1 | $f_{max}$ | 52 Hz | 52.5 Hz |
| A1-2 | $f_{max}$ | 52 Hz | 51.5 Hz |
| A2-1 | $f_{min}$ | 47 Hz | 46.5 Hz |
| A2-2 | $f_{min}$ | 47 Hz | 47.5 Hz |
| A5-1 | ROCOF | 2 Hz/s | 2.2 Hz/s |
| A5-2 | ROCOF | 2 Hz/s | 1.8 Hz/s |
| A6-1 | ROCOF | -2 Hz/s | -2.2 Hz/s |
| A6-2 | ROCOF | -2 Hz/s | -1.8 Hz/s |

It can be observed that the power plant trips correctly during the events out of the permitted range with suffix -1. For underfrequency events beyond the limits, the power plant is tripped, which increases the power imbalance, and hence, the system frequency deviation. ROCOF events result into a slower trip of the power plant, which depends on the measuring window for the computation of frequency gradient used in *PowerFactory* simulation package.

**Frequency response** This feature has been parameterised with values within an acceptable range in the SEIE grid code by reproducing test case A2-2, as indicated in Appendix C. Frequency response for both high and low frequencies has been tested based on an underfrequency event, because frequency decreases during the drop but increases (and decreases) alternatively during recovery, until the steady-state situation. Thus, as frequency drops the power plant increases its active power generation, whereas the contrary happens as frequency starts to recover. This behaviour can be observed in in Figure 8.4, where simulation results are plotted. The power output of the PV plant in p.u. has been calculated respect of its rated active power.

**LVRT** According to the LVRT requirement in the SEIE, two events have been simulated by adjusting the fault duration: an event within the permitted range with $t_{dip}$ = 250 ms (B1-2) and an event outside the permitted range with $t_{dip}$ = 650 ms (B1-1). Test B2, corresponding to unbalanced faults, is out of the scope of the practical application, because the generating unit model under study does not include the ability to ride-through unbalanced faults. LVRT test cases are listed in Table 8.8.

**Table 8.8. Case 1: LVRT test cases**

| Test case | Parameter | Limit | Test value |
|---|---|---|---|
| B1-1 | $V_{dip,3Ph}$ | 0 p.u. (0.5 s) | 0 p.u. (0.650 s) |
| B1-2 | $V_{dip,3Ph}$ | 0 p.u. (0.5 s) | 0 p.u. (0.250 s) |

Figure 8.5 shows voltage profiles at the PCC for both events with limit profile based on SEIE regulation. The power generation asset meets the regulations in Spain; it

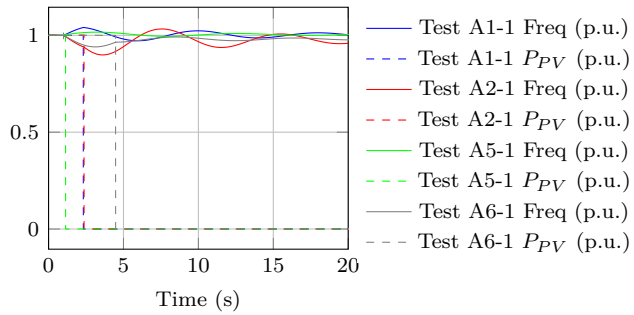


(a) Events out of the permitted range

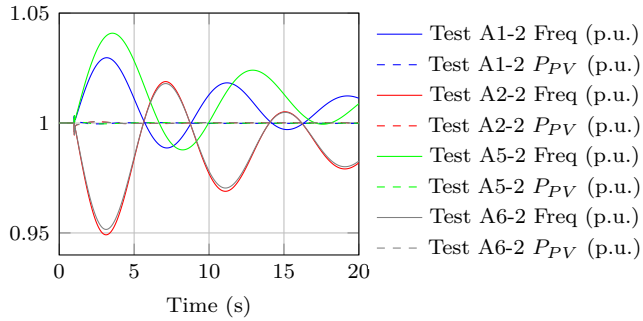


(b) Events within the permitted range

**Figure 8.3. Case 1: validation of the procedure for frequency ride-through**

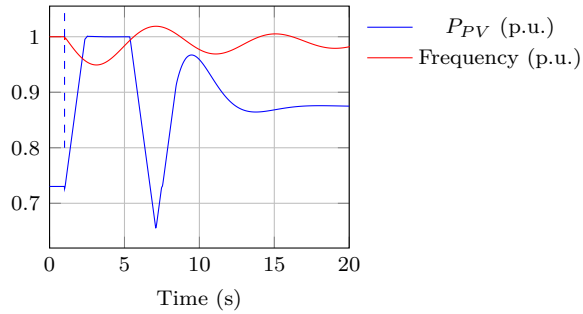


**Figure 8.4. Case 1: validation of the procedure for frequency response**

trips during event B1-1 and remains connected and generating during event B1-2. In test case B1-2 shown in Figure 8.5(d), the power plant remains connected and there is an active and reactive power output. The power output is related to the output current requirements in Spain, which are active during 10 seconds from the event of the fault.

**Output current during faults** According to most grid codes, active and reactive current injection as a function of voltage can be specified by some reference

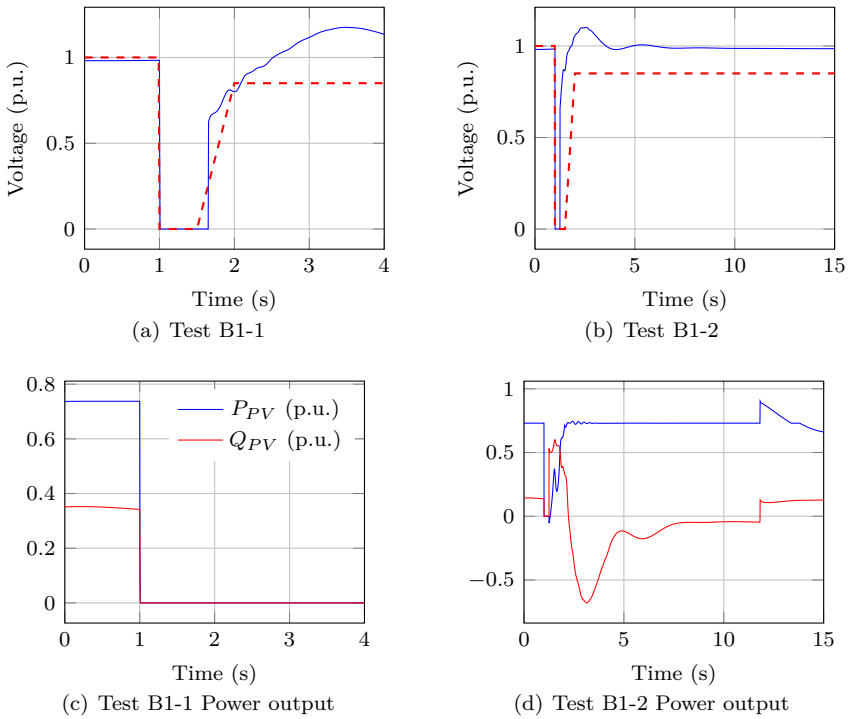


**Figure 8.5. Case 1: validation of the procedure for LVRT**

points. Adjustment values for SEIE regulation are indicated in Appendix C. The control block of the equivalent converter of the power plant has been accordingly parameterised with values within an acceptable range in the SEIE grid code.

The event leading to the current injection tests for balanced faults is TEST B1-2, which corresponds to a balanced LVRT situation. Both active and reactive power are shown in Figure 8.5(d) as required for tests B3 and B4. Support during fault has been specified to be active during 10 seconds after the recovery. Tests B5 and B6, corresponding to current contribution during faults for unbalanced faults, is out of the scope of the practical application, because the generating unit model does not include the ability to contribute to unbalanced faults.

**Unbalance** Unbalance test cases are listed in Table 8.9. Only voltage unbalance has been considered, because current unbalance adjustment condition leads to instability as indicated in Section 8.2. Three-phase loading has been selected as unbalancing event.

Figure 8.6(a) shows the unbalance at the PCC after the grid model adjustment, whereas 8.6(b) plots the action of the protection relay (ANSI function 47) which trips the PV plant. When unbalance is below the limit value, the power plant remains connected.

**Table 8.9. Case 1: unbalance test cases**

| Test case | Parameter | Limit | Test value |
|---|---|---|---|
| C1-1 | VUF | 2 % | 2.5 % |
| C1-2 | VUF | 2 % | 1.5 % |

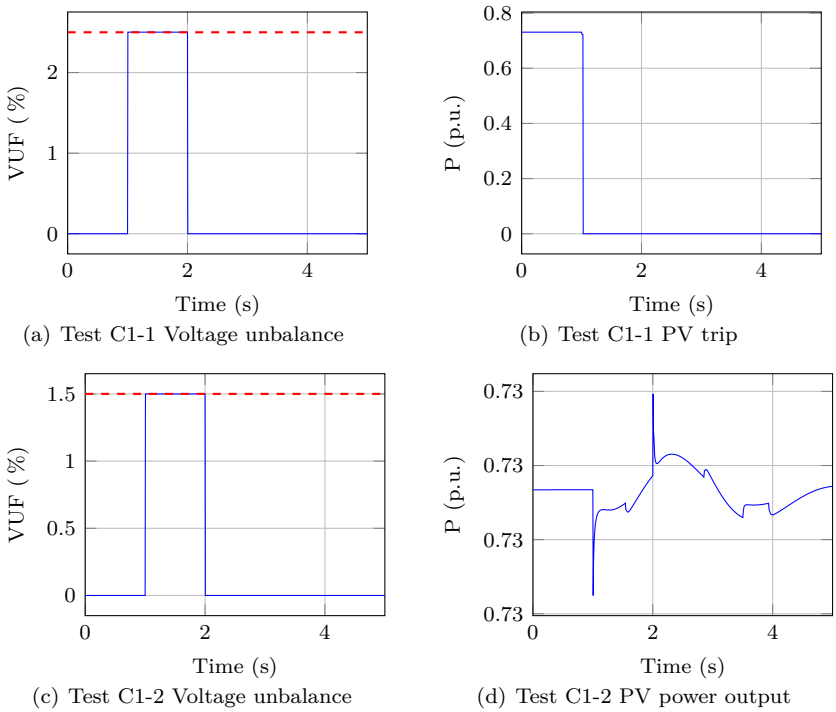


(a) Test C1-1 Voltage unbalance
(b) Test C1-1 PV trip
(c) Test C1-2 Voltage unbalance
(d) Test C1-2 PV power output

**Figure 8.6. Case 1: validation of the procedure for VUF**

**Summary** By using the particular grid model conveniently parameterised, events have been correctly emulated. Thus, the control and protection algorithms of the PV power plant have been assessed with respect of the compliance of the selected grid code provisions. The performance of the power plant and the compliance of the grid code have been correctly demonstrated for all test cases under study. Table 8.10 summarises the results of the grid code compliance verification for **Case 1**.

**Table 8.10. Case 1: summary of grid code compliance verification**

| Test case | Description | Action | Pass/Fail |
|---|---|---|---|
| A1-1 | Maximum frequency | ANSI 81O trips | ✓ |
| A1-2 | Maximum frequency | PV remains connected | ✓ |
| A2-1 | Minimum frequency | ANSI 81U trips | ✓ |
| A2-2 | Minimum frequency | PV remains connected | ✓ |
| A3-1, A3-2 | High frequency event | Not tested | – |
| A4-1, A4-2 | Low frequency event | Not tested | – |
| A5-1 | Positive ROCOF | ANSI 81R trips | ✓ |
| A5-2 | Positive ROCOF | PV remains connected | ✓ |
| A6-1 | Negative ROCOF | ANSI 81R trips | ✓ |
| A6-2 | Negative ROCOF | PV remains connected | ✓ |
| A7 | Frequency response for high frequencies | Control module decreases $P_{PV}$ | ✓ |
| A8 | Frequency response for low frequencies | Control module increases $P_{PV}$ | ✓ |
| B1-1 | Balanced LVRT | Converter module trips | ✓ |
| B1-2 | Balanced LVRT | PV remains connected | ✓ |
| B2-1, B2-2 | Unbalanced LVRT | Not tested | – |
| B3 | $I_a$ during balanced LVRT | Converter module $I_a = f(V)$ | ✓ |
| B4 | $I_q$ during balanced LVRT | Converter module $I_q = f(V)$ | ✓ |
| B5 | $I_a$ during unbalanced LVRT | Not tested | – |
| B6 | $I_q$ during unbalanced LVRT | Not tested | – |
| C1-1 | Voltage unbalance | ANSI 47 Trips | ✓ |
| C1-2 | Voltage unbalance | PV remains connected | ✓ |
| C2-1, C2-2 | Current unbalance | Not tested | – |

Note: -1:outside the permitted range; -2:within the permitted range

# Chapter 9

# Practical application: Terceira island

## 9.1 Introduction

The methodology proposed in this thesis will be validated by the application to three island study cases. This chapter verifies the methodology with **Case 2**: a medium size island, with dynamic data available but no grid code under force. The selected island is Terceira, in the Açores archipelago. The main power station is the Thermal Power Plant (TPP) of Belo Jardim (CTBJ), with an installed capacity over 76 MVA and based on 10 Diesel engines. Regarding renewable power generation, there is a WPP named Serra do Cume, first comissionned in 2008 with 4.5 MW and currently upgraded to 9 MW, as well as some mini-hydroelectric power stations in Cidade, Nasce d'Agua and São João de Deus. The description and characteristics of the power grid are annexed in Appendix D.

It has been assumed that a new wind farm is planned to be installed at Quatro Ribeiras 30 kV substation, where available data is as indicated in Table 9.1. Currently, there is no grid code under force regarding the connection of RES in Terceira. As an alternative, the parameterisation of particular grid models can be based on real performance results, described in Section 9.2. Thus, the operation of Terceira power grid can be emulated by using simple parameterised grid models. Particular grid models have been parameterised and their validity verified in Section 9.3. Finally, the performance of the new renewable power plant model connected to the parameterised grid model has been tested by means of simulation in Section 9.4.

## 9.2 Performance analysis

The static and dynamic operation of Terceira island have been simulated, based on data in [154] and on typical values for lacking parameters. Credible operation scenarios have been defined in this section, as base for steady-state and dynamic operation studies.

**Table 9.1. Characteristics of PCC in Terceira island**

| Parameter | Value |
|---|---|
| Peak load | 35.194 MW |
| Valley load | 14.149 MW |
| Voltage at PCC | 30 kV |
| $S_{sc,max}$ at PCC | 87.57 MVA |
| $S_{sc,min}$ at PCC | 37.39 MVA |

### 9.2.1 Description of operation scenarios

The operation scenarios differ in the level of demand, instantaneous wind power generation, generation dispatch and available reserve margins. The combination of the load and generation scenarios leads to several study cases, which are summed up in Table 9.2.

Two load scenarios have been considered: summer peak *SP* and winter valley *WV*, which correspond respectively to the maximum and minimum demand levels in 2012 [154], adding up a total peak demand slightly over 35 MW and a valley demand of 14 MW. Load demand in each bus in the system is indicated in Appendix D.

On the other hand, three wind power generation situations have been defined: zero wind *0W*, normal wind *NW* (50 % of installed capacity, i.e. 4.5 MW), and peak wind *PW* (100 % of installed capacity, i.e. 9 MW) at the WPP Serra do Cume. In other words, three penetration ratios have been considered: 0 %, 12.78 % and 25.57 % over peak load. However, under valley scenario, instantaneous penetration results into higher values. The WTGs are operated at a constant power factor ($cos\varphi = 0.95$ inductive).

**Table 9.2. Summary of study cases in Terceira island**

| Case Id. | SP | WV | 0W | NW | PW |
|---|---|---|---|---|---|
| 1 | ✓ | | ✓ | | |
| 2 | ✓ | | | ✓ | |
| 3 | ✓ | | | | ✓ |
| 4 | | ✓ | ✓ | | |
| 5 | | ✓ | | ✓ | |
| 6 | | ✓ | | | ✓ |

The Diesel generating units at Belo Jardim shall supply the demand not covered by the wind farm, plus the corresponding losses (including generation losses and transmission network losses). However, it must be taken into account that there must be some spinning reserve in the system. It is especially important for non-interconnected power systems such as Terceira. In this case, the standard N-1 criterion has been

used: spinning reserve should be able to cover the outage of any generator or wind park. It should be pointed out that this approach does not give an optimal spinning reserve, but it is still used in practice today, and can be useful to illustrate the performance of an isolated power grid [155].

Conventional generating units have been commited by choosing the combination with the lowest cost, following an economic dispatch algorithm only based on fuel consumption and respecting technical minima of the generating units. Generation dispatch for each study case is summarised in Appendix D.

### 9.2.2 Operation in steady-state

Under the steady-state operation, voltage and loading of the power system have been studied. The reactive power compensation scenarios have been taken into account. On one hand, capacitor banks have been installed at the weakest buses (i.e. Vinha Brava and Angra do Heroismo) as indicated in [154] during peak demand. Thus, for *Study Cases 1 to 3* two subcases have been defined: *a* subcase for scenario with reactive power compensation, and *b* subcase without compensation.

In steady-state, voltage levels range between 0.9-1.1 p.u., as required by the grid code. The highest average voltages at both 15 and 30 kV happen under *Study Case 4* and 5, i.e. under valley demand and no or little amount of wind power. On the other hand, the lowest voltage levels appear during peak demand, when no capacitor bank is connected. Lowest levels show up at the 15 kV bus of substations Vinha Brava (SEVB), Angra do Heroismo (SEAH) and Quatro Ribeiras (SEQR), whereas highest voltages occur at Belo Jardim. Voltage levels in steady-state for the study cases in Table 9.2 are compared in Figure 9.1 separately for the 15 kV network.

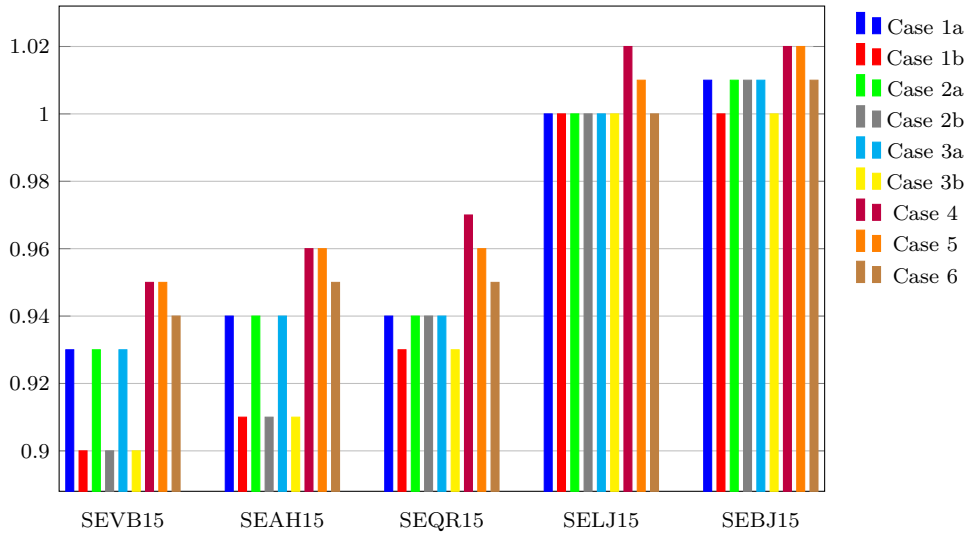


**Figure 9.1. Voltage levels in steady-state at 15 kV in Terceira island**

Besides, lines and transformers prove to be correctly dimensioned, as no overload occurs. Only with a topology change such as the partitioning of substations SEBJ30 and SEBJ15, and under maximum demand (*Study Case 1* and *Study Case 3*), the transformer SEBJ-T1 happens to be overloaded.

**N-1 contingency analysis under different operation scenarios** Line trips and transformer outages have been considered as N-1 contingencies. Some of the contingencies (e.g. trip of Praia da Vitoria-Lajes and Lajes-Quatro Ribeiras lines) lead to the outage of the whole substations of Lajes and Quatro Ribeiras. For the rest of the contingencies, during peak demand and with full wind power generation, voltage can fall below 0.9 p.u. at Vinha Brava and Angra do Heroismo substations at 15 kV, if no reactive power compensation is applied. The trip of the line Praia da Vitoria-Vinha Brava 1 also leads to a similar situation under *Study Case 2* and *Study Case 3*.

**N-2 contingency analysis under different operation scenarios** The simultaneous trip of transmission lines *Vinha Brava-Angra do Heroismo 1* and *Vinha Brava-Angra do Heroismo 2*, and *Praia da Vitoria-Vinha Brava 1* and *Praia da Vitoria-Vinha Brava 2* have been identified as probable N-2 contingencies. The loss of the double line from Vinha Brava to Angra do Heroismo leads to the outage of the whole substation of Angra do Heroismo. The second double contingency results in the overloading of both lines Praia da Vitoria-Serra do Cume and Serra do Cume-Vinha Brava 20 % over the rated capacity.

**Short-circuit levels** Three-phase short-circuits have been simulated in all the buses in the system. Maximum magnitude values correspond to *Study Case 1*, especifically at bus SEBJ30, obtaining a short-circuit power value of 285.78 MVA. For the same study case, lowest magnitude corresponds to bus SEQR15. Lowest values result from *Study Case 6* as expected, because it is the configuration with least synchronous generation. At bus SEBJ30, magnitude decreases to 55.02 MVA for the minimum short-circuit value. The lowest values at 30 kV correspond to SEQR30 with 37.39 MVA and at 15 kV, to bus SEQR15 with 30.49 MVA.

### 9.2.3 Transient operation

**Generation loss** For each study case, the loss of the biggest generator on-line has been simulated, and results are displayed in Figure 9.2. As it can be observed, frequency response differs depending not only on the demand scenario, but also on the generation loss. Therefore, unit dispatch is also of importance, as it determines the system inertia and the available spinning reserve.

The maximum deviation occurs under valley demand, upon the loss of the biggest generating unit in the power system and with the highest wind power penetration. However, recovery for *Study Case 5* takes a longer time, and definitively, stability is lost for *Study Case 6*. Table 9.3 indicates maximum frequency response parameters for the stable study cases: the initial ROCOF, the minimum frequency and the steady-state frequency deviation, taking into account the loss of the biggest generating unit in the system.

**Table 9.3. Frequency after loss of generation in Terceira island**

| Study case | ROCOF (Hz/s) | $f_{min}$ (Hz) | $f_{ss}$ (Hz) |
|---|---|---|---|
| 1 | -0.89 | 49.26 | 49.77 |
| 2 | -1.21 | 48.96 | 49.68 |
| 3 | -1.56 | 48.69 | 49.6 |
| 4 | -2.2 | 48.2 | 49.43 |
| 5 | -2.32 | 48.06 | 49.41 |
| 6 | - | - | - |

However, in order to avoid such low frequency values, isolated power grids often use Under Frequency Load Shedding (UFLS) practices. Therefore, lacking other reference, UCTE practices have been applied [1]. As shown in Figure 9.2, frequency excursion is then smaller, but during the recovery the frequency boosts and reaches unadmissible values. Down reserve is not sufficient and an active power mismatch appears in the system with more generation than load. If only the first stage of the UFLS is configured, the result is better (Figure 9.2 (b)).

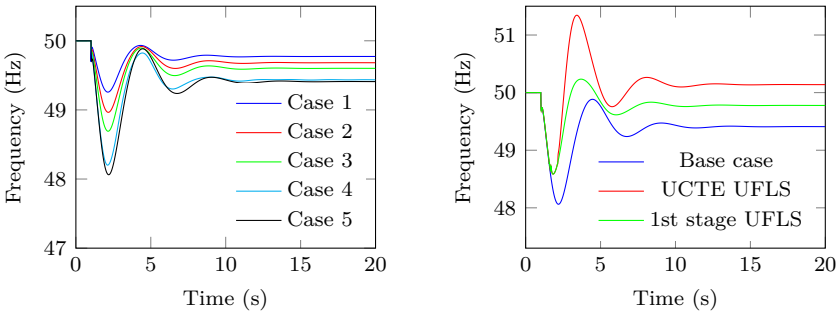


(a) UFLS disabled (b) Case 5 with UFLS included

**Figure 9.2. Frequency deviation after loss of generation in Terceira island**

**Load event** The loss of the Praia de Vitoria load has been simulated for the peak demand study cases, and the loss of Vinha Brava 1 for the valley demand. Both correspond to highest load buses under mentioned scenarios. All cases for frequency deviation are illustrated in Figure 9.3(a). The largest stable frequency deviation corresponds to *Study Case 6*, with a maximum value of 51.4 Hz, 2.2 Hz/s of ROCOF, and a steady-state value of 50.33 Hz. It is the result for the scenarios with WTGs including an overfrequency power reduction logic as frequency response algorithm, based on Spanish grid code. If the frequency response of WTGs is disabled, the frequency deviation is higher as shown in Figure 9.3(b). The figure compares frequency deviation for *Study Case 6* as worst case with (continuous line) and without (dashed

[1] 1st stage: 49 Hz 15 % of load; 2nd stage: 48.7 Hz 15 % of load; 3rd stage: 48.4 Hz 10 % of load; 4th stage: 48 Hz 10 % of load

line) frequency response logic. A maximum value of 51.89 Hz, 2.3 Hz/s of ROCOF, and a steady-state value of 50.6 Hz have been attained in this case.

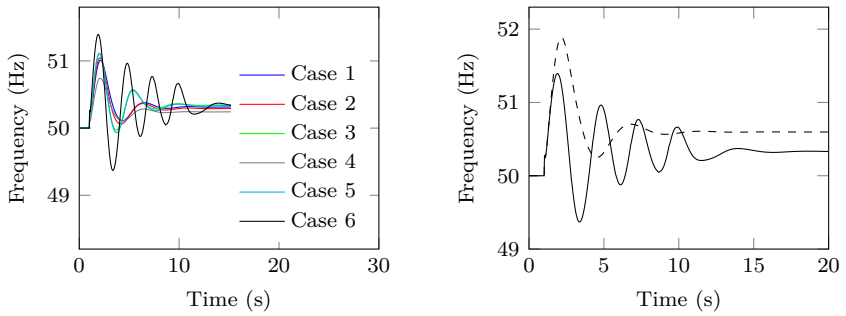


(a) WTGs including frequency response

(b) Case 6 with WTGs without frequency response

**Figure 9.3. Frequency deviation after load loss in Terceira island**

**Faults** According to [154], most of the voltage dips in Terceira in 2012 were caused by thermal production outages and some of them caused by faults. Most of them were dips with a low magnitude (i.e. high residual voltage) and a duration shorter than 200 ms. However, most of the events with a low residual voltage have durations between 200 and 500 ms. Therefore, three-phase short-circuits have been simulated with a duration of 250 ms at main buses in the system. In order to obtain a real typical LVRT envelope, more detailed studies should be carried out. Certainly, protection systems would have to be modelled, as was performed for New Zealand in [156], following studies with simulation of faults at various locations and different fault clearance scenarios. But this aspect is out of the scope of this thesis.

System performance during a fault at the wind farm substation has been analysed, by comparing voltage magnitude at the faulted bus for the study cases in Figure 9.4(a). Indeed, this is the worst location for a fault, as WTGs will be most closely affected. Recovery from the fault is slower under valley demand. As wind generation increases, as contribution to short-circuit current is also reduced, the situation can be worse.

Transient stability is guaranteed after a fault with a 250 ms duration. Longer short-circuits have been applied at PESC bus as shown in Figure 9.4(b) for *Study Case 1*. Overvoltage magnitude on voltage recovery is higher as fault duration increases and recovery is also delayed. Transient stability is certainly lost sooner under peak demand scenarios with higher short-circuit values. For faults longer than 500 ms, some generators fall out of step under some cases and stability is lost.

On the other hand, upon the occurrence of a short-circuit phase angle and frequency also change suddenly. If active power need is high and the system has a low overall inertia, ROCOF can be high and frequency nadir values very low, inducing the UFLS systems to act. Frequency deviation during short-circuits has been hereby studied for peak and valley demand scenarios. Higher values of frequency were found for the

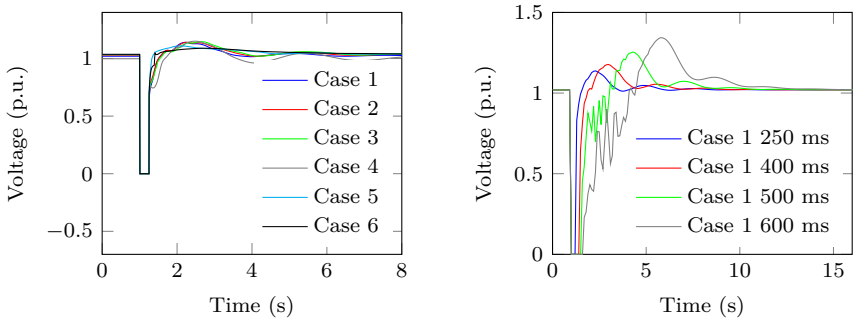


(a) Dip duration 250 ms (b) Effect of voltage dip duration

**Figure 9.4. Voltage dip magnitude after a three-phase fault at Serra do Cume**

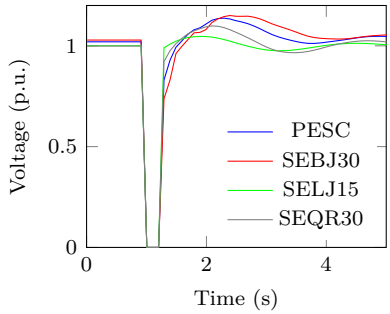


**Figure 9.5. Voltage dips in Terceira island**

peak case. Moreover, as fault duration increases, so does frequency deviation. Both aspects can be observed in Figure 9.6 and Figure 9.7(a).

In addition, frequency deviation has been compared for short-circuits at different locations: bus PESC, bus SEBJ30 with the highest short-circuit value, and buses SELJ15 and SEQR30 with the lowest short-circuit values at 15 and 30 kV levels. As seen in Figure 9.7(b), frequency deviation is highest during faults at strongest buses with a maximum of 51.86 Hz and a minimum of 48.74 Hz for a short-circuit of 250 ms at SEBJ30 with a ROCOF of almost 5 Hz/s. At the weakest buses the frequency deviation is within ±0.2 Hz, barely noticeable.

In Figure 9.5, bolted three-phase short-circuits have been simulated for *Study Case 1* at different buses. Voltage recovery is shown to be the fastest for faults at SELJ15 and slowest and with highest overvoltage at SEBJ30. In addition, a fault at SELJ15 causes a voltage dip with a low magnitude barely noticeable at the rest of the buses, while a fault at SEBJ30 causes the opposite effect.

Regarding unbalanced faults, Figure 9.8 shows voltage dip magnitude at fault point after different types of short-circuits for *Study Case 1*. Highest angle shifts occurs during three-phase and single-phase short-circuits.

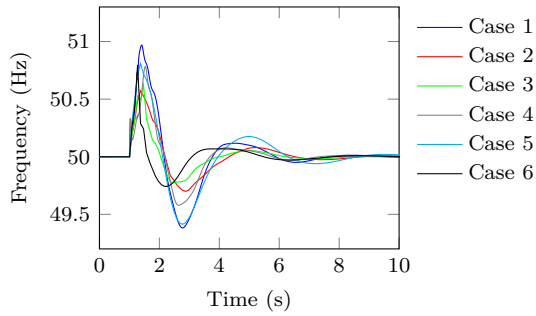


**Figure 9.6. Frequency deviation for a short-circuit at PESC bus**

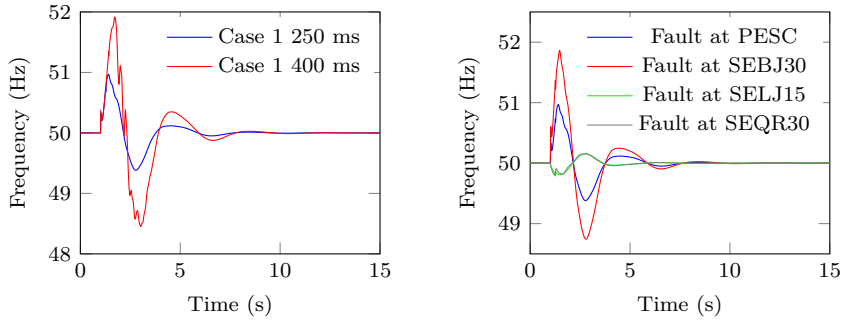


(a) Effect of voltage dip duration (PESC) (b) Case 1 250 ms at different locations

**Figure 9.7. Frequency deviation for a short-circuit at different locations**

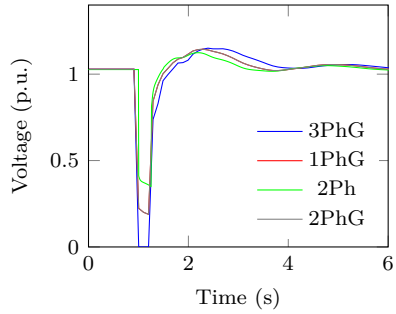


**Figure 9.8. Voltage dip magnitude after a fault at SEBJ30**

On the other hand, the effect of bolted three-phase short-circuits (250 ms) at different locations in the island under the worst scenario (*Study Case 1*) has been studied at Quatro Ribeiras 30 kV substation in Figure 9.9(a). Dip magnitude is higher for the most remote substation, Vinha Brava. Short-circuits at different voltage locations are attenuated because of transformer stations. The same applies for unbalanced faults in Figure 9.9(b), 9.9(c) and 9.9(d). Double-phase short-circuits have a voltage around 0.5 p.u. with a lowest value of 0.42 p.u. when the fault is at the same substation of

observance, i.e. Quatro Ribeiras.

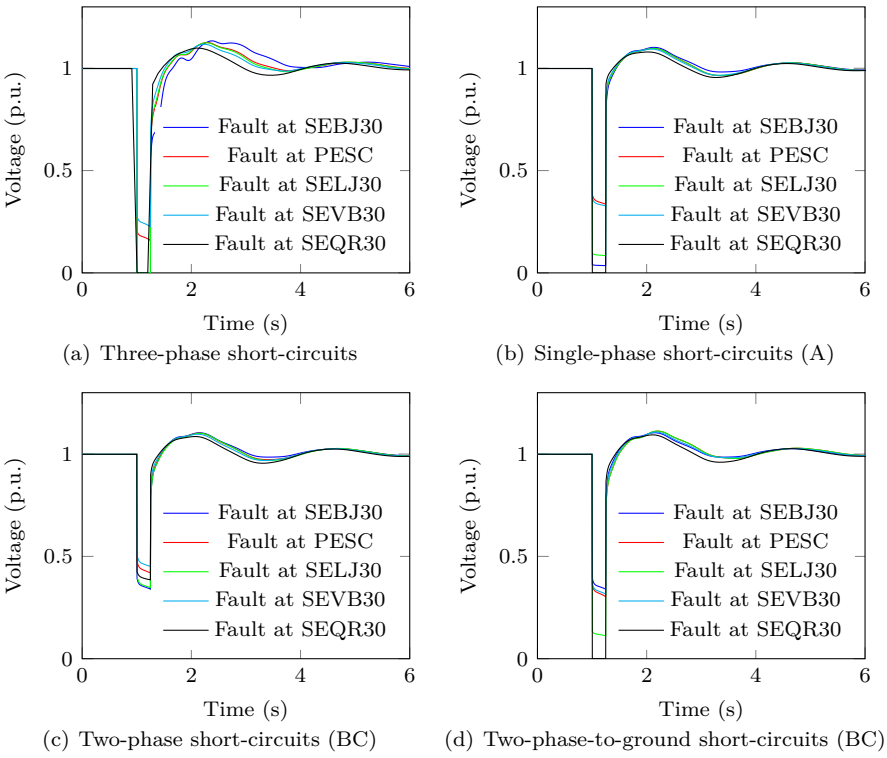


(a) Three-phase short-circuits
(b) Single-phase short-circuits (A)
(c) Two-phase short-circuits (BC)
(d) Two-phase-to-ground short-circuits (BC)

**Figure 9.9. Voltage dip magnitude at SEQR30**

Regarding voltage unbalance, VUF rises temporarily up to around 100 % for two-phase and two-phase-to-ground shunt faults with no fault impedance. Regarding single-phase faults, voltage unbalance is higher for *Study Case 6*, as the grid is weaker in that case. Values resulting from short-circuit at SEBJ30 and PESC are displayed in Figure 9.10. Voltage unbalance propagation depends on the fault position and network topology. So, it can increase or attenuate as it propagates. However, those are transient unbalances.

One and two open phase events have also been analysed in 30 kV transmission lines. Regarding Praia da Vitoria-Vinha Brava 1, only positive sequence voltage appears which barely changes during the disturbance. The voltage angle phase shift is also unnoticeable. For disturbances at Quatro Ribeiras-Lajes1, maximum values of $VUF = 3.3\,\%$ for an open phase and $VUF = 28.06\,\%$ for two open phases can be measured at SEQR30. For more distant substations, VUF is always under 5 %. Unbalance for asymmetrical loading or unbalanced power generation sources are hereby covered, because reference [154] does not report any case.

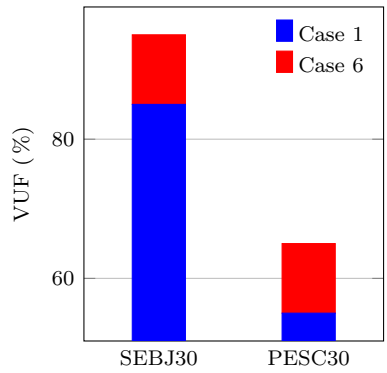


**Figure 9.10. Voltage unbalance in Terceira island**

**Line loss** As the power system is almost radial, after the loss of transmission lines in Terceira, some substations may become unsupplied. It is the case for *Praia da Vitoria-Lajes* and *Lajes-Quatro Ribeiras* lines. Lines Vitoria-Vinha Brava 1 and Vinha Brava-Angra do Heroismo 1, belonging to the two double circuits in the island, have been tripped, and the dynamic behaviour of the system has been analysed. Lines have been tripped at instant t=1 s and reclosed at instant t=2 s. During the line loss, voltage drops at every substation and phase-angle momentarily change slightly. Figure 9.11 shows the results after Vinha Brava-Vitoria line loss for *Study Case 1* in continuous line and *Study Case 6* in dashed line. Influence is higher under valley demand.

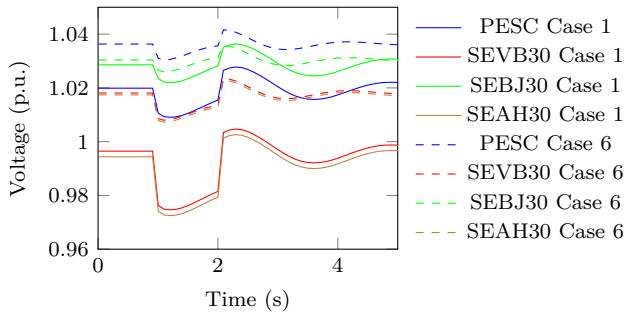


**Figure 9.11. Voltage after Vinha Brava-Vitoria line loss**

### 9.2.4 Synthesis

Results for dynamic operation in Terceira island are summarised in Table 9.4, regarding most critical scenarios. Frequency results apply at any point of the power system, whereas for the rest of parameters performance results depend on the point of disturbance and measurement, i.e. the PCC at Quatro Ribeiras 30 kV substation.

In steady-state, voltage levels are within the admissible range and no remarkable overload occurs. However, under N-1 contingency situation, undervoltage can happen

**Table 9.4. Synthesis of performance results in Terceira island**

| Event | Study Case | Parameter | Value |
|---|---|---|---|
| Generation loss | 5 | $ROCOF-$ | -2.32 Hz/s |
| Generation loss | 5 | $f_{ss,l}$ | 49.41 Hz |
| Generation loss | 5 | $f_{min}$ | 48.06 Hz |
| Load loss | 6 | $ROCOF+$ | 2.3 Hz/s |
| Load loss | 6 | $f_{ss,h}$ | 50.6 Hz |
| Load loss | 6 | $fmax$ | 51.89 Hz |
| 3PhG fault | 1 | $V_{dip,3PhG}$ | 0 |
| 1PhG fault (a) | 1 | $V_{dip,1PhG}$ | 0 |
| 2PhG fault (bc) | 1 | $V_{dip,2PhG}$ | 0 |
| 2Ph fault (bc) | 1 | $V_{dip,2Ph}$ | 0.42 |
| 1PhG fault (a) | 6 | VUF | 100 % |
| 2PhG fault (bc) | 6 | VUF | 100 % |
| 2Ph fault (bc) | 6 | VUF | 100 % |
| 1 Open phase | 6 | VUF | 3.3 % |
| 2 Open phases | 6 | VUF | 28.06 % |

under peak demand and full wind power generation, if no reactive power compensation is applied. The analysis of N-2 contingencies shows probable overloading in some transmission lines. Regarding transient operation, high ROCOF and frequency deviations are reached under valley demand. Besides, UFLS settings have to be carefully selected, as frequency recovery can result inadmissible. Regarding short-circuit analysis, stability can be compromised for faults close to Serra do Cume wind farm under peak demand scenarios. It has also been noted that frequency excursions are high under peak demand scenarios. During a short-circuit, voltage dip magnitude reaches very low values at almost all substations in the island. Moreover, voltage unbalance attains high values under unbalanced short-circuits and open phase events, whereas observed phase-angle shifts are barely noticeable.

## 9.3 Parameterisation of grid models

For each of the three requirements under study, the particular grid has been parameterised based on corresponding formulae in Chapter 5, 6 and 7 in Part III. Açores islands have no special requirement for renewable power generation connection. Main requirements are at distribution level. Therefore, in order to demonstrate a reliable integration, following perspectives can be considered: new grid code rules can be issued, based on deep steady-state and dynamic operation analysis, requirements from other similar systems can be adopted, or typical operation can be emulated.

For Terceira island, the latter approach has been pursued, based on results obtained in Section 9.2. Thus, the adjustment has been carried out based on limit values at the PCC as obtained in the performance analysis in Section 9.2. This approach is valid for *Frequency ride-through* and *LVRT*. However, as no unbalanced loading was reported in Terceira in [154], adjustment for unbalance has been based in the power quality standard under force in the island.

The parameterised grid model has been simulation with *PowerFactory* simulation software package and results compared to adjustment values and real performance operation, so as to verify the validity of the parameterisation methodology.

### 9.3.1 Adjustment results

**Frequency ride-through** The worst underfrequency deviation, but stable case, corresponds to *Study Case 5* under valley demand and fair wind power. Regarding overfrequency deviation due to load trip, highest values are to be found under *Study Case 6*, valley demand and high wind power. The load asset in the equivalent grid model represents the sum of the valley demand and system losses. Wind energy is represented as a negative load. As underfrequency and overfrequency events correspond to different scenarios, loads are different and so is generation dispatch.

The results of the adjustment methodology are stated in Table 9.5. The loss of a single generating unit in Terceira can result into a up to 16 % of the total installed capacity. Therefore, the values for maximum and minimum frequency have been calculated with (5.50). For underfrequency events, *Generator 1* has a rated power of $S_N = 15.25$ MVA, with $H_{eq} = 2.5s$, $R_{eq} = 0.05$ and $T_{eq} = 6$. The installed capacity of *Generator 2* is $S_N = 7.625$ MVA with the same characteristics. Load demand has been equally divided between *Load 1* and *Load 2*. On the other hand, for overfrequency events, *Generator 1* has a rated power of $S_N = 7.625$ MVA, with $H_{eq} = 2.5s$, $R_{eq} = 0.05$ and $T_{eq} = 6$. The installed capacity of *Generator 2* is $S_N = 7.625$ MVA with the same characteristics. Equivalencing is based on system data in Terceira.

**Table 9.5: Case 2: parameterisation of particular grid model for frequency ride-through**

| Test | Parameter | Limit | $G_2$ | Load 1 | Load 2 |
|---|---|---|---|---|---|
| A1 | $f_{max}$ | 51.89 Hz | - | 3.24 MW | 2.21 MW |
| A2 | $f_{min}$ | 48.06 Hz | 2.2 MW | 4.965 MW | 4.965 MW |
| A3 | $f_{ss,h}$ | 50.6 Hz | - | 1.85 MW | 3.6 MW |
| A4 | $f_{ss,l}$ | 49.41 Hz | 3.6 MW | 4.965 MW | 4.965 MW |
| A5 | $ROCOF+$ | 2.3 Hz/s | - | 1.94 MW | 3.51 MW |
| A6 | $ROCOF-$ | -2.32 Hz/s | 3.54 MW | 4.965 MW | 4.965 MW |

**LVRT** For LVRT, the divider model has been selected as particular grid model due to the relative small size of the island. The fault duration is based on assumptions

in Section 9.2. The results of the adjustment methodology are stated in Table 9.6. Resistive faults and inductive sources have been assumed, based on the sensitivity study in Chapter 6. $Z_{l1}$ has been adjusted in order to obtain the maximum $S_{sc}$ at the PCC taking into account the generator internal impedance. $Z_{l2}$ has been adjusted to the lowest possible magnitude at the PCC. For two-phase short-circuits, the lowest magnitude at the PCC is 0.42 p.u. However, the minimum voltage if all sequence impedances are considered equal is 0.5 p.u. Therefore, this value has been selected for the parameterisation. On the other hand, two other aspects have been carefully considered for double-phase short-circuits:

- Load modelling: voltage dependence of load has been taken into account. The load asset in the equivalent grid model represents the sum of the valley demand and system losses.
- Pre-fault voltage: for a higher accuracy, fault resistance has been calculated based on pre-fault voltage 0.9662 p.u. with a resulting value of $R_f = 0.697\Omega$.

An alternative could be not to include a load asset in the particular grid model, as it is not strictly necessary.

**Table 9.6. Case 2: parameterisation of particular grid model for LVRT**

| Test | Parameter | Limit | $Z_{l1}$ | $Z_{l2}$ | $G_1$ | Load |
|---|---|---|---|---|---|---|
| B1 | $V_{dip,3Ph}$ | 0 p.u. (0.25 s) | 1.25Ω | 0 | 76.45 MVA | 35.64 MW |
| B2 1PhG | $V_{dip,1PhG}$ | 0 p.u. (0.25 s) | 1.25Ω | 0 | 76.45 MVA | 35.64 MW |
| B2 2Ph | $V_{dip,2Ph}$ | 0.5 p.u. (0.25 s) | 1.25Ω | 0.697Ω | 76.45 MVA | 35.64 MW |

**Unbalance** As in steady-state the power system shows no unbalance [154], the Portuguese standard NP EN 50160 has been taken as reference for the adjustment with a maximum voltage unbalance of 2 %. There is no reference to current unbalance. As a consequence, the parameterisation of the particular grid model for current unbalance has been left out of the scope of this chapter. The selected scenario is valley demand with minimum short-circuit value ($S_{sc,min}$) corresponding to *Study Case 6*, as voltage unbalance results into higher values.

The results of the adjustment methodology are stated in Table 9.7. All sequence impedances have been considered equal and a value of $LUF = 2$ for three-phase loads. The single load corresponds to $P_{bc} = 0.75$ MW and the three-phase load $P_a = 0.625MW$ and $P_b = P_c = 1.25MW$.

**Table 9.7. Case 2: parameterisation of particular grid model for unbalance**

| Test | Parameter | Limit | $Z_{l1}$ | $Z_{l2}$ | $G_1$ | Load |
|---|---|---|---|---|---|---|
| C1 | VUF | 2 % | $5.18 \cdot j\Omega$ | 0Ω | 15.25 MVA | $R_{bc} = 1203.3\Omega$<br>$Ra = 479.86\Omega, R_b = 239.93\Omega$ |

### 9.3.2 Verification of the parameterisation

The validity of the parameterised grid model has been verified by means of simulation. The parameterised models have been implemented in *Power Factory* Digsilent software package and the obtained results benchmarked against the performance results for frequency ride-through and three-phase and single-phase-to-ground LVRT, and limit values for double-phase LVRT and voltage unbalance. Figure 9.12 shows the results of the adjustment for *Frequency Ride-Through* requirement. Plots in blue correspond to the parameterised grid model and those in green to real performance results. The adjustment for the rest of requirements can be verified in Figure 9.13. Limit values are pointed out in red and plots with dashed lines to real performance results.

The relative errors between the theoretical model and the simulation results have been computed for each technical requirement and can be looked up in Table 9.8. Errors are below $\pm 10\,\%$ for all the test cases. Hence, the parameterised grid models can be hereby validated.

**Table 9.8. Case 2: parameterised grid model validation results**

| Test | Parameter | Limit | Result | Error (%) | Verification |
|---|---|---|---|---|---|
| A1 | $fmax$ | 51.89 Hz | 51.86 Hz | -0.06 % | ✓ |
| A2 | $f_{min}$ | 48.06 Hz | 48.11 Hz | 0.1 % | ✓ |
| A3 | $f_{ss,h}$ | 50.6 Hz | 50.6 Hz | 0 % | ✓ |
| A4 | $f_{ss,l}$ | 49.41 Hz | 49.4 Hz | -0.02 % | ✓ |
| A5 | ROCOF+ | 2.3 Hz/s | 2.24 Hz/s | -2.61 % | ✓ |
| A6 | ROCOF- | -2.32 Hz/s | -2.26 Hz/s | -1.26 % | ✓ |
| B1 | $V_{dip,3Ph}$ | 0 p.u. | 0 p.u. | 0 % | ✓ |
| B2 | $V_{dip,1PhG}$ | 0 p.u. | 0 p.u. | 0 % | ✓ |
| B2 | $V_{dip,2Ph}$ | 0.5 p.u. | 0.509 p.u. | -1.8 % | ✓ |
| C1 (1Ph load) | VUF | 2 % | 1.99 % | -0.5 % | ✓ |
| C1 (3Ph load) | VUF | 2 % | 1.97 % | -0.5 % | ✓ |

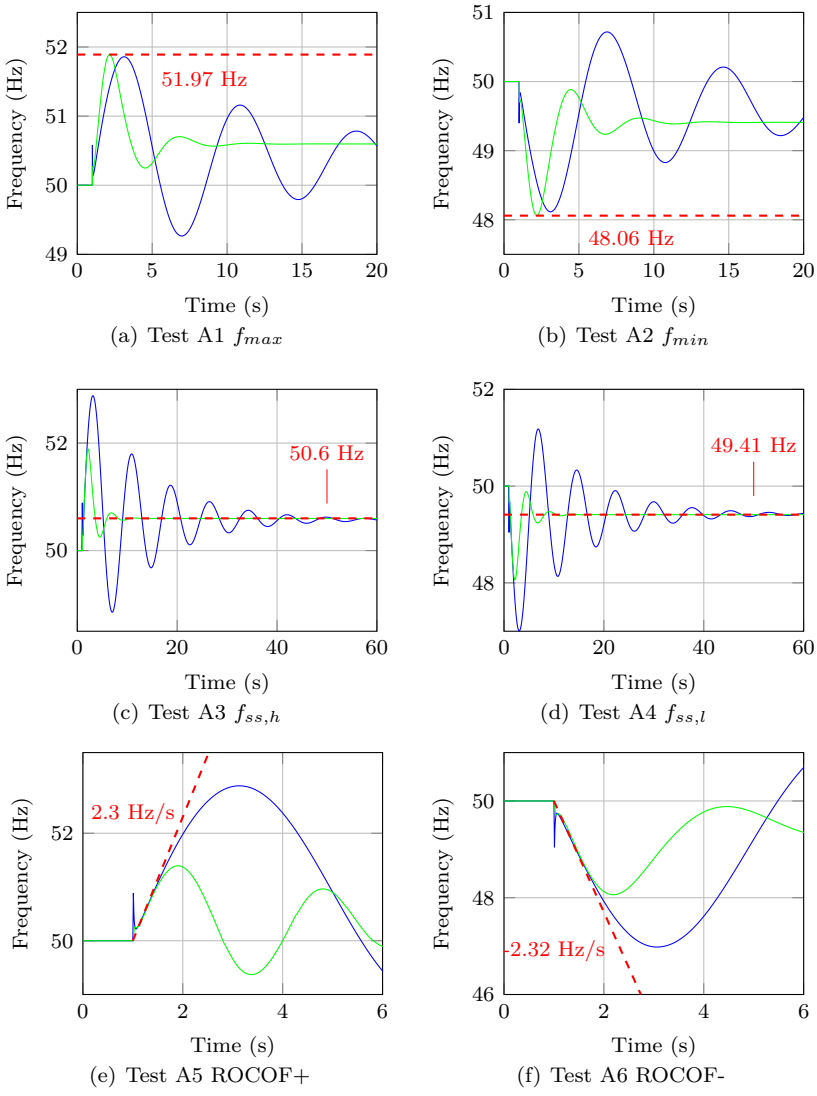


(a) Test A1 $f_{max}$ (b) Test A2 $f_{min}$

(c) Test A3 $f_{ss,h}$ (d) Test A4 $f_{ss,l}$

(e) Test A5 ROCOF+ (f) Test A6 ROCOF-

**Figure 9.12. Case 2: verification of adjustment of frequency ride-through**

## 9.4 Practical application of the methodology

The installation of a new wind farm at Quatro Ribeiras in Terceira island is under study. It will be connected to the substation with a 7.5 km long 30 kV line. Initially, 5 MW will be installed and the power plant will be later upgraded. The PCC of the wind farm has the characteristics indicated in Table 9.1. The SCR at the PCC under valley demand is 6.7, which is low. This aspect should be taken into account.

The wind farm has been modelled with *PowerFactory* software package, based on a

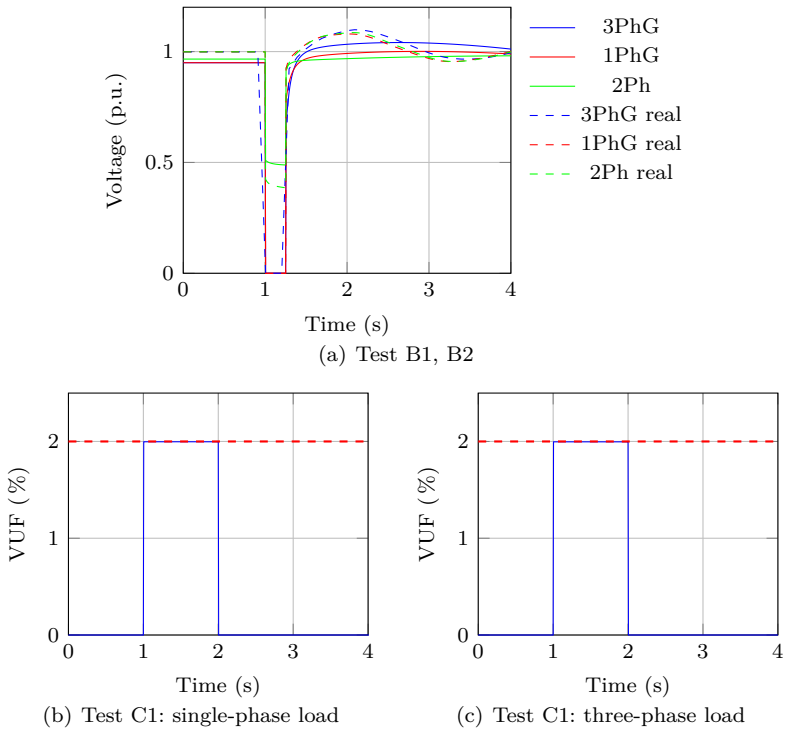


(a) Test B1, B2

(b) Test C1: single-phase load

(c) Test C1: three-phase load

**Figure 9.13. Case 2: verification of the rest of parameters**

grey-box user model and parameterised according to values indicated in Appendix C, where the user model and the equivalent grid model are also described. The methodology has been applied so as to verify if the new power plant is able to remain connected and contribute actively to the real performance in the island as simulated in Section 9.2.

For remain connected requirements, two events have been simulated by adjusting the simplified equivalent grid for each of the compliance tests defined in Chapter 4: an event outside usual range in the power grid (indicated suffix -1 in test identificator), and an event within the usual range (indicated suffix -2 in test identificator). Limit values are based on real performance in Section 9.3, unless for unbalance requirement that is limited by the Portuguese standard under force. For active support requirements, generator contribution is showed by simulating an event within limits.

**Frequency ride-through** Frequency ride-through test cases are listed in Table 9.9. For *Frequency ride-through* validation, the frequency response block of the plant has been disabled, so as to be able to observe the trip of the plant when frequency is beyond permitted values. This feature can be achieved by conveniently adjusting the protection relay settings of the generation asset. In addition, for a better observance of ROCOF events under/overfrequency events have been disabled for test cases A5 and A6. Test cases A3 and A4 have not been considered, because only primary

protection relays have been configured in the model.

**Table 9.9. Case 2: frequency ride-through test cases**

| Test | Parameter | Limit | Test value |
|---|---|---|---|
| A1-1 | $f_{max}$ | 51.89 Hz | 52 Hz |
| A1-2 | $f_{max}$ | 51.89 Hz | 51.5 Hz |
| A2-1 | $f_{min}$ | 48.06 Hz | 47.5 Hz |
| A2-2 | $f_{min}$ | 48.06 Hz | 48.5 Hz |
| A5-1 | ROCOF | 2.3 Hz/s | 2.5 Hz/s |
| A5-2 | ROCOF | 2.3 Hz/s | 1.5 Hz/s |
| A6-1 | ROCOF | -2.32 Hz/s | -2.5 Hz/s |
| A6-2 | ROCOF | -2.32 Hz/s | -1.5 Hz/s |

Figure 9.14 plots the system frequency and the power output of the power plant for each case. The power output is expressed in p.u. with respect of initial power reference. It can be stated that the power plant trips correctly during the events out of the permitted range. For underfrequency events beyond the limits, the power plant is tripped, which increases the power imbalance, and hence, the system frequency deviation. ROCOF events result into a slower trip of the power plant, which depends on the measuring window for the computation of frequency gradient used in PowerFactory simulation package.

**Frequency response** This feature has been parameterised with values within an acceptable range in the SEIE grid code by reproducing test cases A2-2 and A1-2, as indicated in Appendix C. Frequency response for both high (A2-2) and low (A1-2) frequencies has been tested. The simulation results are plotted in Figure 9.15. The power output of the PV plant corresponds to the initial power flow in per unit. As the frequency nadir, values are lower than in Case 1, the action of the control algorithm is also faster. The parameters of the *Control Module* may need to be reconsidered.

**LVRT** Two events have been simulated by adjusting the fault duration: an event outside the usual range with $t_{dip} = 150$ ms and an event within the permitted range with $t_{dip} = 500$ ms. Only balanced short-circuits have been applied. Test B2, corresponding to unbalanced faults, is out of the scope of the practical application, because the generating unit model under study does not include the ability to ride-through unbalanced faults.

Figure 9.16 shows voltage profiles at the PCC for both events with a limit profile based on real performance results. The power generation asset remains connected and generating during event B1-2, and trips during event B1-1. In test case B1-2 shown in Figure 9.16(d), it can be observed that the power plant remains connected. The power output changes after 10 seconds, after finishing LVRT injection. This aspect is further covered in next paragraph.

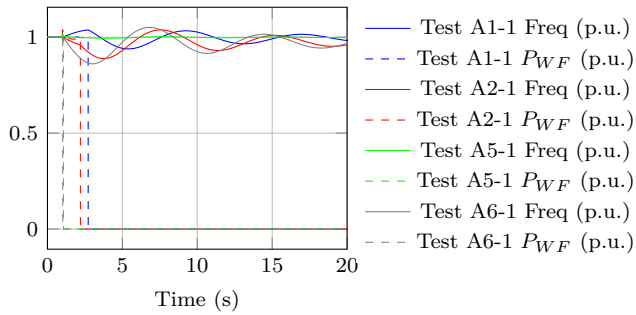


(a) Events out of the permitted range

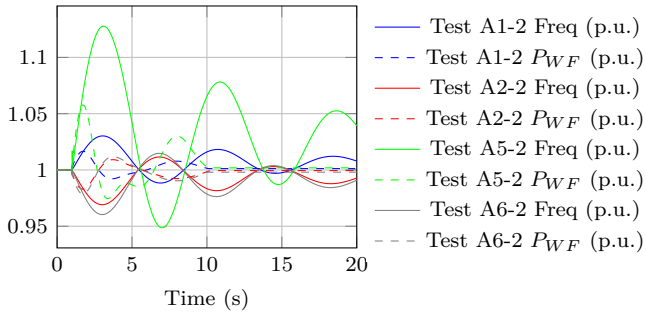


(b) Events within the permitted range

**Figure 9.14. Case 2: validation of the procedure for frequency ride-through**

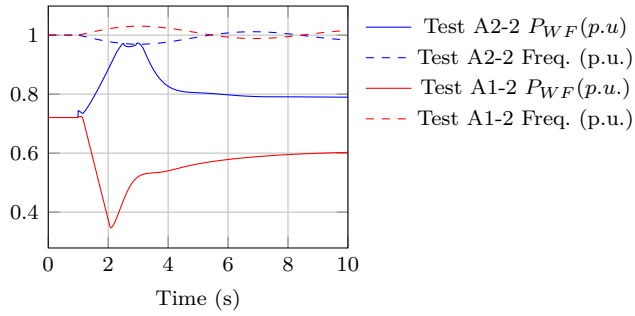


**Figure 9.15. Case 2: validation of the procedure for frequency response**

**Output current during faults** In order to maintain the transient stability in Terceira island, the new wind farm can contribute with active and reactive power during short-circuits. Thus, the control block of the equivalent converter of the power plant has been parameterised with values based on the SEIE grid code. According to most grid code, active and reactive current injection in function of voltage can be specified by some reference points. Adjustment values are indicated in Appendix C.

The event corresponding to the current injection tests for balanced faults is TEST B2-2, which corresponds to a balanced LVRT situation. Both current and corres-

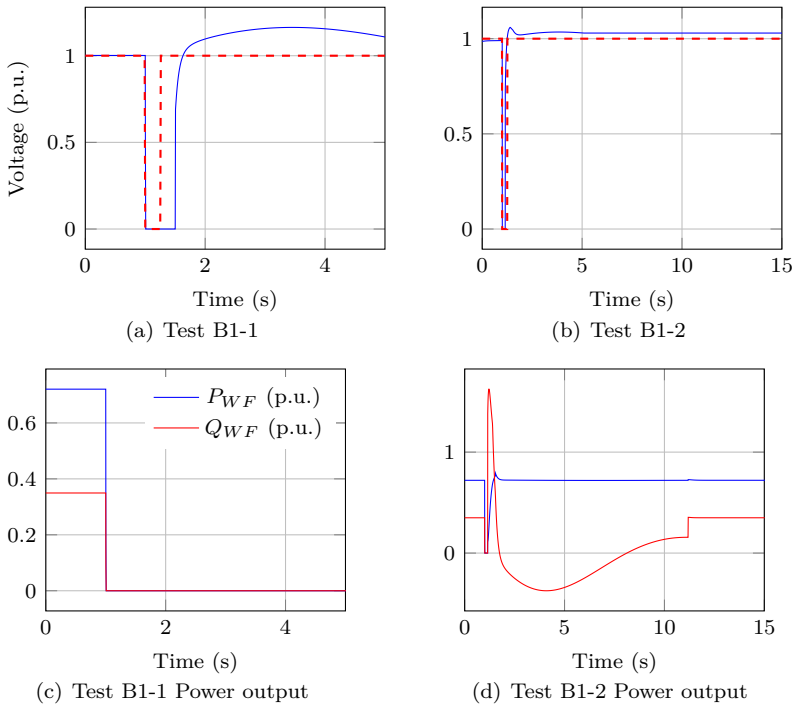


(a) Test B1-1 (b) Test B1-2

(c) Test B1-1 Power output (d) Test B1-2 Power output

**Figure 9.16. Case 2: validation of the procedure for LVRT**

ponding power in p.u. are shown in Figure 9.16(d). Support during fault has been specified to be active still 10 seconds after the recovery. Tests B5 and B6, corresponding to current contribution during faults for unbalanced faults, is out of the scope of the practical application, because the generating unit model does not include the ability to contribute to unbalanced faults.

**Unbalance** Unbalance test cases are listed in Table 9.10. Unbalance values in the performance study were low and transitory, and no unbalancing load has been reported. So, the adjustment has been carried out based on the Portuguese power quality standard. Only voltage unbalance has been considered, because current unbalance is not included in the regulation. Single-phase loading has been selected as unbalancing event because it leads to higher unbalances. Frequency protection functions and frequency response have been disabled.

**Table 9.10. Case 2: unbalance test cases**

| Test case | Parameter | Limit | Test value |
|---|---|---|---|
| C1-1 | VUF | 2 % | 2.5 % |
| C1-2 | VUF | 2 % | 1.5 % |

Figure 9.17(a) shows the unbalance at PCC after the grid adjustment, whereas Figure

9.17(b) plots the action of the protection relay with trip of the wind farm. When unbalance is below the limit value, the power plant remains connected.

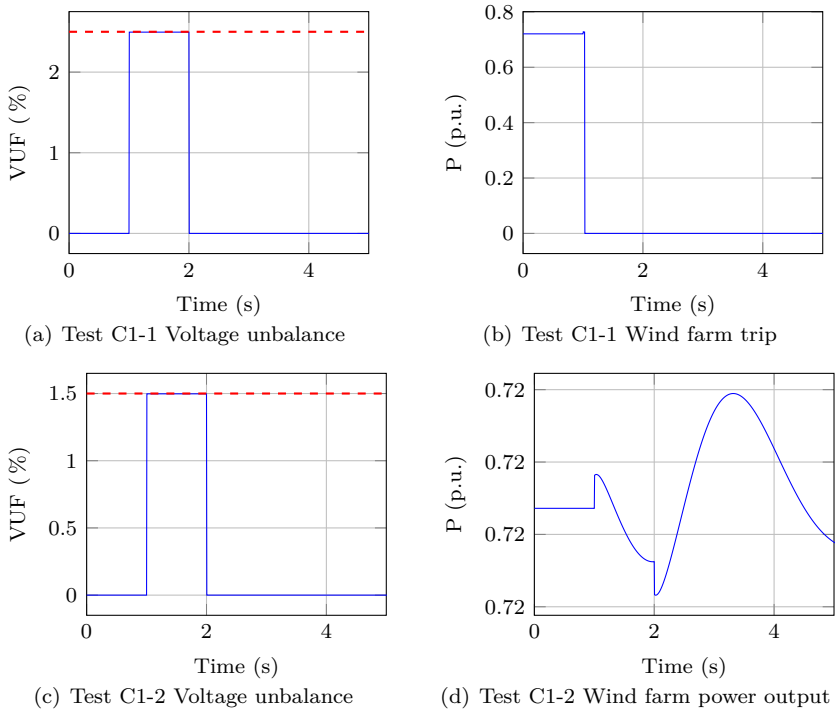


(a) Test C1-1 Voltage unbalance
(b) Test C1-1 Wind farm trip
(c) Test C1-2 Voltage unbalance
(d) Test C1-2 Wind farm power output

**Figure 9.17. Case 2: validation of the procedure for VUF**

**Summary** The application of the methodology for **Case 2** is based on real performance results and some grid code limits. By using the particular grid model conveniently parameterised, events have been correctly emulated. Thus, the control and protection algorithms of the wind power plant have been assessed with respect of the connection to Terceira island. The performance of the power plant and the emulation of real performance have been correctly demonstrated for all test cases under study. Table 9.11 summarises the results of the practical application of the methodology for **Case 2**.

**Table 9.11. Case 2: summary of grid code compliance verification**

| Test case | Description | Action | Pass/Fail |
|---|---|---|---|
| A1-1 | Maximum frequency | ANSI 81O trips | ✓ |
| A1-2 | Maximum frequency | Wind Farm (WF) remains connected | ✓ |
| A2-1 | Minimum frequency | ANSI 81U trips | ✓ |
| A2-2 | Minimum frequency | WF remains connected | ✓ |
| A3-1, A3-2 | High frequency event | Not tested | – |
| A4-1, A4-2 | Low frequency event | Not tested | – |
| A5-1 | Positive ROCOF | ANSI 81R trips | ✓ |
| A5-2 | Positive ROCOF | WF remains connected | ✓ |
| A6-1 | Negative ROCOF | ANSI 81R trips | ✓ |
| A6-2 | Negative ROCOF | WF remains connected | ✓ |
| A7 | Frequency response for high frequencies | Control module decreases $P_{WF}$ | ✓ |
| A8 | Frequency response for low frequencies | Control module increases $P_{WF}$ | ✓ |
| B1-1 | Balanced LVRT | Converter module trips | ✓ |
| B1-2 | Balanced LVRT | WF remains connected | ✓ |
| B2-1, B2-2 | Unbalanced LVRT | Not tested | – |
| B3 | $I_a$ during balanced LVRT | Converter module $I_a = f(V)$ | ✓ |
| B4 | $I_q$ during balanced LVRT | Converter module $I_q = f(V)$ | ✓ |
| B5 | $Ia$ during unbalanced LVRT | Not tested | – |
| B6 | $Iq$ during unbalanced LVRT | Not tested | – |
| C1-1 | Voltage unbalance | ANSI 47 Trips | ✓ |
| C1-2 | Voltage unbalance | WF remains connected | ✓ |
| C2-1, C2-2 | Current unbalance | Not tested | – |

Note: -1:outside the permitted range; -2:within the permitted range

# Chapter 10

# Practical application: Fuerteventura-Lanzarote islands

## 10.1 Introduction

The methodology proposed in this thesis will be validated by the application to three island study cases. This chapter verifies the methodology with **Case 3**: a medium size island, with dynamic data available and grid code under force. The selected power grids for the practical application are Fuerteventura and Lanzarote, two Canarian islands. Since 1977, both islands have been electrically linked: first, by a 33 kV undersea cable, and from 2005 with a 66 kV undersea cable. Its repowering to a double 132 kV link is expected for the coming years. Currently, the main power stations are the Thermal Power Plant (TPP) Las Salinas (in Fuerteventura island) with an installed capacity of 213 MVA, corresponding to 2 gas turbines and 9 Diesel units, and the TPP Punta Grande (in Lanzarote island) with an installed capacity of 244.57 MVA and 3 gas turbines and 9 Diesel units. There are also 4 small size wind farms: Los Valles with an installed capacity of 7.65 MW, Montaña Mina of 1.125 MW, Cañada del Río of 18.4 MW, and Cañada de la Barca with 1.12 MW. Further details are included in Appendix E.

It has been assumed that an existing wind farm is planned to be upgraded at Montaña de la Mina (Lanzarote). The characteristics of the connection point in Lanzarote are indicated in Table 10.1. A performance study has been carried out in Section 10.2 by simulation with *PowerFactory* Digsilent software package. Thus, the performance of the power system can be characterised and used for the parameterisation of the particular grid models, when necessary. The validity of the adjustment has been verified in Section 10.3. Finally, the performance of the renewable power plant model connected to the parameterised grid model has been tested by means of simulation in Section 10.4.

## 10.2 Performance analysis

The static and dynamic operation of Fuerteventura-Lanzarote islands have been simulated, based on [157], [153] and [158]. Credible operation scenarios have been defined in this section, as base for a steady-state and dynamic operation study.

**Table 10.1. Characteristics of PCC in Lanzarote island**

| Parameter | Interconnected systems | Separated systems |
|---|---|---|
| Voltage | 66 kV | |
| Peak load | 251.1 MW | 137 MW |
| Valley load | 115.74 MW | 66.05 MW |
| Maximum $S_{sc,max}$ | 699.15 MVA | 616.22 MVA |
| Minimum $S_{sc,min}$ | 411.26 MVA | 337.61 MVA |

### 10.2.1 Description of operation scenarios

The operation scenarios differ in the level of demand, instantaneous wind power generation, generation dispatch and available reserve margins.

Two load scenarios have been considered : winter peak $WP$ and winter valley $WV$, which correspond to the maximum and minimum demands in 2013.

Three wind power generation situations have been defined: zero wind $0W$, normal wind $NW$ (50 % of installed capacity, i.e. 14.15 MW), and peak wind $PW$ (100 % of installed capacity, i.e. 28.3 MW), which correspond to 5.63 % and 11.27 % of peak demand. During valley load, penetration ratios are higher, but still lower than in Terceira island. WTGs operate with a fixed power factor: in the case of Squirrel Cage Induction Generators (SCIGs), $cos\varphi = 0.95$, and $cos\varphi = 1$ for the rest of the generating units.

The combination of the load and generation scenarios leads to several study cases, which are summed up in Table 10.2.

**Table 10.2. Summary of study cases in Fuerteventura-Lanzarote**

| Case Id. | WP | WV | 0W | NW | PW |
|---|---|---|---|---|---|
| 1 | ✓ | | ✓ | | |
| 2 | ✓ | | | ✓ | |
| 3 | ✓ | | | | ✓ |
| 4 | | ✓ | ✓ | | |
| 5 | | ✓ | | ✓ | |
| 6 | | ✓ | | | ✓ |

The demand not covered by wind power generation, plus the system losses (including generation losses and transmission network losses), is supplied by the TPPs Punta Grande and Las Salinas. However, there must be some spinning reserve in the system. TSO establishes the hourly merit order for conventional generation groups taking into account variable costs. Renewable energy has priority in access and priority in dispatching, if technical conditions make it feasible. Moreover, unit commitment

depends on the power exchange between Fuerteventura and Lanzarote subsystems. Generation dispatch is summarised in Appendix E.

### 10.2.2 Operation in steady-state

Under peak demand scenario, some issues arise in steady-state. On one hand, power system infrastructure issues are evident, especially in Fuerteventura, where the overhead line from Las Salinas to Gran Tarajal substation is already overloaded to a 118 % of its capacity in steady-state. This aspect will hopefully be relieved in the future by the upgrading of the link to a new double circuit of 132 kV. On the other hand, all buses in Fuerteventura except for Las Salinas TPP show extremely low voltage levels under peak demand scenario. Limit voltage levels are 0.94 and 1.06 for 66 kV networks as referred in [159]. Matas Blancas substation has a lowest voltage level of 0.81 p.u. under *Study Case 1*, independently from the active power exchange situation between both subsystems. It can be concluded that the islands surely rely on emergency power stations for peak demand scenarios, which have not been considered in the modelisation.

**N-1 contingency analysis under different operation scenarios** Any transmission line or transformer failure in Fuerteventura leads to the loss of electricity supply in wide areas of the island, as it is a radial network with a simple circuit. Nevertheless, if Las Salinas-Corralejo line is tripped, Corralejo substation can still remain fed by Lanzarote subsystem, even if voltage at Corralejo substation decreases to the minimum voltage limit permitted for N-1 contingency situations, i.e. 0.91 p.u. On the other hand, Lanzarote is weakly meshed, and the situation is slightly better, and voltage levels are within permitted range.

**N-2 contingency analysis under different operation scenarios** According to [159], N-2 contingencies refer to double circuit trips, or successive failure of generating group and transmission line. There is only one double circuit line in Fuerteventura-Lanzarote system, which corresponds to the Punta Grande-Macher link. Its outage overloads both Macher-San Bartolomé and Punta Grande-San Bartolomé lines, the first with 10 % and the latter with around 30 % of its capacity, above the maximum permitted overload of 15 % [159]. This worst case corresponds to peak demand without wind power. However, for any of the peak load scenarios Punta Grande-San Bartolomé line is over the maximum permitted overload.

**Short-circuit levels** Three-phase short-circuits have been simulated in all the buses in the system. Maximum magnitude values correspond to *Study Case 2*, as following the economic dispatch the same synchronous generating units as in *Study Case 1* are on-line. But in addition, WTGs do also contribute more modestly. Maximum short-circuit values are found at the substations corresponding to the TPP PCCs, with 1003 MVA at Las Salinas, 1125.43 MVA at Punta Grande and 601.97 MVA at Corralejo. Lowest values result from *Study Case 6* as expected, because it is the configuration with least synchronous generation. If both systems are isolated due to the inter-island link trip, short-circuit values are still lower, with 276.21 MVA at Las Salinas bus, 369.93 MVA at Corralejo, and 424.38 MVA at Punta Grande.

Short-circuit values are smaller in Fuerteventura, with 136.02 MVA at Matas Blancas, 169.41 MVA at Corralejo substation, or still 134.79 MVA at Cañada del Río wind farm PCC.

### 10.2.3 Transient operation

**Generation loss** Simulations are based on the separate economic dispatch results for the islands under an interconnected situation. For each study case, the loss of the biggest generator on-line has been simulated, and results are displayed in Figure 10.1.

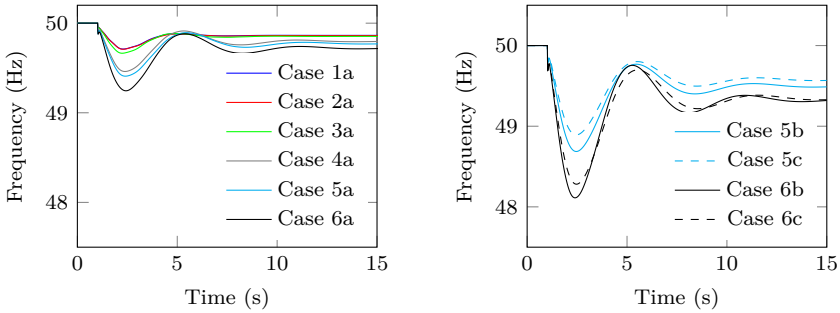


(a) Interconnected subsystems (b) Separated subsystems

**Figure 10.1: Frequency deviation after loss of generation in Fuerteventura-Lanzarote**

The maximum frequency deviation occurs under valley demand, upon the loss of the biggest generating unit in the power system and with highest wind power penetration. The unit commitment and economic dispatch have been done separately, and for each subsystem a spinning reserve up to the biggest generating unit on-line has been respected. Therefore, upon the trip of a generator, there is still a very high overall reserve. However, if the interconnection between both islands is under fault, the spinning reserve would be reduced, and therefore, the frequency excursion would be higher. Figure 10.1 shows frequency deviation with interconnected and separated subsystems for worst scenarios, after loss in Punta Grande or in Las Salinas. Frequency deviation is similar for both cases.

Frequency deviation is above 49 Hz, unless for cases *Study Case 4c*, *Study Case 5b*, *Study Case 6b*, and *Study Case 6c*. UFLS could be acceptable for those cases as it is stated in the regulation. Applying the UCTE UFLS practice to *Study Case 6b* (with the lower frequency nadir), frequency excursion is smaller (48.76 Hz). In addition, the final frequency value before the action of secondary control is also higher (49.66 Hz), as shown in Figure 10.2(a). First two stages of UFLS logic do trip.

In addition, a credible contingency could be the disconnection between both islands. This event has been simulated for *Study Case 6a* after the trip of Playa Blanca-Corralejo link in Figure 10.2(b). In this case, frequency rises in Fuerteventura and drops in Lanzarote because of the power exchange between both islands, with Fuer-

teventura exporting and Lanzarote importing, which corresponds to the most usual situation.

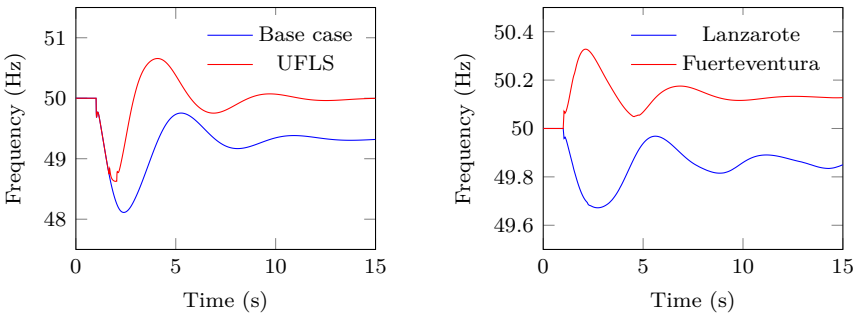


(a) Study case 6b (b) Study case 6a

**Figure 10.2. Frequency deviation under valley demand in Fuerteventura-Lanzarote**

Table 10.3 indicates maximum frequency response parameters for worst cases: the initial ROCOF, the minimum frequency and the steady-state frequency deviation, taking into account the loss of the biggest generating unit in the system. Subcase *a* refers to an interconnected situation, *b* to separated subsystems with loss in Lanzarote, and *c* to separated subsystems with loss in Fuerteventura.

**Table 10.3. Frequency after loss of generation in Fuerteventura-Lanzarote**

| Study case | ROCOF (Hz/s) | $f_{min}$ (Hz) | $fss$ (Hz) |
|---|---|---|---|
| 6a | -0.8 | 49.24 | 49.72 |
| 6b | -1.97 | 48.11 | 49.32 |
| 6c | -1.79 | 48.28 | 49.34 |

**Load event** For the interconnected system, the loss of Punta Grande load has been simulated corresponding to the highest load bus both under peak and valley demand. When the systems are separated because of a disturbance, the most loaded bus in Fuerteventura is Matas Blancas and Punta Grande in Lanzarote. All cases for frequency deviation are illustrated in Figure 10.3. Besides, the interconnected and separated systems have been compared for the worst study case including WTGs with no frequency response. Frequency response parameters for higher frequency deviations are summarised in Table 10.4.

**Faults** The highest short-circuit levels are reached for three-phase faults at Punta Grande. Figure 10.4(a) compares voltage magnitude at Punta Grande substation for the scenarios under study, where wind farms do not contribute. Voltage recovery seems quicker for low demand scenarios. Fault duration has been increased for *Study Case 1* in Figure 10.4(b), and above 400 ms duration faults some generators are out of step, losing the transient stability of the system.

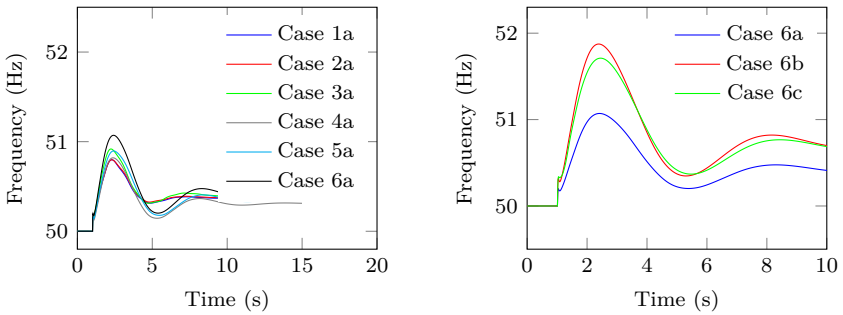


(a) Interconnected subsystems (b) Comparison for study case 6

**Figure 10.3. Frequency deviation after load loss in Fuerteventura-Lanzarote**

**Table 10.4. Frequency after loss of load in Fuerteventura-Lanzarote**

| Study case | ROCOF (Hz/s) | $fmax$ (Hz) | $fss$ (Hz) |
|---|---|---|---|
| 6a | 1.08 | 51.07 | 50.4 |
| 6b | 1.98 | 51.87 | 50.7 |
| 6c | 1.94 | 51.71 | 50.66 |

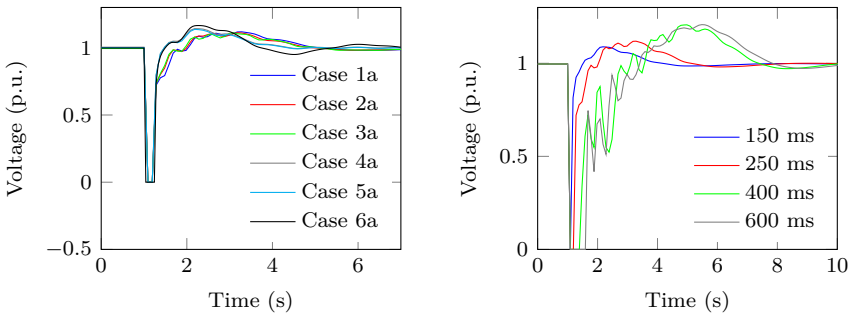


(a) Dip duration 250 ms (b) Effect of voltage dip duration

**Figure 10.4. Voltage dip magnitude after a fault at Punta Grande**

However, for a balanced fault at Matas Blancas, transient stability is maintained for much longer dips as seen in Figure 10.5(a). If a three-phase short-circuit with a duration of 250 ms is applied at different locations of the power system, Figure 10.5(b) shows that recovery is slower and overvoltage higher if the fault is at power station buses. Oscillations are also more evident for faults at Punta Grande and Las Salinas. Fault propagation also differs depending on the fault location. Whereas during a fault at Punta Grande, dip magnitude is around 0.6 p.u. at most buses, for short-circuits at a weaker and more distant location like Matas Blancas substation, dip magnitude remains above 0.8 p.u. On the other hand, if a fault happens at Corralejo -located in Fuerteventura but close to Lanzarote- the voltage dip propagates to most of the system with some importance.

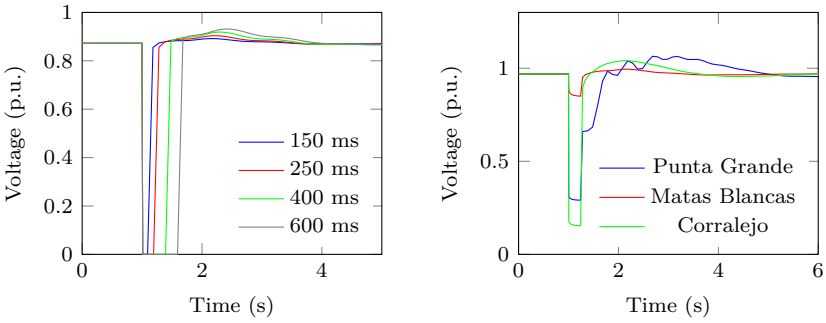


(a) Effect of voltage dip duration (b) Dip propagation at Punta Blanca

**Figure 10.5. Voltage dip magnitude after a fault at Matas Blancas**

During short-circuits synchronous generators' speed changes. Hence, system frequency also changes. Maximum frequency is reached with high demand scenarios, up to 51.04 Hz under *Study Case 1* and 5.92 Hz/s of ROCOF as observed in Figure 10.6.

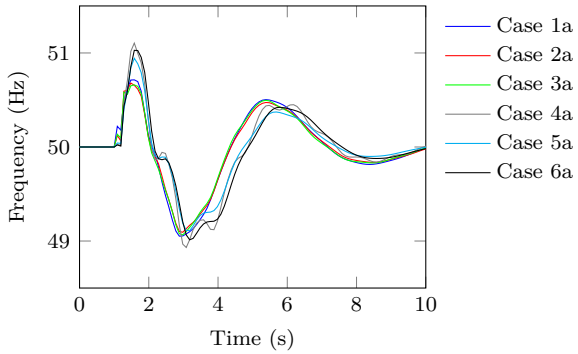


**Figure 10.6. Frequency deviation during short-circuit at Punta Grande**

Regarding unbalanced faults, Figure 10.7(a) shows voltage dip magnitude at fault point after different types of short-circuits for *Study Case 1*. Recovery is slower and with higher overvoltage for balanced faults. Angle shifts occurs during short-circuits are plotted in Figure 10.7(b).

The effect of bolted three-phase short-circuits (300 ms) at different locations in the island (66 kV) under the worst scenario has been studied at Montaña Mina (PCC) in Figure 10.8(a) and 10.8(b). The worst scenario is peak demand and interconnected subsystems. Dip magnitude is higher for the most remote substation, that are situated in Fuerteventura. For faults at the TPPs, stability is compromised as some generator fall out of step during the simulation. Short-circuits at lower voltage locations are attenuated because of transformer stations. The same applies for unbalanced faults in Figure 10.8(c), 10.8(d), 10.9(a), 10.9(b), 10.9(c) and 10.9(d).

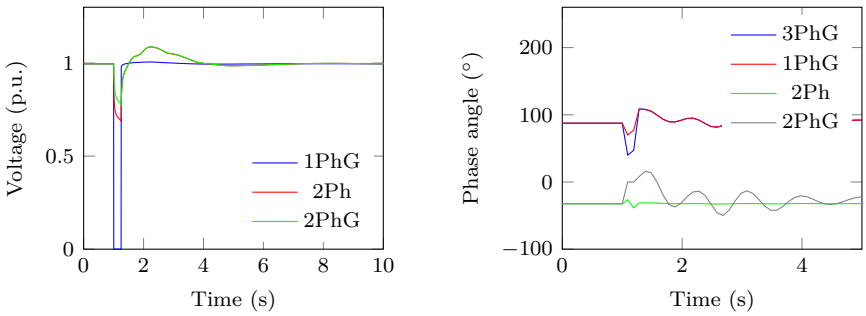


(a) Voltage dip magnitude (b) Phase angle

**Figure 10.7: Voltage dip during unbalanced faults at Punta Grande in Fuerteventura-Lanzarote**

Double-phase short-circuits have a voltage around 0.5 p.u. with a lowest value of 0.42 p.u. when the fault is at the same substation of observance, i.e. Montaña Mina. During single-phase short-circuits, voltage at the non-faulty phase A rises up to 1.6 at Macher. Under two-phase-to-ground faults, highest overvoltage is 1.2 p.u. at Corralejo 66 kV substation.

When subsystems are separated, short-circuit power at the PCC is lower. But the difference is barely remarkable on the dip magnitude, as seen in Figure 10.10 for two-phase short-circuits.

On the other hand, voltage unbalance rises up to around 100 % for two-phase and two-phase-to-ground shunt faults with no fault impedance. Regarding single-phase faults, voltage unbalance is higher for *Study Case 6*, as the grid is weaker in that case: 3.87 % under *Study Case 1* and 7.5 % under *Study Case 6*. Values resulting from single-phase short-circuit at Punta Grande, Corralejo and Matas Blancas are displayed in Figure 10.7. Voltage unbalance is notably higher at the fault point for Matas Blancas, as weakest bus in the system. However, unbalance propagation is deeper for faults at Corralejo, situated on the limit of both subsystems, as can be concluded from data in Table 10.5.

One open and two open phase events have also been analysed. Frequency, voltage magnitude and phase-angles change due to this disturbance with some magnitude. In the case of the link between both islands, frequency deviation is highest under *Study Case 6*, with a ±0.4 Hz excursion, while it only attains ±0.2 Hz under *Study Case 1*. If the disturbance is permanent, stability is lost for both cases. However, it is not a credible disturbance, concerning underground cables. Playa Blanca-Macher is an overhead line, but still stability is lost under both unbalancing events.

**Line loss** If the link between both islands is lost, frequency deviates and voltage magnitude and phase-angle change. The evolution depends on the initial power exchange between the islands. When Fuerteventura is exporting energy to Lanzarote (base case for interconnected islands scenario), frequency in this subsystem increases after the loss of the interconnection, as well as voltage magnitude. The contrary happens in Lanzarote. Some of the generators go out of step, as well, which happens

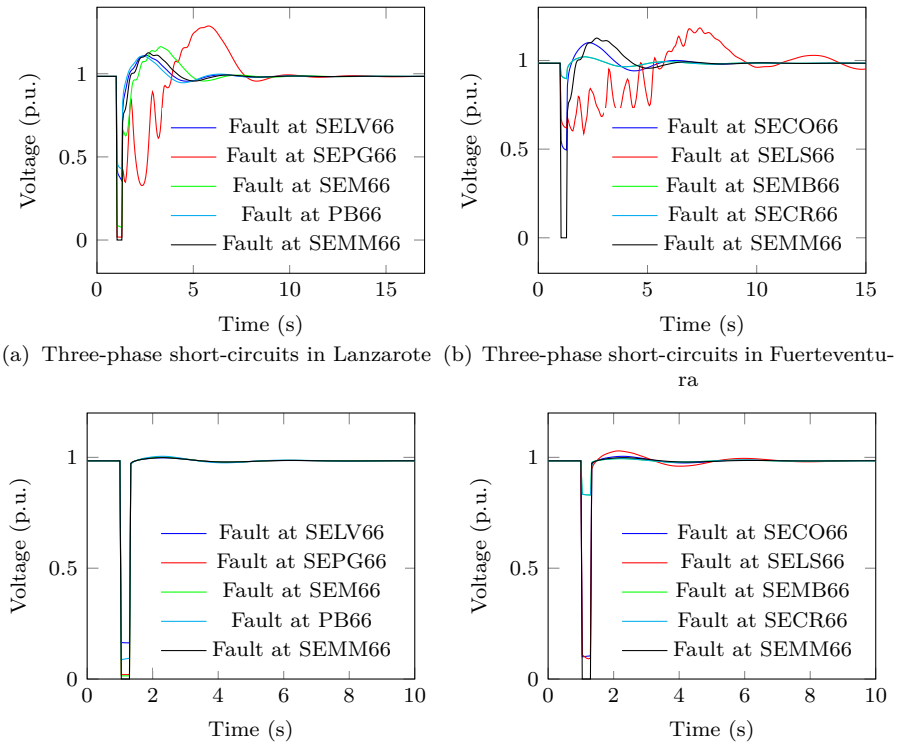


(a) Three-phase short-circuits in Lanzarote (b) Three-phase short-circuits in Fuerteventura

(c) Single-phase short-circuits (A) in Lanzarote (d) Single-phase short-circuits (A) in Fuerteventura

**Figure 10.8. Voltage dip magnitude at Montaña Mina 66 kV (I)**

**Table 10.5. Voltage unbalance due to single-phase faults under *Study Case 6***

| Fault point | Measurement point | VUF |
|---|---|---|
| Punta Grande | Punta Grande | 7.5 % |
| | Corralejo | 5.14 % |
| | Matas Blancas | 3.12 % |
| | Macher | 5.14 % |
| Corralejo | Punta Grande | 7.54 % |
| | Corralejo | 16.11 % |
| | Matas Blancas | 9.43 % |
| | Macher | 16.11 % |
| Matas Blancas | Punta Grande | 2.44 % |
| | Corralejo | 4.95 % |
| | Matas Blancas | 23.59 % |
| | Macher | 4.95 % |

faster under *Study Case 1*.

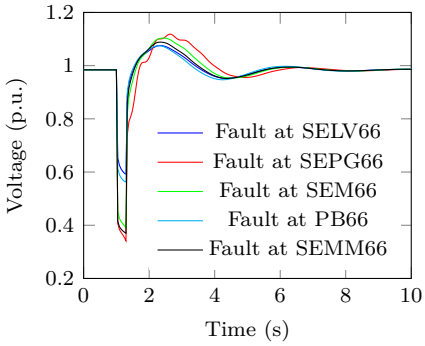


(a) Two-phase short-circuits (BC) in Lanzarote

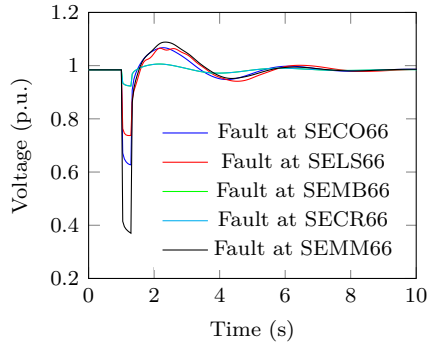


(b) Two-phase short-circuits (BC) in Fuerteventura

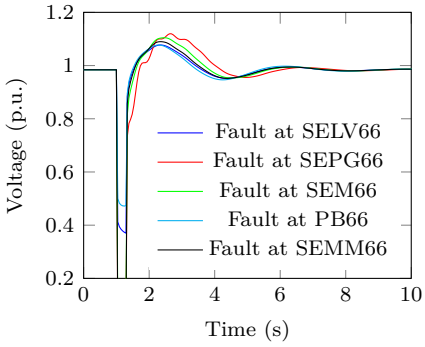


(c) Two-phase short-circuits-to-ground (BC) in Lanzarote

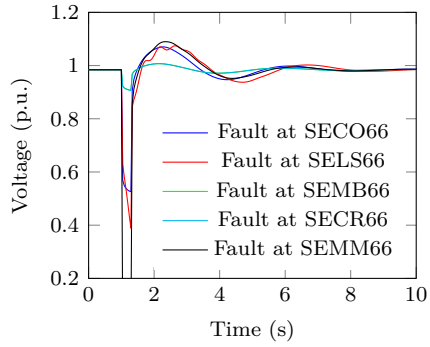


(d) Two-phase short-circuits-to-ground (BC) in Fuerteventura

**Figure 10.9. Voltage dip magnitude at Montaña Mina 66 kV (II)**

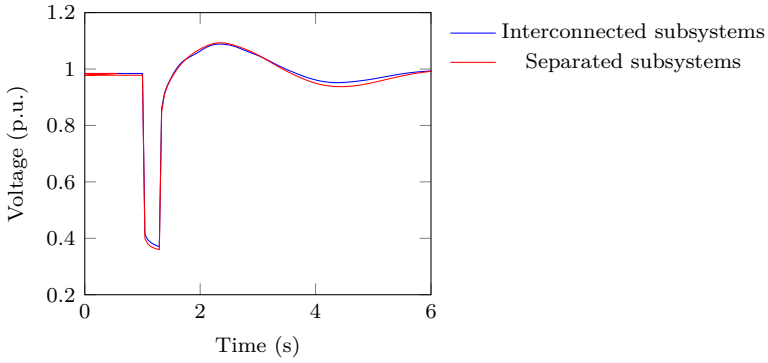


**Figure 10.10. Two-phase short-circuit at Montaña Mina 66 kV**

The loss of one of the double circuit Macher-Punta Grande has also been simulated. Resulting frequency is lower than the rated frequency, although the difference is small (0.01 Hz in steady-state). Worst case for frequency deviation is *Study Case 1*,

while phase-angle jumps are highest under *Study Case 6* with a maximum of 2°. If the islands are electrically separated, voltage deviations and phase shift are higher. Phase-shift in Lanzarote is not instantaneous and increases with time, and in some cases the subsystem may lose its stability. On the other hand, Fuerteventura island is radial, and therefore, the loss of any line results into a black-out.

### 10.2.4 Synthesis

Results for the dynamic operation in Fuerteventura-Lanzarote subsystem are gathered in Table 10.6, summing up the most critical scenarios. Frequency results apply at any point of the power system, whereas for the rest of parameters performance results depend on the point of disturbance and measurement, i.e. the PCC at Montaña Mina 66 kV substation.

**Table 10.6. Synthesis of performance results in Fuerteventura-Lanzarote**

| Event | Case | Parameter | Value[a] | Value[b] | Value[c] |
|---|---|---|---|---|---|
| Generation loss | 6 | $ROCOF-$ | -0.8 Hz/s | -1.97 Hz/s | -1.79 Hz/s |
| Generation loss | 6 | $f_{ss,l}$ | 49.72 Hz | 49.32 Hz | 49.34 Hz |
| Generation loss | 6 | $f_{min}$ | 49.24 Hz | 48.11 Hz | 48.28 Hz |
| Load loss | 6 | $ROCOF+$ | 1.08 Hz/s | 1.98 Hz/s | 1.94 Hz/s |
| Load loss | 6 | $f_{ss,h}$ | 50.4 Hz | 50.7 Hz | 50.66 Hz |
| Load loss | 6 | $f_{max}$ | 51.07 Hz | 51.87 Hz | 51.71 Hz |
| 3PhG fault | 1 | $V_{dip,3PhG}$ | 0 p.u. | 0 p.u. | - |
| 1PhG fault (a) | 1 | $V_{dip,1PhG}$ | 0 p.u. | 0 p.u. | - |
| 2PhG fault (bc) | 1 | $V_{dip,2PhG}$ | 0 p.u. | 0 p.u. | - |
| 2Ph fault (bc) | 1 | $V_{dip,2Ph}$ | 0.41 p.u. | 0.41 p.u. | - |
| 1PhG fault (a) | 6 | VUF | 100 % | 100 % | - |
| 2PhG fault (bc) | 6 | VUF | 100 % | 100 % | - |
| 2Ph fault (bc) | 6 | VUF | 100 % | 100 % | - |
| 1 Open phase | 6 | VUF | 1.9 % | 2.5 % | - |
| 2 Open phases | 6 | VUF | 15 % | 31.4 % | - |

Note: [a]: Interconnected; [b]: Separated, Lanzarote; [c]: Separated, Fuerteventura

It can be concluded that with the available data about the power system topology and assets, the situation in the Fuerteventura-Lanzarote system is compromised under steady-state and dynamic operation. Under steady-state operation, even under no contingency situation, voltage levels might happen to be out the admissible range, and transmission lines overloaded. The situation is worse in Fuerteventura island, which shows more acute infrastructure problems. Short-circuit levels are higher than

in Terceira island, as the power system size is bigger both in terms of peak load and installed capacity. Frequency deviations after a power mismatch event are not so critical as in Terceira, except for the separated subsystem scenario. Transient stability during short-circuits is maintained for most cases, but can be compromised for faults at the TPPs. The propagation of voltage dips is not as wide as in Terceira island due to the bigger size of the subsystems. Nonetheless, very high frequency events can be observed for three-phase short-circuits under peak demand scenario. Voltage unbalance reaches critical values under unbalanced short-circuits and open phase events, especially at the weakest buses in the system and under the weakest scenarios. When the islands are electrically separated, voltage deviations and phase-angle jumps are higher, even if no troublesome values are reached.

The energetic planning for the Canary islands, called PECAN (Plan Energético de Canarias), indicates in [160] future upgrading of the power network with the construction of new transmission lines and repowering of the system with new power stations, both conventional and renewable type for the coming years.

## 10.3 Parameterisation of grid models

For each of the three requirements under study, the particular grid has been parameterised based on corresponding formulae in Chapter 5, 6 and 7 in Part III. In **Case 3**, both grid code provisions and real performance results are available. As a consequence, the methodology could be applied as grid code verification tool or real operation emulation. For the first purpose, particular grid models would have to be parameterised based on grid code limits. For the second purpose, on the contrary, the adjustment could be based on simulation results for most critical scenarios in Section 10.2. Table 10.7 compares real performance results and grid code limits in the SEIE for the test cases under study. Real operation results for unbalance have not been included, because no unbalanced loading is reported in the available information. More restrictive values correspond to grid code limits. It can be observed that for most of the values grid code limits are very close to real performance results. It is hereby proved that regulation is adequate for Fuerteventura-Lanzarote system. As a consequence, the methodology could be applied as grid code verification tool or real operation emulation. Exceptions are frequency nadir and two-phase short-circuits. Regarding frequency minimum, it can be due to the fact that the SEIE grid code also applies in smaller systems where deeper frequency values could be attained. In the case of two-phase short-circuits the discordance can be put down on the fact that if all sequence impedances are considered equal, the minimum dip magnitude is 0.5 p.u. Therefore, it has also been selected as adjustment value hereby. The values finally selected for parameterising the particular grid models are in boldface.

The parameterised grid model has been simulated with *PowerFactory* simulation software package and the results compared to adjustment values and real performance operation, so as to verify the validity of the parameterisation methodology.

**Table 10.7. Synthesis of test cases with possible adjustment values**

| Test case | Parameter | Performance result | Grid code |
|---|---|---|---|
| A1 | $f_{max}$ | 51.87 Hz | **52 Hz** |
| A2 | $f_{min}$ | 48.11 Hz | **47 Hz** |
| A3 | $f_{ss,h}$ | 50.7 Hz | **50.25 Hz** |
| A4 | $f_{ss,l}$ | 49.32 Hz | **49.75 Hz** |
| A5 | $ROCOF+$ | 1.98 Hz | **2 Hz/s** |
| A6 | $ROCOF-$ | -1.97 Hz | **-2 Hz/s** |
| B1 | $V_{dip,3Ph}$ | 0 p.u. | **0 p.u.** |
| B2 1 PhG | $V_{dip,1PhG}$ | 0 p.u. | **0 p.u.** |
| B2 2 Ph | $V_{dip,2Ph}$ | 0.41 p.u. | **0.5 p.u.** |
| C1 | VUF | - | **2 %** |
| C2 | CUF | - | **5 %** |

### 10.3.1 Adjustment results

**Frequency ride-through** The worst underfrequency and overfrequency deviations correspond to *Study Case 6* under valley demand and high wind power. The load asset in the equivalent grid model represents the sum of the valley demand and system losses, as well considering wind energy contributing with no frequency response.

The most adverse situation can happen in Lanzarote when the power system is separated. However, grid code limits are more restrictive, as indicated in Table 10.7. Therefore, the particular grid model adapted to Lanzarote has been parameterised for grid code limits. The values for maximum and minimum frequency have been calculated with (5.50), as power mismatch is over 10 %. The adjustment results are shown in Table 10.8. Regarding the equivalent generator *Generator 1*, the rated power is $S_N = 78.4$ MVA, with $H_{eq} = 3.25s$, $R_{eq} = 0.052$ and $T_{eq} = 6s$ for the generation scenario under study, based on real scenario values. The installed capacity of *Generator 2* is $S_N = 30.5$ MVA, with $H_2 = 3.53s$, $R_{eq} = 0.075$ and $T_{eq} = 6s$. Equivalencing is based on system data in Lanzarote.

**LVRT** For LVRT, the divider model has been selected as particular grid model because only dip magnitude has been adjusted. The fault duration is based on the SEIE grid code. The results of the adjustment methodology are stated in Table 10.9. Resistive faults and an inductive source have been considered, based on the sensitivity study in Chapter 6. $\underline{Z}_{l1}$ has been adjusted in order to obtain the maximum $S_{sc}$ at the PCC, when both islands are interconnected, taking into account the generator internal impedance. $Z_{l2}$ has been adjusted to the lowest possible magnitude at the PCC. The load asset in the equivalent grid model represents the sum of the valley demand and system losses. For two-phase short-circuits, load modelling concerns mentioned in Chapter 9 do also apply, especially due to the big size of the

**Table 10.8: Case 3: parameterisation of particular grid model for frequency ride-through**

| Test | Parameter | Limit | *Generator 2* | *Load 1* | *Load 2* |
|---|---|---|---|---|---|
| A1 | $f_{max}$ | 52 Hz | - | 39.51 MW | 18.34 MW |
| A2 | $f_{min}$ | 47 Hz | 20.36 MW | 28.925 MW | 28.925 MW |
| A3 | $f_{ss,h}$ | 50.25 Hz | - | 48.13 MW | 9.72 MW |
| A4 | $f_{ss,l}$ | 49.75 Hz | 7.54 MW | 28.925 MW | 28.925 MW |
| A5 | $ROCOF+$ | 2 Hz/s | - | 28.84 MW | 29.01 MW |
| A6 | $ROCOF-$ | -2 Hz/s | 20.38 MW | 28.925 MW | 28.925 MW |

peak load. A fault resistance of $R_f = 0.399\Omega$ has been added upon the short-circuit application for the two-phase short-circuit.

**Table 10.9. Case 3: parameterisation of particular grid model for LVRT**

| Test | Parameter | Limit | $\underline{Z}_{l1}$ | $\underline{Z}_{l2}$ | $G_1$ | Load |
|---|---|---|---|---|---|---|
| B1 | $V_{dip,3Ph}$ | 0 p.u. (0.5 s) | 4.21Ω | 0 | 452.39 MVA | 257.8 MW |
| B2 1PhG | $V_{dip,1PhG}$ | 0 p.u. (0.5 s) | 4.21Ω | 0 | 452.39 MVA | 257.8 MW |
| B2 2Ph | $V_{dip,2Ph}$ | 0.5 p.u. (0.5 s) | 4.21Ω | 0.399Ω | 452.39 MVA | 257.8 MW |

**Unbalance** The selected scenario is valley demand with minimum short-circuit value ($S_{sc,min}$) corresponding to *Study Case 6* with separated subsystems, as voltage unbalance results into higher values.

The results of the adjustment methodology are stated in Table 10.10. All sequence impedances have been considered equal and a value of $LUF = 2$ for three-phase loads. For the VUF adjustment, resulting active power absorbed by the single-phase unbalanced load is $P_{bc} = 6.75MW$ and for the three-phase ungrounded star loads, $P_a = 5.64MW$ and $P_b = P_c = 11.29MW$. Regarding CUF, $P_a = 360.29MW$ and $P_b = P_c = 720.59MW$, values that are over the capacity and stability limits of the power grid.

**Table 10.10. Case 3: parameterisation of particular grid model for unbalance**

| Test | Parameter | Limit | $\underline{Z}_{l1}$ | $G_1$ | Load |
|---|---|---|---|---|---|
| C1 | VUF | 2 % | $4.5 \cdot j\Omega$ | 108.9 MVA | $R_{bc} = 644.87\Omega$<br>$R_a = 257.18\Omega, R_b = 128.59\Omega$ |
| C2 | CUF | 5 % | $4.5 \cdot j\Omega$ | 108.9 MVA | $R_a = 4.03\Omega, R_b = 2.015\Omega$ |

### 10.3.2 Verification of the parameterisation

The validity of the parameterised grid model has been verified by means of simulation. The models have been implemented in *PowerFactory* Digsilent software package and the obtained results benchmarked against the simulation performance results. Figure 10.11 shows the results of the adjustment for *Frequency Ride-Through* requirement. Plots in blue correspond to the parameterised grid model and those in green to real performance results. The adjustment for the rest of requirements can be verified in Figure 10.12. Limit values are pointed out in red and plots with dashed lines to real performance results.

The relative errors have been computed for each technical requirement and can be looked up in Table 10.11. Errors are below ±10 % for all the test cases. Hence, the parameterised grid models can be hereby validated.

**Table 10.11. Case 3: theoretical model verification results**

| Test | Parameter | Limit | Result | Error ( %) |
|---|---|---|---|---|
| A1 | $f_{max}$ | 52 Hz | 51.96 Hz | -0.08 % |
| A2 | $f_{min}$ | 47 Hz | 46.94 Hz | -0.13 % |
| A3 | $f_{ss,h}$ | 50.25 Hz | 50.248 Hz | -0.004 % |
| A4 | $f_{ss,l}$ | 49.75 Hz | 49.75 Hz | 0 % |
| A5 | ROCOF+ | 2 Hz/s | 1.94 Hz/s | -3 % |
| A6 | ROCOF- | -2 Hz/s | -1.95 Hz/s | 2.5 % |
| B1 | $V_{dip,3Ph}$ | 0 p.u. | 0 p.u. | 0 % |
| B2 | $V_{dip,1PhG}$ | 0 p.u. | 0 p.u. | 0 % |
| B2 | $V_{dip,2Ph}$ | 0.5 p.u. | 0.5 p.u. | 0 % |
| C1 (1Ph load) | VUF | 1.99 % | 1.99 % | -0.5 % |
| C1 (3Ph load) | VUF | 2 % | 1.99 % | 0 % |

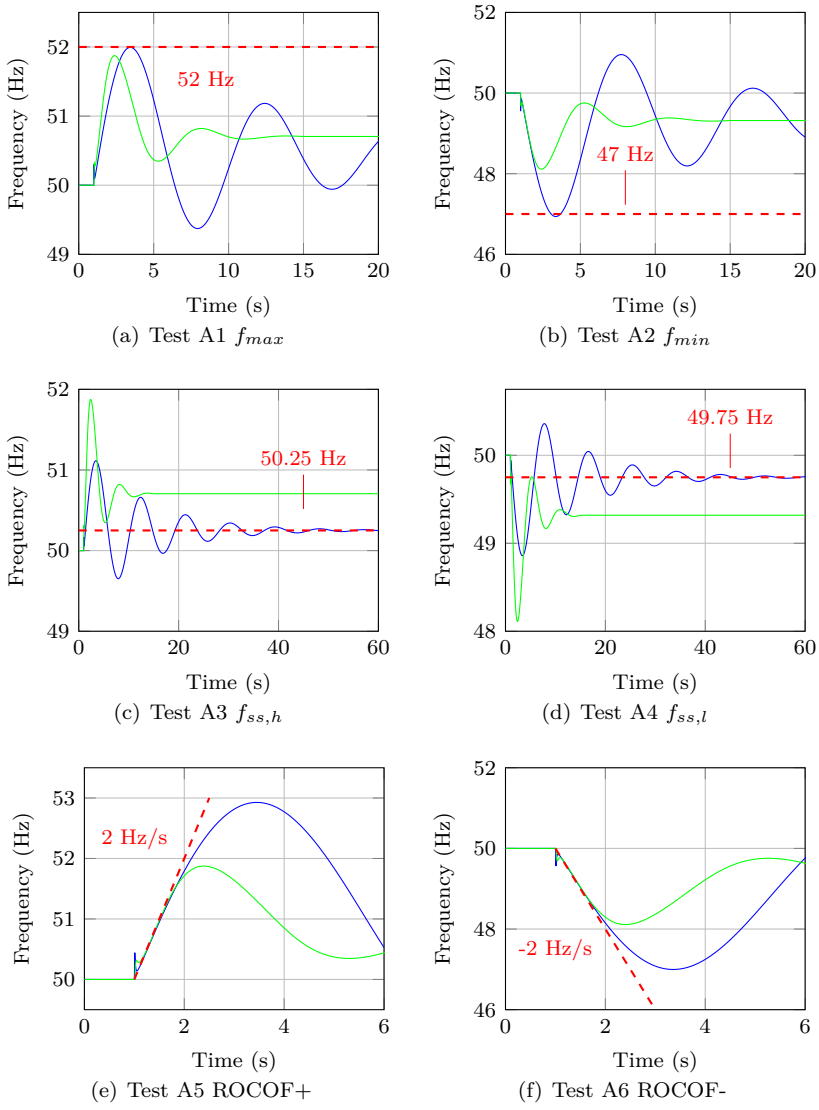


(a) Test A1 $f_{max}$ (b) Test A2 $f_{min}$

(c) Test A3 $f_{ss,h}$ (d) Test A4 $f_{ss,l}$

(e) Test A5 ROCOF+ (f) Test A6 ROCOF-

**Figure 10.11. Case 3: verification of adjustment of frequency ride-through**

## 10.4 Practical application of the methodology

The installation of 105 MW of wind power was approved in 2007, but has not been still executed [158]. In this practical application, the methodology will be used to perform compliance tests to an existing wind farm, which has been upgraded: the wind farm at Montaña de la Mina in Lanzarote. Initially, the wind farm consisted of 5 old generation induction generators (Appendix E) with a total installed capacity of 1.125 MW. The new wind farm will consist of 4 WTGs of 2 MW. The PCC of the

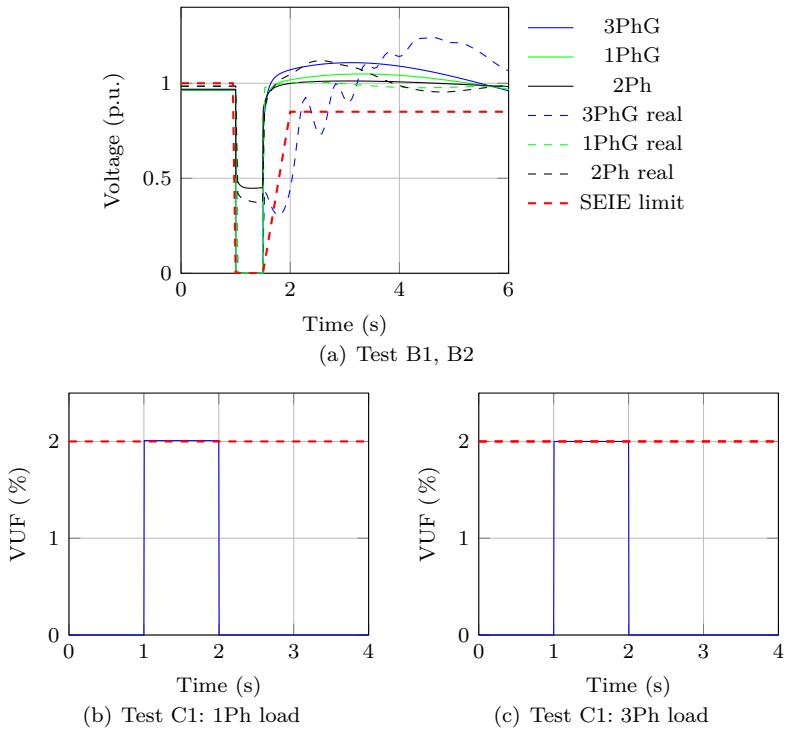


(a) Test B1, B2

(b) Test C1: 1Ph load

(c) Test C1: 3Ph load

**Figure 10.12. Case 3: verification of the rest of parameters**

wind farm has the characteristics indicated in Table 10.1. The SCR at the PCC is over 40, even under most demanding scenarios.

The wind farm has been modelled with *PowerFactory* software package, based on a grey-box user model, and parameterised according to values indicated in Appendix C, where the user model and the equivalent grid model are also described. The methodology has been applied so as to verify if the new power plant complies with the technical provisions in the SEIE grid code regarding the requirements under study.

For remain connected requirements, two events have been simulated by adjusting the simplified equivalent grid for each of the compliance tests defined in Chapter 4: an event outside usual range in the power grid (indicated suffix -1 in test identificator), and an event within the usual range (indicated suffix -2 in test identificator). Limit values are based on Section 10.3. For active support requirements, generator contribution is showed by simulating an event within limits.

**Frequency ride-through** Frequency ride-through test cases are listed in Table 10.12. For *Frequency ride-through* validation, the frequency response block of the plant has been disabled, so as to be able to observe the trip of the plant when frequency is beyond permitted values. This feature can be achieved by conveniently adjusting the protection relay settings of the generation asset. In addition, for a

better observance of ROCOF events under/overfrequency events have been disabled for test cases A5 and A6. Test cases A3 and A4 have not been considered, because only primary protection relays have been configured in the model.

**Table 10.12. Case 3: frequency ride-through test cases**

| Test case | Parameter | Limit | Test value |
|---|---|---|---|
| A1-1 | $f_{max}$ | 52 Hz | 52.5 Hz |
| A1-2 | $f_{max}$ | 52 Hz | 51.5 Hz |
| A2-1 | $f_{min}$ | 47 Hz | 46.5 Hz |
| A2-2 | $f_{min}$ | 47 Hz | 47.5 Hz |
| A5-1 | ROCOF | 2 Hz/s | 2.5 Hz/s |
| A5-2 | ROCOF | 2 Hz/s | 1.5 Hz/s |
| A6-1 | ROCOF | -2 Hz/s | -2.5 Hz/s |
| A6-2 | ROCOF | -2 Hz/s | -1.5 Hz/s |

Figure 10.13(a) plots the system frequency for each case and Figure 10.13(a) the power output of the power plant. The power output is expressed in p.u. with respect of initial power reference. It can be observed that the power plant trips correctly during the events out of the permitted range. For underfrequency events beyond the limits, the power plant is tripped, which increases the power imbalance, and hence, the system frequency deviation.

**Frequency response** The converter model includes primary frequency control characteristics. This feature has been parameterised with values within an acceptable range in the SEIE grid code by reproducing test case A2-2. Frequency response for both high and low frequencies has been tested based on an underfrequency event, because frequency decreases during the drop but increases (and decreases) alternatively during recovery, until the steady-state situation. Thus, as frequency drops the power plant increases its active power generation, whereas the contrary happens as frequency starts to recover. This behaviour can be observed in in Figure 10.14, where simulation results are plotted.

**LVRT** Two events have been simulated by adjusting the fault duration for each of the compliance tests defined in Chapter 4: an event within the permitted range with $t_{dip} = 250$ ms and an event outside the permitted range with $t_{dip} = 650$ ms. Test B2, corresponding to unbalanced faults, is out of the scope of the practical application, because the generating unit model under study does not include the ability to ride-through unbalanced faults.

Figure 10.15 shows voltage profiles at the PCC for both events with limit profile based on SEIE regulation. The power generation asset meets the regulations in Spain, as it remains connected and generating during event B1-2, and trips during event B1-1. In test case B1-2 shown in Figure 10.15(d), it can observed that the power plant remains connected and there is an active and reactive power output.

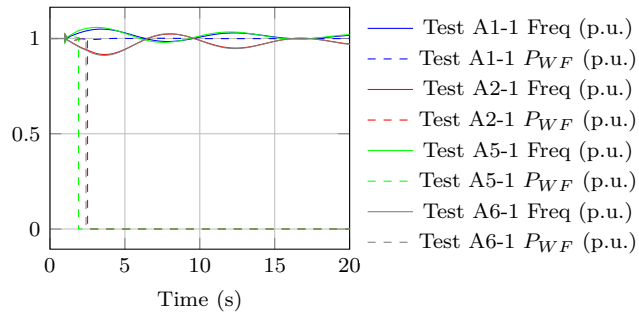


(a) Events out of the permitted range

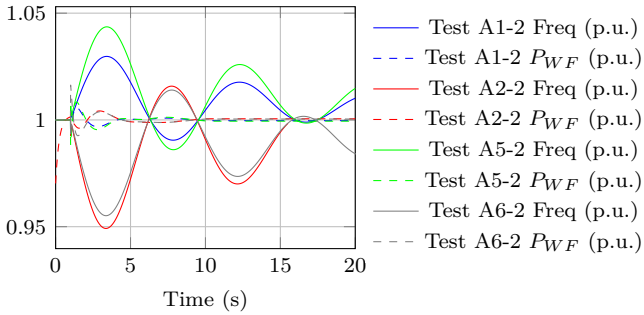


(b) Events within the permitted range

**Figure 10.13. Case 3: validation of the procedure for frequency ride-through**

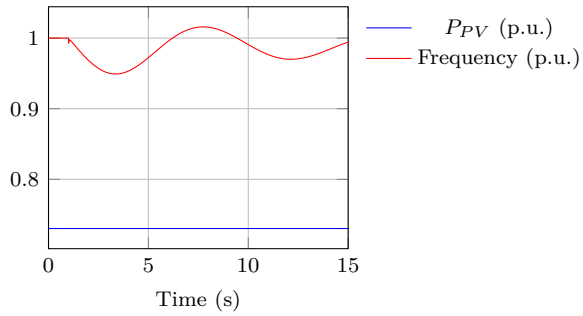


**Figure 10.14. Case 3: validation of the procedure for frequency response**

Test B2, corresponding to unbalanced faults, is out of the scope of the practical application, because the generating unit models only contain positive sequence.

**Output current during faults** In order to maintain transient stability, the upgraded wind farm can contribute with active and reactive power during balanced short-circuits. Thus, the control block of the equivalent converter of the power plant has been parameterised with values based on the SEIE grid code. According to most grid codes (Chapter 4), active and reactive current injection in function of voltage can be specified by some reference points. Adjustment values for SEIE regulation

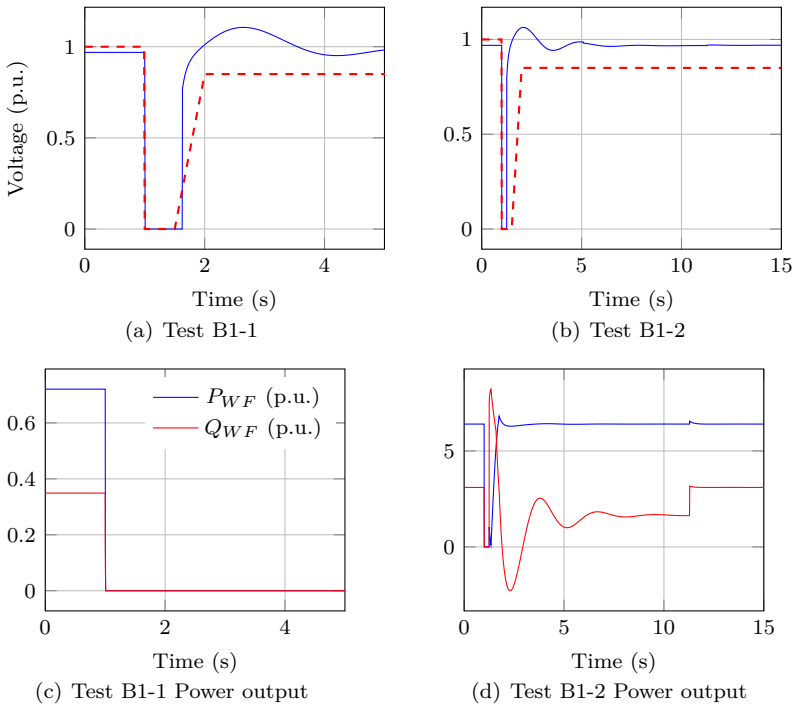


(a) Test B1-1 (b) Test B1-2

(c) Test B1-1 Power output (d) Test B1-2 Power output

**Figure 10.15. Case 3: validation of the procedure for LVRT**

are indicated in Appendix C.

The event corresponding to the current injection tests for balanced faults is Test B1-2, which corresponds to a balanced LVRT situation. Both current and corresponding power in p.u. are shown in Figure 10.15(d). Support during fault has been specified to be active still 10 seconds after the recovery. Tests B5 and B6, corresponding to current contribution during faults for unbalanced faults, is out of the scope of the practical application, because the generating unit model does not include the ability to contribute to unbalanced faults.

**Unbalance** Unbalance test cases are listed in Table 10.13. Only voltage unbalance has been considered, because current unbalance adjustment condition leads to instability. Single-phase loading has been selected as unbalancing event because it leads to higher unbalances. Frequency protection functions and frequency response have been disabled.

**Table 10.13. Case 3: unbalance test cases**

| Test case | Parameter | Limit | Test value |
|---|---|---|---|
| C1-1 | VUF | 2 % | 2.5 % |
| C1-2 | VUF | 2 % | 1.5 % |

Figure 10.16(a) shows the unbalance at PCC after the grid adjustment, whereas 10.16(b) plots the action of the protection relay with trip of the PV plant. When unbalance is below the limit value, the power plant remains connected.

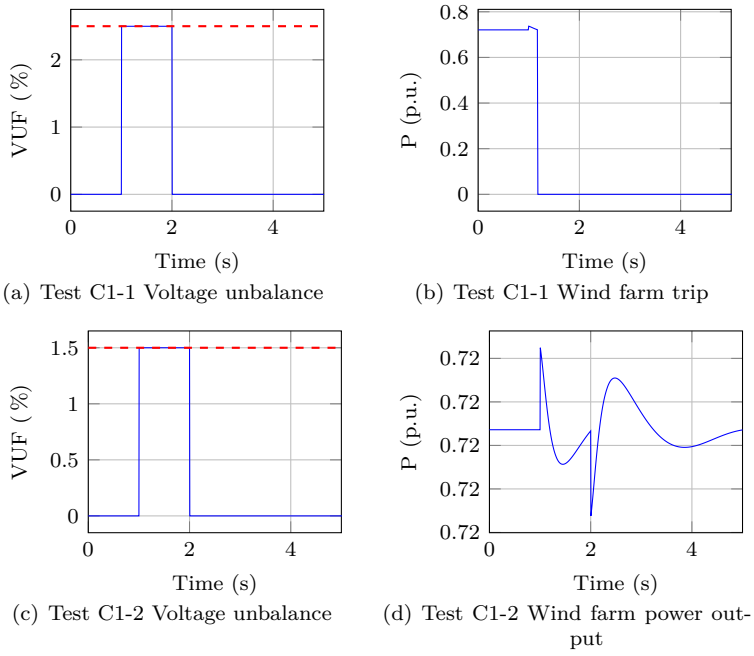


(a) Test C1-1 Voltage unbalance

(b) Test C1-1 Wind farm trip

(c) Test C1-2 Voltage unbalance

(d) Test C1-2 Wind farm power output

**Figure 10.16. Case 3: validation of the procedure for VUF**

**Summary** The application of the methodology for **Case 3** is based on grid code limits. By using the particular grid model conveniently parameterised, events have been correctly emulated. Thus, the control and protection algorithms of the wind power plant have been assessed with respect of the connection to Fuerteventura-Lanzarote system. The performance of the power plant has been correctly demonstrated for all test cases under study. Table 10.14 summarises the results of the practical application of the methodology for **Case 3**.

**Table 10.14. Case 3: summary of grid code compliance verification**

| Test case | Description | Action | Pass/Fail |
|---|---|---|---|
| A1-1 | Maximum frequency | ANSI 81O trips | ✓ |
| A1-2 | Maximum frequency | WF remains connected | ✓ |
| A2-1 | Minimum frequency | ANSI 81U trips | ✓ |
| A2-2 | Minimum frequency | WF remains connected | ✓ |
| A3-1, A3-2 | High frequency event | Not tested | – |
| A4-1, A4-2 | Low frequency event | Not tested | – |
| A5-1 | Positive ROCOF | ANSI 81R trips | ✓ |
| A5-2 | Positive ROCOF | WF remains connected | ✓ |
| A6-1 | Negative ROCOF | ANSI 81R trips | ✓ |
| A6-2 | Negative ROCOF | WF remains connected | ✓ |
| A7 | Frequency response for high frequencies | Control module decreases $P_{WF}$ | ✓ |
| A8 | Frequency response for low frequencies | Control module increases $P_{WF}$ | ✓ |
| B1-1 | Balanced LVRT | Converter module trips | ✓ |
| B1-2 | Balanced LVRT | WF remains connected | ✓ |
| B2-1, B2-2 | Unbalanced LVRT | Not tested | – |
| B3 | $I_a$ during balanced LVRT | Converter module $I_a = f(V)$ | ✓ |
| B4 | $I_q$ during balanced LVRT | Converter module $I_q = f(V)$ | ✓ |
| B5 | $I_a$ during unbalanced LVRT | Not tested | – |
| B6 | $I_q$ during unbalanced LVRT | Not tested | – |
| C1-1 | Voltage unbalance | ANSI 47 Trips | ✓ |
| C1-2 | Voltage unbalance | WF remains connected | ✓ |
| C2-1, C2-2 | Current unbalance | Not tested | – |

Note: -1:outside the permitted range; -2:within the permitted range

# Part V

# Conclusions and future work

# Chapter 11

# Conclusions and future research

## 11.1 Conclusions

The point of departure of this thesis was the review of existing grid codes for the connection of renewable generation assets in the light of harmonisation efforts launched by international organisms. Differences in regulation can be attributed to environmental conditions, government policies, local utility practices, network strength and characteristics, and grid asset types present in the system. Therefore, this thesis analysed the influence of strength in grid codes. Main outcomes point out that in weak power grids wider operating ranges, greater power factor range, more stringent frequency response and more onerous fault ride-through requirements are requested by system operators.

The following step was to study current grid code compliance verification practices. It was concluded that grid code verification, model validation and certification procedures are still under development in many countries, which on the contrary have rather stable, harmonised and complete grid codes. Even if compliance processes are well documented in some countries like the UK, mostly there is usually little information and documents are not clear nor definite. Recently, RES certification has been launched in some countries, such as Germany and Spain. The German regulation encompasses generating unit and system certification. The process includes type testing verification, as well as the provision of simulation models of the assets under certification. The Spanish procedure for wind farm certification is based on the verification of LVRT requirement based on simulation models of the whole wind farm, which are made up by previously validated wind turbine models. However, simulation procedures were found to be scarcely documented and basically focused on FRT requirement. Modelling requirements are more widely standardised, although mostly not adequate for weaker parts of the power grids and EMT studies.

Those weaknesses were addressed in this thesis, with the presentation of a grid code compliance verification methodology aiming to expand simulation technique as an adequate tool to prove compliance with other technical requirements besides LVRT. The methodology presented in this thesis proposed a generic and reduced grid model as equivalent system suitable for both simulating the static and dynamic performance of a selected power system for interconnection and design purposes, and for verifying the compliance of grid code requirements. Depending on the disturbance

to be represented and sensitivity studies of the model parameters, the generic grid model must be particularised, and so obtain a particular grid model. Finally, the grid model has to be parameterised based on grid characteristics and grid code limits, resulting into a parameterised grid model.

Island grids were selected as target because of the importance of RES integration and proper testing and evaluation beforehand. As a consequence, a simulation procedure for most critical rules in this kind of power grids was presented. Selected requirements were *frequency ride-through*, *LVRT* and *unbalance*, with corresponding remain connected and active support provisions. Each of the requirements was theoretically analysed so as to obtain an equivalent grid model able to reproduce any disturbance.

Regarding **frequency ride-through**, existing SFR models are adequate for only thermal generation (Anderson), not straightforward to adjust (Aik), or only valid for small power mismatches (Egido). As an alternative, this thesis presented a procedure for larger disturbances, which are frequent in smaller island grids. Thus, frequency can be calculated by equivalencing the power system considering first-order prime movers.

The theoretical analysis of **fault induced voltage dips** is two-fold. Dip magnitude calculation can be derived by using a simple voltage divider model. However, studying the dynamic evolution results into high-order equations, even for small power grids. Several parameters have an influence, including the characteristics of the network, generating units and fault nature. Hence, in order to streamline parameterisation, only dip magnitude and fault duration were considered in this thesis.

**Voltage and current unbalance** were theoretically analysed considering unbalanced short-circuits, series faults and asymmetrical loading. A sensitivity analysis brought to light that short-circuits and series faults cannot be adjusted so as to obtain usual limit values in the grids codes. Generally, these phenomena either involve very high or very low -in the case of unequal impedances in conveniently transposed lines- transient unbalances. Therefore, parameterisation was limited to unbalanced loading in this thesis.

Finally, the compliance verification methodology was applied to three study cases: three island power systems where a new or an existing renewable power plant must prove fulfilment of a selected grid code or the ability to integrate in a power system.

First, a general medium size island where only minimum data at the PCC is known was considered. The particular equivalent grid models for each of the requirements were parameterised, and the parameterised grid models and corresponding adjustment formulae were validated by comparing simulation results with theoretical adjustment. Then, a new PV power plant under grid code compliance verification was connected to the parameterised grid models. By emulating limit conditions, the correct performance of the power plant was evaluated, both remaining connected when required and contributing with active and reactive power during frequency excursions and voltage dips. Thus, the methodology proposed in this thesis showed to be useful for manufacturers aiming to integrate a new power plant in a medium size island grid where little information about the power system is available.

The second application example was Terceira island, in the Açores archipelago. The island grid was modelled based on system operator information with no current specific technical regulation for the connection of renewable generation assets. Therefore, particular grid models were parameterised based on real performance results at the PCC. For that purpose, the static and dynamic performances of Terceira island were simulated, under most usual operation scenarios and credible contingencies. Thus, limit values for relevant parameters were derived. Terceira island showed to be a power system with favourable renewable energy resources and an encouraging potential for higher penetration rates. In this line of work, the performance of a new wind farm connected at Quatro Ribeiras substation was assessed so as to verify its suitability to undergo limit grid situations and contribute to system performance. The results proved the usefulness of the methodology for cases with similar characteristics as Terceira island.

The last application example was the interconnected power system of Fuerteventura-Lanzarote in the Canary islands. The big size island grid was modelled based on system operator information, and a specific regulation rules the connection of renewable power plants in the Spanish SEIE. The performance analysis brought to light usual technical issues in isolated power systems. Due to economic constraints, investments in electrical infrastructures are often delayed. This seems to be the case for Fuerteventura island, where issues arise even under steady-state operation. For dynamic simulations, worst results were obtained when Fuerteventura and Lanzarote systems are separated. This can be considered as a credible contingency, as currently only a submarine link is available. Low values of frequency upon a power mismatch event were reached in both systems, especially under valley demand scenarios, which could trip UFLS protection relays. So, electricity supply would be compromised for some parts of the network. Simulations showed that attained ROCOF values could also be challenging for converter-based generators. As a consequence of these results, the connection of a new renewable power plant seems unrealistic without undertaking infrastructure upgrades. Hence, the WTG of an existing wind farm was replaced with newer generating units, including control and protection algorithms which must comply with the grid code under force. The parameterisation of the particular grid codes for each of the requirements under assessment can be done either based on real performance results, or in regulation limits. The choice depends on the purpose of the application. In this thesis, most stringent values between both alternatives were considered, corresponding to regulation limits. Thus, it was proved that grid code of the SEIE is on the whole adequate for Fuerteventura-Lanzarote system. The simulation results confirmed the validity of the methodology for a bigger size island grid, where both network information and interconnection regulation for RES are available. In addition, the methodology proved to be adequate for new and existing power plants.

In conclusion, the verification methodology presented in the thesis was proved to be suitable in the light of the application cases. The theoretical study leading to the adjustment procedure was also confirmed to be correct, except for current unbalance. The unbalancing phenomena under study -unbalanced short-circuits, series faults and unbalanced loading- were evidenced to be inadequate for current unbalance

adjustment because they involved unrealistic parameter values. The parameterisation based on unbalancing power generation sources, left out the scope of the thesis, could be a better alternative. Regarding LVRT, equivalencing techniques could be applied to whole power systems. However, the simplifications assumed in the thesis were valid for island power grids due to their limited size and because only voltage dip magnitude was adjusted. Nevertheless, in order to reproduce polygonal profiles as indicated in many grid codes, the use of controllable voltage sources could be a better choice. This alternative would also be a more adequate solution for verifying frequency response of generating units, because often several frequency values are requested to be checked.

## 11.2 Main contributions

Grid codes issued by relevant system operators for the connection of renewable power generation were reviewed and compared. Thus, the influence of system strength on regulation was analysed. On the other hand, regulation provisions regarding modelling, testing and validation of renewable generation units were studied. As a consequence, main shortcomings in current practices were highlighted and used as basis for the proposal of a methodology for the compliance verification.

Moreover, the novel contributions of the thesis are hereby presented.

1. A new grid code compliance verification was presented in this thesis. A T-shaped generic power grid model was proposed as starting point, valid for the emulation of several grid disturbances. The particularisation of the generic model was explained, based on the event types under study. Finally, this document indicated an adjustment methodology leading to a parameterised grid model.

2. System Frequency Response models proposed in the literature were studied and a simplified method for calculating the frequency minimum value was introduced so as to fit small and medium size island power grids, where large power mismatches can appear.

3. Voltage dip characterisation was studied beyond the classical voltage divider model, so as to better analyse transient performance during a short-circuit and its recovery.

4. Sequence circuit connection for series faults and unbalanced loading were mathematically derived. Based on those expressions, complex voltage and current unbalance factors for the unbalancing phenomena under study were computed.

5. Simplified equivalent grid models for the emulation of frequency excursions, voltage dips and unbalances were presented. The expressions for the parameterisation of each particular grid model were hereby presented, taking into account sensitivity studies.

6. Island power systems of Terceira in the Açores and Fuerteventura-Lanzarote in the Canaries were modelled based on available network data. Their operation under steady-state and transient regimes was studied using *PowerFactory*

software package.

7. The methodology was applied to three island examples and the particular grid model parameterisation adapted to the available information. The integration of new or existing RES power plants was simulated using *PowerFactory* software package, based on parameterised grid equivalents. By using the particular grid model conveniently parameterised, events were correctly emulated. Thus, the control and protection algorithms of the renewable power plants were assessed for all test cases under study.

## 11.3 Scientific production

Several contributions of this thesis were communicated to the scientific community with relevant journal and conference papers.

**Journal papers**

[1 ] **A. Etxegarai**, P. Eguia, E. Torres, A. Iturregi and V. Valverde. *"Review of grid connection requirements for generation assets in weak power grids"*. Renewable and Sustainable Energy Reviews, vol. 41. pp. 1501-1514, January 2015.

This paper reviews and compares technical requirements imposed on to generation assets in countries with very distinct characteristics, in order to analyse the influence of weakness and isolation of a power grid on the interconnection conditions imposed by system operators to grid users. Current and future regulation aspects are covered.

[2 ] **A. Etxegarai**, P. Eguia, E. Torres, G. Buigues and A. Iturregi. *"Current procedures and practices on grid code compliance verification of renewable power generation"*. submitted for publication to Renewable and Sustainable Energy Reviews in January 2015.

Generation assets applying for grid connection must comply with certain grid code requirements. Grid code compliance verification shall include revision of documentation covering technical data and models, checking of the requested capabilities, and validation of model performance. These procedures are singular regarding renewable power generation, due to their singular characteristics, specific topologies and short experience. This paper reviews current procedures and practices on grid code compliance verification, encompassing modelling and validation requirements, testing set-ups and certification procedures.

**Conference papers**

[1 ] **A. Etxegarai**, E. Torres and P. Eguia. *"Integrating Distributed Generation into Weak Power Grids "*. 12 Conferencia Luso-Española de Ingeniería Eléctrica XIICLEEE, Ponta Delgada, Açores (Portugal), July 2011.

[2 ] **A. Etxegarai**, P. Eguia, E. Torres and E. Fernandez. *"Impact of wind power in isolated power systems "*. 2012 16th IEEE Electrotechnical Conference

(MELECON), pp. 63-66, Hammamet (Tunis), April 2012.

[3 ] **A. Etxegarai**, E. Torres and P. Eguia. *"Frequency control of isolated power systems with wind power penetration"*. Conferencias Hispano-Lusas de Ingeniería Eléctrica (CHLIE) 2013, Valencia (Spain), July 2013.

[4 ] M. Zubiaga, S. Aurtenetxea, **A. Etxegarai** and E. Torres. *"LVRT dynamic performance analysis in a detailed time domain simulation scenario beyond the impedance divisor fault"*. EPE'13 15th European Conference on Power Electronics and Applications, pp. 1-10, Lille (France), September 2013.

[5 ] M. Zubiaga, S. Aurtenetxea, **A. Etxegarai**, E. Torres, P. Eguia and J. Chivite. *"Frequency restoration in insular grids with high penetration of wind power"*. 39th Annual Conference of the IEEE Industrial Electronics Society IECON'2013, pp. 2045-2050, Vienna (Austria), November 2013.

[6 ] **A. Etxegarai**, E. Torres, I. Zamora, J.I.San Martin and P. Eguia. *"Review of Procedures for Verification of Grid Code Compliance of Renewable Generation"*. International Conference on Renewable Energies and Power Quality (ICREPQ'14), Cordoba (Spain), April 2014.

[7 ] P. Eguia, **A. Etxegarai**, E. Torres, J.I. San Martin and I. Albizu. *"Use of generic dynamic models for photovoltaic plants"*. International Conference on Renewable Energies and Power Quality ICREPQ'15, ISSN 2172-038 X, N. 13, La Coruña (Spain), March 2015.

[8 ] J. I. San Martin, P. Eguia, **A. Etxegarai**, E. Torres and I. Albizu. *"A survey on Innovative Solutions and Projects for the Integration of Renewable Generation in Weak Power Grids"*. International Conference on Renewable Energies and Power Quality ICREPQ'15, ISSN 2172-038 X, N. 13, La Coruña (Spain), March 2015.

[9 ] P. Eguia, **A. Etxegarai**, E. Torres, J.I. San Martin and I. Albizu. *"Modelos dinámicos genéricos de plantas fotovoltaicas: parametrización y validación"*. XVI ERIAC Encuentro Regional Iberoamericano de CIGRÉ, Puerto Iguazú (Argentina), May 2015.

## 11.4 Future research lines

A thesis must be a finite time-bound work. As a consequence, there will always be new papers to review, assumptions to discard, unresolved questions or research paths to explore more deeply. It is certainly the case for the present thesis. But a finishing line has to be drawn (fortunately). Therefore, here go some future research lines that would contribute to further develop the work initiated by this thesis:

- Based on the procedure as outlined in this thesis, the grid code compliance methodology could be extended to:
  - Other usual technical requirements. Regarding *remain connected requirements*, phase-angle jump and HVRT could be best candidates after the

corresponding theoretical study. On the other hand, inertia emulation and oscillation damping are indicated as possible future active support requirements for RES generators.

  - Other kinds of power grids in addition to islands, by selecting the adequate technical provisions and grid disturbances, as well as by carrying out a sensitivity study that takes into account the boundary conditions.

- Load modelling in the equivalent grid could be further studied, taking into account voltage and frequency dependent assets.
- The numerical application of the methodology in this thesis was based on a grey-box RMS plant user model. Instead, validated generic generator models could also be tested, as outlined in some reference documents. Besides, three-phase generator models should be more adequate so as to verify grid code compliance for remaining connected and contributing to the power system stability under unbalancing events.
- The grid equivalent models presented in this dissertation could be used not only to emulate island power operation or verify the grid code compliance of generating units under certification. In addition, they could be applied to further analyse the interaction of converter systems with weak power grids, so as to improve control and protection algorithms and tune control and protection parameters.
- The methodology could be completed with more detailed measuring, passing and accuracy criteria, especially for active requirements.

# Part VI

# Appendices

# Appendix A

# Influence of SFR study model on frequency response

The influence of the SFR study model on frequency response regarding frequency minimum has been analysed for single generating units, as well as the whole power system, based on the analytical study in Section 5.3.

## A.1 Single generating unit models

Frequency behaviour is hereby analysed using different theoretical SFR study models, comparing Kundur model [127], Anderson model [125], and Egido model [123] for a single generating unit. For the Egido model, the parameters of the equivalent first-order model (best suited for reheat steam turbines [126]) have been tuned in open loop. In addition, the fitting time range has been analysed selecting extreme frequency minimum occurrence instant values indicated in Table A.1, i.e. 1 and 20 seconds, as well as some intermediate values.

**Table A.1. Typical frequency minimum time range in different power systems**

| Power system | $t_{min}$ (s) | Reference |
|---|---|---|
| Spanish isolated systems | 1-4 | [123] |
| Large, mixed resource systems | 9 | [161] |
| Crete | 2 | [162] |
| Ireland | 2.75, 3-7 | [163] |
| US eastern interconnection | 2.2-2.5 | [161] |
| WECC | 8-20 | [164] |
| New Zealand | 4 | [165] |

On the other hand, two simplified model types based on Egido model have been selected, with non-tunable and tunable $k$ parameter (calculated from the droop constant $K_i$) hereinafter called *Egido1* and *Egido2* methods, which correspond respectively to *one* parameter estimation ($T$ time constant) and *two* parameter estimation ($k$ and

$T$ constants). Estimation results are indicated in Table A.2, obtained from a step input to Kundur model (the most detailed model among those under analysis) with parameters in Table 5.2 based on different fitting times. It can be concluded that lower $k$ and $T$ values are obtained as fitting time is shorter.

**Table A.2. Parameter estimation for a single generating unit**

| Fitting time | Egido1 | | Egido2 | |
|---|---|---|---|---|
| | $k$ | $T$ (s) | $k$ | $T$ (s) |
| 1 s | 20 | 0.41 s | 18.41 | 0.41 s |
| 3 s | 20 | 0.73 s | 15.62 | 0.73 s |
| 5 s | 20 | 1.21 s | 11.97 | 1.21 s |
| 10 s | 20 | 2.44 s | 15.62 | 2.44 s |
| 20 s | 20 | 3.82 s | 18.41 | 3.82 s |

Resulting frequency deviations after a generation loss of 0.2 p.u. have been plotted for different fitting time ranges in Figure A.1 and compared to Kundur model as the most detailed model. It can be concluded that the two parameter estimation method *Egido2* gives a more exact result for predicting the system frequency behaviour for the initial instants (included the frequency nadir). On the other hand, fitting time range, hereinafter referred to as $t_f$, is highly important. If a time range close to the frequency minimum instant is chosen, the estimation for the first instants is more precise.

Figure A.2 compares the frequency response in a power system with a single reheat steam turbine generator after a generation loss of 0.2 p.u. including Kundur, Anderson and Egido method. For the Egido model, only *Egido2* is considered based on the real minimum frequency instant for the detailed model (i.e. 2 seconds) resulting in parameters $k = 8.77$ and $T = 0.5452$ s. The equivalent first-order model fits perfectly the detailed model response. The frequency nadir can be analytically approximated based on [123] or directly solved (e.g. using Laplace transform). Both results are indicated in Table A.3.

**Table A.3. Comparison of SFR models**

| Parameter | Kundur | Anderson | Egido2[a] | Egido2[b] |
|---|---|---|---|---|
| $f_{min}$ | 48.73 Hz | 48.87 Hz | 49.25 Hz | 48.73 Hz |
| $t_{min}$ | 2.1 s | 2.31 s | 1.2 s | 2.1 s |

a: Approximation

b: Directly solved

The result obtained by solving directly the first-order equivalent system corresponds correctly to the detailed model response. Using Egido method, the difference between both is notable. In fact, the simplification only suffices for small disturbances. The bigger is $P_0$ the mismatch disturbance, so it is the calculation error.

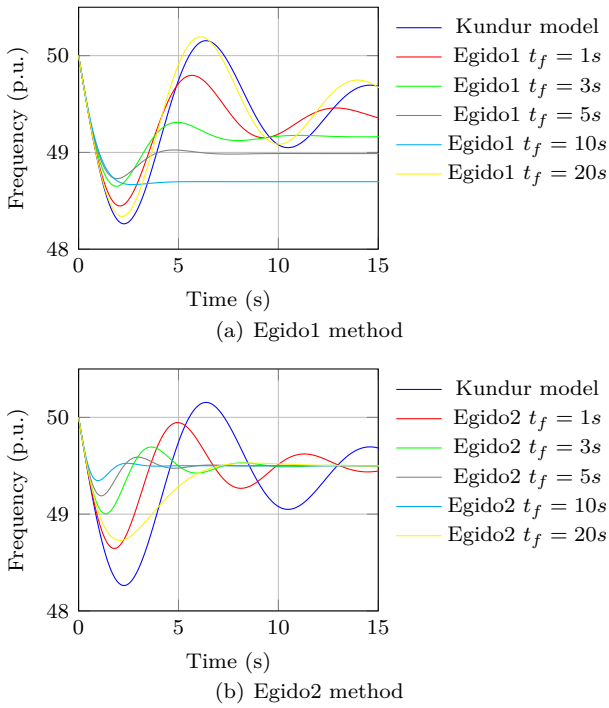


(a) Egido1 method

(b) Egido2 method

**Figure A.1. Study of Egido model**

It can be concluded that when power mismatch is high, the method proposed by Egido introduces a significant error in the estimation of frequency minimum. For smaller disturbances, the error is reduced. Hence, the method is not adequate for small and even medium size isolated power systems, where the loss of a single generating unit could represent a high proportion of total installed capacity.

## A.2 Whole power system models

The effect of the theoretical model on frequency response has been also analysed for a whole power system. Anderson model [125], Aik model [130], and Egido model [123] approaches for multi-generator power systems have been compared. Three simple cases have been considered as illustration, based on a small power system made up of two thermal generating units:

- **Case A**: two identical generating units (parameters in Table 5.2).
- **Case B**: two generating units with different inertia constants ($H_1 = 2.5s$ and $H_2 = 4s$) and rest of the parameters identical (Table 5.2).
- **Case C**: two generating units with different inertia constants ($H_1 = 2.5s$ and $H_2 = 4s$) and different turbine parameters ($T_{RH,1} = 5s$ and $T_{RH,1} = 8s$)

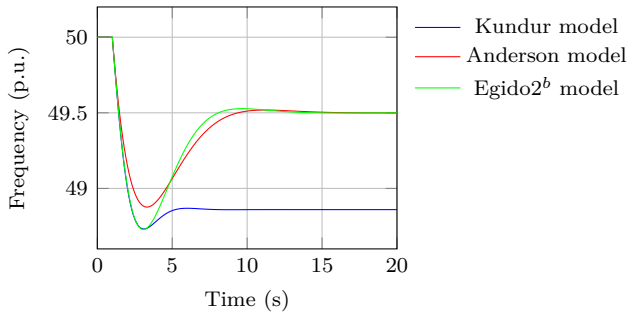


**Figure A.2. Comparison of single reheat steam turbine-generator models**

**Table A.4. Parameter estimation for 2 generating units**

| Case | Unit | Fitting time | $k$ | $T$ (s) |
|---|---|---|---|---|
| Case A | 1 | 2 s | 8.77 | 0.5452 s |
| | 2 | 2 s | 8.77 | 0.5452 s |
| Case B | 1 | 1.5 s | 8.22 | 0.47 s |
| | 2 | 2 s | 8.77 | 0.5452 s |
| Case C | 1 | 1.5 s | 10.43 | 0.3995 s |
| | 2 | 2.3 s | 8.2 | 0.62 s |

First, equivalent first model parameters have been estimated for each of the generating units in the system, based on Egido method and indicated in Table A.4. As inertia constant is lower, estimation fitting range is also narrower, because the frequency nadir happens earlier. In addition, both $k$ and $T$ parameters have been normalised.

Figure A.3 compares the frequency response for a multigenerator system for Case A, Case B and Case C, a after a generation loss of 0.2 p.u.

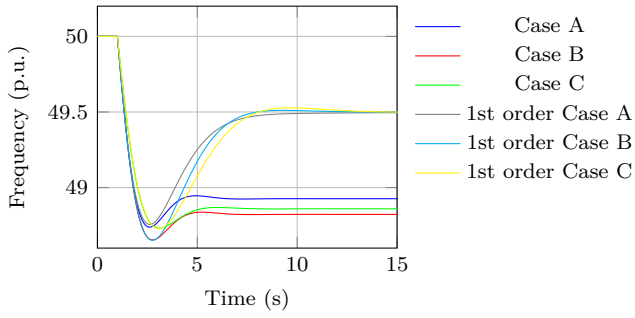


**Figure A.3. Comparison of SFR models for a multi-generator system**

Regarding the calculation of the minimum frequency, taking into account that the two generating units have the same power rating, Anderson method can only be ap-

**Table A.5. Frequency response for the multi-generator system**

| Case | Method | $f_{min}$ (Hz) | $t_{min}$ (s) |
|---|---|---|---|
| Case A | Kundur | 48.73 Hz | 2.016 s |
| | Anderson | 48.87 Hz | 2.31 s |
| | Egido2[a] | 49.25 Hz | 1.2 s |
| | Egido2[b] | 48.73 Hz | 2.1 s |
| Case B | Kundur | 48.65 Hz | 1.757 s |
| | Anderson | 48.83 Hz | 2 s |
| | Egido2[a] | 49.388 Hz | 0.7956 s |
| | Egido2[b] | 48.65 Hz | 1.76 s |
| Case C | Kundur | 48.75 Hz | 1.62 s |
| | Anderson | - | - |
| | Egido2[a] | 49.53 Hz | 0.6149 s |
| | Egido2[b] | 48.74 Hz | 1.61 s |

a: Approximation

b: Directly solved

plied to Cases A and B, and only to underdamped second-order systems. Calculation results are indicated in Table A.5.

It can be concluded that as in power systems with a single generating unit, Egido method is not adequate for small isolated power systems, as errors are included for power mismatches below 0.1 p.u.

# Appendix B

# Application of symmetrical components for unbalancing phenomena

## B.1 Introduction

This appendix presents the connection of sequence circuits for short-circuit faults, series faults and unbalanced loading. The mathematical derivation of sequence circuit connection for series faults and unbalanced loading is hereby indicated, excluding out short-circuit faults as it is widely documented in classical texts [152]. Expressions for voltage and current calculation at PCC are also indicated.

## B.2 Shunt faults

### B.2.1 Connection of sequence circuits

Figures B.1, B.2 and B.3 indicate the connection of sequence circuits for short-circuit faults.

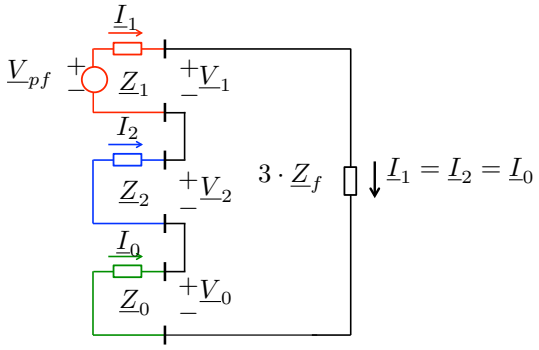


**Figure B.1. Sequence circuit connection for a single-phase short-circuit**

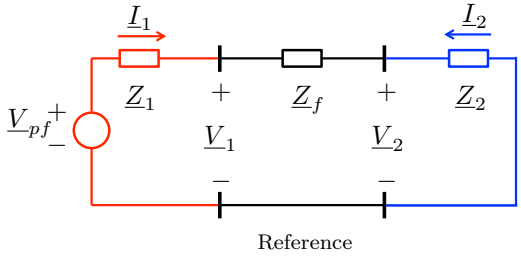


**Figure B.2. Sequence circuit connection for a double-phase short-circuit**

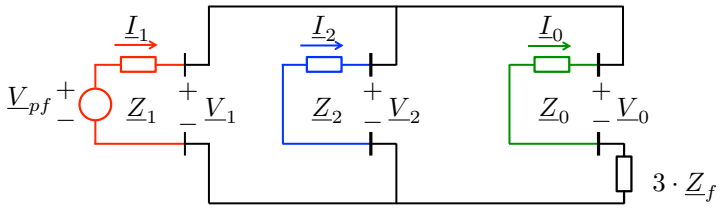


**Figure B.3. Sequence circuit connection for a double-phase to ground short-circuit**

## B.2.2 Current calculation

**Three-phase short-circuit**

$$\underline{I}_{a1} = \underline{I}_a = \underline{V}_{pf} \cdot \frac{1}{\underline{Z}_1 + \underline{Z}_f} \tag{B.1}$$

The negative and zero sequence currents are null: $\underline{I}_{a2} = 0$, $\underline{I}_{a0} = 0$.

**Single-phase short-circuit (phase A)**

$$\underline{I}_{a1} = \underline{I}_{a2} = \underline{I}_{a0} = \underline{V}_{pf} \cdot \frac{1}{\underline{Z}_1 + \underline{Z}_2 + \underline{Z}_0 + 3 \cdot \underline{Z}_f} \tag{B.2}$$

**Double-phase short-circuit (phases B and C)**

$$\underline{I}_{a1} = -\underline{I}_{a2} = \underline{V}_{pf} \cdot \frac{1}{\underline{Z}_1 + \underline{Z}_2 + \underline{Z}_f} \tag{B.3}$$

The zero sequence current is null: $\underline{I}_{a0} = 0$.

**Double-phase-to-ground short-circuit (phases B and C)**

$$\underline{I}_{a1} = \underline{V}_{pf} \cdot \frac{1}{\underline{Z}_1 + \underline{Z}_f + \dfrac{(\underline{Z}_f + \underline{Z}_2) \cdot (\underline{Z}_0 + \underline{Z}_f + 3 \cdot \underline{Z}_t)}{\underline{Z}_2 + \underline{Z}_0 + 2 \cdot \underline{Z}_f + 3 \cdot \underline{Z}_t}} \tag{B.4}$$

$$\underline{I}_{a2} = -\underline{I}_{a1} \cdot \frac{\underline{Z}_0}{\underline{Z}_0 + \underline{Z}_2} \tag{B.5}$$

$$\underline{I}_{a0} = -\underline{I}_{a1} \cdot \frac{\underline{Z}_2}{\underline{Z}_0 + \underline{Z}_2} \tag{B.6}$$

### B.2.3 Voltage calculation

Voltage during short-circuits has been calculated at the faulted point, considering a fault impedance $Z_f$ equal for any phase in fault. Positive, negative and zero sequence voltage at the faulted phase(s) are indicated below.

**Three-phase short-circuit**

$$\underline{V}_{a1} = \underline{V}_{pf} \cdot \frac{\underline{Z}_f}{\underline{Z}_1 + \underline{Z}_f} \tag{B.7}$$

The negative and zero sequence voltages are null: $\underline{V}_{a2} = 0$, $\underline{V}_{a0} = 0$.

$$\underline{V}_a = \underline{V}_b = \underline{V}_c = \underline{V}_{pf} \cdot \frac{\underline{Z}_f}{\underline{Z}_1 + \underline{Z}_f} \tag{B.8}$$

**Single-phase short-circuit (phase A)**

$$\underline{V}_{a1} = \underline{V}_{pf} \cdot \left(1 - \frac{\underline{Z}_1}{\underline{Z}_1 + \underline{Z}_2 + \underline{Z}_0 + 3 \cdot \underline{Z}_f}\right) \tag{B.9}$$

$$\underline{V}_{a2} = \underline{V}_{pf} \cdot \frac{-\underline{Z}_2}{\underline{Z}_1 + \underline{Z}_2 + \underline{Z}_0 + 3 \cdot \underline{Z}_f} \tag{B.10}$$

$$\underline{V}_{a0} = \underline{V}_{pf} \cdot \frac{-\underline{Z}_0}{\underline{Z}_1 + \underline{Z}_2 + \underline{Z}_0 + 3 \cdot \underline{Z}_f} \tag{B.11}$$

$$\underline{V}_a = \underline{V}_{pf} \cdot \frac{3 \cdot \underline{Z}_f}{\underline{Z}_1 + \underline{Z}_2 + \underline{Z}_0 + 3 \cdot \underline{Z}_f} \tag{B.12}$$

**Double-phase short-circuit (phases B and C)**

$$\underline{V}_{a1} = \underline{V}_{pf} \cdot \left(1 - \frac{\underline{Z}_1}{\underline{Z}_1 + \underline{Z}_2 + \underline{Z}_f}\right) \tag{B.13}$$

$$\underline{V}_{a2} = \underline{V}_{pf} \cdot \frac{\underline{Z}_2}{\underline{Z}_1 + \underline{Z}_2 + \underline{Z}_f} \tag{B.14}$$

The zero sequence voltage is null: $\underline{V}_{a0} = 0$.

$$\underline{V}_a = \underline{V}_{pf} \cdot \frac{2 \cdot \underline{Z}_2 + \underline{Z}_f}{\underline{Z}_1 + \underline{Z}_2 + \underline{Z}_f} \tag{B.15}$$

**Double-phase-to-ground short-circuit (phases B and C)**

$$\underline{V}_{a1} = \underline{V}_{pf} \cdot \left(1 - \frac{\underline{Z}_1}{\underline{Z}_1 + \underline{Z} + \underline{Z}_f}\right) \tag{B.16}$$

$$\underline{V}_{a2} = \underline{V}_{pf} \cdot \left(\frac{\underline{Z}_2}{\underline{Z}_1 + \underline{Z} + \underline{Z}_f} \cdot \frac{\underline{Z}_0 + \underline{Z}_f + 3 \cdot \underline{Z}_t}{\underline{Z}_2 + \underline{Z}_0 + 2 \cdot \underline{Z}_f + 3 \cdot \underline{Z}_t}\right) \tag{B.17}$$

$$\underline{V}_{a0} = \underline{V}_{pf} \cdot \frac{\underline{Z}_0}{\underline{Z}_1 + \underline{Z} + \underline{Z}_f} \cdot \left(1 - \frac{\underline{Z}_0 + \underline{Z}_f + 3 \cdot \underline{Z}_t}{\underline{Z}_2 + \underline{Z}_0 + 2 \cdot \underline{Z}_f + 3 \cdot \underline{Z}_t}\right) \tag{B.18}$$

where $\underline{Z} = \dfrac{\left(\underline{Z}_2 + \underline{Z}_f\right) \cdot \left(\underline{Z}_0 + \underline{Z}_f + 3 \cdot \underline{Z}_t\right)}{\underline{Z}_2 + \underline{Z}_0 + 2 \cdot \underline{Z}_f + 3 \cdot \underline{Z}_t}$.

## B.3 Series faults

### B.3.1 Connection of sequence circuits

**Unequal series impedances** The mathematical derivation of the sequence circuit connection for unequal series impedances has been adapted from [152]. Voltage between points F and F' indicated as faulted points can be calculated:

$$\underline{V}_{abc} - \underline{V}_{a'b'c'} = \underline{Z}_{abc} \cdot \underline{I}_{abc} \tag{B.19}$$

Transforming phase impedance matrix into sequence impedance matrix:

$$\underline{Z}_{012} = \underline{A}^{-1} \cdot \underline{Z}_{abc} \cdot \underline{A} \tag{B.20}$$

where $\underline{A} = \begin{pmatrix} 1 & 1 & 1 \\ 1 & \underline{a}^2 & \underline{a} \\ 1 & \underline{a} & \underline{a}^2 \end{pmatrix}$.

Considering that the three phase have respectively $\underline{Z}_{aa}$, $\underline{Z}_{bb}$ and $\underline{Z}_{cc}$ series impedance, $\underline{Z}_{012}$ can be calculated.

$$\underline{Z}_{012} = \frac{1}{3} \cdot \begin{pmatrix} \underline{Z}_{aa} + \underline{Z}_{bb} + \underline{Z}_{cc} & \underline{Z}_{aa} + \underline{a}^2 \cdot \underline{Z}_{bb} + \underline{a} \cdot \underline{Z}_{cc} & \underline{Z}_{aa} + \underline{Z}_{bb} + \underline{Z}_{cc} \\ \underline{Z}_{aa} + \underline{a} \cdot \underline{Z}_{bb} + \underline{a}^2 \cdot \underline{Z}_{cc} & \underline{Z}_{aa} + \underline{Z}_{bb} + \underline{Z}_{cc} & \underline{Z}_{aa} + \underline{a}^2 \cdot \underline{Z}_{bb} + \underline{a} \cdot \underline{Z}_{cc} \\ \underline{Z}_{aa} + a^2 \underline{Z}_{bb} + \underline{a} \cdot \underline{Z}_{cc} & \underline{Z}_{aa} + \underline{a} \cdot \underline{Z}_{bb} + \underline{a}^2 \cdot \underline{Z}_{cc} & \underline{Z}_{aa} + \underline{Z}_{bb} + \underline{Z}_{cc} \end{pmatrix} \tag{B.21}$$

In order to simplify the equation below, series impedance in phases B and C are considered equal. Therefore:

$$\underline{Z}_{012} = \frac{1}{3} \cdot \begin{pmatrix} \underline{Z}_{aa} + 2 \cdot \underline{Z}_{bb} & \underline{Z}_{aa} - \underline{Z}_{bb} & \underline{Z}_{aa} - \underline{Z}_{bb} \\ \underline{Z}_{aa} - \underline{Z}_{bb} & \underline{Z}_{aa} + 2 \cdot \underline{Z}_{bb} & \underline{Z}_{aa} - \underline{Z}_{bb} \\ \underline{Z}_{aa} - \underline{Z}_{bb} & \underline{Z}_{aa} - \underline{Z}_{bb} & \underline{Z}_{aa} + 2 \cdot \underline{Z}_{bb} \end{pmatrix} \tag{B.22}$$

Voltage drop between points F and F' can be calculated using following expression:

$$\underline{V}_{aa'-012} = \underline{V}_{a-012} - \underline{V}_{a'-012} = \underline{Z}_{012} \cdot \underline{I}_{012} \tag{B.23}$$

Adding and subtracting rows and combining expressions:

$$\underline{V}_{aa'-1} - \underline{Z}_{bb} \cdot \underline{I}_{a1} = \frac{1}{3} \cdot (\underline{Z}_{aa} - \underline{Z}_{bb}) \cdot (\underline{I}_{a0} + \underline{I}_{a1} + \underline{I}_{a2}) \tag{B.24}$$

From previous equations it can be deduced that sequence circuits are connected as indicated in Figure B.4.

The positive sequence current can be calculated as:

$$\underline{I}_{a1} = \frac{\underline{V}_{pf}}{\underline{Z}_t} \tag{B.25}$$

where $\underline{Z}_t = \underline{Z}_{bb} + \underline{Z}_1 + \underline{Z}^{''}$ and $\underline{Z}^{''} = \dfrac{(\underline{Z}_2 + \underline{Z}_{bb}) \cdot (\underline{Z}_0 + \underline{Z}_{bb}) \cdot \left( \dfrac{\underline{Z}_{aa} - \underline{Z}_{bb}}{3} \right)}{\underline{Z}_2 + 2 \cdot \underline{Z}_{bb} + \underline{Z}_0 + \dfrac{\underline{Z}_{aa} - \underline{Z}_{bb}}{3}}$.

By inspection of Figure B.4:

$$\underline{I}_{a2} = -\underline{I}_{a1} \cdot \frac{\underline{Z}^{''}}{\underline{Z}_{bb} + \underline{Z}_2} \tag{B.26}$$

and

$$\underline{I}_{a0} = -\underline{I}_{a1} \cdot \frac{\underline{Z}^{''}}{\underline{Z}_{bb} + \underline{Z}_0} \tag{B.27}$$

**One phase open** It can considered a particularisation of unequal series impedances case, in which case impedance in phase A $\underline{Z}_{aa}$ is infinite and $\underline{Z}_{bb}$ and $\underline{Z}_{cc}$ are finite. Therefore, the sequence circuit connection is as shown in Figure B.5.

By inspection of Figure B.5:

$$\underline{I}_{a1} = \frac{\underline{V}_{pf}}{\underline{Z}_t} \tag{B.28}$$

where $\underline{Z}_t = \underline{Z}_{bb} + \underline{Z}_1 + \underline{Z}$ and $\underline{Z} = \dfrac{(\underline{Z}_2 + \underline{Z}_{bb}) \cdot (\underline{Z}_0 + \underline{Z}_{bb})}{\underline{Z}_2 + 2 \cdot \underline{Z}_{bb} + \underline{Z}_0}$.

By inspection of Figure B.5:

$$\underline{I}_{a2} = -\underline{I}_{a1} \cdot \frac{\underline{Z}}{\underline{Z}_{bb} + \underline{Z}_2} \tag{B.29}$$

and

$$\underline{I}_{a0} = -\underline{I}_{a1} \cdot \frac{\underline{Z}}{\underline{Z}_{bb} + \underline{Z}_0} \tag{B.30}$$

**Two phases open** It can considered a particularisation of unequal series impedances case, in which case impedance in phase A $\underline{Z}_{aa}$ is finite and $\underline{Z}_{bb}$ and $\underline{Z}_{cc}$ are infinite. The boundary conditions are $\underline{I}_b = \underline{I}_c = 0$ and $\underline{V}_{aa'} = \underline{Z}_{aa} \cdot \underline{I}_a$.

Transforming to sequence currents:

$$\underline{I}_{a0} = \underline{I}_{a1} = \underline{I}_{a2} = \frac{1}{3} \cdot \underline{I}_a \tag{B.31}$$

The sequence currents are all equal. Based on the boundary conditions:

$$\underline{V}_{aa'-1} + \underline{V}_{aa'-2} + \underline{V}_{aa'-0} = \underline{Z}_{aa} \cdot (\underline{I}_{a1} + \underline{I}_{a2} + \underline{I}_{a0}) \tag{B.32}$$

Funderlinea Rearranging:

$$\left(\underline{V}_{aa'-0} - \underline{Z}_a \cdot \underline{I}_{a0}\right) + \left(\underline{V}_{aa'-1} - \underline{Z}_{aa} \cdot \underline{I}_{a1}\right) + \left(\underline{V}_{aa'-2} - \underline{Z}_{aa} \cdot \underline{I}_{a2}\right) \tag{B.33}$$

Therefore, the sequence circuit connection is as shown in Figure B.6.

Figures B.4, B.5 and B.6 indicate the connection of sequence circuits for series faults, as concluded analytically.

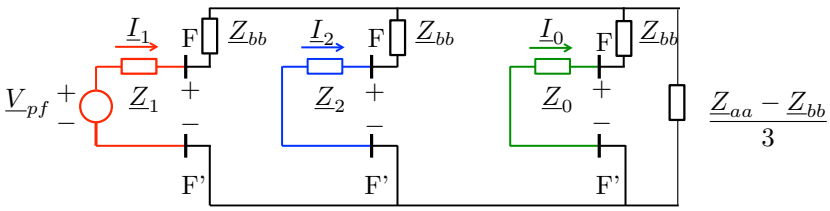


**Figure B.4. Sequence circuit connection for unequal series impedances**

## B.3.2 Sequence voltage drop calculation

### Unequal series impedances

$$\underline{\Delta V}_{a1} = \underline{V}_{pf} \cdot \left(1 - \frac{\underline{Z}_1}{\underline{Z}_1 + \underline{Z}_{bb} + \underline{Z}''}\right) \tag{B.34}$$

$$\underline{\Delta V}_{a2} = \frac{\underline{Z}_2 \cdot \underline{V}_{pf}}{\underline{Z}_1 + \underline{Z}_{bb} + \underline{Z}''} \cdot \frac{\underline{Z}'''}{\underline{Z}_2 + \underline{Z}_0 + 2 \cdot \underline{Z}_{bb} + \frac{\underline{Z}_{aa} - \underline{Z}_{bb}}{3}} \tag{B.35}$$

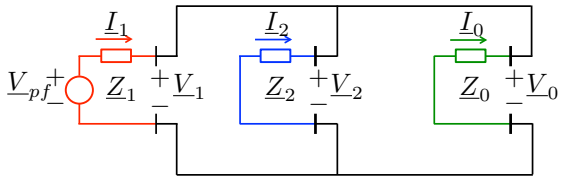


**Figure B.5. Sequence circuit connection for one phase open**

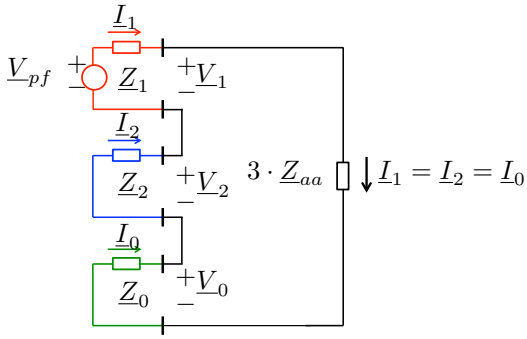


**Figure B.6. Sequence circuit connection for two open phases**

$$\underline{\Delta V}_{a0} = \frac{\underline{Z}_0 \cdot \underline{V}_{pf}}{\underline{Z}_1 + \underline{Z}_{bb} + \underline{Z}''} \cdot \frac{\underline{Z}'}{\underline{Z}_2 + \underline{Z}_0 + 2 \cdot \underline{Z}_{bb} + \dfrac{\underline{Z}_{aa} - \underline{Z}_{bb}}{3}} \tag{B.36}$$

**One phase open**

$$\underline{\Delta V}_{a1} = \underline{V}_{pf} \cdot \left(1 - \frac{\underline{Z}_1}{\underline{Z}_1 + \underline{Z}_{bb} + \underline{Z}''''}\right) \tag{B.37}$$

$$\underline{\Delta V}_{a2} = \frac{\underline{Z}_2 \cdot \underline{V}_{pf}}{\underline{Z}_1 + \underline{Z}_{bb} + \underline{Z}''''} \cdot \frac{\underline{Z}_0 + \underline{Z}_{bb}}{\underline{Z}_2 + \underline{Z}_0 + 2 \cdot \underline{Z}_{bb}} \tag{B.38}$$

$$\underline{\Delta V}_{a0} = \frac{\underline{Z}_0 \cdot \underline{V}_{pf}}{\underline{Z}_1 + \underline{Z}_{bb} + \underline{Z}''} \cdot \left(1 - \frac{\underline{Z}_0 + \underline{Z}_{bb}}{\underline{Z}_2 + \underline{Z}_0 + 2 \cdot \underline{Z}_{bb}}\right) \tag{B.39}$$

**Two phases open**

$$\underline{\Delta V}_{a1} = \underline{V}_{pf} \cdot \left(1 - \frac{\underline{Z}_1}{\underline{Z}_1 + \underline{Z}_2 + \underline{Z}_0 + 3 \cdot \underline{Z}_{aa}}\right) \tag{B.40}$$

$$\underline{\Delta V}_{a2} = -\frac{\underline{Z}_2 \cdot \underline{V}_{pf}}{\underline{Z}_1 + \underline{Z}_2 + \underline{Z}_0 + 3 \cdot \underline{Z}_{aa}} \tag{B.41}$$

$$\underline{\Delta V}_{a0} = -\frac{\underline{Z}_0 \cdot \underline{V}_{pf}}{\underline{Z}_1 + \underline{Z}_2 + \underline{Z}_0 + 3 \cdot \underline{Z}_{aa}} \tag{B.42}$$

where $\underline{Z}^{'} = \dfrac{(\underline{Z}_2 + \underline{Z}_{bb}) \cdot \left(\dfrac{\underline{Z}_{aa} - \underline{Z}_{bb}}{3}\right)}{\underline{Z}_2 + \underline{Z}_{bb} + \dfrac{\underline{Z}_{aa} - \underline{Z}_{bb}}{3}}$, $\underline{Z}^{''} = \dfrac{(\underline{Z}_2 + \underline{Z}_{bb}) \cdot (\underline{Z}_0 + \underline{Z}_{bb}) \cdot \left(\dfrac{\underline{Z}_{aa} - \underline{Z}_{bb}}{3}\right)}{\underline{Z}_2 + 2 \cdot \underline{Z}_{bb} + \underline{Z}_0 + \dfrac{\underline{Z}_{aa} - \underline{Z}_{bb}}{3}}$,

$\underline{Z}^{'''} = \dfrac{(\underline{Z}_0 + \underline{Z}_{bb}) \cdot \left(\dfrac{\underline{Z}_{aa} - \underline{Z}_{bb}}{3}\right)}{\underline{Z}_0 + \underline{Z}_{bb} + \dfrac{\underline{Z}_{aa} - \underline{Z}_{bb}}{3}}$, and $\underline{Z}^{''''} = \dfrac{(\underline{Z}_2 + \underline{Z}_{bb}) \cdot (\underline{Z}_0 + \underline{Z}_{bb})}{\underline{Z}_2 + 2 \cdot \underline{Z}_{bb} + \underline{Z}_0}$,

### B.3.3 Sequence current calculation

**Unequal series impedances**

$$\underline{I}_{a1} = \frac{\underline{V}_{pf}}{\underline{Z}_t} \tag{B.43}$$

where $\underline{Z}_t = \underline{Z}_{bb} + \underline{Z}_1 + \underline{Z}$ and $\underline{Z} = \dfrac{(\underline{Z}_2 + \underline{Z}_{bb}) \cdot (\underline{Z}_0 + \underline{Z}_{bb})}{\underline{Z}_2 + 2 \cdot \underline{Z}_{bb} + \underline{Z}_0}$.

$$\underline{I}_{a2} = -\underline{I}_{a1} \cdot \frac{\underline{Z}^{''}}{\underline{Z}_{bb} + \underline{Z}_2} \tag{B.44}$$

$$\underline{I}_{a0} = -\underline{I}_{a1} \cdot \frac{\underline{Z}^{''}}{\underline{Z}_{bb} + \underline{Z}_0} \tag{B.45}$$

**One phase open**

$$\underline{I}_{a1} = \frac{\underline{V}_{pf}}{\underline{Z}_t} \tag{B.46}$$

where $\underline{Z}_t = \underline{Z}_{bb} + \underline{Z}_1 + \underline{Z}$ and $\underline{Z} = \dfrac{(\underline{Z}_2 + \underline{Z}_{bb}) \cdot (\underline{Z}_0 + \underline{Z}_{bb})}{\underline{Z}_2 + 2 \cdot \underline{Z}_{bb} + \underline{Z}_0}$.

$$\underline{I}_{a2} = -\underline{I}_{a1} \cdot \frac{\underline{Z}}{\underline{Z}_{bb} + \underline{Z}_2} \tag{B.47}$$

$$\underline{I}_{a0} = -\underline{I}_{a1} \cdot \frac{\underline{Z}}{\underline{Z}_{bb} + \underline{Z}_0} \tag{B.48}$$

**Two phases open**

$$\underline{I}_{a1} = \underline{I}_{a2} = \underline{I}_{a0} = \frac{\underline{V}_{pf}}{\underline{Z}_1 + \underline{Z}_2 + \underline{Z}_0 + 3 \cdot \underline{Z}_{aa}} \tag{B.49}$$

## B.4 Unbalanced loads

Any three-phase load connected in delta can be converted into a ungrounded star connected three-phase load based on equations (B.50) to (B.52) corresponding to Kennelly theorem.

$$\underline{Z}_a = \frac{\underline{Z}_{ab} \cdot \underline{Z}_{ca}}{\underline{Z}_{ab} + \underline{Z}_{bc} + \underline{Z}_{ca}} \tag{B.50}$$

$$\underline{Z}_b = \frac{\underline{Z}_{ab} \cdot \underline{Z}_{bc}}{\underline{Z}_{ab} + \underline{Z}_{bc} + \underline{Z}_{ca}} \tag{B.51}$$

$$\underline{Z}_c = \frac{\underline{Z}_{bc} \cdot \underline{Z}_{ca}}{\underline{Z}_{ab} + \underline{Z}_{bc} + \underline{Z}_{ca}} \tag{B.52}$$

### B.4.1 Connection of sequence circuits

**Single-phase load connected to line voltage** A single-phase load connected to line voltage is analogous to a double-phase short-circuit. For a single-phase load connected between phases B and C, $\underline{I}_a = \underline{I}_{ab}$, $\underline{I}_b = \underline{I}_{bc} - \underline{I}_{ab}$ and $\underline{I}_c = \underline{I}_{bc}$. On the other hand, voltage between phases B and C can be calculated:

$$\underline{V}_b - \underline{V}_c = \underline{Z}_{bc} \cdot \underline{I}_b \tag{B.53}$$

Based on the symmetrical components theory, sequence current and voltages are computed. For sequence currents, no zero sequence current flows and positive and negative sequence currents: $\underline{I}_{a1} = -\underline{I}_{a2}$. As to sequence voltages:

$$\underline{V}_{a1} - \underline{V}_{a2} = \underline{Z}_{bc} \cdot \underline{I}_{a1} \tag{B.54}$$

Therefore, only positive and negative sequence networks exist and they are shunt connected through load impedance $Z_{bc}$, as indicated in Figure B.7. Thus, it can be stated that:

$$\underline{I}_{a1} = -\underline{I}_{a2} = \frac{\underline{V}_{pf}}{\underline{Z}_1 + \underline{Z}_2 + \underline{Z}_{bc}} \tag{B.55}$$

The zero sequence current is null: $\underline{I}_{a0} = 0$.

**Three-phase loads connected to phase voltages** As star neutral wire is ungrounded, $\underline{I}_a + \underline{I}_b + \underline{I}_c = 0$. Therefore, there is no zero sequence current circulation: $\underline{I}_{a0} = 0$. Expressions for phase voltage calculation:

$$\begin{pmatrix} \underline{V}_a \\ \underline{V}_b \\ \underline{V}_c \end{pmatrix} = \begin{pmatrix} \underline{Z}_a & 0 & 0 \\ 0 & \underline{Z}_b & 0 \\ 0 & 0 & \underline{Z}_c \end{pmatrix} \cdot \begin{pmatrix} \underline{I}_a \\ \underline{I}_b \\ \underline{I}_c \end{pmatrix} \tag{B.56}$$

Using B.20, the sequence impedance matrix is obtained.

$$\underline{Z}_{012} = \frac{1}{3} \cdot \begin{pmatrix} \underline{Z}_a + \underline{Z}_b + \underline{Z}_c & \underline{Z}_a + \underline{a}^2 \cdot \underline{Z}_b + \underline{a} \cdot \underline{Z}_c & \underline{Z}_a + \underline{a} \cdot \underline{Z}_b + \underline{a}^2 \cdot \underline{Z}_c \\ \underline{Z}_a + \underline{a} \cdot \underline{Z}_b + \underline{a}^2 \cdot \underline{Z}_c & \underline{Z}_a + \underline{Z}_b + \underline{Z}_c & \underline{Z}_a + \underline{a}^2 \cdot \underline{Z}_b + \underline{a} \cdot \underline{Z}_c \\ \underline{Z}_a + \underline{a}^2 \cdot \underline{Z}_b + \underline{a} \cdot \underline{Z}_c & \underline{Z}_a + \underline{a} \cdot \underline{Z}_b + \underline{a}^2 \cdot \underline{Z}_c & \underline{Z}_a + \underline{Z}_b + \underline{Z}_c \end{pmatrix} \tag{B.57}$$

In order to simplify the equation below, $Z_b = Z_c$ is considered [166]. Therefore:

$$\underline{Z}_{012} = \frac{1}{3} \cdot \begin{pmatrix} \underline{Z}_a + 2 \cdot \underline{Z}_b & \underline{Z}_a - \underline{Z}_b & \underline{Z}_a - \underline{Z}_b \\ \underline{Z}_a - \underline{Z}_b & \underline{Z}_a + 2 \cdot \underline{Z}_b & \underline{Z}_a - \underline{Z}_b \\ \underline{Z}_a - \underline{Z}_b & \underline{Z}_a - \underline{Z}_b & \underline{Z}_a + 2 \cdot \underline{Z}_b \end{pmatrix} \tag{B.58}$$

Voltage drop in phase A can be calculated using following expression:

$$\underline{V}_{a-012} = \underline{Z}_{012} \cdot \underline{I}_{012} \tag{B.59}$$

Adding and subtracting rows and combining expressions:

$$\underline{V}_{a1} - \underline{Z}_b \cdot \underline{I}_{a1} = \frac{1}{3} \cdot (\underline{Z}_a - \underline{Z}_b) \cdot (\underline{I}_{a0} + \underline{I}_{a1} + \underline{I}_{a2}) \tag{B.60}$$

From previous equations, it can be deduced that sequence circuits are connected as indicated in Figure B.8.

By inspection of Figure B.8:

$$\underline{I}_{a1} = \frac{\underline{V}_{pf}}{\underline{Z}_t} \tag{B.61}$$

where $\underline{Z}_t = \underline{Z}_b + \underline{Z}_1 + \underline{Z}$ and $\underline{Z} = \dfrac{(\underline{Z}_2 + \underline{Z}_b) \cdot \dfrac{(\underline{Z}_a - \underline{Z}_b)}{3}}{\underline{Z}_2 + 2 \cdot \underline{Z}_b + \dfrac{(\underline{Z}_a - \underline{Z}_b)}{3}}$.

By inspection of Figure B.5:

$$\underline{I}_{a2} = -\underline{I}_{a1} \cdot \frac{\underline{Z}}{\underline{Z}_b + \underline{Z}_2} \tag{B.62}$$

**Three-phase loads connected to phase voltages with grounded neutral**
Expressions for phase voltage calculation:

$$\begin{pmatrix} \underline{V_{ag}} \\ \underline{V_{bg}} \\ \underline{V_{cg}} \end{pmatrix} = \begin{pmatrix} \underline{Z}_a + \underline{Z}_N & 0 & 0 \\ 0 & \underline{Z}_b + \underline{Z}_N & 0 \\ 0 & 0 & \underline{Z}_c + \underline{Z}_N \end{pmatrix} \cdot \begin{pmatrix} \underline{I}_a \\ \underline{I}_b \\ \underline{I}_c \end{pmatrix} \tag{B.63}$$

Using B.20, the sequence impedance matrix can be obtained.

$$\underline{Z}_{012} = \frac{1}{3} \cdot \begin{pmatrix} \underline{Z}_a + \underline{Z}_b + \underline{Z}_c + 9 \cdot + \underline{Z}_N & \underline{Z}_a + \underline{a}^2 \cdot \underline{Z}_b + \underline{a} \cdot \underline{Z}_c & \underline{Z}_a + \underline{a} \cdot \underline{Z}_b + \underline{a}^2 \cdot \underline{Z}_c \\ \underline{Z}_a + \underline{a} \cdot \underline{Z}_b + \underline{a}^2 \cdot \underline{Z}_c & \underline{Z}_a + \underline{Z}_b + \underline{Z}_c & \underline{Z}_a + \underline{a}^2 \cdot \underline{Z}_b + \underline{a} \cdot \underline{Z}_c \\ \underline{Z}_a + \underline{a}^2 \cdot \underline{Z}_b + \underline{a} \cdot \underline{Z}_c & \underline{Z}_a + \underline{a} \cdot \underline{Z}_b + \underline{a}^2 \cdot \underline{Z}_c & \underline{Z}_a + \underline{Z}_b + \underline{Z}_c \end{pmatrix} \tag{B.64}$$

In order to simplify the equation below, $Z_b = Z_c$ is considered [166]. Therefore:

$$\underline{Z}_{012} = \frac{1}{3} \cdot \begin{pmatrix} \underline{Z}_a + 2 \cdot \underline{Z}_b + 9 \cdot \underline{Z}_N & \underline{Z}_a - \underline{Z}_b & \underline{Z}_a - \underline{Z}_b \\ \underline{Z}_a - \underline{Z}_b & \underline{Z}_a + 2 \cdot \underline{Z}_b & \underline{Z}_a - \underline{Z}_b \\ \underline{Z}_a - \underline{Z}_b & \underline{Z}_a - \underline{Z}_b & \underline{Z}_a + 2 \cdot \underline{Z}_b \end{pmatrix} \tag{B.65}$$

Voltage drop in phase A can be calculated using following expression:

$$\underline{V}_{ag-012} = \underline{V}_{an-012} + \underline{V}_{ng-012} = \underline{Z}_{012} \cdot \underline{I}_{012} \tag{B.66}$$

Adding and subtracting rows and combining expressions:

$$\underline{V_{ag1}} - \underline{Z}_b \cdot \underline{I}_{a1} = \frac{1}{3} \cdot (\underline{Z}_a - \underline{Z}_b) \cdot (\underline{I}_{a0} + \underline{I}_{a1} + \underline{I}_{a2}) \tag{B.67}$$

From previous equations, it be can deduced that sequence circuits are connected as indicated in Figure B.9.

The positive sequence current can be calculated as:

$$\underline{I}_{a1} = \frac{\underline{V}_{pf}}{\underline{Z}_t} \tag{B.68}$$

where $\underline{Z}_t = \underline{Z}_b + \underline{Z}_1 + \underline{Z}$ and $\underline{Z} = \dfrac{(\underline{Z}_2 + \underline{Z}_b) \cdot (\underline{Z}_0 + 3 \cdot \underline{Z}_N + \underline{Z}_b) \cdot \left( \dfrac{\underline{Z}_a - \underline{Z}_b}{3} \right)}{\underline{Z}_2 + 2 \cdot \underline{Z}_b + \underline{Z}_0 + 3 \cdot \underline{Z}_N + \dfrac{\underline{Z}_a - \underline{Z}_b}{3}}$.

By inspection of Figure B.9:

$$\underline{I}_{a2} = -\underline{I}_{a1} \cdot \frac{\underline{Z}}{\underline{Z}_b + \underline{Z}_2} \tag{B.69}$$

and

$$\underline{I}_{a0} = -\underline{I}_{a1} \cdot \frac{\underline{Z}}{\underline{Z}_b + 3 \cdot \underline{Z}_N + \underline{Z}_0} \tag{B.70}$$

**Three-phase loads connected to line voltages** It can be easily derived that no zero current flows out of a delta connected three-phase load. The sequence network connection can be derived from the ungrounded star three-phase load. Any delta connected three-phase load can be converted into an equivalent star load following equations (B.50) to (B.52). For the sake of simplicity, $Z_{ab} = Z_{ca}$ is assumed. Therefore, equivalent sequence impedance matrix becomes:

$$\underline{Z}_{012} = \frac{1}{3} \cdot \begin{pmatrix} \underline{X} + 2 \cdot \underline{Y} & \underline{X} - \underline{Y} & \underline{X} - \underline{Y} \\ \underline{X} - \underline{Y} & \underline{X} + 2 \cdot \underline{Y} & \underline{X} - \underline{Y} \\ \underline{X} - \underline{Y} & \underline{X} - \underline{Y} & \underline{X} + 2 \cdot \underline{Y} \end{pmatrix} \tag{B.71}$$

where $\underline{X} = \dfrac{\underline{Z}_{ab} \cdot \underline{Z}_{ab}}{2 \cdot \underline{Z}_{ab} + \underline{Z}_{bc}}$ and $\underline{Y} = \dfrac{\underline{Z}_{ab} \cdot \underline{Z}_{bc}}{2 \cdot \underline{Z}_{ab} + \underline{Z}_{bc}}$.

Figures B.7, B.8, B.9 and B.10 indicate the connection of sequence circuits for unbalanced loading, as concluded analytically.

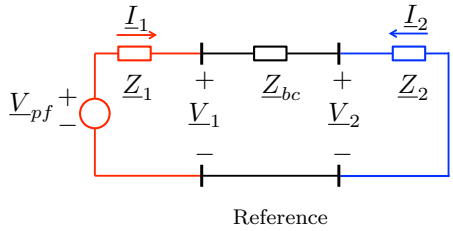


**Figure B.7. Sequence circuit connection for single-phase load**

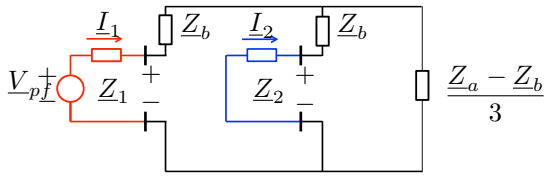


**Figure B.8. Sequence circuit connection for three-phase load in ungrounded star**

## B.4.2 Sequence voltage calculation

Voltage due to unbalanced load has been calculated between at the PCC of the load and its positive, negative and zero sequence components are indicated below.

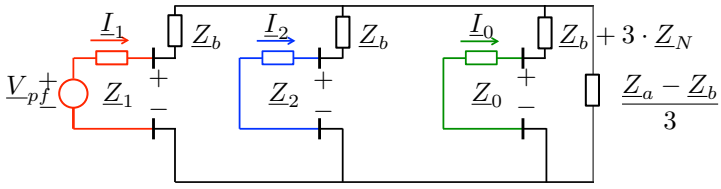


**Figure B.9. Sequence circuit connection for three-phase load in grounded star**

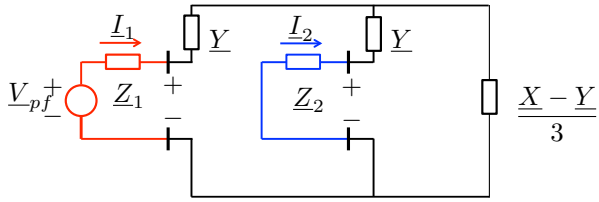


**Figure B.10. Sequence circuit connection for a three-phase load in delta connection**

### Single phase load connected to line voltages

$$\underline{V}_{a1} = \underline{V}_{pf} \cdot \left(1 - \frac{\underline{Z}_1}{\underline{Z}_1 + \underline{Z}_2 + \underline{Z}_{bc}}\right) \tag{B.72}$$

$$\underline{V}_{a2} = \frac{\underline{Z}_2 \cdot \underline{V}_{pf}}{\underline{Z}_1 + \underline{Z}_2 + \underline{Z}_{bc}} \tag{B.73}$$

The zero sequence voltage is null: $\underline{V}_{a0} = 0$.

### Three-phase load in ungrounded star connection

$$\underline{V}_{a1} = \underline{V}_{pf} \cdot \left(1 - \frac{\underline{Z}_1}{\underline{Z}_1 + \underline{Z}_b + \underline{Z}'}\right) \tag{B.74}$$

$$\underline{V}_{a2} = \frac{\underline{Z}_2 \cdot \underline{V}_{pf} \cdot \dfrac{\underline{Z}_a - \underline{Z}_b}{3}}{\left(\underline{Z}_2 + \underline{Z}_b + \dfrac{\underline{Z}_a - \underline{Z}_b}{3}\right) \cdot \left(\underline{Z}_2 + \underline{Z}_b + \underline{Z}'\right)} \tag{B.75}$$

The zero sequence voltage is null: $\underline{V}_{a0} = 0$.

### Three-phase load in grounded star connection

$$\underline{V}_{a1} = \underline{V}_{pf} \cdot \left(1 - \frac{\underline{Z}_1}{\underline{Z}_1 + \underline{Z}_b + \underline{Z}''}\right) \tag{B.76}$$

$$\underline{V}_{a2} = \frac{\underline{Z}_2 \cdot \underline{V}_{pf}}{\underline{Z}_1 + \underline{Z}_b + \underline{Z}^{''}} \cdot \frac{\underline{Z}^{'''}}{\underline{Z}_2 + \underline{Z}_0 + 2 \cdot \underline{Z}_b + \frac{\underline{Z}_a - \underline{Z}_b}{3}} \tag{B.77}$$

$$\underline{V}_{a0} = \frac{\underline{Z}_0 \cdot \underline{V}_{pf}}{\underline{Z}_1 + \underline{Z}_b + \underline{Z}^{''}} \cdot \frac{\underline{Z}^{'}}{\underline{Z}_2 + \underline{Z}_0 + 2 \cdot \underline{Z}_b + \frac{\underline{Z}_a - \underline{Z}_b}{3}} \tag{B.78}$$

**Three-phase load in delta connection** Formulae for ungrounded star load can be applied for three-phase loads connected in delta, where $\underline{Z}^{'} = \frac{(\underline{Z}_2 + \underline{Z}_b) \cdot \left(\frac{\underline{Z}_a - \underline{Z}_b}{3}\right)}{\underline{Z}_2 + \underline{Z}_b + \frac{\underline{Z}_a - \underline{Z}_b}{3}}$, $\underline{Z}^{''} = \frac{(\underline{Z}_2 + \underline{Z}_b) \cdot (\underline{Z}_0 + \underline{Z}_b) \cdot \left(\frac{\underline{Z}_a - \underline{Z}_b}{3}\right)}{\underline{Z}_2 + 2 \cdot \underline{Z}_b + \underline{Z}_0 + \frac{\underline{Z}_a - \underline{Z}_b}{3}}$ and $\underline{Z}^{'''} = \frac{(\underline{Z}_0 + \underline{Z}_b) \cdot \left(\frac{\underline{Z}_a - \underline{Z}_b}{3}\right)}{\underline{Z}_0 + \underline{Z}_b + \frac{\underline{Z}_a - \underline{Z}_b}{3}}$.

### B.4.3 Sequence current calculation

**Single phase load connected to line voltages**

$$\underline{I}_{a1} = -\underline{I}_{a2} = \frac{\underline{V}_{pf}}{\underline{Z}_1 + \underline{Z}_2 + \underline{Z}_{bc}} \tag{B.79}$$

The zero sequence current is null: $\underline{I}_{a0} = 0$.

**Three-phase load in ungrounded star connection**

$$\underline{I}_{a1} = \frac{\underline{V}_{pf}}{\underline{Z}_t} \tag{B.80}$$

where $\underline{Z}_t = \underline{Z}_b + \underline{Z}_1 + \underline{Z}$ and $\underline{Z} = \frac{(\underline{Z}_2 + \underline{Z}_b) \cdot \frac{(\underline{Z}_a - \underline{Z}_b)}{3}}{\underline{Z}_2 + 2 \cdot \underline{Z}_b + \frac{(\underline{Z}_a - \underline{Z}_a)}{3}}$.

$$\underline{I}_{a2} = -\underline{I}_{a1} \cdot \frac{\underline{Z}}{\underline{Z}_b + \underline{Z}_2} \tag{B.81}$$

The zero sequence current is null: $\underline{I}_{a0} = 0$.

**Three-phase load in grounded star connection**

$$\underline{I}_{a1} = \frac{\underline{V}_{pf}}{\underline{Z}_t} \tag{B.82}$$

where $\underline{Z}_t = \underline{Z}_b + \underline{Z}_1 + \underline{Z}$ and $\underline{Z} = \dfrac{(\underline{Z}_2 + \underline{Z}_b) \cdot (\underline{Z}_0 + 3 \cdot \underline{Z}_N + \underline{Z}_b) \cdot \left( \dfrac{\underline{Z}_a - \underline{Z}_b}{3} \right)}{\underline{Z}_2 + 2 \cdot \underline{Z}_b + \underline{Z}_0 + 3 \cdot \underline{Z}_N + \dfrac{\underline{Z}_a - \underline{Z}_b}{3}}$.

$$\underline{I}_{a2} = -\underline{I}_{a1} \cdot \frac{\underline{Z}}{\underline{Z}_b + \underline{Z}_2} \tag{B.83}$$

$$\underline{I}_{a0} = -\underline{I}_{a1} \cdot \frac{\underline{Z}}{\underline{Z}_b + 3 \cdot \underline{Z}_b + \underline{Z}_0} \tag{B.84}$$

# Appendix C

# Numerical application: power system and power plant modelisation

## C.1 Introduction

The thesis includes the practical application of the methodology to three study cases. This appendix gathers the modelisation and simulation data for the three cases. The simulation has been carried out by using *PowerFactory* DigSilent software package. The model of the renewable power plants considered in the study cases is based on a common plant model for all the cases and is described in Section C.2. Then, the power plant model parameterisation and its connection layout to the parameterised grid models are detailed in Section C.3, C.4, and C.5 respectively for the medium size island (general case), Terceira island and Fuerteventura-Lanzarote system.

## C.2 Power plant model description

The power plants of the three numerical applications of the methodology presented in this thesis have a common plant model, based on a positive sequence RMS *Composite Frame*. This model refers to the *Generic Renewable Generator Model* proposed by the WECC [167]. The model is already implemented in some simulation software packages such as PSLF, PowerWorld or PSS/E. In this case, the generic model has been carried out by user models in *Power Factory* including some modifications suited for an inverter manufacturer. Therefore, the user models are grey-box models and consist of static generators connected to converter systems. The block diagram is indicated in Figure C.1.

The RMS model has nine slots. The *Static Generator*, *V&F Control Bus*, *V Inverter Bus*, *P&Q Inverter Bus*, and *Phase-Locked Loop (PLL)* slots are built-in models. The rest are common user models. The converter includes active grid support functions, as required in many grid codes. The methodology hereby presented covers primary frequency regulation based on a droop function, as well as active and reactive current injection during LVRT. Therefore, only dynamic parameters regarding these functions are indicated for *Control Module Common Model* and *Converter Module*

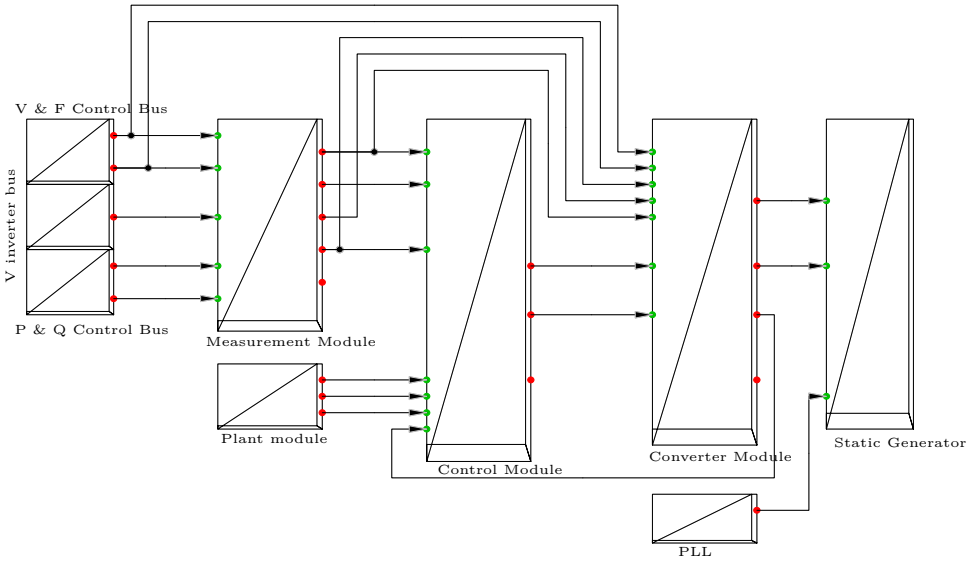


**Figure C.1. Converter RMS model in block diagrams**

*Common Model* in following sections. In order to test the control for low frequencies, the output of plant must be curtailed. However, in field, it has to be considered that for low frequency response, the plant only responds if there is resource availability so as to increase production. Primary frequency response can be disabled by setting a very large deadband (e.g. 1 p.u.). On the other hand, the RMS model only provides active and reactive current injection during balanced faults under LVRT operation mode. Therefore, current injection for unbalanced faults is out of the scope of the model abilities. The LVRT function trips the power plant when voltage is out of the permitted range.

In addition, the static generator includes the relay model ABB DPU200R, with following ANSI protection functions activated: 47 phase-sequence voltage, 81O overfrequency, 81R ROCOF and 81U underfrequency relays.

## C.3 Model parameterisation: application to a medium size island (Case 1)

This section includes the parameterisation, modelling and simulation of both the photovoltaic plant and the equivalent grid model.

### C.3.1 Photovoltaic power plant: description and parameterisation

The new PV plant to be installed in Gomera island generates at 400 V. A constant irradiation is considered. Then, voltage is stepped up to 20 kV by the plant transfor-

mer (20/0.4 kV, 2.5 MVA), and connected by an overhead line of 5 km to the PCC. The parameterised grid model is connected to this connecting point. Table C.1 details the impedances of the system elements. All sequence impedances are considered equal. The plant connection layout is shown in Figure C.2.

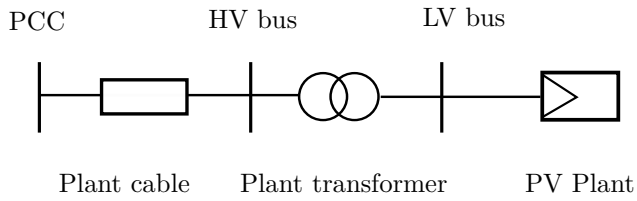


**Figure C.2. PV plant connection layout**

**Table C.1. Case 1: system impedance data (20 kV 100 MVA base)**

| Element | R(p.u.) | X(p.u.) |
|---|---|---|
| Plant cable | 1 | 0.175 |
| Plant transformer | 0.3075 | 2.38 |

In PowerFactory, a PV plant in power flow can be represented by a static generator. An equivalent inverter and step-up transformer representing 2 lumped inverters have been configured with ratings in Table C.2, operating with a ± 0.9 power factor. The operation point is set at 80 % of the rating: $P_{PV} = 1.3$ MW and $Q_{PV} = 0.63$ MW.

**Table C.2. Case 1: inverter and static generator ratings**

| Parameter | Single inverter | Equivalent generator |
|---|---|---|
| Nameplate rating | 800 kW | |
| Generator rating | 0.89 MVA | 1.78 MVA |
| $P_{max}$ | 0.8 MW | 1.6 MW |
| $P_{min}$ | 0 W | 0 W |
| $Q_{max}$ | 0.39 MVAr | 0.78 MVAr |
| $Q_{min}$ | -0.39 MVAr | -0.78 MVAr |

Primary frequency response has been adjusted with parameters in Table C.3 corresponding to the Control Module, based on optimal performance results and within SEIE limits. LVRT protection function and current injection have been set to parameters in Tables C.4 C.5, and C.6 corresponding to the Converter Module. Both features are based on the Spanish SEIE grid code graphs and limit values: voltage versus time for LVRT and current versus voltage for current injection. Reactive current injection covers both undervoltage and overvoltage. Intermediate values are

interpolated by the converter control system. Besides, the relay model must be parameterised with values in Table C.7, based on grid code limits.

**Table C.3. Case 1: parameters of Control Module**

| Parameter | Value | Description | SEIE limits |
|---|---|---|---|
| `dbfreq(p.u.)` | 0.002 | Deadband | ±30 mHz to ±200 mHz |
| `R`(p.u.) | 0.05 | Droop | 0.02-0.066 |
| `d_ppr_max`(p.u.) | 1 | Maximum limit | - |
| `d_ppr_min`(p.u.) | -1 | Minimum limit | - |
| `Ramp_pr`(p.u./s) | 0.2 | Response ramp | 0.2 |

**Table C.4. Case 1: parameters of Converter Module (LVRT)**

| Parameter | Description | Value | SEIE limits |
|---|---|---|---|
| `VRTime`(s) | Voltage recovery time | 10 | <30 s |
| `Vmin_1t`(s) | Vmin curve point 1 (t) | 0.02 | 0 |
| `Vmin_1V`(p.u.) | Vmin curve point 1 (V) | 0 | 0 |
| `Vmin_2t`(s) | Vmin curve point 2 (t) | 0.5 | 0.5 |
| `Vmin_2V`(p.u.) | Vmin curve point 2 (V) | 0 | 0 |
| `Vmin_3t`(s) | Vmin curve point 3 (t) | 1 | 1 |
| `Vmin_3V`(p.u.) | Vmin curve point 3 (V) | 0.85 | 0.85 |

**Table C.5. Case 1: parameters of Converter Module (Reactive current injection)**

| Parameter | Description | Value | SEIE limits |
|---|---|---|---|
| Iq_LV_1V | Iq LV curve point 1 (V) | 0.95 p.u. | 0.95 p.u. |
| Iq_LV_1I | Iq LV curve point 1 | 0.287 p.u. | 0.287 p.u. |
| Iq_LV_2V | Iq LV curve point 2 (V) | 0.85 p.u. | 0.85 p.u. |
| Iq_LV_2I | Iq LV curve point 2 | 0.6 p.u. | 0.6 p.u. |
| Iq_LV_3V | Iq LV curve point 3 (V) | 0.5 p.u. | 0.5 p.u. |
| Iq_LV_3I | Iq LV curve point 3 | 0.9 p.u. | 0.9 p.u. |
| Iq_LV_4V | Iq LV curve point 4 (V) | 0 p.u. | 0 p.u. |
| Iq_LV_4I | Iq LV curve point 4 | 1 p.u. | 1 p.u. |
| Iq_HV_1V | Iq HV curve point 1 (V) | 1.05 p.u. | 1.05 p.u. |
| Iq_HV_1I | Iq HV curve point 1 | -0.287 p.u. | -0.287 p.u. |
| Iq_HV_2V | Iq HV curve point 2 (V) | 1.15 p.u. | 1.15 p.u. |
| Iq_HV_2I | Iq HV curve point 2 | -0.6 p.u. | -0.6 p.u. |
| Iq_HV_3V | Iq HV curve point 3 (V) | 1.5 p.u. | 1.5 p.u. |
| Iq_HV_3I | Iq HV curve point 3 | -0.9 p.u. | -0.9 p.u. |

**Table C.6. Case 1: parameters of Converter Module (Active current injection)**

| Parameter | Description | Value | SEIE limits |
|---|---|---|---|
| Id_LV_1V | Id curve point 1 (V) | 0 p.u. | 0 |
| Id_LV_1I | Id LV curve point 1 (V) | 0 p.u. | 0 |
| Id_LV_2V | Id LV curve point 2 (V) | 0.5 p.u. | 0.5 |
| Id_LV_2I | Id LV curve point 2 (V) | 0 p.u. | 0-0.53 p.u. |
| Id_LV_3V | Id LV curve point 3 (V) | 0.95 p.u. | 0.95 p.u. |
| Id_LV_3I | Id LV curve point 3 (V) | 1 p.u. | 1 p.u. |

**Table C.7. Case 1: relay parameters**

| Function | Value |
|---|---|
| 47 | 0.02 % |
| 81O | 52 Hz |
| 81R | ± 2 Hz/s |
| 81U | 47 Hz |

### C.3.2 Parameterised grid model

Table C.8 indicates the parameterisation of the particular grid model for the numerical application case regarding the power flow in the system for frequency ride-through.

**Table C.8: Case 1: parameterisation of particular grid model for frequency ride-through**

| Test case | Limit | G2 | Load 1 | Load 2 |
|---|---|---|---|---|
| A1-1 | 52.5 Hz | - | 3.46 MW | 2.44 MW |
| A1-2 | 51.5 Hz | - | 4.44 MW | 1.46 MW |
| A2-1 | 46.5 Hz | 2.28 MW | 2.95 MW | 2.95 MW |
| A2-2 | 47.5 Hz | 1.63 MW | 2.95 MW | 2.95 MW |
| A5-1 | 2.2 Hz/s | - | 3.05 MW | 2.85 MW |
| A5-2 | 1.8 Hz/s | - | 3.57 MW | 2.33 MW |
| A6-1 | -2.2 Hz/s | 1.9 MW | 2.95 MW | 2.95 MW |
| A6-2 | -1.8 Hz/s | 1.55 MW | 2.95 MW | 2.95 MW |

*Generator 1* (G1) has a rated capacity of $S_N = 10$ MVA, with $H_1 = 2.16s$. The rated capacity of *Generator 2* (G2) is 5 MVA with the same characteristics. Both generators have a governor based on a user model, representing a first-order turbine-governor model. The user model is based on the steam turbine TGOV1 model [168] and shown in Figure C.3. Parameters of the turbine-governor model are indicated in Table C.9.

**Table C.9. Parameters of first-order turbine-governor model**

| Parameters | Generator 1 | Generator 2 |
|---|---|---|
| $A_t$ | 1 | 1 |
| $D_t$ | 0 | 0 |
| $R$ | 0.061 | 0.061 |
| $P_N$ | 10 MVA | 5 MVA |
| $T_1$ | 6.1 s | 6.1 s |

For LVRT, the divider model has been selected as particular grid model because distances between assets in the island are short. The parameterisation of the particular grid model was indicated in Table 8.3. *Generator 1* includes the turbine-governor system as indicated in Table C.9 and the AVR represented by model SEXS with parameters in Table C.10. Its rated power is 25 MVA, with inertia $H_1 = 2.5$ s and $X''_d = X''_q = 0.21$ p.u.

Voltage unbalance has been simulated by the connection of an unbalanced three-

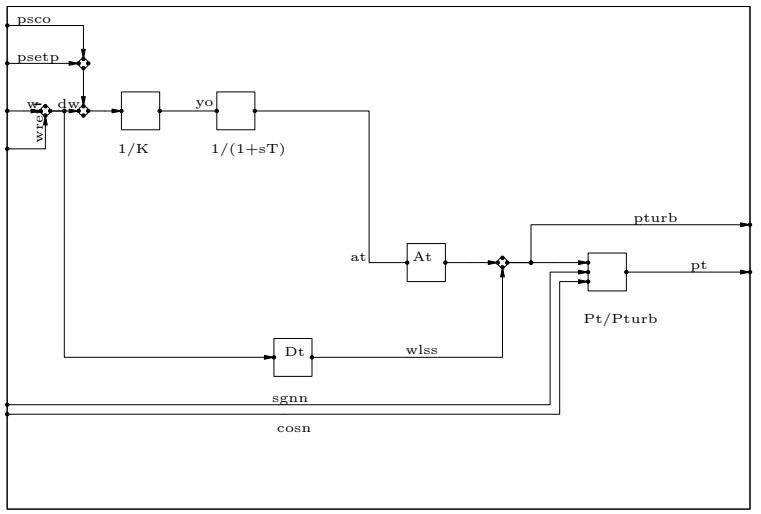


**Figure C.3. First-order turbine-governor model**

**Table C.10. Parameters of AVR model SEXS**

| Parameters | Value |
|---|---|
| $T_b$ | 10 |
| $T_a$ | 2 |
| $K$ | 100 |
| $T_e$ | 0.5 |
| $E_{min}$ | -3 |
| $E_{max}$ | 3 |

phase load *Load2* consuming the active power indicated in Table C.11. The rated power of *Generator 1* is 15 MVA, with $H_1 = 2.16$ s, $X'd = 0.25$ p.u. and $X''d = 0.21$ p.u. It includes the turbine-governor system as indicated in Table C.9 and the AVR represented by model SEXS with parameters in Table C.10.

**Table C.11. Case 1: parameterisation of particular grid model for voltage unbalance**

| Test case | Test value | Load2 |
|---|---|---|
| C1 | 2 % | $P_a = 1$ MW, $P_b = P_c = 2$ MW |
| C1-1 | 2.5 % | $P_a = 1.255$ MW, $P_b = P_c = 2.5$ MW |
| C1-2 | 1.5 % | $P_a = 0.75$ MW, $P_b = P_c = 1.5$ MW |

## C.4 Model parameterisation: application to Terceira island (Case 2)

This section includes the parameterisation, modelling and simulation of both the wind farm to install in Terceira and the equivalent grid model.

### C.4.1 Wind farm: description and parameterisation

The WTGs at the new wind farm to be installed in Terceira island at Quatro Ribeiras generate at 400 V. Then, voltage is stepped up to 30 kV by the WTG transformer (30/0.4 kV, MVA), and connected by an 7.5 km long overhead line to the PCC. The parameterised grid model is connected to this connecting point. Table C.12 details the impedances of the system elements. All sequence impedances are considered equal. The plant connection layout is shown in Figure C.4.

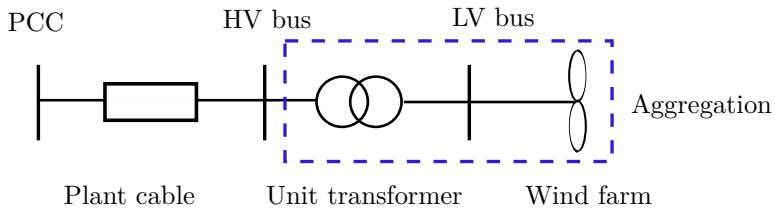


**Figure C.4. Wind farm connection layout in Terceira**

**Table C.12. Case 2: system impedance data (30 kV 100 MVA base)**

| Element | R(p.u.) | X(p.u.) |
|---|---|---|
| Plant cable | 0.138 | 0.202 |
| Plant transformer | 0 | 0.03 |

In PowerFactory, a wind farm in power flow can be represented by a static generator. An equivalent inverter and step-up transformer representing 2 lumped inverters have been configured with ratings in Table C.13, operating with a $\pm$ 0.9 power factor. The operation point is set at 80 % of the rating: $P_{WF} = 4$ MW and $Q_{WF} = 1.94$ MW.

Primary frequency response has been adjusted with parameters in Table C.3 corresponding to the Control Module, based on real performance results. LVRT protection function and current injection has been adjusted with parameters in Tables C.14, C.5, and C.15 corresponding to the Converter Module. They are partially based on performance results and the SEIE grid code limits.Reactive current injection covers both undervoltage and overvoltage. The active current injection is also based in the SEIE grid code, but the values have been adapted to the island characteristics. Intermediate values are interpolated by the converter control system. The protection function is based on the performance study.

**Table C.13. Case 2: inverter and static generator ratings**

| Parameter | Single inverter | Equivalent generator |
|---|---|---|
| Nameplate rating | 2.5 MW | |
| Generator rating | 2.78 MVA | 5.55 MVA |
| $P_{max}$ | 2.5 MW | 5 MW |
| $P_{min}$ | 0 W | 0 W |
| $Q_{max}$ | 1.2 MVAr | 2.4 MVAr |
| $Q_{min}$ | -1.2 MVAr | -2.4 MVAr |

**Table C.14. Case 2: parameters of Converter Module (LVRT)**

| Parameter | Description | Value |
|---|---|---|
| `VRTime`(s) | Voltage recovery time | 10 |
| `Vmin_1t`(s) | Vmin curve point 1 (t) | 0.02 |
| `Vmin_1V`(p.u.) | Vmin curve point 1 (V) | 0 |
| `Vmin_2t`(s) | Vmin curve point 2 (t) | 0.25 |
| `Vmin_2V`(p.u.) | Vmin curve point 2 (V) | 0 |
| `Vmin_3t`(s) | Vmin curve point 3 (t) | 1 |
| `Vmin_3V`(p.u.) | Vmin curve point 3 (V) | 1 |

**Table C.15. Case 2: parameters of Converter Module (Active current injection)**

| Parameter | Description | Value | SEIE limits |
|---|---|---|---|
| `Id_LV_1V` | Id curve point 1 (V) | 0 p.u. | 0 |
| `Id_LV_1I` | Id LV curve point 1 (V) | 0 p.u. | 0 |
| `Id_LV_2V` | Id LV curve point 2 (V) | 0.25 p.u. | 0.5 |
| `Id_LV_2I` | Id LV curve point 2 (V) | 0 p.u. | 0-0.53 p.u. |
| `Id_LV_3V` | Id LV curve point 3 (V) | 0.95 p.u. | 0.95 p.u. |
| `Id_LV_3I` | Id LV curve point 3 (V) | 1 p.u. | 1 p.u. |

Besides, the relay model must be parameterised with values in Table C.16, based on real performance results and grid code limits in the case of unbalance.

## C.4.2 Parameterised grid model

Table C.17 indicates the parameterisation of the particular grid model for the numerical application case regarding the power flow in the system for frequency ride-through.

Maximum frequency deviations correspond to different scenarios regarding demand

**Table C.16. Case 2: relay parameters**

| Function | Value |
|---|---|
| 47 | 0.02 % |
| 81O | 51.89 Hz |
| 81R | ± 2.3 Hz/s |
| 81U | 48.06 Hz |

**Table C.17: Case 2: parameterisation of particular grid model for frequency ride-through**

| Test case | Limit | G2 | Load 1 | Load 2 |
|---|---|---|---|---|
| A1-1 | 52 Hz | - | 3.07 MW | 2.38 MW |
| A1-2 | 51.5 Hz | - | 3.67 MW | 1.78 MW |
| A2-1 | 47.5 Hz | 2.97 MW | 4.965 MW | 4.965 MW |
| A2-2 | 48.5 Hz | 1.78 MW | 4.965 MW | 4.965 MW |
| A5-1 | 2.5 Hz/s | - | 1.64 MW | 3.81 MW |
| A5-2 | 1.5 Hz/s | - | 3.16 MW | 2.29 MW |
| A6-1 | -2.5 Hz/s | 3.81 MW | 4.965 MW | 4.965 MW |
| A6-2 | -1.5 Hz/s | 2.29 MW | 4.965 MW | 4.965 MW |

and generation dispatch. For underfrequency events, *Generator 1* has a rated power of $S_N = 15.25$ MVA, with $H_{eq} = 2.5s$, $R_{eq} = 0.05$ and $T_{eq} = 6$. The installed capacity of *Generator 2* is $S_N = 7.625$ MVA with the same characteristics. Load demand has been equally divided between *Load 1* and *Load 2*. On the other hand, for overfrequency events, *Generator 1* has a rated power of $S_N = 7.625$ MVA, with $H_{eq} = 2.5s$, $R_{eq} = 0.05$ and $T_{eq} = 6$. The installed capacity of *Generator 2* is $S_N = 7.625$ MVA with the same characteristics. Both generators have a governor based on a user model, representing a first-order turbine-governor model. The user model is based on the steam turbine TGOV1 model [168] and shown in Figure C.3. Parameters of the turbine-governor model are indicated in Table C.18 for both generators and for underfrequency (UF) and overfrequency (OF) events.

**Table C.18. Parameters of First-order turbine-governor model**

| Parameters | Generator 1 | Generator 2 |
|---|---|---|
| $A_t$ | 1 | 1 |
| $D_t$ | 0 | 0 |
| $R$ | 0.05 | 0.05 |
| $P_N$ | 15.25 MVA (UF), 7.625 MVA (OF) | 7.625 MVA |
| $T_1$ | 6 s | 6 s |

For LVRT, the divider model has been selected as particular grid model because distances between assets in Terceira are short. The parameterisation of the particular grid model was indicated in Table 9.6. *Generator 1* includes the turbine-governor system as indicated in Table C.18 and the AVR represented by model SEXS with parameters in Table C.10. It is the same model and values as used in the complete power system model (Appendix D). Its rated power is 76.45 MVA, with inertia $H_1 = 2.5$ s and $X''_d = X''_q = 0.32$ p.u. based on assumed data for the complete power system case.

Voltage unbalance has been simulated by the connection of an unbalanced single-phase load *Load2* consuming the active power indicated in Table C.19. Single-phase load has been selected as unbalancing event, because it results in higher unbalances in the system. The rated power of *Generator 1* is 15.25 MVA, with $H_1 = 2.5$ s, $X'd = 0.4$ p.u. and $X''d = 0.32$ p.u. It includes the turbine-governor system as indicated in Table C.18 and the AVR represented by model SEXS with parameters in Table C.10.

**Table C.19. Case 2: parameterisation of particular grid model for voltage unbalance**

| Test case | Test value | Load2 |
|---|---|---|
| C1 | 2 % | $P_a = 0.75$ MW |
| C1-1 | 2.5 % | $P_a = 0.93$ MW |
| C1-2 | 1.5 % | $P_a = 0.56$ MW |

## C.5 Model parameterisation: application to Lanzarote-Fuerteventura island system (Case 3)

This section includes parameterisation, modelling and simulation of both the wind farm to upgrade in Fuerteventura-Lanzarote and the equivalent grid model.

### C.5.1 Wind farm: description and parameterisation

The wind farm at Montaña de la Mina in Lanzarote will be upgraded. The WTGs at the new wind farm generate at 400 V. Then, voltage is stepped up to 30 kV by the WTG transformer (30/0.4 kV, MVA), and stepped up again at the wind farm substation up to 66 kV. The PCC is located at Montaña Mina 66 kV substation. The parameterised grid model is connected to this connecting point. Table C.20 details the impedances of the system elements. All sequence impedances are considered equal. The plant connection layout is shown in Figure C.5.

In PowerFactory, a wind farm in power flow can be represented by a static generator. An equivalent inverter and step-up transformer representing 4 lumped inverters have been configured with ratings in Table C.21, operating with a ± 0.9 power factor range. The operation point is set at 80 % of the rating: $P_{WF} = 6.4$ MW and $Q_{WF} = 3$ MW.

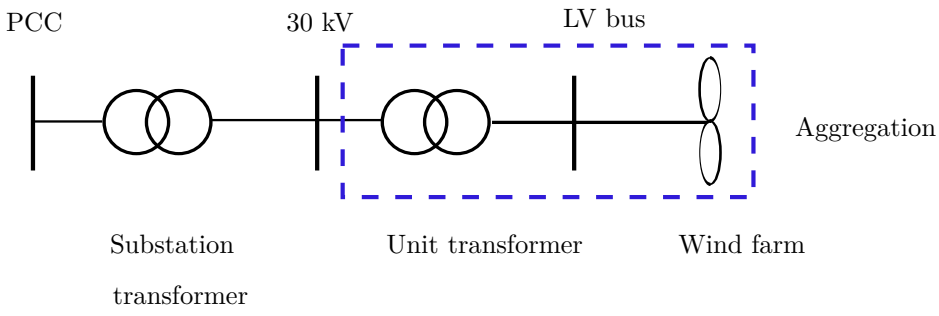


**Figure C.5. Wind farm connection layout in Lanzarote**

**Table C.20. CASE 3: system impedance data (66 kV 100 MVA base)**

| Element | R(p.u.) | X(p.u.) |
|---|---|---|
| Plant transformer | 0.00099 | 0.05999 |
| Substation transformer | 0.006 | 0.075 |

**Table C.21. Case 3: inverter and static generator ratings**

| Parameter | Single inverter | Equivalent generator |
|---|---|---|
| Nameplate rating | 2 MW | |
| Generator rating | 2.22 MVA | 8.88 MVA |
| $P_{max}$ | 2 MW | 8 MW |
| $P_{min}$ | 0 W | 0 W |
| $Q_{max}$ | 0.97 MVAr | 3.87 MVAr |
| $Q_{min}$ | -0.97 MVAr | -3.87 MVAr |

The parameters of the inverter can be found in Section C.3, as both cases have been parameterised for the SEIE grid code.

## C.5.2 Parameterised grid model

The loss of a single generating unit in Fuerteventura-Lanzarote system for the worst case results into a 13.23 % of the total installed capacity. When the subsystems are separated, the ratio increases up to a 18.8 %. Therefore, the values for maximum and minimum frequency have been calculated with (5.50). Table C.22 indicates the parameterisation of the particular grid model for the numerical application case regarding the power flow in the system for frequency ride-through.

*Generator 1* (G1) has a rated capacity of $S_N = 78.4$ MVA, with $H_1 = 3.25s$, which is the equivalent inertia value in the system. The rated capacity of *Generator 2* (G2) is 30.5 MVA with $H_2 = 3.53s$. Both generators have a governor based on a user

**Table C.22: Case 3: parameterisation of particular grid model for frequency ride-through**

| Test case | Limit | G2 | Load 1 | Load 2 |
|---|---|---|---|---|
| A1-1 | 52.5 Hz | - | 34.93 MW | 22.92 MW |
| A1-2 | 51.5 Hz | - | 44.1 MW | 13.75 MW |
| A2-1 | 46.5 Hz | 23.75 MW | 28.925 MW | 28.925 MW |
| A2-2 | 47.5 Hz | 16.96 MW | 28.925 MW | 28.925 MW |
| A5-1 | 2.5 Hz/s | - | 21.59 MW | 36.26 MW |
| A5-2 | 1.5 Hz/s | - | 36.09 MW | 21.76 MW |
| A6-1 | -2.5 Hz/s | 25.48 MW | 28.925 MW | 28.925 MW |
| A6-2 | -1.5 Hz/s | 15.29 MW | 28.925 MW | 28.925 MW |

model, representing a first-order turbine-governor model. The user model is based on the steam turbine TGOV1 model [168] and shown in Figure C.3. Parameters of the turbine-governor model are indicated in Table C.23.

**Table C.23. Parameters of First-order turbine-governor model**

| Parameters | Generator 1 | Generator 2 |
|---|---|---|
| $A_t$ | 1 | 1 |
| $D_t$ | 0 | 0 |
| $R$ | 0.052 | 0.07 |
| $P_N$ | 78.4 MVA | 30.5 MVA |
| $T_1$ | 6 s | 6 s |

For LVRT, the divider model has been selected as particular grid model because only dip magnitude has been adjusted. The parameterisation of the particular grid model was indicated in Table 9.6. *Generator 1* includes the turbine-governor system as indicated in Table C.23 and the AVR represented by model SEXS with parameters in Table C.10. It is the same model and values as used in the complete power system model (Appendix D). Its rated power is 452.39 MVA, with inertia $H_1 = 3.69$ s and $X''_d = X''_q = 0.21$ p.u., based on assumed data for the complete power system case.

Voltage unbalance has been simulated by the connection of an unbalanced single-phase load *Load2* consuming the active power indicated in Table C.24. The rated power of *Generator 1* is 108.9 MVA, with $H_1 = 3.33$ s, $X'd = 0.4$ p.u. and $X''d = 0.21$ p.u. It includes the turbine-governor system as indicated in Table C.23 for *Generator 1* and the AVR represented by model SEXS with parameters in Table C.10.

**Table C.24. Case 3: parameterisation of particular grid model for voltage unbalance**

| Test case | Test value | Load2 |
|---|---|---|
| C1 | 2 % | $P_a = 6.75$ MW |
| C1-1 | 2.5 % | $P_a = 8.44$ MW |
| C1-2 | 1.5 % | $P_a = 5.06$ MW |

# Appendix D

# Description of Terceira island

## D.1 Introduction

Figure D.1 shows the single line diagram of the Terceira island based on [154], with main power stations: TPP Belo Jardim with an installed capacity of 76453 kVA with 10 Diesel generators (4 of them supplied by gas-oil, 6 of them by fuel-oil) and 2 emergency generators (not included in this study), and the WPP Serra do Cume, with 10 WTGs adding up 9 MW. Mini-hydroelectric power stations of Cidade, Nasce d'Agua and Sao Joao de Deus are not included. Substations are named with abbreviated labels. PESC corresponds to Sierra to Cume wind farm, SEVB to Vinha Brava, SEAH to Angra do Heroismo, SEQR to Quatro Ribeiras, SELJ to Lajes, SEBJ Belo Jardim.

## D.2 Characteristics of the power system in Terceira

### D.2.1 Characteristics of transmission lines

The main characteristics of 30 kV transmission lines in Terceira island are displayed in Table D.1. OH corresponds to *overhead* line and UG to *underground* line.

### D.2.2 Description of generator characteristics

Table D.2 summarises the main data of all the power plants in the island of Terceira. Hydroelectric power plants are connected to the low voltage distribution network, and because of their small size are let out of the scope of this work.

#### D.2.2.1 Belo Jardim

All synchronous generators are salient pole generators, which are typical for internal combustion machines and hydraulic turbines, and a power factor of 0.8 has been considered. The technical minimum is set to 40 % of the rated power. The selected generator model is *GENSAL*, a linearised representation of a synchronous machine with salient poles that assumes equal mutual inductance rotor modelling. It must be noted that actually demand is covered by only units G5BJ to G10BJ 99 % of the year.

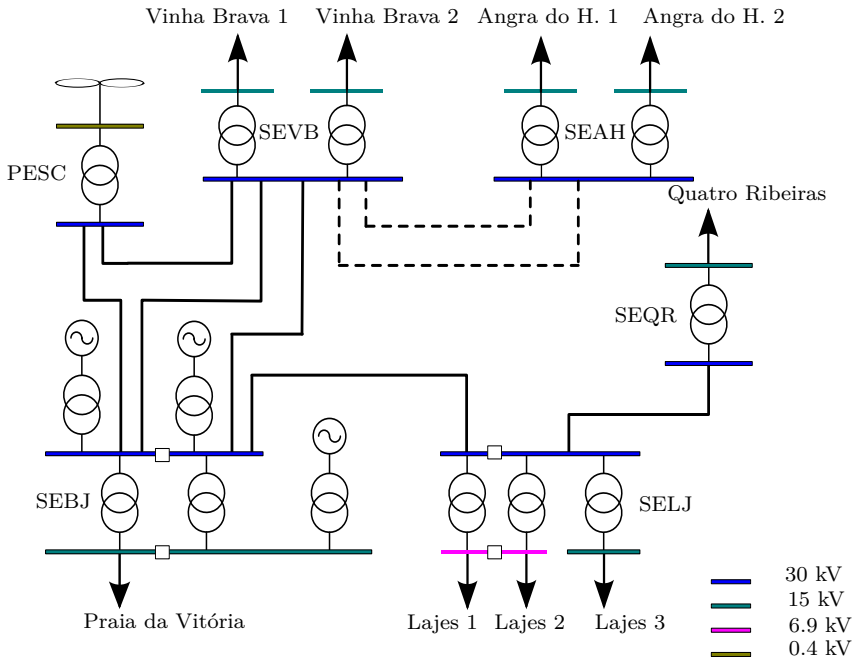


**Figure D.1. Single line diagram of Terceira island**

This is due to the fact that G1BJ to G4BJ use gas-oil as fuel, whereas the rest of the units are supplied with fuel-oil [169] -although they use gas-oil for starting up)-which is cheaper and less polluting. In addition, generating units G5BJ, G7BJ, G9JB and G10BJ have waste heat recovery, and hence, a higher overall efficiency [170]: 93 % against an average 77 %. Generator dispatch is influenced by aforementioned factors. Parameter values are based on criteria mentioned in [171] and [172].

Tables D.3, D.4 and D.5 gather the technical data of the synchronous generator, voltage regulator and speed regulator models, respectively, at Belo Jardim TPP. The speed regulation system needs to be selected according to a driving machine coupled with the generator. In the case of Belo Jardim, the driving machine is an internal combustion motor that runs on fuel, that can be modelled with the Woodward diesel governor model *DEGOV1*. In this model, in addition to the motor, a governor and an actuator for gas flow are also modelled. On the other hand, for the representation of the voltage regulator, simplified model SEXS is adopted. Generator parameter values are based on [173] and [162], as well as on the criteria mentioned in [171] and [172] for the unknown parameters.

### D.2.2.2 Serra do Cume

On the other hand, the generation park in Terceira is also made up of wind farm in Serra do Cume equipped with 10 WTGs Enercon E44 900 kW. These turbines are variable speed and gearless and the generator is an ENERCON direct-drive annular

**Table D.1. Parameters of 30 kV transmission lines in Terceira island**

| Line | Type | Length (km) | $R(\Omega)$ | $X(\Omega)$ | $B(\mu S)$ |
|---|---|---|---|---|---|
| Vitória-Vinha Brava 1 | OH | 13.61 | 3.3753 | 4.9404 | 43.3 |
| Vitória-Vinha Brava 2 | OH | 13.42 | 1.3527 | 5.2177 | 1.46 |
| Vitória-Vinha Brava 2 | UG | 0.54 | 0.086 | 0.05589 | 0.362 |
| Vitória-S. do Cume | OH | 3.56 | 0.8829 | 1.2923 | 11.3 |
| Vitória-S. do Cume | UG | 0.2 | 0.0484 | 0.02196 | 0.292 |
| Vinha Brava-S. do Cume | OH | 10.03 | 2.4874 | 3.6404 | 31.9 |
| Vinha Brava-S. do Cume | UG | 0.2 | 0.0484 | 0.02196 | 0.294 |
| Vitória-Lajes | OH | 3.81 | 0.9449 | 1.383 | 12.1 |
| Vitória-Lajes | UG | 1.09 | 0.2639 | 0.1197 | 1.61 |
| Lajes-Quatro Ribeiras | OH | 14.15 | 2.929 | 5.1322 | 3.35 |
| Lajes-Quatro Ribeiras | UG | 1.51 | 0.3656 | 0.1658 | 83.6 |
| Vinha Brava-Angra 1 | UG | 2.34 | 0.5665 | 0.2569 | 130 |
| Vinha Brava-Angra 2 | UG | 2.38 | 0.5762 | 0.2613 | 132 |

**Table D.2. List of power stations in Terceira island**

| Power station | Installed capacity | Type | Id. Generators |
|---|---|---|---|
| Cidade | 900 kVA | Hydro | G1CHCD |
| Nasce d'Agua | 560 kVA | Hydro | G1CHNA |
| Sao Joao de Deus | 330 kVA | Hydro | G1CHSJ |
| Belo Jardim | 76453 kVA | Fuel | G1BJ-G10BJ |
| Serra do Cume | 9000 kW | Wind | WT1SC-WT10SC |

**Table D.3. Technical data from Belo Jardim power plant (G1BJ-G10BJ)**

| Parameters | G1,G2 | G3 | G4 | G5,G7 | G6,G8 | G9,G10 |
|---|---|---|---|---|---|---|
| $U_N$ **(kV)** | 6.6 | 10 | 6.6 | 6 | 6 | 6 |
| $S_N$ **(kVA)** | 3910 | 3750 | 3575 | 7625 | 7625 | 15404 |
| $P_N$ **(kW)** | 3128 | 3000 | 2860 | 6100 | 6100 | 12323.2 |
| $P_{max}$ **(kW)** | 2408.56 | 2310 | 2202.2 | 5673 | 4880 | 11460.58 |
| $P_{min}$ **(kW)** | 1251.2 | 1200 | 1144 | 2440 | 2440 | 4929.28 |
| $H_s$ **(s)** | 2 | 2 | 2 | 2.5 | 2.5 | 2.5 |
| $X_d$ **(p.u.)** | 1.6 | 1.6 | 1.6 | 1.6 | 1.6 | 1.2 |
| $X_q$ **(p.u.)** | 1.04 | 1.04 | 1.04 | 1.04 | 1.04 | 0.72 |
| $X'_d$ **(p.u.)** | 0.4 | 0.4 | 0.4 | 0.4 | 0.4 | 0.36 |
| $X_l$ **(p.u.)** | 0.224 | 0.224 | 0.224 | 0.224 | 0.224 | 0.168 |
| $X''_d$ **(p.u.)** | 0.32 | 0.32 | 0.32 | 0.32 | 0.32 | 0.24 |
| $X''_q$ **(p.u.)** | 0.32 | 0.32 | 0.32 | 0.32 | 0.32 | 0.24 |
| $T'_{d0}$ **(s)** | 4 | 4 | 4 | 4 | 4 | 5 |
| $T''_{d0}$ **(s)** | 0.035 | 0.035 | 0.035 | 0.035 | 0.035 | 0.5 |
| $T''_{q0}$ **(s)** | 0.05 | 0.05 | 0.05 | 0.05 | 0.05 | 0.06 |
| $S(1.0)$ **(s)** | 0.15 | 0.15 | 0.15 | 0.15 | 0.15 | 0.15 |
| $S(1.2)$ **(s)** | 0.4 | 0.4 | 0.4 | 0.4 | 0.4 | 0.4 |

**Table D.4: Voltage regulator model SEXS technical data from the thermal power plants in Terceira island**

| $T_b$ | $Ta$ | $K$ | $Te$ (s) | $Emax$ (p.u.) | $E_{min}$ (p.u.) |
|---|---|---|---|---|---|
| 10 | 2 | 100 | 0.5 | 3 | -3 |

**Table D.5: Speed regulator model DEGOV1 technical data from Belo Jardim power plant (G1BJ-G10BJ)**

| Parameters | G1,G2 | G3 | G4 | G5-G8 | G9,G10 |
|---|---|---|---|---|---|
| $T_1$ (s) | 0.2 | 0.2 | 0.2 | 0.2 | 0.2 |
| $T_2$ (s) | 0.3 | 0.3 | 0.3 | 0.3 | 0.3 |
| $T_3$ (s) | 0.5 | 0.5 | 0.5 | 0.5 | 0.5 |
| $T_4$ (s) | 0.25 | 0.25 | 0.25 | 0.25 | 0.25 |
| $T_5$ (s) | 0.1 | 0.1 | 0.1 | 0.1 | 0.1 |
| $T_6$ (s) | 0.2 | 0.2 | 0.2 | 0.2 | 0.2 |
| $K$ | 8 | 8 | 8 | 9 | 10 |
| $TD$ (s) | 0.05 | 0.05 | 0.05 | 0.05 | 0.05 |
| $T_{max}$ | 1 | 1 | 1 | 1 | 1 |
| $T_{min}$ | 0 | 0 | 0 | 0 | 0 |
| Droop | 0.05 | 0.05 | 0.05 | 0.05 | 0.05 |
| $Te$ (s) | 0 | 0 | 0 | 0 | 0 |

generator (Permanent Magnet Synchronous Generator (PMSG)).

**Table D.6. Fully rated converter parameters in Terceira island**

| $u_{sc}$ | $P_{cu}$ | $K_d$ | $T_d$ | $K_q$ | $T_q$ |
|---|---|---|---|---|---|
| 10 % | 10 kW | 5 | 0.01 s | 5 | 0.01 s |

### D.2.3 Power transformers

The power transformer characteristics at the main substations in Terceira are described in Table D.7. The power transformer characteristics corresponding to the synchronous generators at Belo Jardim thermal power plant are described in Table D.8, and those corresponding to Serra do Cume wind farm in Table D.9.

## D.3 Case study

### D.3.1 Load scenarios

Table D.10 indicates the active and reactive power demand of the loads under peak and valley demand situations.

Static loads have been considered.

**Table D.7. Power transformer characteristics in Terceira island**

| Substation | Id | Connection | U | $S_N$ | R(p.u.) | X(p.u.) |
|---|---|---|---|---|---|---|
| SEBJ | TP1 | YNd11 | 31.46/15 kV | 10 | 0.0027 | 0.0748 |
| SEBJ | TP2 | YNd11 | 31.5/15 kV | 10 | 0.0055 | 0.0728 |
| SEVB | TP1 | YNd11 | 31.5/15 kV | 10 | 0.0077 | 0.0843 |
| SEVB | TP2 | YNd11 | 31.5/15 kV | 10 | 0.0035 | 0.0760 |
| SEAH | TP1 | YNd11 | 31.51/15 kV | 5 | 0.0066 | 0.0677 |
| SEAH | TP2 | YNd11 | 31.51/15 kV | 5 | 0.0066 | 0.0677 |
| SELJ | TP1 | YNd11 | 31.5/6.9 kV | 6.25 | 0.0051 | 0.0682 |
| SELJ | TP2 | YNd11 | 31.5/6.9 kV | 6.25 | 0.0051 | 0.0682 |
| SELJ | TP3 | YNd11 | 31.5/15 kV | 1 | 0.0199 | 0.0566 |
| SEQR | TP1 | YNd11 | 31.48/15 kV | 10 | 0.0063 | 0.0868 |

Note. Values in p.u. referred to the rated capacity of the transformers

**Table D.8. Power transformer characteristics at Belo Jardim**

| Id | Connection | U | $S_N$ | R(p.u.) | X(p.u.) |
|---|---|---|---|---|---|
| TP G1 | Yd5 | 15/6.6 kV | 4 | 0.0094 | 0.0945 |
| TP G2 | Yd5 | 15.5/6.6 kV | 4 | 0.0095 | 0.1005 |
| TP G3 | Yd5 | 15.5/10 kV | 4 | 0.0094 | 0.1006 |
| TP G4 | YNd5 | 15.5/6.6 kV | 4 | 0.0070 | 0.0907 |
| TP G5 | YNd5 | 31.56/6 kV | 8 | 0.0030 | 0.058 |
| TP G6 | YNd5 | 31.56/6 kV | 8 | 0.0030 | 0.0571 |
| TP G7 | YNd5 | 31.56/6 kV | 8 | 0.0030 | 0.0587 |
| TP G8 | YNd5 | 31.56/6 kV | 8 | 0.0039 | 0.0565 |
| TP G9 | YNd5 | 31.56/6 kV | 15.5 | 0.0081 | 0.0786 |
| TP G10 | YNd5 | 31.56/6 kV | 15.5 | 0.0082 | 0.0776 |

Note. Values in p.u. referred to the rated capacity of the transformers

**Table D.9. Power transformer characteristics at Serra do Cume**

| Id | Connection | U | $S_N$ | R(p.u.) | X(p.u.) |
|---|---|---|---|---|---|
| TP1-TP5 | Dy5 | 30/0.4 kV | 1 | 0.0130 | 0.0378 |
| TP6-TP10 | Dy5 | 30/0.4 kV | 1 | 0.0186 | 0.0555 |

Note. Values in p.u. referred to the rated capacity of the transformers

### D.3.2 Generation dispatch

Thermal generation (without taking into account losses and spinning reserve) is indicated in Table D.11 for each study case.

Thermal generating unit dispatch can be programmed so as to minimise overall cost, power system losses, or environmental impact. In addition, generating unit maximum and minimum output constraint, maximum ramps and required spinning reserve shall be taken into account. However, for the Terceira system, only maximum and minimum output constraint is known. Therefore, for the unit commitment two steps have been followed. First, the on-line generating units have been chosen based

**Table D.10. Load scenarios in Terceira island, 2012**

| Load Id. | Peak demand | | Valley demand | |
|---|---|---|---|---|
| Lajes 1 | 2.016 MW | 0.505 MVAr | 0.989 MW | 0.201 MVAr |
| Lajes 2 | 2.148 MW | 0.706 MVAr | 1.107 MW | 0.364 MVAr |
| Lajes 3 | 0.405 MW | 0.123 MVAr | 0.182 MW | 0.112 MVAr |
| Quatro Ribeiras | 2.259 MW | 1.302 MVAr | 0.751 MW | 0.612 MVAr |
| Angra do Heroismo 1 | 3.181 MW | 1.251 MVAr | 1.237 MW | 0.742 MVAr |
| Angra do Heroismo 2 | 3.012 MW | 1.152 MVAr | 0.583 MW | 0.16 MVAr |
| Vinha Brava 1 | 6.601 MW | 3.578 MVAr | 3.594 MW | 2.119 MVAr |
| Vinha Brava 2 | 6.629 MW | 3.495 MVAr | 2.429 MW | 1.232 MVAr |
| Praia da Vitoria | 8.443 MW | 4.975 MVAr | 3.277 MW | 3.006 MVAr |
| **Total** | 35.194 MW | 17.087 MVAr | 14.149 MW | 8.548 MVAr |

**Table D.11. Thermal generation scenarios in Terceira island**

| Case | Total generation | Wind power | Thermal generation |
|---|---|---|---|
| **Case 1** | 35.194 MW | 0 MW | 35.194 MW |
| **Case 2** | 35.194 MW | 4.5 MW | 30.694 MW |
| **Case 3** | 35.194 MW | 9 MW | 26.194 MW |
| **Case 4** | 14.149 MW | 0 MW | 14.149 MW |
| **Case 5** | 14.149 MW | 4.5 MW | 9.649 MW |
| **Case 6** | 14.149 MW | 9 MW | 5.149 MW |

on the demand scenarios for each study case, and taking into account the spinning reserve to cover. For each scenario, at least two generating units must be programmed in order to guarantee security in a N-1 condition. In addition, system losses have also to be covered. As a second step, an economic dispatch have been performed (without taking into account losses), based on data available in [162], and respecting maximum and minimum output constraints. The cost functions are indicated below:

$$C_1 = C_2 = C_3 = 146.44 + 4.7593 \cdot P + 0.06237 \cdot P^2 \tag{D.1}$$

$$C_4 = 219.66 + 5.4915 \cdot P + 0.069559 \cdot P^2 \tag{D.2}$$

$$C_5 = C_6 = C_7 = C_8 = 73.22 + 4.0271 \cdot P + 0.054915 \cdot P^2 \tag{D.3}$$

$$C_9 = C_10 = 117.9585 + 6.8798 \cdot P + 0.7595 \cdot P^2 \tag{D.4}$$

The optimal unit commitment is summarised in Table D.12, where on-line generators are marked. Smallest Diesel generators (i.e. G3, G4) are normally left for emergency situations.

Table D.12. On-line generators for each study case in Terceira island

| Case Id. | G1 | G2 | G5 | G6 | G7 | G8 | G9 | G10 |
|---|---|---|---|---|---|---|---|---|
| 1 | ✓ | ✓ | ✓ | ✓ | ✓ | ✓ | ✓ | ✓ |
| 2 | | | ✓ | ✓ | ✓ | ✓ | ✓ | ✓ |
| 3 | | | | ✓ | ✓ | ✓ | ✓ | ✓ |
| 4 | | | | | | ✓ | ✓ | ✓ |
| 5 | | | | ✓ | ✓ | ✓ | | |
| 6 | | | | | ✓ | ✓ | | |

# Appendix E

# Description of Fuerteventura-Lanzarote system

## E.1 Introduction

Figure E.1 shows the single line diagram of the Fuerteventura-Lanzarote, where the system is weakly meshed and a unique corridor links substations from north to south. Main power stations are the TPP Las Salinas (in Fuerteventura island) with an installed capacity of 231.4 MW, with 3 gas turbines and 9 Diesel units, the TPP Punta Grande (in Lanzarote island) with an installed capacity of 212.5 MW and 2 gas turbines and 8 Diesel units, and finally, 4 small size wind farms: Los Valles with an installed capacity of 7.65 MW, Montaña Mina of 1.125 MW, Cañada del Río of 18.4 MW, and Cañada La Barca with 1.12 MW. Further details are included in Appendix E. In addition, due to the high demand in the more distant substation, i.e. Matas Blancas, emergency generators have been installed close to Gran Tarajal substation. Those generators are not included in the present study. Substations are named with abbreviated labels in Figure E.1. In Fuerteventura, SECB corresponds to Cañada La Barca, SECR corresponds to Cañada del Río, SEMB to Matas Blancas, SEGT to Gran tarajal, SELS to Las Salinas, and SECO to Corralejo. In Lanzarote, SELV corresponds to Los Valles, SEMM to Montaña Mina, SESB to san Bartolomé, SEM to Macher, and SEPB to Playa Blanca.

## E.2 Characteristics of the power system Fuerteventura-Lanzarote

### E.2.1 Characteristics of transmission lines

The main characteristics of transmission lines are displayed in Table E.1. The data is based on [157] available in 2013 and the information about the conductor types in [153]. OH corresponds to *overhead* line and UG to *underground* line.

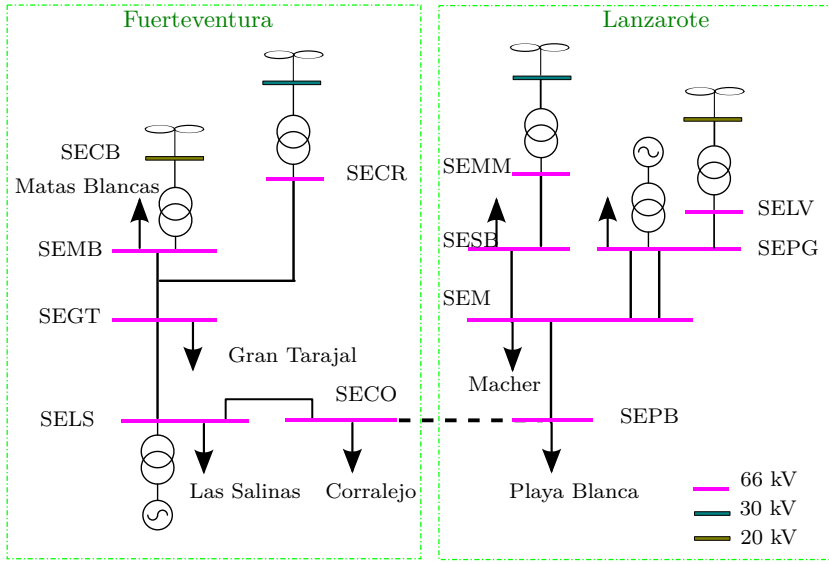


**Figure E.1. Single line diagram of Fuerteventura-Lanzarote system**

### E.2.2 Description of generator characteristics

Table E.3 summarises main data form all the power plants in the Fuerteventura-Lanzarote system. F indicates power stations belonging to Fuerteventura and L those in Lanzarote. Regarding Diesel engines, in Lanzarote mostly 4 cylinder units are used except for G4PG-G6PG, and in Fuerteventura all are 4 cylinder engines. In addition, the wind farm Montaña Mina is connected to the substation of San Bartolomé and Los Valles at Punta Grande substation. In Fuerteventura, on the other hand, both Cañada del Río and Cañada de la Barca are connected at Matas Blancas substation. In Fuerteventura, 4 MW of photovoltaic generation are also installed, but have not been considered in this study.

Tables E.4, E.6, E.6, E.8 and E.9 gather the technical data of the synchronous generator, speed regulator and voltage regulator models at Punta Grande TPP. On the other hand, Tables E.5, E.6, E.7 and E.9 gather the technical data of the synchronous generator, speed regulator and voltage regulator models at Las Salinas TPP. Speed regulator and voltage regulator models for Diesel engines are based on [174].

At Punta Grande, G1PG-G8PG are Diesel generating units, while G9PG and G10PG are gas turbines. At Las Salinas, all the units are Diesel engines, except for units G10LS-G12LS which are gas turbines. Table E.2 summarises the models used in *Power Factory* simulation software.

For all synchronous generators, a power factor of 0.8 has been considered, and the technical minimum is set to 40 % of the rated power for Diesel engines and 20 % for gas turbines. Parameter values are based on criteria mentioned in [171] and [172], as well as data available in [123]. Reactive power limits are set between 0.5/-0.3 p.u.

**Table E.1: Parameters of 66 kV transmission lines in Fuerteventura-Lanzarote system**

| Line | Type | Length (km) | $R(\Omega)$ | $X(\Omega)$ | $B(\mu S)$ |
|---|---|---|---|---|---|
| Las Salinas-G. Tarajal | OH | 38.77 | 4.9354 | 15.4964 | 111.4133 |
| Las Salinas-G. Tarajal | UG | 1.27 | 0.166 | 0.07112 | 118.11 |
| Las Salinas-Corralejo | UG | 1.27 | 0.166 | 0.07112 | 118.11 |
| Las Salinas-Corralejo | OH | 23.33 | 2.9699 | 9.325 | 67.0434 |
| Las Salinas-Corralejo | UG | 0.95 | 0.1216 | 0.05785 | 74.1 |
| G. Tarajal-Matas Blancas | OH | 6.45 | 0.8211 | 2.5781 | 18.5353 |
| G. Tarajal-Matas Blancas | UG | 2.56 | 0.3346 | 0.1434 | 238.08 |
| Corralejo-Playa Blanca | UG | 5 | 0.689 | 0.294 | 425 |
| Corralejo-Playa Blanca | US | 15 | 0.9015 | 2.07 | 631.46 |
| Corralejo-Playa Blanca | UG | 1.5 | 0.225 | 0.0882 | 127.5 |
| Playa Blanca-Macher | OH | 17.4 | 2.215 | 6.9548 | 50 |
| Macher-S. Bartolomé | OH | 9.87 | 1.2564 | 3.945 | 28.3634 |
| Macher-S. Bartolomé | UG | 0.85 | 0.1172 | 0.04998 | 72.25 |
| Macher-Punta Grande 1 | UG | 21.59 | 2.9773 | 1.2695 | 1835.5 |
| Macher-Punta Grande 2 | UG | 21.59 | 2.9773 | 1.2695 | 1835.5 |
| S. Bartolomé-Punta Grande | OH | 8.06 | 1.02604 | 3.2216 | 23.162 |
| S. Bartolomé-Punta Grande | UG | 0.85 | 0.1172 | 0.04998 | 72.25 |
| Los Valles-Punta Grande | OH | 8.06 | 1.02604 | 3.2216 | 23.162 |

for round rotor generators, and 0.5/-0.4 p.u. for salient poles generators.

**Table E.2. List of models**

| Element | Model |
|---|---|
| Round rotor generator | GENROU |
| Salient poles generator | GENSAL |
| Gas turbine | GAST |
| Diesel motor | DEGOV1 |
| Voltage regulator | IEEET1 |

**Table E.3. List of power stations in Fuerteventura-Lanzarote system**

| Power station | System | Technology | Installed capacity | Id. |
|---|---|---|---|---|
| Las Salinas | F | D, GT | 185.07 MW | G1-G12LS |
| Punta Grande | L | D, GT | 212.11 MW | G1-G12PG |
| Los Valles | L | DFIG | 7650 kW | WT1-WT9LV |
| Montaña de la Mina | L | IG | 1125 kW | WT1-WT5MM |
| Cañada de la Barca | F | IG | 1125 kW | WT1-WT5CB |
| Cañada del Río | F | DFIG | 18.4 MW | WT1-WT8CR |

**Table E.4. Technical data from the thermal power plant Punta Grande, Lanzarote**

| Parameters | G1-G3PG | G4-G5PG | G6PG | G7-G10PG | G11PG | G12PG |
|---|---|---|---|---|---|---|
| **Technology** | D | D | D | D | GT | GT |
| $U_N$ **(kV)** | 6.6 | 11.3 | 11.3 | 11.3 | 11.3 | 11.3 |
| $S_N$ **(MVA)** | 9.4 | 19.375 | 30.5 | 23 | 31.25 | 46.87 |
| $P_N$ **(MW)** | 7.52 | 15.50 | 24.39 | 18.4 | 25 | 37.5 |
| $P_{max}$ **(MW)** | 6.49 | 12.85 | 20.51 | 17.2 | 19.6 | 32.34 |
| $P_{min}$ **(MW)** | 3 | 6.2 | 9.756 | 7.36 | 5 | 7.5 |
| $Hs$ **(s)** | 1.19 | 3.66 | 3.53 | 3.53 | 7.5 | 1.95 |
| $X_d$ **(p.u.)** | 1.6 | 2.16 | 2.2 | 1.5 | 1.7 | 1.735 |
| $X_q$ **(p.u.)** | 1.04 | 2.074 | 2.112 | 1.06 | 1.632 | 1.651 |
| $X_d'$ **(p.u.)** | 0.48 | 0.41 | 0.308 | 0.3 | 0.247 | 0.196 |
| $X_q'$ **(p.u.)** | - | 0.54 | 0.55 | - | 0.379 | 0.395 |
| $X_l$ **(p.u.)** | 0.224 | 0.164 | 0.132 | 0.16 | 0.119 | 0.095 |
| $X_d''$ **(p.u.)** | 0.32 | 0.26 | 0.209 | 0.184 | 0.162 | 0.15 |
| $X_q''$ **(p.u.)** | 0.32 | 0.26 | 0.209 | 0.184 | 0.162 | 0.15 |
| $T_{d0}'$ **(s)** | 4 | 4.75 | 4.75 | 4.75 | 5.228 | 5.51 |
| $T_{d0}''$ **(s)** | 0.035 | 0.035 | 0.035 | 0.035 | 0.023 | 0.04 |
| $T_{q0}'$ **(s)** | - | 0.7 | 0.7 | - | 0.411 | 0.7 |
| $T_{q0}''$ **(s)** | 0.05 | 0.05 | 0.05 | 0.05 | 0.056 | 0.05 |
| $S(1.0)$ **(s)** | 0.15 | 0.15 | 0.15 | 0.15 | 0.101 | 0.14 |
| $S(1.2)$ **(s)** | 0.4 | 0.4 | 0.4 | 0.4 | 0.441 | 0.65 |

### E.2.3 Power transformers

The power transformer data is indicated in Tables E.10,E.11, E.12, and E.13 and partially based on [153], [154] and [172]. No load losses are dismissed.

## E.3 Case study

### E.3.1 Load scenarios

Peak and valley scenarios are indicated in Table E.14, based on data supplied at [175], [153] and [176].

### E.3.2 Generation dispatch

Currently, the relation between installed generation to peak demand is around 1.6 in Lanzarote and 2.8 in Fuerteventura, considering them as separate power systems. Due to the low relation value in Lanzarote, emergency engines have been installed in Punta Grande. Some years ago, Fuerteventura used to export energy to Lanzarote island. However, currently the interconnection between both islands often plays a role only under emergency situations [177] for two reasons: the limited capacity of the interconnection link, constrained by the capacity of the undersea cable to 64 MVA, and because of the increasing demand in Fuerteventura. In the future, if the

**Table E.5. Technical data from the thermal power plant Las Salinas, Fuerteventura**

| Parameters | G1-G2LS | G3LS | G4-G5LS | G6LS | G7-G9LS | G10LS | G11LS |
|---|---|---|---|---|---|---|---|
| **Technology** | D | D | D | D | D | GT | GT |
| $U_N$ **(kV)** | 6.6 | 6.6 | 6.6 | 11.3 | 11.3 | 11.3 | 11.3 |
| $S_N$ **(MVA)** | 5.4 | 6.3 | 9.4 | 30 | 23 | 31.25 | 46.87 |
| $P_N$ **(MW)** | 4.32 | 5.04 | 7.52 | 24 | 18.4 | 25 | 37.5 |
| $P_{max}$ **(MW)** | 3.82 | 4.11 | 6.21 | 20.51 | 17.2 | 21.85 | 29.4 |
| $P_{min}$ **(MW)** | 1.73 | 2.016 | 3 | 9.76 | 7.36 | 5 | 7.5 |
| $Hs$ **(s)** | 1.75 | 1.73 | 2.16 | 3.53 | 3.53 | 7.5 | 1.95 |
| $X_d$ **(p.u.)** | 1.3 | 1.7 | 1.6 | 2.2 | 1.5 | 1.7 | 1.735 |
| $X_q$ **(p.u.)** | 0.84 | 1.04 | 1.04 | 2.112 | 1.06 | 1.632 | 1.651 |
| $X'_d$ **(p.u.)** | 0.386 | 0.368 | 0.48 | 0.308 | 0.3 | 0.247 | 0.196 |
| $X'_q$ **(p.u.)** | - | - | - | 0.55 | - | 0.379 | 0.395 |
| $X_l$ **(p.u.)** | 0.219 | 0.16 | 0.224 | 0.132 | 0.16 | 0.119 | 0.095 |
| $X''_d$ **(p.u.)** | 0.29 | 0.233 | 0.32 | 0.209 | 0.184 | 0.162 | 0.15 |
| $X''_q$ **(p.u.)** | 0.29 | 0.233 | 0.32 | 0.209 | 0.184 | 0.162 | 0.15 |
| $T'_{d0}$ **(s)** | 4 | 4 | 4 | 4.75 | 4.75 | 5.228 | 5.51 |
| $T''_{d0}$ **(s)** | 0.035 | 0.035 | 0.035 | 0.035 | 0.035 | 0.023 | 0.04 |
| $T'_{q0}$ **(s)** | - | - | - | 0.7 | - | 0.411 | 0.7 |
| $T''_{q0}$ **(s)** | 0.05 | 0.05 | 0.05 | 0.05 | 0.05 | 0.056 | 0.05 |
| $S(1.0)$ **(s)** | 0.15 | 0.15 | 0.15 | 0.15 | 0.15 | 0.101 | 0.14 |
| $S(1.2)$ **(s)** | 0.4 | 0.4 | 0.4 | 0.4 | 0.4 | 0.441 | 0.65 |

**Table E.6: Speed regulator model DEGOV1 technical data from the thermal power plant at Punta Grande**

| Parameters | G1-G3PG | G4-G5PG | G6PG | G7-G10PG |
|---|---|---|---|---|
| $T_1$ **(s)** | 0.2 | 0.2 | 0.2 | 0.2 |
| $T_2$ **(s)** | 0.3 | 0.3 | 0.3 | 0.3 |
| $T_3$ **(s)** | 0.5 | 0.5 | 0.5 | 0.5 |
| $T_4$ **(s)** | 1 | 0.5 | 0.5 | 0.25 |
| $T_5$ **(s)** | 0.1 | 0.1 | 0.1 | 0.1 |
| $T_6$ **(s)** | 0.2 | 0.2 | 0.2 | 0.2 |
| $K$ | 8 | 10 | 9 | 9 |
| $TD$ **(s)** | 0.05 | 0.05 | 0.05 | 0.05 |
| $T_{max}$ | 0.8 | 0.8 | 0.81 | 0.8 |
| $T_{min}$ | 0 | 0 | 0 | 0 |
| Droop | 0.075 | 0.07 | 0.07 | 0.05 |
| $T_e$ **(s)** | 0 | 0 | 0 | 0.5 |

interconnection capacity between both islands increases, demand could be covered in both islands like a unique power system [177].

Therefore, the generation dispatches have been initially calculated separately. Thermal generation (without taking into account losses and spinning reserve) is indicated in Table E.15 for each study case.

**Table E.7: Speed regulator model DEGOV1 technical data from the thermal power plant at Las Salinas**

| Parameters | G1-G2LS | G3LS | G4-G5LS | G6LS | G7-G9LS |
|---|---|---|---|---|---|
| $T_1$ (s) | 0.2 | 0.2 | 0.2 | 0.2 | 0.2 |
| $T_2$ (s) | 0.3 | 0.3 | 0.3 | 0.3 | 0.3 |
| $T_3$ (s) | 0.5 | 0.5 | 0.5 | 0.5 | 0.5 |
| $T_4$ (s) | 1 | 1 | 0.5 | 0.5 | 0.25 |
| $T_5$ (s) | 0.1 | 0.1 | 0.1 | 0.1 | 0.1 |
| $T_6$ (s) | 0.2 | 0.2 | 0.2 | 0.2 | 0.2 |
| $K$ | 7 | 7 | 8 | 9 | 9 |
| $TD$ (s) | 0.05 | 0.05 | 0.05 | 0.05 | 0.05 |
| $T_{max}$ | 0.8 | 0.8 | 0.8 | 0.81 | 0.8 |
| $T_{min}$ | 0 | 0 | 0 | 0 | 0 |
| **Droop** | 0.075 | 0.075 | 0.075 | 0.07 | 0.05 |
| $T_e$ (s) | 0 | 0 | 0 | 0 | 0 |

**Table E.8: Speed regulator model GAST technical data from the thermal power plants in Fuerteventura-Lanzarote**

| Parameters | Value |
|---|---|
| $T_1$ (s) | 0.4 |
| $T_2$ (s) | 0.1 |
| $T_3$ (s) | 3 |
| $A_T$ | 1 |
| $K_T$ | 2 |
| $Vmax$ | 1 |
| $V_{min}$ | -0.05 |
| $D_{turb}$ | 0 |
| $R$ | 0.05 |

**Table E.9: Voltage regulator model IEEET1 technical data from the thermal power plants in Fuerteventura-Lanzarote system**

| Parameters | Value |
|---|---|
| $K_a$ | 200 |
| $K_e$ | 1 |
| $K_f$ | 0.1 |
| $Ta$ (s) | 0.84 |
| $T_e$ (s) | 0.3 |
| $T_r$ (s) | 0.023 |
| $T_f$ (s) | 1 |
| $E_1$ | 2.47 |
| $S(E_1)$ | 0.035 |
| $E_2$ | 3.5 |
| $S(E_2)$ | 0.6 |
| $V_{max}$ (p.u.) | 3.5 |
| $V_{min}$ (p.u.) | -2.5 |

**Table E.10. Power transformer characteristics at Punta Grande**

| Id | Connection | U | $S_N$ (MVA) | X(%) | R(%) |
|---|---|---|---|---|---|
| TG1-TG3PG | YNd11 | 6.6/66 kV | 10 MVA | 9 | 0.5 |
| TG4-TG5PG | YNd11 | 11.3/66 kV | 20 MVA | 10 | 0.45 |
| TG6PG | YNd11 | 11.3/66 kV | 30 MVA | 10 | 0.35 |
| TG7-TG10PG | YNd11 | 11.3/66 kV | 25 MVA | 10 | 0.4 |
| TG11PG | YNd11 | 11.3/66 kV | 35 MVA | 10.5 | 0.4 |
| TG12PG | YNd11 | 11.3/66 kV | 50 MVA | 11.5 | 0.3 |

**Table E.11. Power transformer characteristics at Las Salinas**

| Id | Connection | U | $S_N$ (MVA) | X(%) | R(%) |
|---|---|---|---|---|---|
| TG1 | YNd11 | 6.6/66 kV | 5 MVA | 7.5 | 0.55 |
| TG2-TG5LS | YNd11 | 6.6/66 kV | 10 MVA | 9 | 0.5 |
| TG6 | YNd11 | 11.3/66 kV | 30 MVA | 10 | 0.35 |
| TG7-TG9LS | YNd11 | 11.3/66 kV | 25 MVA | 10 | 0.4 |
| TG10LS | YNd11 | 11.3/66 kV | 35 MVA | 10.5 | 0.4 |
| TG11LS | YNd11 | 11.3/66 kV | 50 MVA | 11.5 | 0.3 |

**Table E.12. Power transformer characteristics at wind park substations**

| Id | Connection | U | $S_N$ (MVA) | X(%) | R(%) |
|---|---|---|---|---|---|
| TP WT1LV-WT8LV | Dyn5 | 30/0.4 kV | 1 | 3.78 | 1.30 |
| TP WT1CR-WT9CR | Dyn5 | 30/0.4 kV | 2.5 | 5.951672 | 0.76 |
| TP WT1CB-WT5CB | Dyn5 | 30/0.4 kV | 0.3 | 3.64 | 1.66 |
| TP WT1MM-WT5MM | Dyn5 | 30/0.4 kV | 0.3 | 3.64 | 1.66 |

**Table E.13. Power transformer characteristics at wind park substations**

| Id | Connection | U | $S_N$ | R(%) | X(%) |
|---|---|---|---|---|---|
| Montaña de la Mina | YNd11 | 30/66 kV | 5 MVA | 7.5 | 0.6 |
| Los Valles | YNd11 | 30/66 kV | 10 MVA | 9 | 0.55 |
| Cañada de la Barca | YNd11 | 30/66 kV | 5 MVA | 7.5 | 0.6 |
| Cañada del Rio | YNd11 | 30/66 kV | 20 MVA | 10 | 0.4 |

The regulation corresponding to the OP 2.2 [178] establishes that the initial generation dispatch shall be determined minimising the variable costs. The variable costs include the costs of the fuel, starting or spinning reserve costs, and variable costs of operation and maintenance. However, only variable costs related to the fuel consumption has been taken into account for this study. They can be calculated for each generating group based on [179]. Thus, cost functions are indicated in Table E.16. Recently, some reports have been issued containing recommendations to improve the technical and economic efficiency of the insular systems [158], which are out of the scope of this thesis.

In addition, in the OP 1 [178] it is stated that the primary regulation reserve shall be at least 50 % of the highest dispatch assigned to any on-line generating unit.

**Table E.14. Load scenarios in Fuerteventura-Lanzarote, 2013**

| Load Id | Peak demand | | Valley demand | |
|---|---|---|---|---|
| Las Salinas | 34.9 MW | 7.1 MVAr | 15.21 MW | 3.09 MVAr |
| Gran Tarajal | 10.2 MW | 2.1 MVAr | 4.42 MW | 0.9 MVAr |
| Matas Blancas | 48.1 MW | 9.8 MVAr | 21 MW | 4.26 MVAr |
| Corralejo | 20.9 MW | 4.2 MVAr | 9.1 MW | 1.85 MVAr |
| **Total Fuerteventura** | 114.1 MW | 23.2 MVAr | 49.73 MW | 10.1 MVAr |
| Playa Blanca | 31.7 MW | 6.4 MVAr | 15.25 MW | 3.1 MVAr |
| Macher | 27.8 MW | 5.7 MVAr | 13.4 MW | 2.72 MVAr |
| San Bartolomé | 13.7 MW | 2.8 MVAr | 6.64 MW | 1.34 MVAr |
| Punta Grande | 63.8 MW | 13 MVAr | 30.76 MW | 6.25 MVAr |
| **Total Lanzarote** | 137 MW | 27.9 MVAr | 66.05 MW | 13.41 MVAr |
| **Total** | 251.1 MW | 51.1 MVAr | 115.74 MW | 23.51 MVAr |

**Table E.15. Thermal generation scenarios in Fuerteventura-Lanzarote system**

| Case | Total | Wind | Thermal | Thermal L | Thermal F |
|---|---|---|---|---|---|
| **Case 1** | 251.1 MW | 0 MW | 251.1 MW | 137 MW | 114.1 MW |
| **Case 2** | 251.1 MW | 14.15 MW | 235.95 MW | 132.61 MW | 104.34 MW |
| **Case 3** | 251.1 MW | 28.3 MW | 222.8 MW | 128.22 MW | 94.57 MW |
| **Case 4** | 115.74 MW | 0 MW | 115.74 MW | 66.05 MW | 49.73 MW |
| **Case 5** | 115.74 MW | 14.15 MW | 101.59 MW | 61.66 MW | 39.97 MW |
| **Case 6** | 115.74 MW | 28.3 MW | 87.44 MW | 52.27 MW | 30.21 MW |

Note. L:Lanzarote, F:Fuerteventura

In addition, the sum of the primary and secondary reserve must be 100 % of the biggest generator on-line, the loss of interconnections to other islands or the loss of wind power (among other reasons). The biggest generating unit in Lanzarote corresponds to unit G12PG of 32.34 MW, and in Fuerteventura, to unit G11LS of 29.40 MW. However, gas turbines only generate in peak demand scenarios due to higher variable costs. Therefore, the maximum daily reserve is normally provided by the biggest Diesel units, i.e. units G6PG and G6LS of 20.51 MW. Regarding wind power, installed capacity amounts to 8.775 MW and 19.525 MW respectively in Lanzarote and Fuerteventura. Therefore, it shall not be considered for the reserve requirement calculation, as it can certainly be smaller than the biggest generator on-line. On the other hand, considering both islands as a unique power system, the spinning reserve could be minimised, being divided between the power stations of Punta Grande and Las Salinas. But in that case, the spinning reserve would not be guaranteed upon the loss of the interconnection between both islands.

The optimal unit commitment is summarised in Tables E.17 and E.18, where on-line generators are marked. For Punta Grande power plant G2PG and G3PG are reserved as emergency generators.

**Table E.16. Cost functions in Lanzarote and Fuerteventura**

| Generator Id. | Cost function (euros) |
|---|---|
| G1PG | $C = 118.786 + 166.55 \cdot P + 0.7915 \cdot P^2$ |
| G2PG | $C = 118.786 + 166.55 \cdot P + 0.7915 \cdot P^2$ |
| G3PG | $C = 118.786 + 166.55 \cdot P + 0.7915 \cdot P^2$ |
| G4PG | $C = 253.8 + 119.2588 \cdot P + 1.08 \cdot P^2$ |
| G5PG | $C = 253.8 + 119.2588 \cdot P + 1.08 \cdot P^2$ |
| G6PG | $C = 565.299 + 102.6 \cdot P + 1.1323 \cdot P^2$ |
| G7PG | $C = 709.5361 + 77.157 \cdot P + 2.681 \cdot P^2$ |
| G8PG | $C = 709.5361 + 77.157 \cdot P + 2.681 \cdot P^2$ |
| G9PG | $C = 709.5361 + 77.157 \cdot P + 2.681 \cdot P^2$ |
| G10PG | $C = 709.5361 + 77.157 \cdot P + 2.681 \cdot P^2$ |
| G11PG | $C = 1802.4628 + 194.7847 \cdot P + 0.2494 \cdot P^2$ |
| G12PG | $C = 2260.6778 + 171.373 \cdot P + 0.1047 \cdot P^2$ |
| G1LS | $C = 37.436 + 166.93 \cdot P + 1.7559 \cdot P^2$ |
| G2LS | $C = 37.436 + 166.93 \cdot P + 1.7559 \cdot P^2$ |
| G3LS | $C = 25.6922 + 178.6465 \cdot P + 1.309 \cdot P^2$ |
| G4LS | $C = 117.9585 + 166.8798 \cdot P + 0.7595 \cdot P^2$ |
| G5LS | $C = 117.9585 + 166.8798 \cdot P + 0.7595 \cdot P^2$ |
| G6LS | $C = 565.299 + 102.6 \cdot P + 1.132 \cdot P^2$ |
| G7LS | $C = 709.5361 + 77.1571 \cdot P + 2.681 \cdot P^2$ |
| G8LS | $C = 709.5361 + 77.1571 \cdot P + 2.681 \cdot P^2$ |
| G9LS | $C = 709.5361 + 77.1571 \cdot P + 2.681 \cdot P^2$ |
| G10LS | $C = 1804.61 + 194.49 \cdot P + 0.2587 \cdot P^2$ |
| G11LS | $C = 2260.6778 + 171.3735 \cdot P + 0.1047 \cdot P^2$ |

**Table E.17. On-line generators in Punta Grande for each study case**

| Case Id. | G1PG | G4PG | G5PG | G6-G9PG | G10-G12PG |
|---|---|---|---|---|---|
| 1 | | ✓ | ✓ | ✓ | ✓ |
| 2 | | ✓ | ✓ | ✓ | ✓ |
| 3 | | ✓ | ✓ | ✓ | ✓ |
| 4 | | ✓ | ✓ | ✓ | |
| 5 | | | ✓ | ✓ | |
| 6 | ✓ | | | ✓ | |

**Table E.18. On-line generators in Las Salinas for each study case**

| Case Id. | G1-G4LS | G5LS | G6-G8LS | G9LS | G10LS | G11LS |
|---|---|---|---|---|---|---|
| 1 | ✓ | ✓ | ✓ | ✓ | ✓ | ✓ |
| 2 | ✓ | ✓ | ✓ | ✓ | ✓ | ✓ |
| 3 | ✓ | ✓ | ✓ | ✓ | | ✓ |
| 4 | | ✓ | ✓ | ✓ | | |
| 5 | | | ✓ | ✓ | | |
| 6 | | | ✓ | | | |

# Bibliography


[1] "IEEE Guide for Planning DC Links Terminating at AC Locations Having Low Short-Circuit Capacities," *IEEE Std 1204-1997*, p. i, 1997.

[2] G. Delille, B. Francois, and G. Malarange, "Dynamic frequency control support by energy storage to reduce the impact of wind and solar generation on isolated power system's inertia," *IEEE Transactions on Sustainable Energy*, vol. 3, no. 4, pp. 931–939, 2012.

[3] M. Farias, P. Battaiotto, and M. Cendoya, "Wind farm to Weak-Grid connection using UPQC custom power device," in *Industrial Technology (ICIT), 2010 IEEE International Conference on*, 2010, pp. 1745–1750.

[4] J.O. Tande, G. di Marzio, and K.Uhlen, "System Requirements for Wind Power Plants," SINTEF Energy Research, Tech. Rep., Nov. 2007.

[5] N. Strachan and D. Jovcic, "Stability of a Variable-Speed permanent magnet wind generator with weak AC grids," *Power Delivery, IEEE Transactions on*, vol. 25, no. 4, pp. 2779–2788, 2010.

[6] I. D. Margaris, A. D. Hansen, N. A. Cutululis, P. Sorensen, and N. D. Hatziargyrou, *Operation and Control of Wind Farms in Non-Interconnected Power Systems*. InTech, 2011, vol. Chapter 8. [Online]. Available: http://orbit.dtu.dk/fedora/objects/orbit:64000/datastreams/file_5678103/content

[7] E. Haesen, F. Minne, J. Driesen, and M.H. J. Bollen, "Hosting capacity for motor starting in weak grids," *International Conference on Future Power Systems*, pp. 1–6, Nov. 2005.

[8] H. Haeder, "EU Islands: towards a sustainable energy future," EURELECTRIC, Tech. Rep. D/2012/12.105/24, Jun. 2012. [Online]. Available: http://www.eurelectric.org/media/38999/eu_islands_-_towards_a_sustainable_energy_future_-_eurelectric_report_final-2012-190-0001-01-e.pdf

[9] D. Marín, "Intégration des éoliennes dans les réseaux électriques insulaires," Ph.D. dissertation, Ecole Centrale de Lille, Laboratoire d'Electrotechnique et d'Electronique de Puissance de Lille, Lille, France, 2009.

[10] C. A. Bellés, "Electric vehicles charging from surplus wind power in non-connected islands," Master's thesis, Department of Mechanical and Aerospace Engineering, University of Strathclyde, 2012. [Online]. Available: http://www.esru.strath.ac.uk/Documents/MSc_2012/Ara.pdf

[11] P. Gardner and I. Papadopoulos, "The limiting factors for wind integration,"

Copenhagen, Apr. 2012. [Online]. Available: http://www.gl-garradhassan.com/assets/downloads/The_Limiting_Factors_for_Wind_Integration.pdf

[12] M. H. Ahmed, "New Models and Analytical Frameworks for Power Systems with Wind Generation Penetration," Ph.D. dissertation, University of Waterloo, Waterloo, Ontario, Canada, 2012. [Online]. Available: https://uwspace.uwaterloo.ca/bitstream/handle/10012/6792/Ahmed_Mohamed.pdf?sequence=1

[13] C. K. Simoglou, E. G. Kardakos, E. A. Bakirtzis, D. I. Chatzigiannis, S. I. Vagropoulos, A. V. Ntomaris, P. N. Biskas, A. Gigantidou, E. J. Thalassinakis, A. G. Bakirtzis, and J. P. S. Catalão, "An advanced model for the efficient and reliable short-term operation of insular electricity networks with high renewable energy sources penetration," *Renewable and Sustainable Energy Reviews*, vol. 38, pp. 415–427, Oct. 2014.

[14] A. Bizuayehu, P. Medina, J. P. Catalao, E. Rodrigues, and J. Contreras, "Analysis of electrical energy storage technologies' state-of-the-art and applications on islanded grid systems," in *T D Conference and Exposition, 2014 IEEE PES*, Apr. 2014, pp. 1–5.

[15] S. A. Papathanassiou and N. G. Boulaxis, "Power limitations and energy yield evaluation for wind farms operating in island systems," *Renewable Energy*, vol. 31, no. 4, pp. 457–479, Apr. 2006.

[16] "Workpackage 2 : Market applications in specific island power systems," STORIES project, Tech. Rep., Mar. 2009. [Online]. Available: http://ec.europa.eu/energy/intelligent/projects/sites/iee-projects/files/projects/documents/stories_market_applications_for_energy_storage_methods.pdf

[17] N. Hamsic, A. Schmelter, A. Mohd, E. Ortjohann, E. Schultze, A. Tuckey, and J. Zimmermann, "Increasing renewable energy penetration in isolated grids using a flywheel energy storage system," in *International Conference on Power Engineering, Energy and Electrical Drives, 2007. POWERENG 2007*, Apr. 2007, pp. 195–200.

[18] K. Burman, D. Olis, V. Gevorgian, A. Warren, R. Butt, P. Lilienthal, and J. Glassmire, "Integrating Renewable Energy into the Transmission and Distribution System of the U.S. Virgin Islands," Energy Development in Island Nations EDIN, Tech. Rep. NREL/TP-7A20-51294, Sep. 2011. [Online]. Available: http://www.edinenergy.org/pdfs/51294.pdf

[19] J. Kumagai, "The smartest, greenest grid," *IEEE Spectrum*, vol. 50, no. 5, pp. 42–47, May 2013.

[20] "Arreté du 23 avril 2008 relatif aux prescriptions techniques de conception et de fonctionnement pour le raccordement au réseau public de transport d'électricité d'une installation de production d'énergie électrique," *Ministère de l'Ecologie*, Jul. 2010. [Online]. Available: http://www.legifrance.gouv.fr/affichTexte.do;jsessionid=1A8F4D7DE73520F89503063607E22F86.tpdjo10v_2?cidTexte=LEGITEXT000018728709&dateTexte=20120225

[21] J. Kaldellis, "Maximum wind potential exploitation in autonomous electrical networks on the basis of stochastic analysis," *Journal of Wind Engineering and Industrial Aerodynamics*, vol. 96, no. 8âĂŞ9, pp. 1412–1424, Aug. 2008. [Online]. Available: http://www.sciencedirect.com/science/article/pii/S0167610508001013

[22] D. Weisser and R. S. Garcia, "Instantaneous wind energy penetration in isolated electricity grids: concepts and review," *Renewable Energy*, vol. 30, no. 8, pp. 1299–1308, Jul. 2005. [Online]. Available: http://www.sciencedirect.com/science/article/pii/S0960148104004021

[23] Eric Vales, "Actu-environment," May 2012. [Online]. Available: http://www.actu-environnement.com/ae/news/eric-vales-reseaux-insulaires-stockage-energie-eolienne-15707.php4

[24] M. Charlet, "SEI EDF guadeloupe," Jun. 2009. [Online]. Available: http://interreg-caraibes.fr/IMG/pdf/MR_CHARLET_Compatibility_Mode_.pdf

[25] O. Göksu, *Control of Wind Turbines during Symmetrical and Asymmetrical Grid Faults*, ser. PhD Thesis. Department of Energy Technology, Aalborg University, 2012.

[26] "Decreto Regulamentar Regional ÂtN. 15/2004/M. Aprova o Regulamento da Qualidade de Serviço do Sistema Eléctrico de Serviço Público da Região Autónoma da Madeira," *Região Autónoma da Madeira. Presidéncia do Governo*, 2004.

[27] A. Bizuayehu, E. Rodrigues, S. Santos, J. Catalao, and J. Contreras, "Assessment on baseline and higher order grid security criteria: Prospects for insular grid applications," in *2014 IEEE PES General Meeting | Conference Exposition*, Jul. 2014, pp. 1–5.

[28] M. Harper, "Review of Strategies and Technologies for Demand-Side Management on Isolated Mini-Grids," Lawrence Berkeley National Laboratory, Schatz Energy Research Center, California, USA, Tech. Rep. LBNLÂŋâĂŘ6223E, Mar. 2013. [Online]. Available: http://www.cleanenergyministerial.org/Portals/2/pdfs/Review_of_Strategies_and_Technologies_for_DSM_on_MiniGrids.pdf

[29] K. De Vos, A. G. Petoussis, J. Driesen, and R. Belmans, "Revision of reserve requirements following wind power integration in island power systems," *Renewable Energy*, vol. 50, pp. 268–279, Feb. 2013.

[30] H. Vasconcelos, C. Moreira, A. Madureira, J. Lopes, and V. Miranda, "Advanced Control Solutions for Operating Isolated Power Systems: Examining the Portuguese islands." *IEEE Electrification Magazine*, vol. 3, no. 1, pp. 25–35, Mar. 2015.

[31] P. Tielens, S. De Rijcke, K. Srivastava, M. Reza, A. Marinopoulos, and J. Driesen, "Frequency support by wind power plants in isolated grids with varying

generation mix," in *2012 IEEE Power and Energy Society General Meeting*, Jul. 2012, pp. 1–8.

[32] M. Zubiaga, S. Aurtenetxea, J. Chivite, A. Etxegarai, E. Torres, and P. Eguia, "Frequency restoration in insular grids with high penetration of wind power," in *IECON 2013 - 39th Annual Conference of the IEEE Industrial Electronics Society*, Nov. 2013, pp. 2045–2050.

[33] M. Mohseni and S. M. Islam, "Review of international grid codes for wind power integration: Diversity, technology and a case for global standard," *Renewable and Sustainable Energy Reviews*, vol. 16, no. 6, pp. 3876 – 3890, 2012.

[34] Z. Yong, D. Zhengang, and L. Xuelian, "Comparison of Grid Code Requirements with Wind Turbine in China and Europe," in *Power and Energy Engineering Conference (APPEEC), 2010 Asia-Pacific*, 2010, pp. 1–4.

[35] M. P. Comech, M. García-Gracia, S. Martín Arroyo, and M. A. Martínez Guilén, "Wind farms and grid codes," in *From Turbine to Wind Farms - Technical Requirements and Spin-Off Products*, G. Krause, Ed. InTech, Apr. 2011. [Online]. Available: http://www.intechopen.com/books/from-turbine-to-wind-farms-technical-requirements-and-spin-off-products/wind-farms-and-grid-codes

[36] M. Gustavo and J. Gimenez, "Technical and regulatory exigencies for grid connection of wind generation," in *Wind Farm - Technical Regulations, Potential Estimation and Siting Assessment*, G. O. Suvire, Ed. InTech, Jun. 2011. [Online]. Available: http://www.intechopen.com/books/wind-farm-technical-regulations-potential-estimation-and-siting-assessment/technical-and-regulatory-exigencies-for-grid-connection-of-wind-generation

[37] M. Altin, O. Goksu, R. Teodorescu, P. Rodriguez, B.-B. Jensen, and L. Helle, "Overview of recent grid codes for wind power integration," in *Optimization of Electrical and Electronic Equipment (OPTIM), 2010 12th International Conference on*, 2010, pp. 1152–1160.

[38] L. Rouco, K. Chan, J. Oesterheld, and S. Keller, "Recent evolution of European grid code requirements and its impact on turbogenerator design," in *Power and Energy Society General Meeting, 2012 IEEE*, 2012, pp. 1–9.

[39] C. Sourkounis and P. Tourou, "Grid Code Requirements for Wind Power Integration in Europe," in *Conference Papers in Energy*, 2013.

[40] F. Díaz-González, M. Hau, A. Sumper, and O. Gomis-Bellmunt, "Participation of wind power plants in system frequency control: Review of grid code requirements and control methods," *Renewable and Sustainable Energy Reviews*, vol. 34, pp. 551–564, Jun. 2014.

[41] J. Merino and C. Veganzones, "State of the art and future trends in grid codes applicable to isolated power systems," in *Proceedings of the 1st Int. e-Conf. on Energies*, Mar. 2014.

[42] "National Electricity Rules Version 59," *Australian Energy Market Commission AEMC*, Oct. 2013.

[43] "Technical regulation 3.2.5 for wind power plants with a power output greater than 11 kW," *Energinet*, Sep. 2010.

[44] "Technical regulation 3.2.3. for thermal power station units of 1.5 MW and higher," *Energinet*, Oct. 2008.

[45] "REFERENTIEL TECHNIQUE HTB Relatif aux prescriptions techniques de conception et de fonctionnement pour le raccordement d'une installation de production d'énergie électrique au réseau public HTB > 50 kV des Zones Non Interconnectées," *EDF-SEI*, Dec. 2008. [Online]. Available: http://sei.edf.com/fichiers/fckeditor/Commun/SEI/corp/PKGC5-nov2008.pdf

[46] "The Grid Code. Issue 5, version 4," *National Grid Electricity Transmission PLC*, Aug. 2013.

[47] "SONI Grid Code," *SONI*, Feb. 2012. [Online]. Available: http://www.soni.ltd.uk/upload/SONI%20GRID%20CODE%202%20FEBRUARY%202012.pdf

[48] "EirGrid grid code v. 4.0." *EirGrid*, Dec. 2011.

[49] "Electricity Industry Participation Code," *Ministry of Economic Development*, Jul. 2013. [Online]. Available: http://www.ea.govt.nz/document/16116/download/act-code-regs/code-regs/the-code/

[50] "Procedimiento de operación P.O. 1 SEIE," *REE*, May 2006. [Online]. Available: http://www.ree.es

[51] "Propuesta modificación P.O. 12.2 SEIE," *REE*, Nov. 2009. [Online]. Available: http://www.ree.es

[52] "Tasmanian Frequency Operating Standard Review. Final report," *Australian Energy Market Commission AEMC*, Dec. 2008.

[53] "Generic Grid Code Format for Wind Power Plants," European Wind Energy Association (EWEA), Tech. Rep., Nov. 2009. [Online]. Available: http://www.ewea.org/fileadmin/ewea_documents/documents/publications/091127_GGCF_Final_Draft.pdf

[54] A. Ellis, "Reactive Power Interconnection Requirements for PV and Wind Plants. Recommendations to NERC," Sandia National Laboratories, Albuquerque, New Mexico, Tech. Rep. SAND201 2 - 1098, Feb. 2012. [Online]. Available: http://energy.sandia.gov/wp/wp-content/gallery/uploads/Reactive-Power-Requirements-for-PV-and-Wind-SAND2012-1098.pdf

[55] "Generator Fault Ride through (FRT) investigation. Literature review," Transpower, Tech. Rep. GEN FRT: S1, Feb. 2009.

[56] W. Qureshi, G. Demler, and N.-K. Nair, "Developing transmission fault ride-through criteria for New Zealand wind farms," in *2011 IEEE Power and Energy Society General Meeting*, Jul. 2011, pp. 1–7.

[57] "Wind integration: International experience. WP2: Review of Grid Codes," Ecar Energy and AEMO, Tech. Rep., Oct. 2011.

[58] W. Christiansen and D. T. Johnsen, "Analysis of requirements in selected grid codes," Technical University of Denmark, Lyngby, Denmark, Tech. Rep., Jan. 2006. [Online]. Available: http://bibing.us.es/proyectos/abreproy/70370/fichero/24.+Analysis+of+the+requirements+in+selected+Grid+Codes.pdf

[59] A. Colmenar-Santos, O. Monzón-Alejandro, D. Borge-Diez, and M. Castro-Gil, "The impact of different grid regulatory scenarios on the development of renewable energy on islands: A comparative study and improvement proposals," *Renewable Energy*, vol. 60, pp. 302–312, Dec. 2013.

[60] "ENTSO-E Network Code for Requirements for Grid Connection Applicable to all Generators," ENTSO-E, Tech. Rep., Mar. 2013.

[61] M. Sjölund, "Study of Grid Code Compliance: Thanet Wind Farm," Uppsala Universitet, Uppsala, Sweden, Examensarbete UPTEC-ES12026, Aug. 2012. [Online]. Available: http://uu.diva-portal.org/smash/get/diva2:548924/FULLTEXT01.pdf

[62] A. Etxegarai, P. Eguia, E. Torres, A. Iturregi, and V. Valverde, "Review of grid connection requirements for generation assets in weak power grids," *Renewable and Sustainable Energy Reviews*, vol. 41, pp. 1501–1514, Jan. 2015.

[63] B. Badrzadeh and A. Halley, "Challenges associated with assessment and testing of fault ride-through compliance of variable power generation in australian national electricity market," *IEEE Transactions on Sustainable Energy*, vol. PP, no. 99, pp. 1–9, 2014.

[64] D. Popovic and I. Wallace, "International Review of Fault Ride Through for Conventional Generators," Kema, Tech. Rep. 16010829, Nov. 2010.

[65] L. Lindgren, J. Svensson, and L. Gertmar, "Generic models for Wind Power Plants. Needs and previous work," Elforsk, Stockholm, Tech. Rep. Elforsk rapport 12:47, Jul. 2012.

[66] P. Southwell and Z. Bozic, "Results of survey of requirements on generator data and the need for confidentiality," *CIGRÉ Electra magazine*, vol. 224, pp. 44–45, Feb. 2006. [Online]. Available: http://c1.cigre.org/Media/SC/C1/Publications/Electra

[67] "The National Electricity Rules," *Australian Energy Market Commission AEMC*. [Online]. Available: http://www.aemc.gov.au/Electricity/National-Electricity-Rules/Current-Rules.html

[68] "Generating System Model Guidelines," *Australian Energy Market Operator AEMO*, Feb. 2008.

[69] "Data and model requirements for generating systems of less than 30 MW," *Australian Energy Market Operato AEMO*, Nov. 2012.

[70] "Dynamic Model Acceptance Guideline," *Australian Energy Market Operator AEMO*, Jun. 2013.

[71] "Technical regulation 3.2.5. for wind power plants with a power output greater than 11 kW," *Energinet*, Sep. 2010. [Online]. Available: http://www.energinet.dk/SiteCollectionDocuments/Engelske%20dokumenter/El/55986-10_v1_Grid%20Code%203%202%205_v%204%201-30%20%20September%202010.pdf

[72] "FGW Technical Guidelines for Power Generating Units Part 3. Determination of electrical characteristics of power generating units and systems connected to MV, HV and EHV grids," *FGW Fördergesellschaft Windenergie und andere Erneuerbare Energien*, May 2013. [Online]. Available: http://www.wind-fgw.de/

[73] "FGW Technical Guidelines for Power Generating Units Part 4. Demands on Modelling and Validating Simulation Models of the Electrical Characteristics of Power Generating Units and Systems," *FGW Fördergesellschaft Windenergie und andere Erneuerbare Energien*, May 2013. [Online]. Available: http://www.wind-fgw.de/

[74] "Connecting and Dispatching New Generation in New Zealand. Overview," Transpower New Zealand Ltd, Tech. Rep., 2007.

[75] "Asset Capability Information Overview. Guideline," Transpower New Zealand Ltd., Tech. Rep. Version 4.1., Oct. 2010.

[76] "Resolución de 24 de julio de 2012, de la secretaría de estado de energía, por la que se aprueba la modificación de los procedimientos de operación del sistema eléctrico peninsular (SEP) P.O.-3.1; P.O.-3.2; P.O.-9 y P.O.-14.4 y los procedimientos de operación de los sistemas eléctricos insulares y extrapeninsulares (SEIE) P.O. SEIE-1 P.O. SEIE-2.2; P.O. SEIE-3.1; P.O. SEIE-7.1; P.O. SEIE-7.2; P.O. SEIE-8.2; P.O. SEIE-9 y P.O. SEIE-2.3 para su adaptación a la nueva normativa eléctrica." *Ministerio de Industria, Energía y Turismo*, Aug. 2012.

[77] "Guía descriptiva del procedimiento de puesta en servicio," *REE*, no. Version 1.0, Jan. 2011. [Online]. Available: http://www.ree.es

[78] "Requisitos de los modelos de instalaciones eólicas, fotovoltaicas y todas aquellas que no utilicen generadores síncronos directamente conectados a la red," *REE*, oct 2010. [Online]. Available: http://www.ree.es

[79] "Condiciones de validación y aceptación de los modelos," *REE*, Oct. 2010. [Online]. Available: http://www.ree.es

[80] "Guidance notes. Power Park Modules," *National Grid*, Sep. 2012.

[81] P. Ravalli and J. Leung, "Dynamic model requirements and model validation in the australian national electricity market," in *2011 IEEE Power and Energy Society General Meeting*, Jul. 2011, pp. 1–5.

[82] S. Zhao and N.-K. Nair, "Assessment of wind farm models from a transmission

system operator perspective using field measurements," *IET Renewable Power Generation*, vol. 5, no. 6, pp. 455–464, Nov. 2011.

[83] J. Feltes and B. Fernandes, "Wind turbine generator dynamic performance with weak transmission grids," in *2012 IEEE Power and Energy Society General Meeting*, Jul. 2012, pp. 1–7.

[84] M. Asmine, J. Brochu, J. Fortmann, R. Gagnon, Y. Kazachkov, C.-E. Langlois, C. Larose, E. Muljadi, J. MacDowell, P. Pourbeik, S. Seman, and K. Wiens, "Model validation for wind turbine generator models," in *2011 IEEE Power and Energy Society General Meeting*, Jul. 2011, pp. 1–1.

[85] T. Gehlhaar, T. Wehrend, H. Lankowski, and D. Schulz, "Need of harmonized generic model standards for flexible grids in a smart future," in *Proceedings*, Aarhus, Denmark, Oct. 2011.

[86] A. Ellis, Y. Kazachkov, E. Muljadi, P. Pourbeik, and J. Sanchez-Gasca, "Description and technical specifications for generic WTG models - a status report," in *Power Systems Conference and Exposition (PSCE), 2011 IEEE/PES*, Mar. 2011, pp. 1–8.

[87] "Generic Solar Photovoltaic System Dynamic Simulation Model Specification," Western Electricity Coordinating Council Modeling and Validation Work Group, WECC Renewable Energy Modeling Task Force, Tech. Rep. Sandia Contract #1047506, Sep. 2012. [Online]. Available: http://www.powerworld.com/files/WECC-Solar-PV-Dynamic-Model-Specification-September-2012.pdf

[88] P. Pourbeik, D. Sullivan, A. Bostrom, J. Sanchez-Gasca, Y. Kazachkov, J. Kowalski, A. Salazar, A. Meyer, R. Lau, D. Davies, and E. Allen, "Generic model structures for simulating static var systems in power system studies - a WECC task force effort," *IEEE Transactions on Power Systems*, vol. 27, no. 3, pp. 1618–1627, Aug. 2012.

[89] S. Cole and R. Belmans, "A proposal for standard VSC HVDC dynamic models in power system stability studies," *Electric Power Systems Research*, vol. 81, no. 4, pp. 967–973, Apr. 2011.

[90] C. Hahn, A. Semerow, M. Luther, and O. Ruhle, "Generic modeling of a line commutated HVDC system for power system stability studies," in *T D Conference and Exposition, 2014 IEEE PES*, Apr. 2014, pp. 1–6.

[91] P. Sorensen, B. Andresen, J. Fortmann, and P. Pourbeik, "Modular structure of wind turbine models in IEC 61400-27-1," in *2013 IEEE Power and Energy Society General Meeting (PES)*, Jul. 2013, pp. 1–5.

[92] L. Hajagos, J. Barton, R. Berube, M. Coultes, J. Feltes, G. Lanier, S. Patterson, L. Pereira, P. Pourbeik, A. Schneider, and R. Jones, "Guidelines for generator stability model validation testing," in *IEEE Power Engineering Society General Meeting, 2007*, Jun. 2007, pp. 1–16.

[93] J. Fortmann, S. Engelhardt, J. Kretschmann, C. Feltes, and I. Erlich, "Validation of an rms dfig simulation model according to new german model validation standard fgw tr4 at balanced and unbalanced grid faults," *Proceedings / 8th International Workshop on the Large-Scale Integration of Wind Power into Power Systems as well as on Transmission Networks for Offshore Wind Wind Power Farms : 14-15 October 2009, Bremen, Germany*, 2009. [Online]. Available: http://www.uni-due.de/ean/downloads/papers/fortmann2009.pdf

[94] L. Pereira, "Introduction and background to synchronous unit testing and model validation in the WSCC," in *IEEE Power Engineering Society 1999 Winter Meeting*, vol. 1, Jan. 1999, pp. 151–156 vol.1.

[95] R. Rifaat, "Independent power producers (IPP) perspectives and experiences with WSCC requirements for generator model validation tests," in *Conference Record of the 2000 IEEE Industry Applications Conference, 2000*, vol. 2, 2000, pp. 924–931 vol.2.

[96] L. Hajagos, "Guidelines for generator stability model validation testing," in *IEEE Power Engineering Society General Meeting, 2003*, vol. 3, Jul. 2003, pp. –1294 Vol. 3.

[97] P. Pourbeik, "Automated parameter derivation for power plant models from system disturbance data," in *IEEE Power Energy Society General Meeting, 2009. PES '09*, Jul. 2009, pp. 1–10.

[98] P. Dandeno, H. Karmaker, C. Azuaje, M. Glinkowski, I. Kamwa, S. Salon, R. Saunders, and S. Umans, "Experience with standstill frequency response (SSFR) testing and analysis of salient pole synchronous machines," *IEEE Transactions on Energy Conversion*, vol. 14, no. 4, pp. 1209–1217, Dec. 1999.

[99] J. Niiranen, S. Seman, J. Matsinen, R. Virtanen, and A. Vilhunen, "Technical Paper: Low voltage ride-through testing of wind turbine converters at ABB helps wind turbines meet the requirements of IEC61400-21 more quickly," ABB, Tech. Rep., 2013.

[100] J. Niiranen, "Experiences on voltage dip ride through factory testing of synchronous and doubly fed generator drives," in *2005 European Conference on Power Electronics and Applications*, 2005, pp. 11 pp.–P.11.

[101] Y. Coughlan, P. Smith, A. Mullane, and M. O'Malley, "Wind turbine modelling for power system stability analysis-a system operator perspective," *IEEE Transactions on Power Systems*, vol. 22, no. 3, pp. 929–936, Aug. 2007.

[102] C. Wessels, R. Lohde, and F. Fuchs, "Transformer based voltage sag generator to perform lvrt and hvrt tests in the laboratory," in *Power Electronics and Motion Control Conference (EPE/PEMC), 2010 14th International*, 2010, pp. T11–8–T11–13.

[103] C. Veganzones, J. A. Sanchez, S. Martinez, C. A. Platero, F. Blazquez, D. Ramirez, J. R. Arribas, J. Merino, N. Herrero, and F. Gordillo, "Voltage dip

generator for testing wind turbines connected to electrical networks," *Renewable Energy*, vol. 36, no. 5, pp. 1588–1594, May 2011.

[104] Y. Yang, F. Blaabjerg, and Z. Zou, "Benchmarking of voltage sag generators," in *IECON 2012 - 38th Annual Conference on IEEE Industrial Electronics Society*, Oct. 2012, pp. 943–948.

[105] Abdullah Al Mahfazur Rahman and Muhammad Usman Sabbir, "Grid code testing by voltage source converter," Master's Thesis in the Master Degree Programme, Electric Power Engineering, Chalmers University of Technology, Göteborg, Sweden, 2012.

[106] [Online]. Available: http://www.4fores.es

[107] "Wind Turbines, Part 21: Measurement and assessment of power quality characteristics of grid connected wind turbines," *IEC-61400-21*, 2008.

[108] E. Muljadi and A. Ellis, "Validation of wind power plant models," in *2008 IEEE Power and Energy Society General Meeting - Conversion and Delivery of Electrical Energy in the 21st Century*, Jul. 2008, pp. 1–7.

[109] Jan Pierik, Johan Morren, Tim van Engelen, Sjoerd de Haan, and Jan Bozelie, "Development and validation of wind farm models for power system studies. alsvik wind farm results," in *Conference Proceedings*, Athens, Greece, 2006. [Online]. Available: http://www.ewea.org/ewec2006/allfiles2/956_Ewec2006fullpaper.pdf

[110] T. Gehlhaar, "Grid code compliance beyond simple LVRT," in *Germanischer Lloyd*, 2012.

[111] "Commissioning requirements for generating systems," *Australian Energy Market Operator AEMO*, Aug. 2012.

[112] "Template for generator compliance programs," *Reliability Panel AEMC*, Jul. 2009.

[113] "Appendix 5.1. Wind power plants with a power output range of 1.5 MW to 25 MW. technical regulation for grid connection TF 3.2.5," *Energinet*, no. Version 4.1, Sep. 2010. [Online]. Available: http://www.energinet.dk/EN/El/Forskrifter/Technical-regulations/Sider/Regulations-for-grid-connection.aspx

[114] "Appendix 5.2. Wind power plants greater than 25 MW. Technical regulation for grid connection TF 3.2.5," *Energinet*, no. Version 4.1, Sep. 2010. [Online]. Available: http://www.energinet.dk/EN/El/Forskrifter/Technical-regulations/Sider/Regulations-for-grid-connection.aspx

[115] "Grid code compliance test procedure," *EirGrid*, Aug. 2010.

[116] "Companion Guide for Testing of Assets," *Transpower*, Oct. 2012.

[117] "Procedure for verification, validation and certification of the requirements of P.O.12.3 on the response of wind farms and photovoltaic plants in the

event of voltage dips," *REE*, no. Version 9, May 2011. [Online]. Available: http://www.aeeolica.org/uploads/documents/1306-pvvc-n9-english.pdf

[118] A. Das and M.-K. Schwarz, "Grid connectivity issues and the importance of GCC," Apr. 2013.

[119] Mike Woebbeking, "IEC TS 61400-22 (first revision of IEC WT 01). The new standard for Wind Turbines and Wind Farms. Onshore and Offshore," Germanischer Lloyd Industrial Services GmbH, Business Segment Wind Energy (GL), Tech. Rep., 2008. [Online]. Available: http://www.gl-group.com/pdf/IEC_TS_61400-22_Woeb.pdf

[120] "IEC 61400-22 Ed1.0. Wind turbines - Part 22: Conformity testing and certification," *IEC International Electrotechnical Commission*, May 2010.

[121] "FGW Technical Guidelines for Power Generating Units Part 8. Certification of the Electrical Characteristics of Power Generating Units and Systems in the Medium-, High- and Highest-voltage grids," *FGW Fördergesellschaft Windenergie und andere Erneuerbare Energien*, May 2013. [Online]. Available: http://www.wind-fgw.de/

[122] "R2 Testing Guideline," *Australian Energy Market Operator AEMO*, 2013.

[123] I. Egido, F. Fernandez-Bernal, P. Centeno, and L. Rouco, "Maximum frequency deviation calculation in small isolated power systems," *Power Systems, IEEE Transactions on*, vol. 24, no. 4, pp. 1731–1738, 2009.

[124] J. Machowski, J. Bialek, and D. J. Bumby, *Power System Dynamics: Stability and Control*. John Wiley & Sons, Aug. 2011.

[125] P. Anderson and M. Mirheydar, "A low-order system frequency response model," *Power Systems, IEEE Transactions on*, vol. 5, no. 3, pp. 720–729, 1990.

[126] L. Sigrist, "Design of UFLS schemes for small isolated power systems. Diseño de esquemas de deslastre de cargas por frecuencia de pequeños sistemas aislados," Ph.D. dissertation, Universidad Pontificia de Comillas, 2010.

[127] P. Kundur, N. J. Balu, and M. G. Lauby, *Power system stability and control*. McGraw-Hill, Jan. 1994.

[128] G. R. Lalor, "Frequency control on an island power system with evolving plant mix," Ph.D. dissertation, University College Dublin, Sep. 2005. [Online]. Available: http://erc.ucd.ie/files/theses/Gill%20Lalor%20-%20Frequency%20Control%20on%20an%20Island%20Power%20System%20with%20Evolving%20Plant%20Mix.pdf

[129] M. Chan, R. Dunlop, and F. Schweppe, "Dynamic Equivalents for Average System Frequency Behavior Following Major Disturbances," *IEEE Transactions on Power Apparatus and Systems*, vol. PAS-91, no. 4, pp. 1637–1642, 1972.

[130] D. L. H. Aik, "A general-order system frequency response model incorporating load shedding: analytic modeling and applications," *IEEE Transactions on Power Systems*, vol. 21, no. 2, pp. 709–717, 2006.

[131] "IEEE Recommended Practice for Functional and Performance Characteristics of Control Systems for Steam Turbine-Generator Units," *IEEE Std 122-1991*, pp. 1–, 1992.

[132] M. Readlay, "Voltage Sag Source Location in Power Systems," Master's thesis, Chalmers University of Technology, Göteborg, Sweden, Dec. 2006. [Online]. Available: http://webfiles.portal.chalmers.se/et/MSc/MakalikiReadlayMSc.pdf

[133] CIGRÉ Working Group C4.110, "Voltage dip immunity of equipment and installations," CIGRÉ, Tech. Rep. 412, Apr. 2010. [Online]. Available: http://www.uie.org/webfm_send/371

[134] S. Papathanassiou and M. Papadopoulos, "Evaluation of voltage dip characteristics in autonomous island networks and correlation with wind turbine FRT curve," in *Electricity Distribution - Part 2, 2009. CIRED 2009. The 20th International Conference and Exhibition on*, 2009, pp. 1–4.

[135] "IEEE Recommended Practice for Monitoring Electric Power Quality," *IEEE Std 1159-1995*, pp. i–, 1995.

[136] M. Bollen, *Understanding power quality problems: voltage sags and interruptions*. IEEE Press, 2000.

[137] ——, "Characterisation of voltage sags experienced by three-phase adjustable-speed drives," *Power Delivery, IEEE Transactions on*, vol. 12, no. 4, pp. 1666 –1671, Oct. 1997.

[138] Zhang Lidong, "Characterisation and assessment of voltage dips," Ph.D. dissertation, Chalmers University of Technology, Göteborg, Sweden, 1999.

[139] Gabriel Olguin, "Stochastic assessment of voltage dips caused by faults in large transmission system," Thesis for the degree of Licentiate of Engineering, Chalmers University of Technology, Göteborg, Sweden, 2003. [Online]. Available: http://webfiles.portal.chalmers.se/et/Lic/OlguinGabrielLic.pdf

[140] Y. Hase, *Handbook of Power Systems Engineering with Power Electronics Applications*. John Wiley & Sons, Oct. 2012.

[141] B. Monchusi, Y. Mitani, L. Changsong, and S. Dechanupaprittha, "Power system stability assessment based on synchronized phasor measurements," in *Power and Energy Conference, 2008. PECon 2008. IEEE 2nd International*, Dec. 2008, pp. 94 –99.

[142] K. Geisler and D. Reitan, "Conversion of transient stability problems to equivalent systems employing an infinite bus," *Proceedings of the IEEE*, vol. 69, no. 6, pp. 758 – 760, Jun. 1981.

[143] B. Yin, R. Oruganti, S. Panda, and A. K. S. Bhat, "An output-power-control strategy for a three-phase PWM rectifier under unbalanced supply conditions," *IEEE Transactions on Industrial Electronics*, vol. 55, no. 5, pp. 2140–2151, 2008.

[144] Y. Zhou, P. Bauer, J. Ferreira, and J. Pierik, "Operation of grid-connected DFIG under unbalanced grid voltage condition," *IEEE Transactions on Energy Conversion*, vol. 24, no. 1, pp. 240–246, 2009.

[145] F. Jiang, Z. Bo, and L. Roumei, "Performance of induction generator in parallel with an unbalanced three phase system," in *1998 International Conference on Power System Technology, 1998. Proceedings. POWERCON '98*, vol. 2, 1998, pp. 1193–1197 vol.2.

[146] I. Margaris, "Work Package 9: Electrical grid. Deliverable D9.3.3 Power system requirements for high wind penetration. Part3: Small island grid," NTUA, Tech. Rep., Sep. 2007. [Online]. Available: http://www.upwind.eu/pdf/Report2007D933Part3.pdf

[147] G. Chicco, F. Corona, R. Porumb, and F. Spertino, "Experimental Indicators of Current Unbalance in Building-Integrated Photovoltaic Systems," *IEEE Journal of Photovoltaics*, vol. 4, no. 3, pp. 924–934, May 2014.

[148] Michal Pokorny, "Analysis of unbalance due to asymmetrical loads," *Iranian Journal of Electrical and Computer Engineering*, vol. 4, no. 1, 2005.

[149] M. Chindris, A. Cziker, A. Miron, H. Balan, A. Iacob, and A. Sudria, "Propagation of unbalance in electric power systems," in *9th International Conference on Electrical Power Quality and Utilisation, 2007. EPQU 2007*, 2007, pp. 1–5.

[150] Y.-J. Wang, "An analytical study on steady-state performance of an induction motor connected to unbalanced three-phase voltage," in *IEEE Power Engineering Society Winter Meeting, 2000*, vol. 1, 2000, pp. 159–164 vol.1.

[151] Prabodha Paravithana, "Contributions towards the development of the TEchnical report IEC/TR 61000-3-13 on voltage unbalance emission allocation," PhD thesis, School of Electrical, Computer and Telecommunications Engineering, University of Wollongong, 2009. [Online]. Available: http://ro.uow.edu.au/theses/834/

[152] P. M. Anderson, *Analysis of faulted power systems*. IEEE Press, Jun. 1995.

[153] J. D. Rodríguez Bordón, "Estudio sobre las interconexiones de los sistemas eléctricos de las islas canarias," Universidad de Las Palmas de Gran Canaria ULPGC, Tech. Rep., Oct. 2011. [Online]. Available: http://acceda.ulpgc.es/

[154] "Caracterização das redes de transporte e distribução da Região Autonoma dos Açores 2012," Electricidade dos Açores S.A., Tech. Rep., Dec. 2012. [Online]. Available: http://www.eem.pt/images/stories/documents/SEPM_2012.pdf

[155] E. Loukarakis and G. Stavrakakis, "Investigation of spinning reserve impact on isolated systems DC interconnection feasibility," in *2011 10th International Conference on Environment and Electrical Engineering (EEEIC)*, May 2011, pp. 1–5.

[156] "Generator fault ride through (frt) investigation. Stage 1," Transpower, Tech. Rep., Feb. 2009.

[157] "Red de Transporte de Canarias," *REE*, Jan. 2013. [Online]. Available: http://www.ree.es/sites/default/files/01_ACTIVIDADES/Documentos/Mapas-de-red/mapa_transporte_canarias_2013.pdf

[158] Pilar Meneses de Quevedo et al., "Report on the scenario analysis for the sinsular electricity grids and development completed for risk analysis tools," Tech. Rep. Singular 7th Framework Programme. Deliverable 6.2, Jul. 2014. [Online]. Available: http://www.singular-fp7.eu

[159] "Procedimientos de operación SEIE," *REE*, 2006. [Online]. Available: http://www.ree.es/operacion/procedimientos_operacion_insulares-extrapeninsulares.asp

[160] "Revisión PECAN 2006-2015," Gobierno de Canarias, Consejería de Empleo, Industria y Comercio, Tech. Rep., Jan. 2012.

[161] N. W. Miller, M. Shao, and S. Venkataraman, "California ISO (CAISO). Frequency Response Study," GE Energy, Tech. Rep., Nov. 2011. [Online]. Available: http://www.uwig.org/Report-FrequencyResponseStudy.pdf

[162] M. H. Osório Pestana de Vasconcelos, "Application of hybrid automatic learning techniques for fast dynamic security assessment of isolated power systems with wind production," Ph.D. dissertation, Faculdade de Engenharia da Universidade do porto, Sep. 1999. [Online]. Available: repositorio-aberto.up.pt/bitstream/10216/19532/2/20260.pdf

[163] J. O'Sullivan, M. Power, M. Flynn, and M. O'Malley, "Modelling of frequency control in an island system," in *IEEE Power Engineering Society 1999 Winter Meeting*, vol. 1, Jan. 1999, pp. 574–579 vol.1.

[164] C. Loutan, "Frequency Control Issues and Related Operational Experience/Efforts to manage Operational Impacts," EPRI, Tech. Rep., Apr. 2012. [Online]. Available: http://mydocs.epri.com/docs/publicmeetingmaterials/4-17-2012/13-Frequency-Control-Issues-Clyde-Loutan.pdf

[165] "AUFLS Scheme Design. Technical Summary," Transpower, Tech. Rep., Aug. 2013. [Online]. Available: http://www.systemoperator.co.nz/sites/default/files/bulk-upload/documents/20130807%20AUFLS%20Scheme%20Design%20Report.pdf

[166] J. L. Blackburn, *Symmetrical Components for Power Systems Engineering*. CRC Press, Jun. 1993.

[167] P. Eguia, A. Etxegarai, E. Torres, S. M. J. Ignacio, and I. Albizu, "Modelos dinámicos genéricos de plantas fotovoltaicas: parametrizaciónn y validación," in *XVI ERIAC Encuentro Regional Iberoamericano de CIGRE*.

[168] Power System Dynamic Performance Committee, Power System Stability Subcommittee, and Task Force on Turbine-Governor Modeling, "Dynamic Models for Turbine-Governors in Power System Studies," IEEE Power & Energy Society, Technical report PES-TR1, Jan. 2013.

[169] "Estudo de impacte ambiental. grupos 5,6,9 e 10 da central termoeléctrica do belo jardim," Ecoprogresso, EDA, Tech. Rep., Jul. 2007. [Online]. Available: http://www.azores.gov.pt/NR/rdonlyres/0C12180D-DB74-467B-B241-A8FB14B5E846/0/RNTGrupos569e10CentralTermoel%C3%A9ctricadoBeloJardim.pdf

[170] "Licenca ambiental n. 5/2008/DRA," Electricidade dos Açores S.A., Tech. Rep., Sep. 2008.

[171] "Informe Final CESI," CESI, Tech. Rep. RETE-A3/012472, 2002. [Online]. Available: http://www.coes.org.pe/DATAWEB2/2003/DEV/CESI/anexo_c.pdf

[172] "Informe Final CESI. Análisis de fiabilidad con criterio probabilístico," CESI, Tech. Rep. RETE-A3/012580, 2002. [Online]. Available: http://www2.osinerg.gob.pe/Proyecto_Normas/2007/CritMetElabPlanTransm/Estudio01-CESI/02Informe01-02-Anexos.pdf

[173] M. A. Mitchell, "Optimization of Under-frequency Load Shedding strategies throught the use of a neural network and a generatic algorithm," Ph.D. dissertation, Faculdade de Engenharia da Universidade do Porto, Jul. 2000. [Online]. Available: http://repositorio-aberto.up.pt/bitstream/10216/11486/2/Texto%20integral.pdf

[174] S. Galrao, "Grid codes for isolated systems," Master's thesis, Instituto Superior Técnico. Universidad Técnica de Lisboa, oct 2010.

[175] "Transmission Code of Practice," *REE*, May 2014. [Online]. Available: http://www.esios.ree.es/web-publica/

[176] G. d. C. Consejería de Empleo, Industria y Comercio, "Anuario energético de canarias. 2012," Tech. Rep., Dec. 2013. [Online]. Available: http://www.gobiernodecanarias.org/industria/publicaciones/ANUARIO_ENERGeTICO_DE_CANARIAS_2012.pdf

[177] "Planificación de los sectores de electricidad y gas 2012-2020. Desarrollo de las redes de transporte," Ministerio de Industria, Turismo y Comercio, Tech. Rep., Jul. 2011. [Online]. Available: http://www.minetur.gob.es/energia/es-ES/Novedades/Documents/PlanificacionElectricidadGas_2012_2020.pdf

[178] "Resolución de 24 de julio de 2012, boe 10/08/12," *Ministerio de Industria, Energía y Turismo*, Aug. 2012.

[179] "Orden ITC/913/2006," *Ministerio de Industria, Energía y Turismo*, Mar. 2012. [Online]. Available: http://www.boe.es/boe/dias/2006/03/31/pdfs/A12484-12556.pdf